GROUNDWATER TEMPERATURE AND FLOW

STUDIES IN THE GREAT BASIN

by

Melissa Dawn Masbruch

A dissertation submitted to the faculty of
The University of Utah
in partial fulfillment of the requirements for the degree of

Doctor of Philosophy

in

Geology

Department of Geology and Geophysics

The University of Utah

December 2013

The University of Utah Graduate School

STATEMENT OF DISSERTATION APPROVAL

The dissertation of **Melissa Dawn Masbruch**

has been approved by the following supervisory committee members:

D. Kip Solomon	, Co-Chair	**10/3/2013** Date Approved
David Chapman	, Co-Chair	**10/3/2013** Date Approved
Victor Heilweil	, Member	**10/3/2013** Date Approved
John Bowman	, Member	**10/3/2013** Date Approved
William Parry	, Member	**10/3/2013** Date Approved

and by **John Bartley**, Chair/Dean of

the Department/College/School of **Geology and Geophysics**

and by David B. Kieda, Dean of The Graduate School.

ABSTRACT

A monitoring network in the alpine Brighton Basin was established to examine the relationship between air, ground, and noble gas groundwater recharge temperatures. Maximum noble gas groundwater recharge temperatures from 25 samples collected over 2 years averaged 2.9±1.2 °C, within the experimental error of the mean ground temperature of 2.3 °C , and vary from 0 to 7 °C, also comparable to ground temperature variations. Mean ground temperatures in the upper 1 m of soil over the 2 years were 1 °C cooler than mean air temperatures. This offset is explained by modeling a snow effect on ground temperature. This study indicates that interpretation of groundwater recharge temperatures derived from noble gases should be attentive to the local ground temperature effects in recharge areas.

Two-dimensional modeling of fluid flow and heat transport are used to quantify effects of groundwater flow on the subsurface thermal regime and determine the lower limit of recharge rates that will produce an observable perturbation such that groundwater temperatures can be used to constrain them. The greatest temperature perturbations occur in the deepest portion of the recharge area. At recharge rates of 10 mm yr^{-1} or less, the hydrologic disturbance to the subsurface thermal regime is almost completely dependent on the recharge rate. At recharge rates higher than this, the hydrologic disturbance is dependent on both the recharge rate and permeability. At recharge rates of 50 mm yr^{-1} and greater, the plume of colder water persists towards the discharge area and could be

easily measured and used to constrain recharge rates to the system.

The Snake Valley area groundwater system was simulated using a three-dimensional model incorporating groundwater flow and heat transport. This study represents one of the first regional modeling efforts to include calibration to groundwater temperatures. The inclusion of temperature observations reduced parameter uncertainties over using just water-level altitude and discharge observations. The distribution of simulated transmissivity includes areas of high transmissivity within and between hydrographic areas. Increased well withdrawals within these areas will likely affect a large portion of the study area, resulting in decreasing groundwater levels and discharge to springs and evapotranspiration.

TABLE OF CONTENTS

LIST OF TABLES

Table

LIST OF FIGURES

Figure

PREFACE

This dissertation consists of three separate manuscripts that have either been published, been submitted for publication, or will be submitted for publication. All three chapters deal with the overarching theme of using groundwater temperatures to quantify various aspects of groundwater systems in the Great Basin.

Chapter 1 is a paper entitled "Air, Ground, and Groundwater Recharge Temperatures in an Alpine Setting, Brighton Basin, Utah" by Melissa D. Masbruch, David S. Chapman, and D. Kip Solomon that was published in volume 48 of Water Resources Research in 2012. This chapter describes results from a detailed monitoring network that was used to examine the relationship between air, ground, and groundwater recharge temperatures in an alpine setting. It is reprinted here with permission from John Wiley and Sons.

Chapter 2 is a paper entitled "Using Groundwater Temperatures to Constrain Recharge Rates in Arid Intermontane Basins" by Melissa D. Masbruch, D. Kip Solomon, and David S. Chapman that will be submitted for publication to a journal yet to be determined. This chapter describes the results of two-dimensional numerical modeling of the combined processes of fluid flow and heat transport which are used to quantify the effects of groundwater flow on the subsurface thermal regime and determine the lower limit of recharge rate that will produce an observable perturbation such that groundwater temperatures can be used to constrain recharge rates.

Chapter 3 is a manuscript entitled "Hydrology and Numerical Simulation of Groundwater Movement and Heat Transport in Snake Valley and Surrounding Areas, Juab, Millard, and Beaver Counties, Utah, and White Pine and Lincoln Counties, Nevada" by Melissa D. Masbruch, Phillip M. Gardner, and Lynette E. Brooks. This manuscript was prepared for publication as an U.S. Geological Survey Scientific Investigations Report and is currently in review. This report describes the construction, calibration, and evaluation of a three-dimensional regional model incorporating groundwater flow and heat transport for Snake Valley and surrounding areas along the Utah-Nevada border. It is reprinted here courtesy of the U.S. Geological Survey.

There are many people to thank that were instrumental in the completion of this work. First and foremost I would like to thank the members of my committee: Kip Solomon, Dave Chapman, Vic Heilweil, John Bowman, and Bill Parry. Their thoughtful guidance, encouragement, and help in solving problems helped keep me focused and moving forward. In preparing this dissertation, they offered invaluable feedback and suggestions for improvement.

I am grateful to my fellow graduate students at the university and colleagues at the U.S. Geological Survey for their friendship, encouragement, humor, and advice. They were always willing to listen and offer helpful suggestions when elicited and helped keep me sane during the writing process.

Finally, this dissertation is dedicated to my family, without whose love and support I would never have made it this far. To my parents, for always encouraging me to follow my dreams, no matter how far away they might take me, and always believing in me. To my brother and his family, and my best friend, for their love and good humor.

And to my dog, Annie, faithful companion of nearly 14 years, and my new dog, Sunshine, for keeping me grounded and making me get outside for fresh air every day. I love you all.

CHAPTER 1

AIR, GROUND, AND GROUNDWATER TEMPERATURES IN AN ALPINE SETTING, BRIGHTON BASIN, UTAH

1.1 Abstract

Noble gases are useful tracers for constraining groundwater recharge temperature and elevation, critical in determining source areas of groundwater recharge in mountainous terrain. A monitoring network in the alpine Brighton Basin in the Wasatch Mountains of northern Utah, USA, was established to examine the relationship between air temperatures, ground temperatures, and noble gas groundwater recharge temperatures. Maximum noble gas groundwater recharge temperatures computed using the closed-system equilibration model from 25 samples collected over the 2 year period 2007 to 2009 averaged 2.96 ± 1.2 °C, within the experimental error of the mean ground temperature of 2.3 °C measured within the probable recharge area. Maximum noble gas recharge temperatures vary from 0 to 7 °C, also comparable to ground temperature variations in the region. Groundwater ages in the collected samples vary from 0 to 7 years, indicating changing flow paths to the collection site during the experiment. Mean ground temperature in the upper 1 m of soil over the 2 year time period is 2.3 °C, which is 1 °C cooler than the mean surface air temperature extrapolated from a nearby meteorological station. This comparison contradicts an earlier observation that mean annual ground temperatures in central Utah are generally warmer than air temperatures.

The offset in the Brighton Basin is explained by modeling a snow effect on ground temperature. This detailed study suggests that interpretation of groundwater recharge temperatures derived from noble gases should be attentive to the complex local ground temperature effects in the recharge areas.

1.2 Introduction

Determining sources of recharge to aquifers is becoming increasingly important as demands on groundwater continue to increase. One such area where water demands are increasing at a rapid rate is the intermountain west of the U.S. Intermountain basin-fill aquifers and underlying permeable bedrock aquifers are a significant source of groundwater in these arid and semiarid regions. Existing studies [*Anderson and Freethey*, 1996; *Gates*, 1995; *Manning and Solomon*, 2003; *Mason*, 1998; *Prudic and Herman*, 1996] have shown that water sourced in the adjacent mountain blocks accounts for one third to nearly all of the groundwater recharge to these basins. Accurate estimations of the amount of mountain-block recharge to these aquifers are important for water resource management planning.

Several studies [*Aeschbach-Hertig et al.*, 1999; *Ballentine and Hall*, 1999; *Manning and Caine*, 2007; *Manning and Solomon*, 2003; *Mazor*, 1991; *Rauber et al.*, 1991; *Zuber et al.*, 1995] have shown noble gases to be useful traces for examining groundwater recharge temperature (T_r) and elevation (H), which in turn can be used to determine source areas of groundwater recharge to the intermountain aquifers. In order to constrain both recharge temperatures and elevations, however, a recharge temperature versus elevation curve (T_r lapse curve) must be developed for the area in question [*Aeschbach-Hertig et al.*, 1999; *Manning and Solomon*, 2003].

The variation of air temperature with elevation is well known from atmospheric science. An average environmental lapse rate is –6.5 °C km^{-1}, intermediate between a dry adiabatic lapse rate of –9.9 °C km^{-1} and a saturated adiabatic lapse rate of –5.0 °C km^{-1}. Studies by *Aeschbach-Hertig et al.* [1999] and *Zuber et al.* [1995] used T_r lapse curves that were developed assuming a consistent relation between T_r and the mean annual air temperature (T_a) at all elevations, either $T_r = T_a$ at all elevations [*Aeschbach-Hertig et al.*, 1999], or $T_r = T_a - 1$ °C at all elevations [*Zuber et al.*, 1995]. In these studies, the noble gas data were used to derive a set of best-fit pairs of H and T_r for each sample by specifying different values of assumed H and then solving for T_r and excess air. The most probable values of H and T_r for each sample were then determined by finding the point of intersection between the suite of best-fit solutions and the assumed recharge lapse curve. This technique was applied to a small number of samples with mixed results; for some samples the derived H values were reasonable, while for others the derived H values were inexplicably too high or too low.

Manning and Solomon [2003] took a more rigorous approach to derive a local T_r lapse curve for the Wasatch Mountains of central Utah. In their study, dissolved noble gases were sampled in 16 springs and mine tunnels at various elevations within the mountain block, and a derived maximum and minimum T_r for each sample was determined using constrained minimum and maximum H values particular to each sampling site. *Manning and Solomon* [2003] then used the derived T_r and H data to develop a T_r lapse curve for the Wasatch Mountains using a least squares linear regression. Their T_r lapse curve has a similar slope (–7.3 °C km^{-1}) to the atmospheric lapse rate (for adiabatic cooling) in the Wasatch Mountains (–6.4 °C km^{-1}); however, it is

approximately 2 to 4 °C cooler than the atmospheric lapse curve (Figure 1-1). Based on all derived minimum and maximum values of T_r, *Manning and Solomon* [2003] concluded that, on average, T_r was about 2 °C cooler than T_a within the Wasatch Mountains. Due to the lack of wells in high alpine recharge areas within the Wasatch Mountains, however, *Manning and Solomon's* [2003] derived recharge lapse curve was never ground-truthed; that is, *Manning and Solomon* [2003] did not measure ground (water table) temperatures in recharge areas to confirm that they were in agreement with the noble gas derived recharge temperatures.

The observation that *Manning and Solomon's* [2003] derived T_r lapse curve is cooler than the atmospheric lapse curve for the Wasatch Mountains is significant in many respects. Generally, shallow water table (10–20 m depth) temperatures are approximately 1 to 2 °C warmer than T_a [*Anderson*, 2005; *Domenico and Schwartz*, 1998], and mean annual soil temperatures can be biased 1 to 4 °C higher than T_a [*Powell et al.*, 1988; *Putnam and Chapman*, 1996] (Figure 1-1). Studies by *Bartlett et al.* [2004, 2005], *Cey* [2009], and *Smith et al.* [1964] have also shown that in areas of prolonged snow cover mean annual ground temperatures may be warmer than T_a as the snow insulates the ground from colder winter air temperatures. *Cey* [2009] has furthermore used numerical simulations to explore the effects of precipitation, water table depth and air temperature variations on mean water table temperatures during groundwater recharge.

Alternatively, under some circumstances snow cover and snow melt may produce cooler mean annual ground temperatures than mean annual air temperatures. *Bartlett et al.* [2004, 2005] show that while snow may insulate the ground from cooler air temperatures during the winter, persistent snow cover in late spring may pin the ground

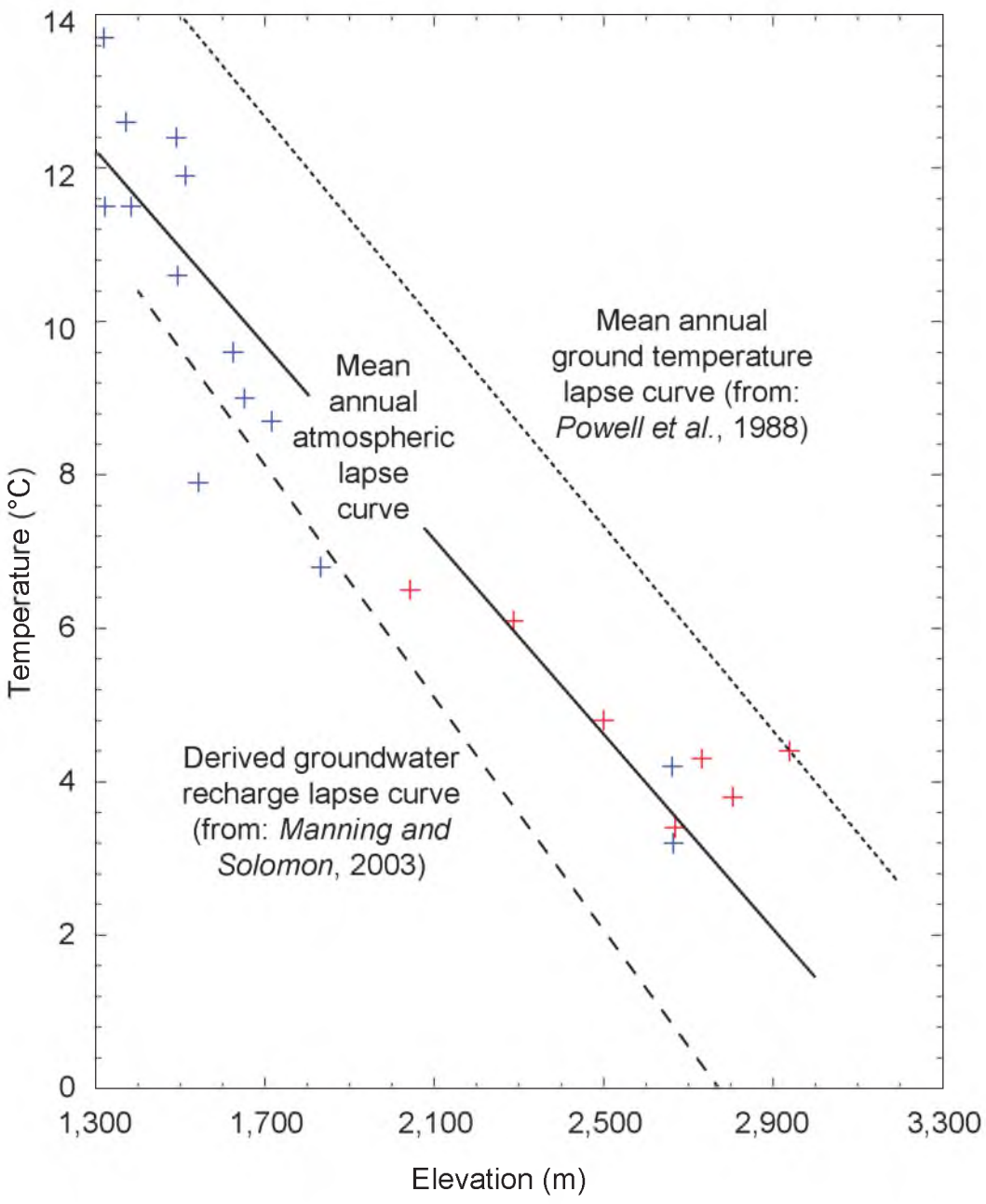

Figure 1-1. Lapse rates of temperature versus elevation in northern and central Utah. Shown are the mean annual atmospheric lapse curve for the Wasatch Mountains (solid line) derived from SNOTEL (red crosses) and Western Regional Climate Center (blue crosses) meteorological station data; groundwater recharge lapse curve from *Manning and Solomon* [2003] for the Wasatch Mountains (dashed line); and mean annual ground temperature lapse curve for sites in central Utah from *Powell et al.* [1988] (dotted line). Modified from: *Masbruch et al.* [2012].

temperature near 0 °C while air temperatures warm during the spring and early summer, producing mean annual ground temperatures that are cooler than T_a. Additionally, as snow melt is often the main source of recharge in mountainous terrain, large volumes of snow melt infiltrating fractured rock may keep temperatures in the unsaturated zone and water table near 0 °C, especially as water table depths may decrease to less than 3 m depth during spring snow melt events [*Buttle*, 1989; *Hill*, 1990; *Klump et al.*, 2006]. Consequently, in many high alpine areas, T_r could be considerably lower than T_a.

To determine why recharge temperatures within the Wasatch Mountains are apparently cooler than mean annual air temperatures, this study investigates the relation between air, ground and groundwater recharge temperatures within the Brighton Basin, a high alpine basin located within the Wasatch Mountains. The area chosen within the Brighton Basin is considered to be an ideal location for several reasons: (1) installation of a shallow monitoring well at a local discharge site where groundwater levels are near land surface was possible; (2) recharge areas within the basin are constrained by the topography of the basin, and span only about a 100 m difference in elevation; they cannot be lower than the elevation of the discharge site at 2,770 m and cannot be much higher than about 2,890 m where there is a break in slope between the basin and the peaks surrounding the basin as it is highly unlikely that groundwater recharge is occurring at the top of the peaks surrounding the basin; and (3) as the topographic map shows, the selected sites exist in a small subbasin, which further limits the location of the probable recharge area contributing water to the discharge site (Figure 1-2). Other subbasins exist northeast and southwest, likely with groundwater flow regimes separate from the sampling sites.

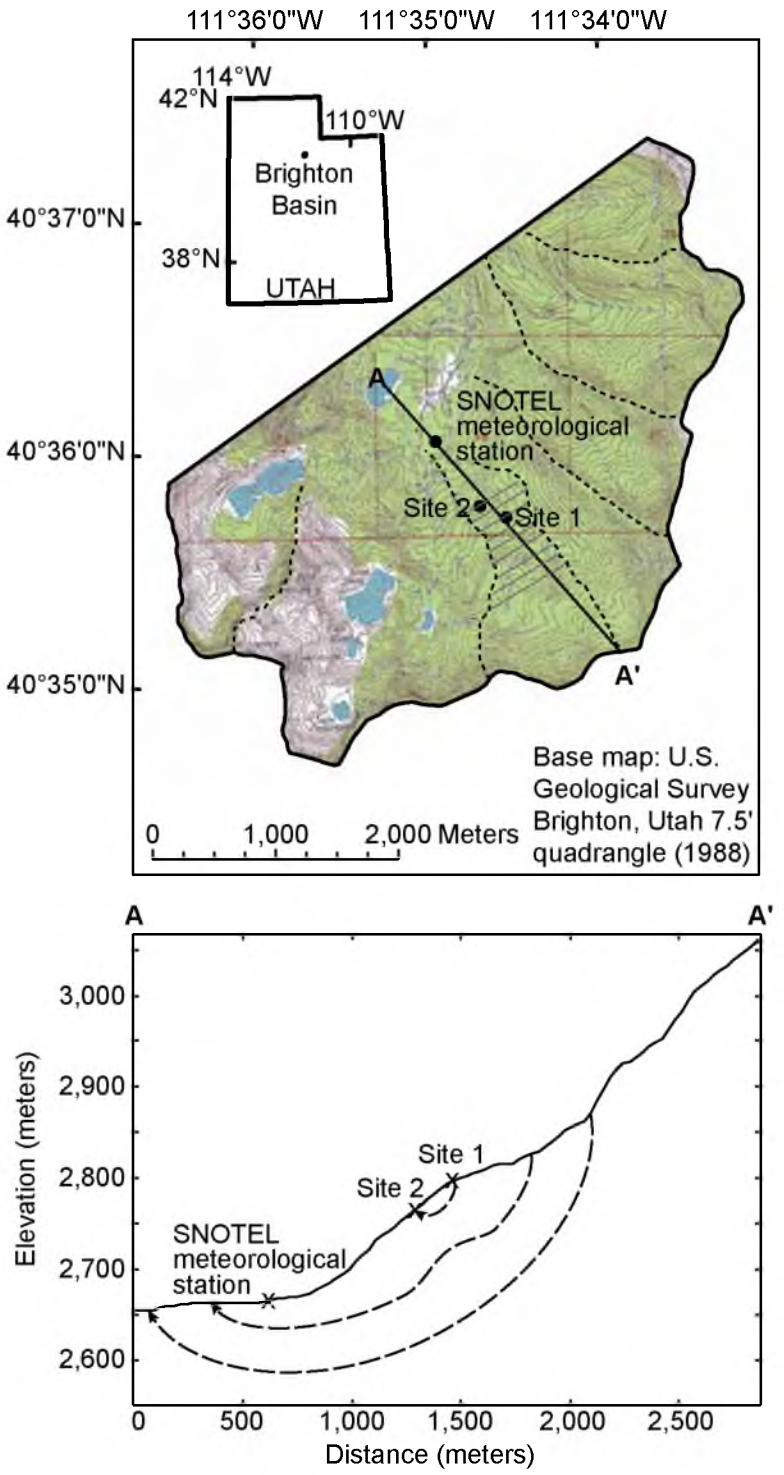

Figure 1-2. (top) Map of land-surface topography of the Brighton Basin, Utah, and locations of monitoring sites. Dotted lines delineate subbasins, and hatchured area represents the probable recharge area for the monitoring sites. (bottom) Two-dimensional cross section of land-surface topography and conceptualization of possible groundwater flow paths (dashed lines) within the basin. Modified from: *Masbruch et al.* [2012].

A monitoring network within the basin was used to compare air, ground, and groundwater recharge temperatures and groundwater ages over a period of more than 2 years. Air temperature and snow depth data were drawn from a meteorological station within the basin that is part of the SNOTEL (Snow Telemetry, Natural Resources Conservation Service National Water and Climate Center) network. Ground temperatures at multiple depths were continuously monitored using temperature probes that were installed at local recharge and discharge areas within the basin. Groundwater temperatures within a shallow well in the discharge area were also continuously monitored. Noble gas and tritium samples from the well were generally collected every 2 to 8 weeks to determine groundwater recharge temperatures and groundwater ages.

This study had three objectives. First, the data collected from the monitoring network were used to examine how the noble gas recharge temperatures relate to ground and air temperatures. Second, the data were used to identify possible seasonal effects in the groundwater recharge temperatures, ages, and flow regime within the basin. Third, the data were used to validate, at least at one point, the derived recharge lapse curve developed by *Manning and Solomon* [2003]. Validation of this lapse curve has implications for using noble gases collected from discharge areas within mountainous terrain to develop a recharge lapse curve, and application of this approach in a variety of high alpine terrains.

1.3 Site Description and Monitoring Network

1.3.1 Site Description

The connection between air, ground, and groundwater recharge temperatures was investigated by establishing a monitoring network within the Brighton Basin, a high

alpine basin located at the head of Big Cottonwood Canyon within the Wasatch Mountains (Figure 1-2). The Wasatch Mountains are located to the east of the Salt Lake Valley in northern Utah and form the eastern margin of the Basin and Range physiographic province. The Brighton Basin ranges in elevation from 2,650 m (8,700 ft) to over 3,200 m (10,500 ft). The peaks surrounding the basin to the north and east are Tertiary igneous intrusions of the Alta and Clayton stocks, and form the divide between the headwaters of Big Cottonwood Creek on the west and Pine Creek on the east [*Stokes*, 1986]. The basin was carved by glaciation, and as a result the basin contains many small glacial moraines.

Mean annual precipitation in the Wasatch Mountains ranges between 50 to 130 cm [*Manning and Solomon*, 2003]; most of this precipitation falls as snow. The Brighton Basin receives an average of 1,270 cm (500 inches) of snow per year. Groundwater recharge in the basin is mainly derived from snowmelt that infiltrates into fractures in the bedrock of the Alta and Clayton stocks, or through the unconsolidated glacial deposits. Groundwater discharge in the basin is to small springs, streams, lakes, and evapotranspiration.

1.3.2 Monitoring Network

Air temperature and snow depth data were drawn from a preexisting SNOTEL meteorological station (SNOTEL site: Brighton, Utah; Site number: 366), located at an elevation of 2,667 m (8,750 ft) within the basin. Multidepth ground temperature probes were installed in two locations within the basin. The first probe was installed in a small glacial moraine (Site 1) at an elevation of approximately 2,790 m within the probable recharge area. The second probe was installed in a wetland/bog type discharge area (Site

2) approximately 230 m downgradient from the glacial moraine, at an elevation of approximately 2,770 m. These probes (also known as MRC (Measurement Research Corporation) probes, constructed by Geneq) consist of a string of precision thermistors epoxied into a single, 109 cm long rod. Five thermistors placed at 7, 12, 22, 52, and 102 cm from the top of the probe were used to measure ground temperatures.

Water temperatures were continuously monitored at a shallow well installed in the wetland area near the probe at Site 2 using a HOBOWater Temp Pro v2 Logger (developed by Onset). The well was constructed using 2-inch diameter PVC tubing with a 30-inch length screen. The bottom of the well is located approximately 1.6 m below land surface. The logger was suspended from the well cap so that it was positioned at approximately the middle of the well screen.

Groundwater recharge temperature and age were determined using noble gas and tritium samples that were collected periodically at the well. Noble gas samples were collected using passive diffusion samplers similar to those shown in *Sanford et al.* [1996]. The samplers were allowed to equilibrate within the well water for at least 24 h. The gases were then measured using a quadrapole mass spectrometer at the University of Utah noble gas laboratory, and from these measured gases a groundwater recharge temperature was determined (see section 1.4.4 below). Tritium samples were collected in 1 L plastic bottles, and were used to determine the apparent groundwater age using the tritium/helium-3 ($^3H/^3He$) dating method [*Solomon and Cook*, 2000].

1.4 Data

1.4.1 SNOTEL Meteorological Station Data

Air temperatures and snow depth were measured at the Brighton meteorological station that is part of the SNOTEL network. Data from this station are archived on the SNOTEL website which can be accessed at *http://www.wcc.nrcs.usda.gov/nwcc/site?sitenum=366&state=ut*. The station has been in operation since 1 October 1985, and has been recording hourly air temperatures since 31 January 1996; before this date, air temperatures were recorded only one to four times per day. Snow depth at the station has been measured hourly since 7 October 1997. Data from the period of 1 March 2007 to 1 March 2009, which encompasses the period of noble gas sampling and ground temperature monitoring, are shown in Figures 1-3 through 1-5 and summarized in Table 1-1.

1.4.2 Ground Temperature Data

Ground temperatures were measured at multiple depths up to 1 m at two locations within the basin, using the MRC probes in conjunction with Campbell Scientific CR-10 data loggers. At both locations, thermistors on the probes were sampled every 60 s, and the mean of 30 measurements were stored every 30 min. At Site 1 the MRC temperature probe was installed on 3 February 2007 in a glacial moraine within the probable recharge area. Ubiquitous subsurface cobbles prevented full penetration of the probe at this site; only two thermistors, therefore, were located below ground at 22 and 72 cm depth, respectively. The water table at this site was not intersected during installation of the probe; however, the soil near the bottom of the hole into which the probe was inserted was very moist, suggesting that the water table at this site was only slightly deeper than

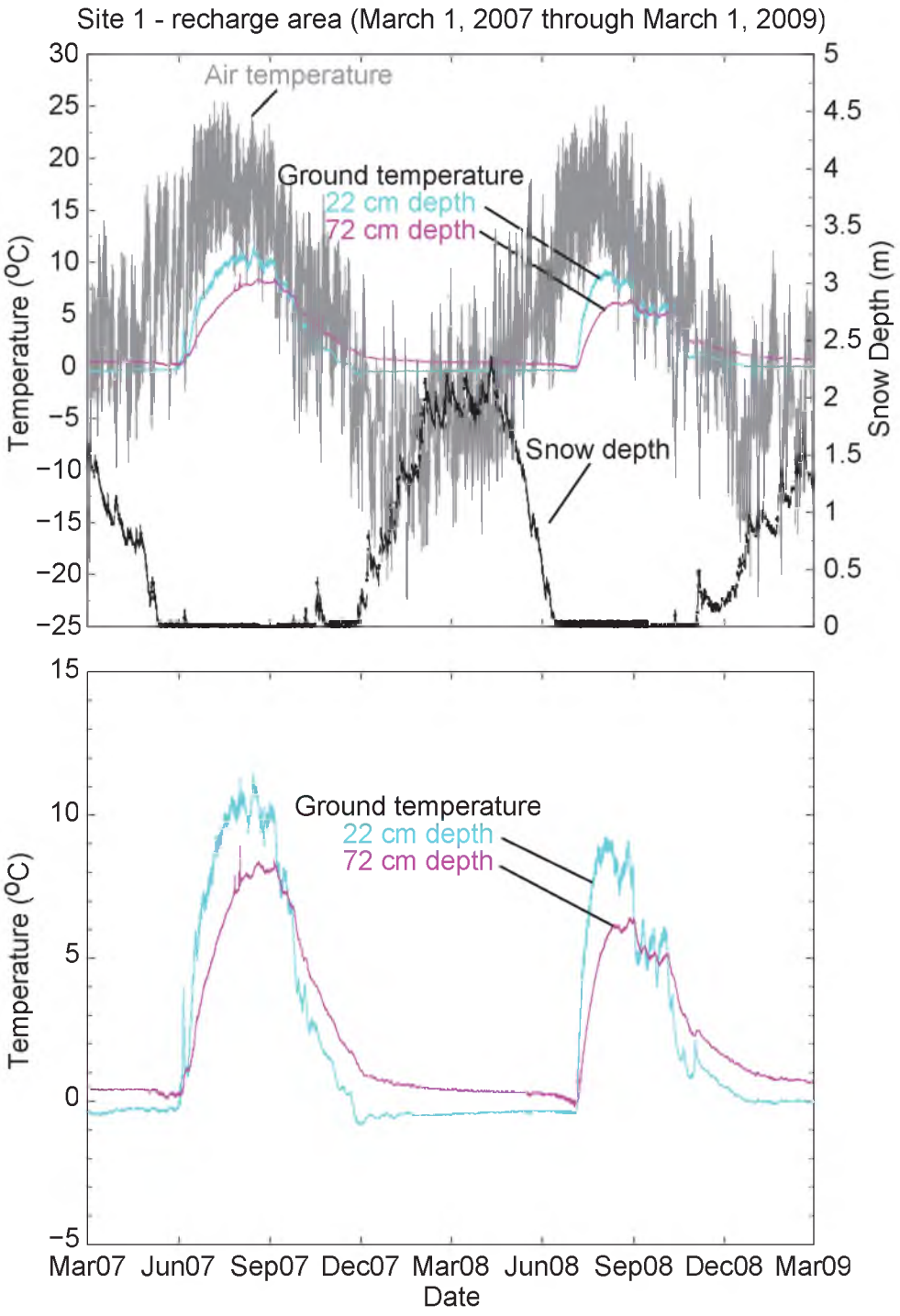

Figure 1-3. Relation of ground temperatures at Site 1 (recharge area) to air temperatures and snow depth. (top) Hourly mean air temperature and snow depth data from the SNOTEL meteorological station, and 30-min mean ground temperature data at Site 1, Brighton Basin, Utah; (bottom) enlargement of the 30-min mean ground temperature data at Site 1. Modified from: *Masbruch et al.* [2012].

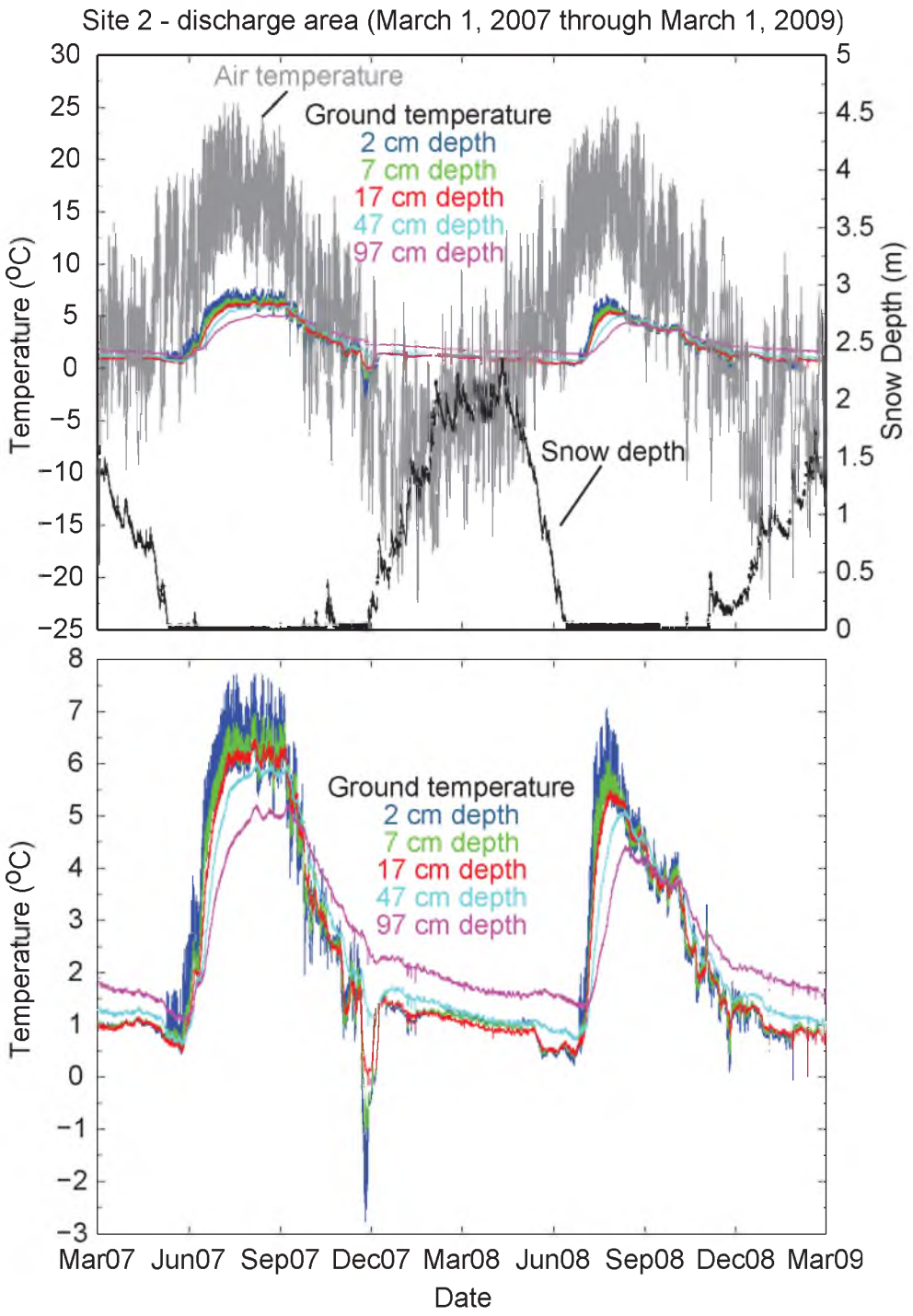

Figure 1-4. Relation of ground temperatures at Site 2 (discharge area) to air temperatures and snow depth. (top) Hourly mean air temperature and snow depth data from the SNOTEL meteorological station, and 30-min mean ground temperature data at Site 2, Brighton Basin, Utah; (bottom) enlargement of the 30-min mean ground temperature data at Site 2. Modified from: *Masbruch et al.* [2012].

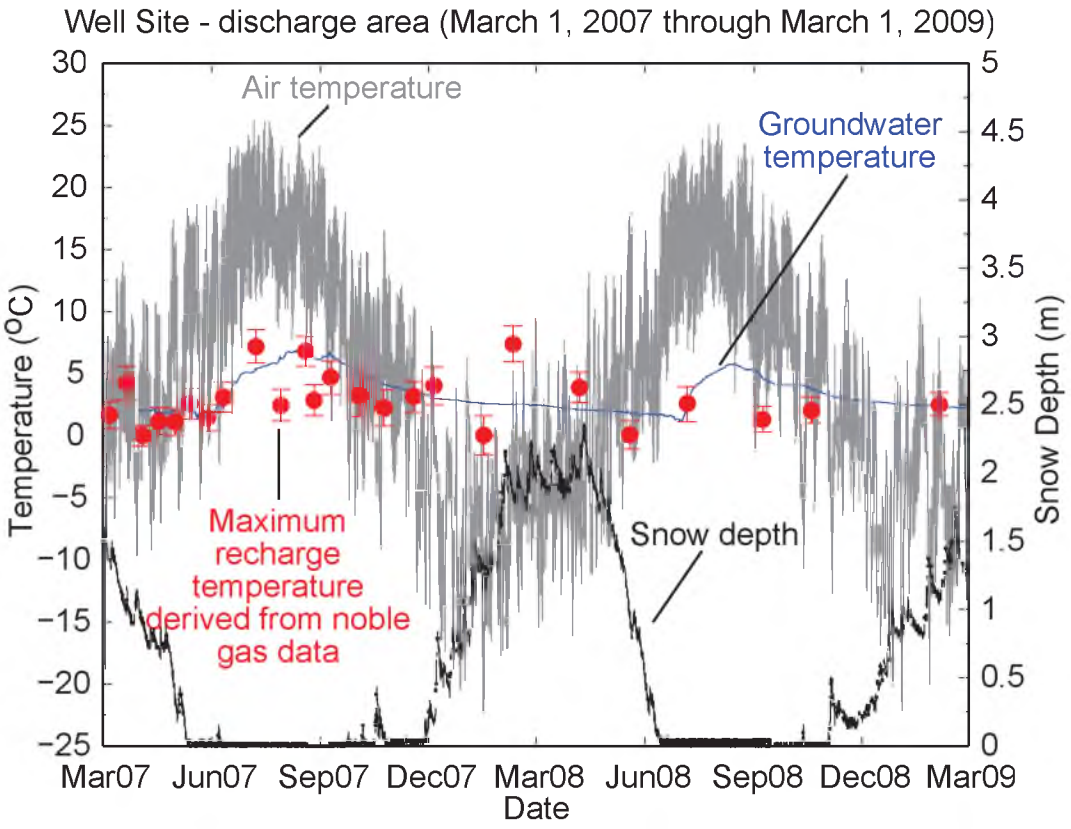

Figure 1-5. Relation of groundwater temperatures from the well at Site 2 (discharge area) and groundwater recharge temperatures to air temperatures and snow depth. Shown are hourly mean air temperature and snow depth data from the SNOTEL meteorological station, 30-min groundwater temperature data from the well, and maximum groundwater recharge temperatures derived from noble gas samples collected from the well, Brighton Basin, Utah. Modified from: *Masbruch et al.* [2012].

Table 1-1. Summary of air (SAT), ground (GT) and groundwater (GWT) temperature data. Modified from: *Masbruch et al.* [2012].

	SNOTEL			Site 1		Site 2					Well
	SAT			GT 22 cm	GT 72 cm	GT 2 cm	GT 7 cm	GT 17 cm	GT 47 cm	GT 97 cm	GWT
2007-2008	Max.	Min.	Mean	Mean	Mean	Mean	Mean	Mean	Mean	Mean	Mean
Mar	14.0	-18.8	0.7	-0.39	0.43	1.00	0.99	0.96	1.24	1.70	2.29[1]
Apr	17.4	-9.2	2.7	-0.29	0.42	1.01	1.04	1.03	1.23	1.58	1.98
May	18.6	-6.0	7.5	-0.28	0.28	0.93	0.85	0.72	0.84	1.24	1.76
Jun	23.3	-2.3	13.4	4.14	2.22	4.03	3.75	3.24	2.63	2.26	3.45
Jul	25.4	8.7	17.2	9.43	6.23	6.32	6.21	6.00	5.45	4.47	5.62
Aug	24.1	6.3	15.6	10.20	8.00	6.40	6.30	6.16	5.86	5.04	6.59
Sep	21.7	-6.4	9.8	7.23	7.21	4.86	4.97	5.08	5.27	4.87	5.99
Oct	16.5	-9.2	4.5	2.48	4.07	2.82	2.88	2.89	3.30	3.76	4.46
Nov	12.1	-13.6	0.8	0.25	1.96	0.71	0.94	1.16	1.92	2.80	3.59
Dec	8.8	-20.5	-7.2	-0.55	0.81	1.06	1.30	1.28	1.54	2.26	2.91
Jan	6.3	-22.4	-7.4	-0.47	0.56	1.17	1.23	1.23	1.51	2.09	2.61
Feb	9.4	-17.3	-5.3	-0.47	0.43	1.21	1.21	1.13	1.34	1.87	2.51
annual mean	–	–	4.4	2.62	2.73	2.64	2.65	2.58	2.68	2.83	3.65[2]

	SNOTEL			Site 1		Site 2					Well
	SAT			GT 22 cm	GT 72 cm	GT 2 cm	GT 7 cm	GT 17 cm	GT 47 cm	GT 97 cm	GWT
2008-2009	Max.	Min.	Mean	Mean	Mean	Mean	Mean	Mean	Mean	Mean	Mean
Mar	7.7	-16.1	-3.6	-0.42	0.38	1.13	1.09	0.98	1.16	1.69	2.31
Apr	13.2	-15.7	-0.9	-0.38	0.34	1.02	0.99	0.88	1.05	1.59	2.06
May	18.0	-9.0	4.2	-0.34	0.29	0.74	0.76	0.72	1.00	1.60	1.85
Jun	22.5	-2.2	10.2	-0.35	0.18	0.52	0.57	0.57	0.85	1.47	1.60
Jul	25.0	6.7	16.1	5.21	2.55	4.46	4.27	3.90	2.99	2.29	3.81
Aug	25.1	3.2	14.8	8.41	6.01	4.85	4.88	4.88	4.81	4.19	5.50
Sep	19.5	-1.3	9.3	5.36	5.24	3.80	3.83	3.83	3.98	3.86	4.42
Oct	16.8	-10.7	4.6	2.45	3.68	2.59	2.64	2.69	3.01	3.24	3.83
Nov	12.6	-12.7	0.5	1.01	2.03	1.54	1.59	1.60	1.91	2.39	3.00
Dec	7.9	-20.2	-5.8	0.19	1.26	1.19	1.25	1.25	1.52	2.04	2.68
Jan	11.1	-22.1	-3.6	-0.02	0.85	0.79	0.86	0.87	1.21	1.83	2.47
Feb	7.8	-16.1	-3.8	0.00	0.73	0.90	0.92	0.85	1.10	1.69	2.29
annual mean	–	–	3.5	1.78	1.97	1.98	1.99	1.94	2.06	2.33	2.99

[1]Value interpolated from differences in monthly data for 2008-2009 vs. 2007-2008

[2]Value calculated as mean of monthly mean data for 2007-2008

79 cm at the time of installation. At Site 2 the MRC temperature probe was installed on 24 February 2007 in a bog/wetland (discharge) area approximately 230 m downgradient from the glacial moraine and Site 1. At this site, the land surface was constantly saturated suggesting that the water table was at, or slightly above, land surface. At Site 2, it was possible to install the probe to a depth of 104 cm, so all five thermistors were below ground at 2, 7, 17, 47, and 97 cm depth. Data for the two probes from the period of 1 March 2007 to 1 March 2009 are shown in Figures 1-3 and 1-4, and summarized in Table 1-1.

1.4.3 Groundwater Temperature Data

In addition to ground temperatures, groundwater temperatures within a shallow well installed in the discharge area (Site 2) near the MRC probe were measured using a HOBO temperature logger. The sensor was suspended from the well cap to a depth of approximately 1.2 m (middle of the well screen); temperatures were logged at 30-min intervals and periodically downloaded throughout the study. The logger in the well was deployed on 31 March 2007. Groundwater temperatures for the period 31 March 2007 to 1 March 2009 are shown in Figure 1-5 and are summarized in Table 1-1.

1.4.4 Noble Gas Groundwater Recharge Temperature Data and Age Data

Noble gas samples for the determination of groundwater recharge temperature and tritium samples for the determination of groundwater age were generally collected every 2 to 8 weeks from 6 February 2007 to 25 May 2009 from the well. Groundwater recharge temperature and age data from the well are shown in Figures 1-5 and 1-6, respectively,

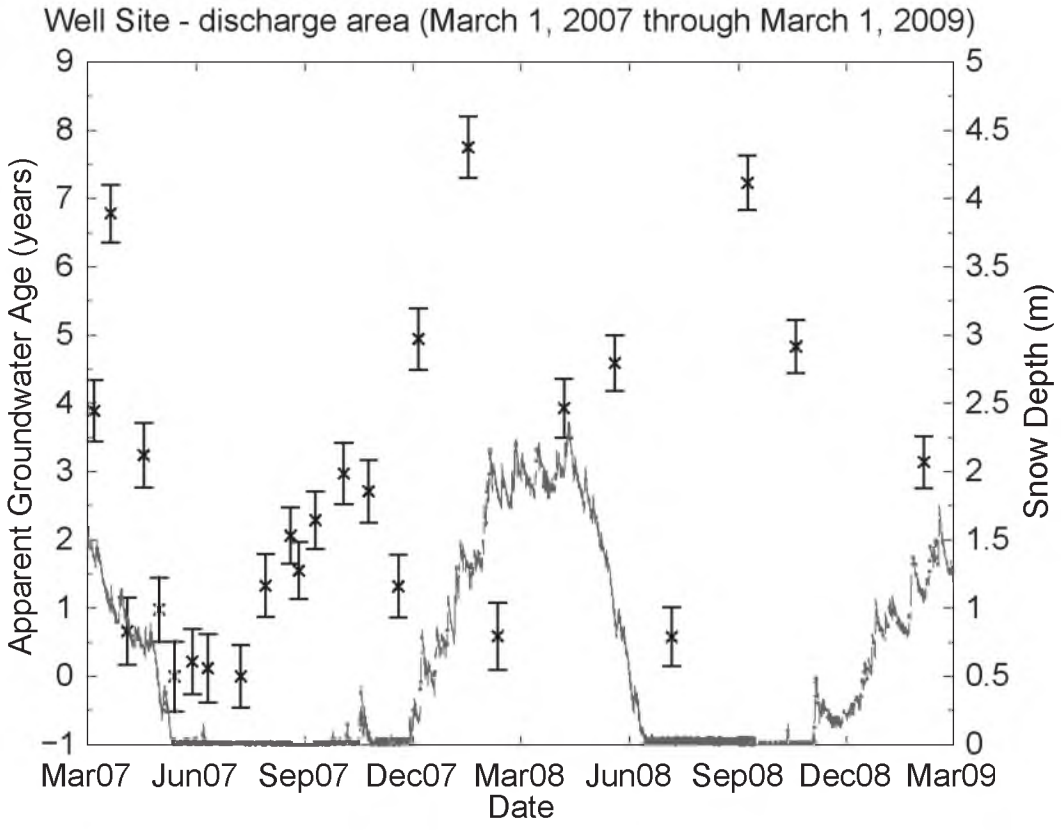

Figure 1-6. Age of groundwater samples (crosses) with 1 s.d. error bars collected from the well. Also shown are hourly mean snow depth data (gray line) from the SNOTEL meteorological station, Brighton Basin, Utah. Modified from: *Masbruch et al.* [2012].

and are summarized in Table 1-2.

Currently, there are several models that are used in the determination of recharge temperatures from noble gas data, which differ in the way in which the ''excess air'' component is treated; these include the total dissolution (TD) model [*Andrews and Lee*, 1979; *Stute and Schlosser*, 1993], the partial re-equilibration (PR) model [*Stute et al.*, 1995], the closed-system equilibration (CE) model [*Aeschbach-Hertig et al.*, 2000; *Ballentine and Hall*, 1999], the multistep partial re-equilibration (MR) model [*Kipfer et al.*, 2002], the partial degassing (rism diopters (PD)) model [*Lippmann et al.*, 2003], the negative pressure (NP) model [*Mercury et al.*, 2004], the oxygen depletion (OD) model [*Hall et al.*, 2005], and the gas diffusion relaxation (GR) model [*Sun et al.*, 2008]. This study uses the CE model for the determination of recharge temperatures from the noble gas data. The purpose of this study was not about comparing results from the different excess air models, but rather about comparing noble gas derived groundwater recharge temperatures with groundwater table temperatures. The consistency between the mean model results and the mean groundwater table temperatures measured within the Brighton Basin suggests that the CE model adequately represents conditions within the basin.

Measured noble gas and tritium concentrations are given in Table 1-2. Using inverse modeling techniques as described by *Aeschbach-Hertig et al.* [1999], these gas concentrations were then used to determine the unknown parameters of recharge temperature, excess air, and the fractionation of the excess air; salinity and recharge elevation (pressure) were prescribed a priori as 0 and 2,768 m, respectively. The inverse modeling technique uses a nonlinear least squares method that finds those values of the

Table 1-2. Summary of noble gas maximum recharge temperatures (T_r), groundwater ages, and measured noble gas and tritium concentrations. Modified from: *Masbruch et al.* [2012].

Sample ID	Collection date	Maximum T_r (°C)	Apparent groundwater age (years)	N_2 (ccSTP/g) x 10^{-2} error: ±5.0%	^{40}Ar (ccSTP/g) x 10^{-4} error: ±3.0%	^{84}Kr (ccSTP/g) x 10^{-8} error: ±4.0%	^{20}Ne (ccSTP/g) x 10^{-7} error: ±2.0%	^{129}Xe (ccSTP/g) x 10^{-9} error: ±5.0%	^{4}He (ccSTP/g) x 10^{-8} error: ±1.0%	R/Ra[1] error: ±1.0%	^{3}H (TU) error: ±5.0%
WA03	20070306	1.6 ± 1.1	3.9 ± 0.4	1.2	3.4	4.8	1.4	3.5	3.5	1.1	6.9
WA04	20070320	4.2 ± 1.4	6.8 ± 0.4	1.2	3.4	4.6	1.5	3.5	3.6	1.2	7.8
WA05	20070403	0.0 ± 0.8	0.7 ± 0.5	1.3	3.5	4.8	1.5	4.0	3.5	1.0	6.9
WA06	20070417	1.2 ± 1.1	3.2 ± 0.5	1.3	3.6	4.8	1.5	3.6	3.8	1.0	6.8
WA07	20070430	1.1 ± 1.1	1.0 ± 0.5	1.4	3.7	5.0	1.6	3.6	3.7	1.0	7.4
WA08	20070513	2.6 ± 1.2	0.0 ± 0.5	1.3	3.6	4.8	1.5	3.5	3.6	1.0	7.1
WA09	20070528	1.4 ± 1.1	0.2 ± 0.5	1.4	3.8	5.1	1.5	3.6	3.6	1.0	7.6
WB10	20070610	3.1 ± 1.2	0.1 ± 0.5	1.3	3.5	4.8	1.5	3.4	3.6	1.0	7.3
WB11	20070708	7.2 ± 1.3	0.0 ± 0.5	1.2	3.2	4.2	1.4	2.9	3.5	1.0	7.9
WA12	20070729	2.5 ± 1.3	1.3 ± 0.5	1.3	3.4	4.6	1.5	3.4	3.8	1.0	7.4
WA13	20070819	6.8 ± 1.2	2.1 ± 0.4	1.2	3.2	4.2	1.5	2.9	3.6	1.1	7.5
WA14	20070826	2.8 ± 1.2	1.6 ± 0.4	1.3	3.5	4.6	1.6	3.5	3.8	1.1	7.7
WB15	20070909	4.7 ± 1.3	2.3 ± 0.4	1.3	3.5	4.5	1.6	3.1	3.8	1.1	7.8
WA16	20071003	3.2 ±1.7	3.0 ± 0.4	1.3	3.4	4.6	1.6	3.4	3.9	1.1	4.5
WA17	20071024	2.2 ± 1.4	2.7 ± 0.5	1.4	3.6	4.9	1.6	3.4	3.8	1.1	7.2
WA18	20071118	3.1 ± 1.2	1.3 ± 0.5	1.3	3.4	4.7	1.6	3.4	3.7	1.1	7.4
WA19	20071205	4.0 ± 1.5	4.9 ± 0.4	1.3	3.4	4.7	1.6	3.1	3.9	1.1	7.0
WA20	20080116	0.0 ± 1.6	7.8 ± 0.4	1.5	3.3	5.5	1.8	3.8	4.5	1.1	7.6
WA21	20080210	7.4 ± 1.4	0.6 ± 0.5	1.2	3.7	4.3	1.5	3.2	3.6	1.0	7.4
WA22	20080406	3.9 ± 1.2	3.9 ± 0.4	1.3	3.5	4.5	1.5	3.2	3.6	1.1	7.4
WA23	20080519	0.1 ± 1.1	4.6 ± 0.4	1.4	3.6	4.9	1.6	4.1	3.8	1.1	7.8
WA24	20080706	2.6 ± 1.4	0.6 ± 0.4	1.3	3.5	4.7	1.6	3.3	3.8	1.0	8.5
WA25	20080908	1.3 ± 1.0	7.2 ± 0.4	1.3	3.5	5.0	1.5	3.4	4.0	1.1	7.7
WB26	20081019	2.1 ± 1.0	4.8 ± 0.4	1.3	3.5	4.9	1.5	3.3	3.8	1.1	8.1
WB27	20090204	2.5 ± 0.9	3.1 ± 0.4	1.3	3.4	4.7	1.4	3.1	3.5	1.1	8.0

[1]R is the $^{3}He/^{4}He$ ratio of the sample; Ra is the $^{3}He/^{4}He$ ratio of air (1.384×10^{-6})

model parameters that minimize χ^2, which is the sum of the squared deviations between the modeled and measured concentrations, normalized to the respective experimental uncertainties [*Aeschbach-Hertig et al.*, 2002]. The reported 1σ (i.e., 1 standard deviation) uncertainties in the recharge temperatures and ages (Table 1-2 and Figures 1-5 and 1-6) were determined using Monte Carlo simulations, whereby the measurement errors of the noble gas and tritium concentrations were varied.

1.5 Results/Discussion

1.5.1 Temperature Data

The data collected from the monitoring network were used to examine how the air, ground, and noble gas groundwater recharge temperatures relate to one another. Additionally, the data were used to identify possible seasonal variations in the groundwater recharge temperatures and ages, which may point to seasonal changes in the groundwater flow regime within the basin. The data were also used to investigate the effects of snow cover on ground temperatures within the basin.

Air temperatures for the period March 2007 to March 2009 varied between –22.4 °C and 25.4 °C (Table 1-1). Maximum temperatures occurred in July and August, while minimum temperatures occurred in January. Monthly mean air temperatures for March to September 2007 were 0.5 to 4.3 °C warmer than monthly mean temperatures for March to September 2008. Conversely, monthly mean air temperatures for December to February 2007 to 2008 were 1.4 to 3.8 °C colder than monthly mean temperatures for December to February 2008 to 2009. Monthly mean temperatures for October and November 2007 and 2008 were fairly similar, with differences of only 0.1 and 0.3 °C. Annual mean temperature for the 2 years was 4.4 and 3.5 °C, respectively. Because Sites

1 and 2 are ~100 m higher in elevation than the meteorological site where air temperatures are measured, there is about a 0.6 °C offset in mean annual air temperatures (cooler) at Sites 1 and 2.

Ground temperatures at Site 1 for the period March 2007 to March 2009 varied between –0.84 and 11.45 °C at 22 cm depth, and between –0.21 and 8.91 °C at 72 cm depth (Figure 1-3), while at Site 2 ground temperatures varied between –2.77 and 7.72 °C at the shallowest depth (2 cm), and between 1.04 and 5.22 °C at the deepest depth (97 cm) (Figure 1-4). As expected, ground temperatures at both of these sites show less variation in minimum and maximum temperatures than air temperatures, with greater attenuation at greater depths. Additionally, ground temperatures at Site 2 show less variation than ground temperatures at Site 1. This difference is likely due to Site 2 lying within a discharge area and groundwater flow through this site further dampens the annual variation in temperatures.

At both Site 1 and Site 2, maximum ground temperatures generally occurred in July or August, lagging behind the timing of maximum air temperatures, with longer lag times occurring at deeper depths. For instance, at Site 1, the deeper thermistor at 72 cm depth reaches its maximum temperature slightly later than the thermistor at 22 cm depth (Figure 1-3); the same can be seen at Site 2 where maximum ground temperatures generally occurred in July for depths of 2, 7, and 17 cm, and in August at 47 and 97 cm depth (Figure 1-4).

Minimum ground temperatures at the shallower depths at both sites (22 cm depth at Site 1 and 2, 7, and 17 cm depth at Site 2) generally occurred in late fall, just before the onset of snow cover (Figures 1-3 and 1-4). Minimum temperatures at the deeper depths

(72 cm depth at Site 1; and 47 and 97 cm depth at Site 2) generally occurred in late spring/early summer during the annual snowmelt event. Additionally, ground temperatures at the shallower depths at both sites were warmer than temperatures at deeper depths from just after the disappearance of the snow cover through the summer months and into early fall; conversely, ground temperatures at the shallower depths were cooler than temperatures at deeper depths during the fall until just after the disappearance of the snow cover (Figures 1-3 and 1-4). Both the difference in the timing of the occurrence of minimum temperatures between the shallower and deeper depths, as well as the relative difference in temperatures between the shallower and deeper depths throughout the year shows that the shallower ground temperatures are more directly influenced by air temperatures, while the deeper ground temperatures are more directly influenced by groundwater flow.

Annual mean ground temperatures at Site 1 were up to 1.18 °C colder than annual mean air temperatures (adjusted for elevation of Site 1) for 2007 to 2008, and 1.12 °C colder than mean annual air temperatures (adjusted for elevation of Site 1) for 2008 to 2009 (Table 1-1). Similarly, annual mean ground temperatures at Site 2 were up to 1.22 °C colder than annual mean air temperatures (adjusted for elevation of Site 2) for 2007 to 2008, and 0.96 °C colder than annual mean air temperatures (adjusted for elevation of Site 2 for 2008 to 2009). These results are consistent with the 2 °C offset between mean annual air temperatures and groundwater recharge temperatures derived by *Manning and Solomon* [2003] for the Wasatch Mountains.

Groundwater temperatures at the well for the period March 2007 to March 2009 varied between 1.10 and 6.89 °C (Figure 1-5). Maximum temperatures generally occurred

in August, attenuated and lagged slightly longer than 1 month after maximum air temperatures. Minimum temperatures occurred in either May 2007 or June 2008 during the annual snow melt event. Annual mean groundwater temperatures for 2007 to 2008 and 2008 to 2009 were 3.65 °C and 2.99 °C, respectively; this is slightly warmer than annual mean ground temperatures at both Site 1 and Site 2, and 0.75 and 0.51 °C colder than the annual mean air temperature (adjusted for elevation of Site 2) for the 2 years. The warmer temperatures at the well versus ground temperatures are likely due to the well measuring deeper temperatures (about 1.2 m depth), and/or from warm water moving up from depth that is typical of discharge areas.

1.5.2 Relation of Air and Ground Temperatures to Temperature at the Water Table

Noble gas samples collected from the well at Site 2 were used to calculate groundwater recharge temperatures, which essentially record the temperature at the water table. The noble gas recharge temperatures reported in this study were calculated at the altitude of the well screen, so they represent the maximum recharge temperatures possible, as it is unlikely that the well is receiving groundwater recharge at a lower elevation than the well screen.

Groundwater recharge temperatures from noble gas samples collected between March 2007 and March 2009 ranged between 0.0 ± 1.6 °C (16 January 2008) and 7.4 ± 1.4 °C (10 February 2008), and averaged 2.9 ± 1.2 °C (Figure 1-5 and Table 1-2), consistent with ground temperatures measured within the basin. Average maximum groundwater recharge temperatures were approximately 0.3 °C warmer to 2.2 °C cooler than annual mean air temperatures (adjusted for elevation of Site 1) from 2007 to 2008,

and were 0.0 to 1.3 °C cooler than annual mean air temperatures (adjusted for elevation of Site 1) from 2008 to 2009. These differences are comparable to the 2 °C difference between groundwater recharge temperatures and mean annual air temperatures inferred by *Manning and Solomon* [2003] for the Wasatch Mountains.

Groundwater recharge temperatures calculated from noble gas samples collected between March and December 2007, appear to track the groundwater temperatures measured at the well, following an attenuated and lagged annual temperature variation. This pattern is pronounced in 2007 with a range of 7 °C between summer and winter samples. Apparent groundwater ages (Figure 1-6 and Table 1-2) from these same samples, however, varied between 0 and 7 years. This seasonal pattern in the noble gas recharge temperatures did not continue into 2008 and 2009 (Figure 1-5), with samples collected after December 2007 showing much more scatter, and no definitive seasonal trends. These data thus show general agreement between noble gas recharge temperatures and groundwater temperatures albeit with some complexity.

Apparent groundwater ages from water collected between March 2007 and March 2009 at the well ranged between 0.0 ± 0.5 years and 7.8 ± 0.4 years (Figure 1-6 and Table 1-2). From March through December 2007, the apparent ages followed a seasonal pattern, with winter samples being 2 to almost 7 years older than late spring/early summer samples. This seasonal age variation points to possible variations in the groundwater flow regime throughout 2007. During times when there is little to no groundwater recharge (i.e., fall/winter) the well is capturing older groundwater. During high recharge times of the year (i.e., the annual snowmelt event during late spring/early summer) these older flow paths are pushed deeper within the aquifer, and are no longer

being captured by the well; the well is capturing flow paths carrying younger water instead. It does not take much change in the depth of the flow paths to change which paths are being captured by the well; in fact, changes in depth as little as 20 cm may produce the seasonal pattern seen in the apparent age data in 2007. Like the noble gas recharge temperatures, the seasonal pattern in apparent age data did not continue into 2008 and 2009. The high scatter in apparent ages and noble gas recharge temperatures suggests that the groundwater flow regime within the Brighton Basin is quite complex, and warrants further study to explain the scatter within the data.

Because the apparent age data suggest groundwater ranging up to 7.8 years, the air temperatures from 2000 to 2007 were also examined to determine differences between groundwater recharge temperatures and air temperatures for these older age samples. Annual mean air temperatures from 2000 to 2007 ranged between 2.9 °C (2002 and 2004) and 4.6 °C (2007), and averaged 3.5 °C (data accessed from SNOTEL website at *http://www.wcc.nrcs.usda.gov/nwcc/site?sitenum=366&state=ut*). Mean maximum groundwater recharge temperatures for the groundwater samples that show ages of being recharged before March 2007 were approximately 0.0 ± 1.2 °C to 1.1 ± 1.2 °C cooler than mean annual air temperatures from 2000 to 2007. Again, this is comparable to, to slightly less than, the 2 °C difference between groundwater recharge temperatures and mean annual air temperatures inferred by *Manning and Solomon* [2003] for the Wasatch Mountains.

1.5.3 Snow Effects

Comparison of changes in monthly mean ground and groundwater temperatures versus changes in monthly mean air temperatures over the 2 year study period illustrate

the effects of snow cover on the ground temperatures within the basin. For example, monthly mean ground and groundwater temperatures for March through May 2007 are comparable to monthly means for March to May 2008 (differences of only 0.00 to 0.36 °C), despite monthly mean air temperatures for March through May 2007 being approximately 3.3 to 4.3 °C warmer than March through May 2008 (Table 1-1). This consistency in ground temperatures is likely due to snow cover insulating the ground from the air temperatures during these times of both years (Figures 1-3 through 1-5). Monthly mean ground and groundwater temperatures for June 2007 were 0.79 to 4.49 °C warmer than monthly mean temperatures for June 2008 (Table 1-1); monthly mean air temperatures for June 2007 also were 3.2 °C warmer than June 2008. The cooler ground temperatures in June 2008 may be attributed to the fact that (1) snow cover persisted one month longer in 2008 than in 2007 (Figures 1-3 through 1-5), resulting in insulating the ground from the warmer air temperatures for a longer period of time in 2008; and/or (2) air temperatures in June 2008 were cooler than air temperatures in 2007. While monthly mean air temperatures from July through September 2007 are only 0.5 to 1.1 °C warmer than July through September 2008, monthly mean ground and groundwater temperatures from July through September 2007 are 0.85 to 4.22 °C warmer than July through September 2008, with the largest differences occurring in July (Table 1-1). Again, this difference may be partly attributed to the snow cover in 2008 persisting longer in the spring and summer months, thereby preventing the ground from warming as much as in 2007 (Figures 1-3 through 1-5). Finally, monthly mean shallow ground temperatures for November to December 2007 are 0.13 to 0.83 °C colder than monthly mean ground temperatures for November to December 2008 (Table 1-1). This is likely due to the later

onset of snow in 2007 than 2008; in 2008, the onset of snow occurred nearly a month earlier than in 2007, thereby insulating the ground from the colder air temperatures for a longer period of time (Figures 1-3 through 1-5).

The snow effects on mean annual ground temperatures were quantified using a numerical model of snow-ground thermal interactions developed by *Bartlett et al.* [2004, 2005]. *Bartlett et al.* [2004] found that snow onset time and duration were the two greatest controlling factors in determining whether the mean annual ground temperature is warmer or cooler than the mean annual air temperature. This temperature difference, called the ''snow effect'' [*Bartlett et al.*, 2004], is plotted in terms of the controlling factors in Figure 1-7 for Brighton Basin, Utah. A snow season can either raise or lower the mean annual ground temperature relative to the air over an annual cycle. Warming of the mean annual ground temperature relative to air occurs when snow onset coincides roughly with the daily mean air temperature falling below 0 °C, and lasting until daily mean air temperatures rise above the freezing point. During this time the ground is insulated by snow from the cold winter temperatures. Depending on the annual surface air temperature (SAT) cycle, this warming can be 2 °C or greater. Alternatively, cooling of the mean annual ground temperature relative to air occurs when the snow onset is late and the duration is long, meaning that snow keeps the ground temperature pinned near 0 °C, long after the daily mean temperature has risen above freezing.

The *Bartlett et al.* [2004] snow model uses inputs of both the annual and diurnal temperature cycles, as well as the diffusivity of the snow pack; however, the model assumes that the thermal properties (diffusivity) of the snow are homogenous and constant in both space and time. In actuality, the snowpack undergoes compaction due to

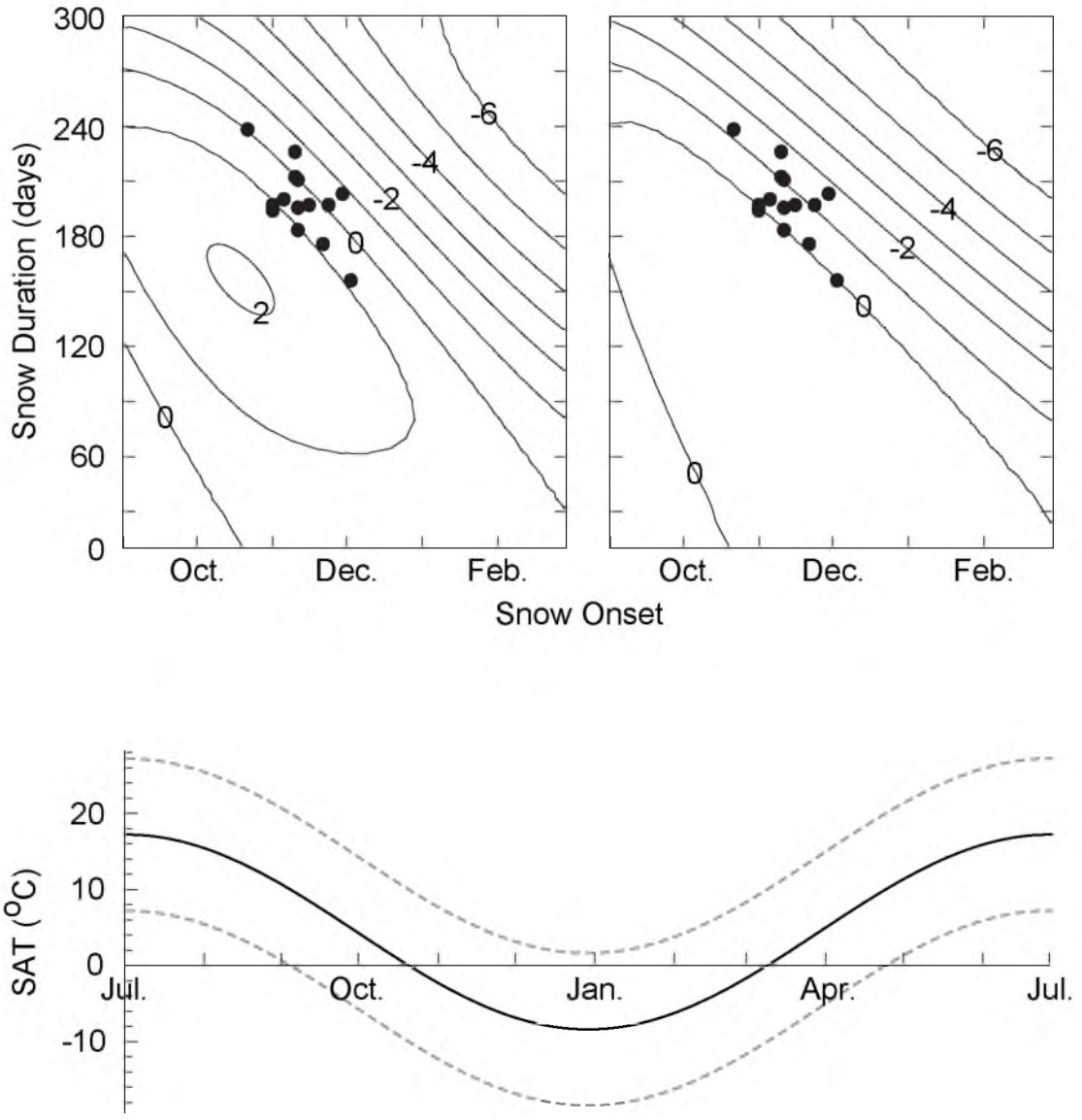

Figure 1-7. The snow effect—influence of snow event onset time and duration on mean annual surface ground temperatures relative to mean annual air temperatures. Contours illustrate the difference in °C between the mean annual surface ground temperature and the driving function (labeled SAT above). The top left panel shows results using an "air-filled" snow thermal diffusivity of 2x10-8 m2/s; the top right panel shows results using an "ice-like" snow thermal diffusivity of 1x10-6 m2/s. The points represent snow onset and duration of annual snow events observed at the Brighton SNOTEL meteorological station from 1997 to 2011.The bottom panel shows the annual driving function (solid line) and the limits of the diurnal fluctuations (dashed lines). Modified from: *Masbruch et al.* [2012].

melting and refreezing, which effectively changes the density and thermal properties of the snow as a function of time [*Bartlett et al.*, 2004]. Therefore, in order to capture the end members of the evolving snowpack and provide a constraint on the snow effect within the Brighton Basin, two simulations of the snow model were run: one with a thermal diffusivity of 2×10^{-8} m^2 s^{-1} which represents a ''fluffy, air-filled'' snow, and one with a thermal diffusivity of 1×10^{-6} m^2 s^{-1} which is representative of a more ''icelike'' snow.

Results from the snow model simulations are shown in Figure 1-7. Figure 1-7 (top left) shows model results for the thermal diffusivity of air-filled snow, and the top right panel shows the model results for the thermal diffusivity of more ice-like snow. Solid dots on Figure 1-7 indicate the onset time and duration for all annual snow events between 1997 and 2011 at the Brighton SNOTEL meteorological station, and indicate that the snow effect at Brighton is between +1.0 °C and –2.0 °C, with a mean snow effect of –1.0 °C. This cooling is consistent with the measured ground, groundwater, and groundwater recharge temperatures within the basin.

1.6 Summary and Conclusions

Although this study did not set out to evaluate noble gas thermometry comprehensively, it does provide details of the thermal regime of both groundwater recharge and discharge areas in an alpine setting. The thermal effects of snow cover in this setting are also studied. Using noble gas temperatures collected from groundwater samples within a discharge area that originates from a highly constrained recharge area, it is concluded that the noble gas recharge temperatures are consistent with surface ground temperatures within the probable recharge area, and that surface ground temperatures are

cooler than mean annual air temperatures.

To determine why groundwater recharge temperatures within the Wasatch Mountains are cooler than mean annual air temperatures, this study investigates the relation between air, ground, and groundwater recharge temperatures within the Brighton Basin, a high alpine basin located within the Wasatch Mountains. Hydrogeologic considerations of this site provide a tight constraint on the location and elevation of recharge areas. A pre-existing meteorological station from the SNOTEL network provided measurements of air temperatures and snow depth. Ground temperature probes were installed in both a local recharge and a local discharge area within the basin to determine the relation between air and shallow ground temperatures at these sites. Additionally, a well was installed in the discharge area that allowed for sampling of noble gases and tritium used to determine groundwater recharge temperature and age. Detailed monitoring over a 2 year period allowed identification of possible seasonal and annual signals in groundwater recharge temperatures and ages. Based on this monitoring, the following conclusions can be drawn:

1. Maximum noble gas groundwater recharge temperatures computed using the CE model from 25 samples collected from March 2007 to March 2009 in the Brighton Basin, Utah, at an elevation of approximately 2,770 m, average 2.9 ± 1.2 °C. This average is within the experimental error of the mean ground temperature of 2.28 °C measured in the probable recharge area over the same time period.
2. The variation in noble gas recharge temperatures is from 0 to 7 °C. This range is also comparable to ground temperature variations in the region throughout the annual cycle. In the first year of monitoring, the noble gas temperatures appear to

follow an attenuated and lagged annual temperature variation similar to the ground temperatures, although the pattern is not replicated in the second year. Because apparent groundwater ages in the collected samples vary from 0 to 7 years, the groundwater flow pattern within the basin is likely complex and warrants further study.

3. Mean ground temperature in the upper 1 m of soil at measurement Sites 1 and 2 over the 2 year time period is 2.32 °C. The ground temperature is 1.05 °C colder than the mean SAT (adjusted for elevation of Sites 1 and 2) of 3.37 °C over the same period. This offset contradicts the trend of surface temperature variation with elevation (lapse rate) in central Utah, whereby ground temperatures are warmer than air temperatures; the offset, however, is explained by a snow effect where late spring and early summer snow cover cools the ground relative to air. Interpretation of groundwater recharge temperatures derived from noble gases, therefore, must be attentive to local ground temperature effects in the probable recharge zones.

These conclusions indicate that in a snow dominated, high alpine area, such as the Brighton Basin, ground temperatures are cooler than air temperatures. The noble gas recharge data corroborate this fact, and the results are consistent with the 2 °C difference between groundwater recharge temperatures and mean annual air temperatures inferred by *Manning and Solomon* [2003] for the Wasatch Mountains. This observation implies that in high alpine areas, the assumption that $T_r = T_a$ may not be valid. It appears that by utilizing noble gas recharge data from discharge points within the mountain block, a more appropriate T_r lapse curve can be derived for the area in question, thereby permitting a

more correct interpretation of recharge altitude and, therefore, sources of recharge to the groundwater system.

1.7 Acknowledgments

We would like to thank Paul Gettings, Tom Marston, Derrick Hasterok, and Angie Vincent for help in the set up and installation of the ground temperature probes and the well. Thanks also go to Marshall Bartlett for the use and running of simulations of his snow model, and to Alan Rigby for help with laboratory analysis of the noble gas samples.

1.8 References

Aeschbach-Hertig, W., F. Peeters, U. Beyerle, and R. Kipfer (1999), Interpretation of dissolved atmospheric noble gases in natural waters, *Water Resour. Res.*, *35*, 2779–2792.

Aeschbach-Hertig, W., F. Peeters, U. Beyerle, and R. Kipfer (2000), Paleotemperature reconstruction from noble gases in ground water taking into account equilibration with entrapped air, *Nature*, *405*, 1040–1044.

Aeschbach-Hertig, W., M. Stute, J. F. Clark, R. F. Reuter, and P. Schlosser (2002), A paleotemperature record derived from dissolved noble gases in groundwater of the Aquia Aquifer (Maryland, USA), *Geochim. Cosmochim. Acta*, *66*, 797–817.

Anderson, M. P. (2005), Heat as a groundwater tracer, *Ground Water*, *43*, 951–968.

Anderson, T. W., and G. W. Freethey (1996), Simulation of groundwater flow in alluvial basins in south-central Arizona and parts of adjacent states, *US Geol. Surv. Prof. Pap. 1406-D*, 78 pp.

Andrews, J. N., and D. J. Lee (1979), Inert gases in groundwater from the Bunter Sandstone of England as indicators of age and paleoclimatic trends, *J. Hydrol.*, *41*, 233–252.

Ballentine, C. J., and C. M. Hall (1999), Determining paleotemperatures and other variables by using an error-weighted, nonlinear inversion of noble gas concentrations in water, *Geochim. Cosmochim. Acta*, *63*, 2315–2336.

Bartlett, M. G., D. S. Chapman, and R. N. Harris (2004), Snow and the ground temperature record of climate change, *J. Geophys. Res.*, *109*, F04008, doi:10.1029/2004JF000224.

Bartlett, M. G., D. S. Chapman, and R. N. Harris (2005), Snow effect on North American ground temperatures, 1950–2002, *J. Geophys. Res.*, *110*, F03008, doi:10.1029/2005JF000293.

Buttle, J. M. (1989), Soil moisture and groundwater responses to snowmelt on a drumlin sideslope, *J. Hydrol.*, *105*, 335–355.

Cey, B. D. (2009), On the accuracy of noble gas recharge temperatures as a paleoclimate proxy, *J. Geophys. Res.*, *114*, D04107, doi:10.1029/ 2008JD010438.

Domenico, P. A., and F. W. Schwartz (1998), *Physical and Chemical Hydrology*, John Wiley and Sons, New York.

Gates, J. S. (1995), Description and quantification of the groundwater basins of the Wasatch Front, Utah, 1904–1994, in *Environmental and Engineering Geology of the Wasatch Front Region, Utah, Utah Geol. Surv. Publ.*, vol. 24, edited by W. R. Lund, Utah Geological Society, Salt Lake City, Utah, 221–248.

Hall, C. M., M. C. Castro, K. C. Lohmann, and L. Ma (2005), Noble gas and stable isotopes in a shallow aquifer in southern Michigan: Implications for noble gas paleotemperature reconstructions for cool climates, *Geophys. Res. Lett.*, *32*, L18404, doi:10.1029/2005GL023582.

Hill, B. R. (1990), Groundwater discharge to a headwater valley, northwestern Nevada, USA, *J. Hydrol.*, *113*, 265–283.

Kipfer, R., W. Aeschbach-Hertig, F. Peeters, and M. Stute (2002), Noble gases in lakes and ground waters, in *Noble Gases in Geochemistry and Cosmochemistry, Rev. Mineral. Geochem.*, vol. 47, edited by D. Porcelli, C. Ballentine, and R. Wieler, 615–700.

Klump, S., M. S. Brennwald, and R. Kipfer (2006), Comment on ''Noble gas and stable isotopes in a shallow aquifer in southern Michigan: Implications for noble gas paleotemperature reconstructions for cool climates'' by Chris M. Hall et al., *Geophys. Res. Lett.*, *33*, L24403, doi:10.1029/2006GL027496.

Lipmann, J., M. Stute, T. Torgersen, D. P. Moser, J. A. Hall, L. Lin, M. Borcsik, R. E. S. Bellamy, and T. C. Onstott (2003), Dating ultra-deep mine waters with noble gases and 36Cl, Witwatersrand Basin, South Africa, *Geochim. Cosmochim. Acta*, *67*, 4597–4619.

Manning, A. H., and J. S. Caine (2007), Groundwater noble gas, age, and temperature signatures in an Alpine watershed: Valuable tools in conceptual model development, *Water Resour. Res.*, *43*, W04404, doi :10.1029/2006WR005349.

Manning, A. H., and D. K. Solomon (2003), Using noble gases to investigate mountain-front recharge, *J. Hydrol.*, *275*, 194–207.

Masbruch, M.D., D.S. Chapman, and D.K. Solomon (2012), Air, ground, and groundwater recharge temperatures in an alpine setting, Brighton Basin, Utah, *Water Resour. Res.*, *48*, W10530, doi:10.1029/2012WR012100.

Mason, J. L. (1998), Ground-water hydrology and simulated effects of development in the Milford area, an arid basin in southwestern Utah, *US Geol. Surv. Prof. Pap. 1409-G*, 69 pp.

Mazor, E. (1991), *Applied Chemical and Isotopic Groundwater Hydrology*, Halsted Press, New York.

Mercury, L., D. L. Pinti, and H. Zeyen (2004), The effect of the negative pressure of capillary water on atmospheric noble gas solubility in ground water and paleotemperature reconstruction, *Earth Planet. Sci. Lett.*, *223*, 147–161.

Powell, W. G., D. S. Chapman, N. Balling, and A. E. Beck (1988), Continental heat-flow density, in *Handbook of.Terrestrial Heat-Flow Density Determination With Guidelines and Recommendations of.the International Heat Flow Commission*, edited by R. Haenel, L. Rybach, and L. Stegena, Kluwer Acad., Boston, Mass., 167–222.

Prudic, D. E., and M. E. Herman (1996), Ground-water flow and simulated effects of development in Paradise Valley, a basin tributary to the Humboldt River in Humboldt County, Nevada, *US Geol. Surv. Prof. Pap. 1409-F*, 92 pp.

Putnam, S. N., and D. S. Chapman (1996), A geothermal climate change observatory: First year results from Emigrant Pass in northwest Utah, *J. Geophys. Res.*, *101*, 21, 877–21, 890.

Rauber, D., H. H. Loosli, H. Schmassmann, and J. N. Andrew (1991), Noble gases in groundwater, in *Applied Isotope Hydrology: A Case Study in Northern Switzerland*, edited by, F. J. Pearson, Jr., et al., Elsevier, Amsterdam, 116–152.

Sanford, W. E., R. G. Shropshire, and D. K. Solomon (1996), Dissolved gas tracers in groundwater: Simplified injection, sampling, and analysis, *Water Resour. Res.*, *32*, 1635–1642.

Smith, G. D., F. Newhall, L. H. Robinson, and D. Swanson (1964), Soil temperature regimes: Their characteristics and predictability, *US Soil Conserv. Serv. Rep., SCS-TP-144*.

Solomon, D. K., and P. G. Cook (2000), ^{3}H and ^{3}He, in *Environmental Tracers in Subsurface Hydrology*, edited by P. G. Cook and A. L. Herczeg, Kluwer Acad., Boston, Mass., 233–260.

Stokes, W. L. (1986), Geology of Utah, *Occas. Pap., 6*, Utah Museum Nat. History, Salt Lake City, Utah.

Stute, M., M. Forster, H. Frischkorn, A. Serejo, J. F. Clark, P. Schlosser, W. S. Broecker, and G. Bonani (1995), Cooling of tropical Brazil (5 °C) during the Last Glacial Maximum, *Science*, *269*, 379–383.

Stute, M., and P. Schlosser (1993), Principles and applications of the noble gas paleothermometer, in *Climate Change in Continental Isotopic Records, Geophys. Monogr. Ser.*, vol. 78, edited by P. K. Swart et al., AGU, Washington, D.C., 89–100.

Sun, T., C. M. Hall, M. C. Castro, K. C. Lohmann, and P. Goblet (2008), Excess air in the noble gas groundwater paleothermometer: A new model based on diffusion in the gas phase, *Geophys. Res. Lett.*, *35*, L19401, doi:10.1029/2008GL035018.

Zuber, A., S. M. Weise, K. Osenbruck, J. Grabczak, and W. Ciezkowski (1995), Age and recharge area of thermal waters in Ladek Spa (Sudeten, Poland) deduced from environmental isotope and noble gas data, *J. Hydrol.*, *167*, 237–349.

CHAPTER 2

USING GROUNDWATER TEMPERATURES TO CONSTRAIN RECHARGE RATES IN ARID INTERMONTANE BASINS

2.1 Abstract

Two-dimensional numerical modeling of the combined processes of fluid flow and heat transport are used to quantify the effects of groundwater flow on the subsurface thermal regime and determine the lower limit of recharge rate that will produce an observable perturbation such that groundwater temperatures can be used to constrain recharge rates. Simulations were executed for a vertical section through a basin with a geometry and moderate to high permeabilities representative of aquifers within the Great Basin. Groundwater recharge rates were varied between 1 and 100 mm yr^{-1}. For all recharge rates and bedrock permeabilities, the greatest temperature perturbations (up to greater than 60 °C) occur in the deepest portion of the recharge area. At lower recharge rates (10 mm yr^{-1} or less), the hydrologic disturbance to the subsurface thermal regime is almost completely dependent on the recharge rate. At recharge rates higher than this, the hydrologic disturbance is dependent on both the recharge rate and the permeability. Bedrock permeabilities appear to control the distance to which the temperature perturbation will extend from the recharge area. At recharge rates of 50 mm yr^{-1} and above, the plume of colder water extends past the recharge area and persists throughout

and under the basin-fill deposits towards the discharge area, at fairly shallow depths. This plume of cooler water could be easily measured and used to constrain recharge rates to the system as a whole. The lower limit of recharge rates needed to produce a thermal perturbation large enough such that groundwater temperatures can be used to constrain recharge rates, therefore, is about 50 mm yr^{-1}.

2.2 Introduction

One of the most difficult hydrologic budget components to determine is groundwater recharge from the infiltration of precipitation, especially in mountainous terrain where hydrologic data may be sparse due to the scarcity of wells. In the Great Basin in the western U.S., groundwater recharge from the infiltration of precipitation primarily occurs in the mountain blocks and is the main source of groundwater to both the mountain-block and adjacent basin aquifers. In recent years, groundwater development within the Great Basin targeting permeable consolidated rock aquifers beneath the basin-fill deposits and in the surrounding mountains has increased [*Masbruch et al.*, 2011]. Accurate estimates of groundwater recharge to these aquifers, therefore, are essential for water resources planning.

Early groundwater studies in the Great Basin, beginning with *Maxey and Eakin* [1949] generally focused on the basin-fill (valley) aquifers, and recharge estimates were calibrated to groundwater discharge in the basin-fill aquifer. These earlier methods did not consider groundwater discharge within the mountain block or recharge to underlying consolidated rock aquifers and, therefore, only considered "net" recharge to the unconsolidated basin-fill aquifer [*Masbruch et al.*, 2011]. More recently, a new class of spatially distributed recharge estimation techniques based on water-balance methods has

been developed for the Great Basin [*Flint and Flint*, 2007a; 2007b; *Flint et al.*, 2011; *Hevesi et al.*, 2003; *Leavesley et al.*, 1983; *Markstrom et al.*, 2008]. These techniques take into account all groundwater recharge and discharge processes within the mountain block and subsequent recharge of a portion of infiltration of runoff to the basin-fill aquifer and, therefore, provide estimates for "total" recharge from precipitation. Uncertainties in these estimates, however, may be as high as ± 50 percent [*Flint et al.*, 2011]. Because of this high uncertainty, finding other methods of constraining groundwater recharge estimates from precipitation is of importance to hydrologic studies within the Great Basin.

Manning and Solomon [2005] showed that groundwater temperatures measured within the Salt Lake Valley, located along the eastern margin of the Great Basin, could be used to constrain recharge rates, as well as subsurface mountain-block to basin-fill groundwater flow. Groundwater temperatures collected from over 50 wells within the Salt Lake basin-fill aquifer showed a cold-water plume extending from the adjacent Wasatch Mountains, which is the recharge area for groundwater in the Salt Lake Valley. *Manning and Solomon* [2005] were able to constrain the absolute magnitude of subsurface inflow of mountain-block groundwater into the basin-fill aquifer, and ultimately groundwater recharge, by using groundwater temperature and age data collected from the basin-fill aquifer in conjunction with a three-dimensional finite element flow and transport model. Results from *Manning and Solomon* [2005] showed that groundwater age data could be used to constrain the lower end of recharge, while groundwater temperature data could be used to constrain the higher end of recharge.

This study focuses on whether the approach used by *Manning and Solomon*

[2005] could be applied to other drier/warmer climatic settings within the Great Basin. A "generic" coupled groundwater flow/thermal model was constructed using hydrologic and thermal characteristics that are typically found in the southern Great Basin, which is a much drier and warmer environment compared to the Salt Lake Valley. This model was used to investigate the relative magnitude of thermal perturbations caused by groundwater flow that may occur within a warmer/drier climate, and to determine recharge rates needed to produce a significant thermal perturbation such that groundwater temperatures might be used to determine or constrain recharge rates.

Previous studies such as *Smith and Chapman* [1983] and *Forster and Smith* [1988; 1989] have used similar modeling techniques to determine the effects of groundwater flow on the subsurface thermal regime by varying parameters such as permeability, anisotropy, water table topography or position, aquifer geometry and properties, and regional heat flow. *Smith and Chapman* [1983] used fully saturated models and specified the position and geometry of the water table; *Forster and Smith* [1988; 1989] included the unsaturated zone, and used infiltration of recharge with a free surface method to let the water table position and geometry vary. *Forster and Smith* [1989] examined the effects of lowering recharge, and concluded that in systems with a deep water table (greater than 50 m) the rate of groundwater recharge best characterizes the potential for an advective disturbance of the subsurface thermal regime. The current study takes this concept one step further in quantifying the lower limit of the amount of recharge needed to produce a significant thermal perturbation such that groundwater temperatures can be used to constrain recharge rates.

2.3 Conceptual Model of Groundwater Flow/Thermal Regime in the Great Basin

The Great Basin is a region of internal drainage in the western United States that covers much of Nevada, western Utah, and parts of California, Oregon, Idaho, and Arizona (Figure 2-1). It is bounded on the east by the Wasatch Range and the Colorado Plateau and on the west by the Sierra Nevada Range. The dominant topography of the area consists of north-south trending valleys and adjacent mountain ranges characteristic of the Basin and Range province.

Groundwater within the Great Basin primarily occurs in basin-fill aquifers composed of unconsolidated deposits that occupy the intermontane valleys, and permeable bedrock aquifers which exist at depth beneath the basin-fill aquifers and are exposed at the surface in the intervening mountain ranges. The bedrock aquifers are predominantly part of a large, regionally extensive set of Paleozoic and early Mesozoic carbonate rocks that underlie most of eastern Nevada, western Utah, and parts of southeastern California and southern Idaho and make up what is known as the carbonate-rock aquifer system [*Prudic et al.*, 1995].

Figure 2-2 shows a conceptualized groundwater flow system between a mountain-block aquifer and an adjacent basin-fill aquifer that is characteristic of the Basin and Range province of the western United States. Groundwater recharge occurs mainly in the mountain blocks and upland areas from precipitation. Natural groundwater discharge occurs to evapotranspiration, springs, and streams/lakes/reservoirs. Because of the connectivity of the underlying consolidated bedrock aquifers, some basins may also receive recharge as subsurface inflow from upgradient basins, or discharge groundwater

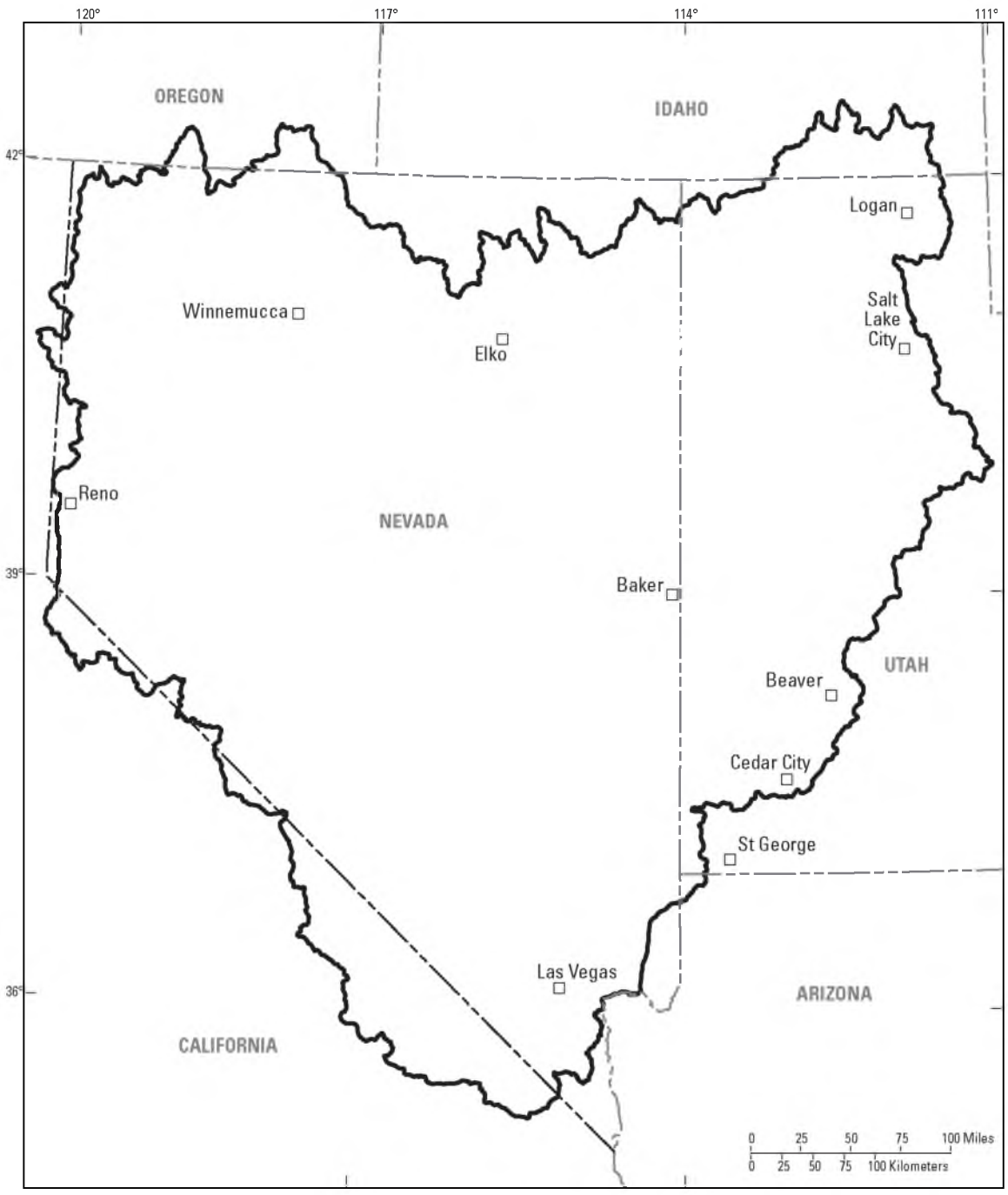

Figure 2-1. Location of the Great Basin, western United States. State boundary data from: *U.S. Census Bureau* [2000].

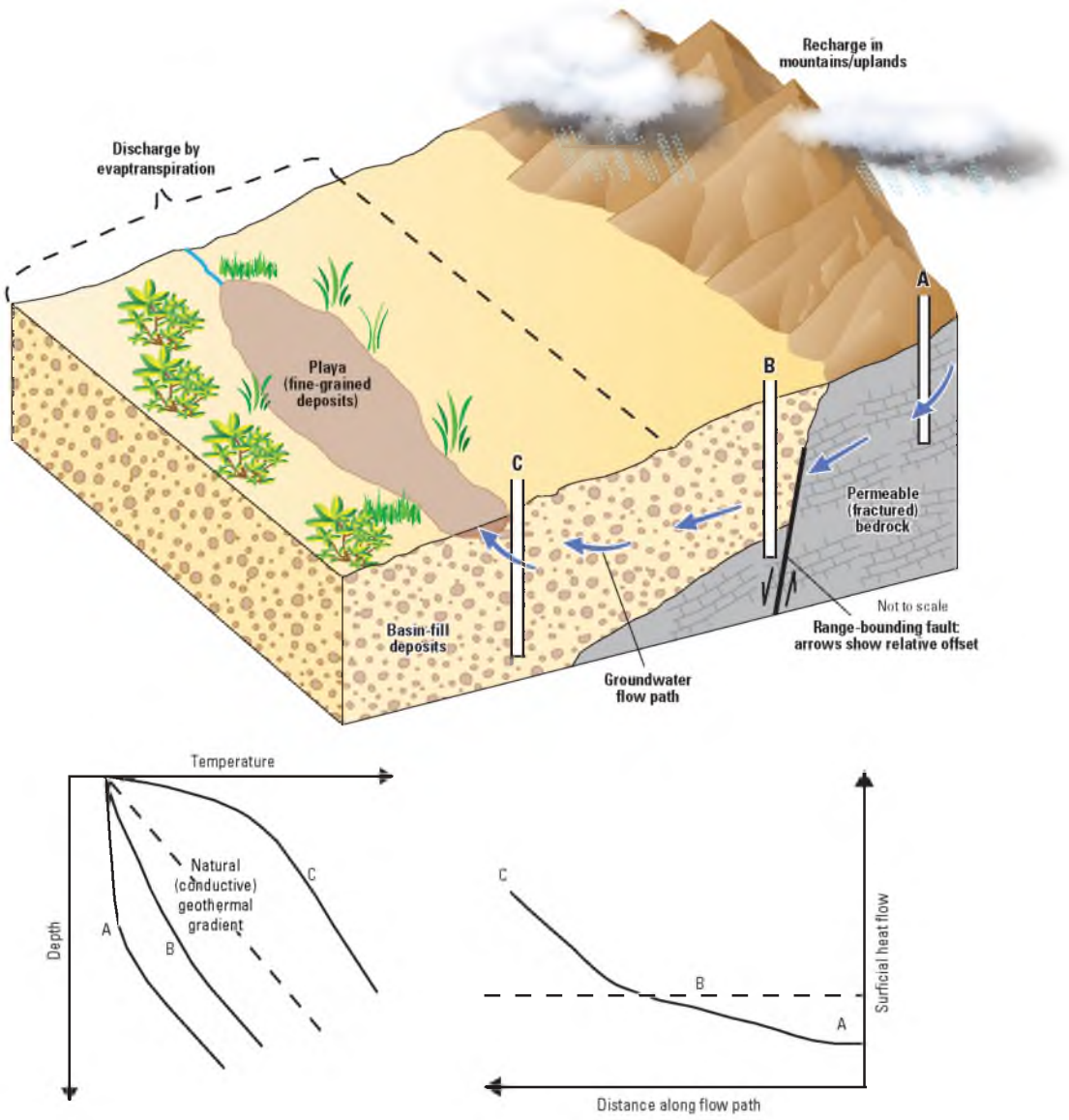

Figure 2-2. Conceptual diagram showing groundwater flow typical of the Great Basin, and how geothermal gradients and surface heat flow may be affected by groundwater flow. Letters in bottom figures correspond to wells A, B, and C in top figure. Also shown are the conductive geothermal gradient and surface heat flow (dashed lines) that would exist if no groundwater flow was occurring. Top panel modified from: *Masbruch et al.* [2011].

through subsurface outflow to downgradient basins. In most basins, however, the range crest and the evapotranspiration/playa or basin-fill stream are considered to be groundwater divides.

It has long been recognized that advective transport of heat by groundwater in the shallow subsurface poses the greatest obstacle in determining heat flow at depth from surface observations [*Lachenbruch and Sass*, 1977]. If groundwater flows are large enough, they will redistribute heat within the subsurface, and alter the natural conductive geotherm (temperature vs. depth) of the area. Figure 2-2 shows a conceptualization of how groundwater flow may redistribute heat. In areas of groundwater recharge, temperatures tend to be lower and will depress the natural conductive geotherm as cold water enters the subsurface. This produces an area of lower than expected heat flow at the surface. Correspondingly, in areas of discharge, groundwater discharge will raise the natural conductive geotherm as warm water at depth is brought to the surface. Changes in the geothermal gradient and distribution of surface heat flow, as well as the associated groundwater temperatures, can be used to assess the magnitude of groundwater flow in an area. Numerous past studies have demonstrated the influence of fluid flow on the subsurface temperature distribution [*Bredehoeft and Papadopulos*, 1965; *Cartwright*, 1971; *Domenico and Palciauskas*, 1973; *Donaldson*, 1962; *Forster and Smith*, 1989; *Parsons*, 1970; *Smith and Chapman*, 1983; *Stallman*, 1963, 1965], and utilized this dependence as an aid in delineating the flow field [*Bredehoeft and Papadopulos*, 1965; *Cartwright*, 1970; *Keys and Brown*, 1978; *Manning and Solomon*, 2005; *Salem et al.*, 2004; *Sorey*, 1971].

Climatically and hydrogeologically, the Salt Lake basin represents a much

cooler/wetter environment compared to areas within the southern Great Basin. Recharge rates within the southern Great Basin are one to three orders of magnitude lower than recharge rates within the Salt Lake basin, and generally range between 0.05 and 34 mm yr^{-1}, with an average rate of 7 mm yr^{-1} [*Masbruch et al.*, 2011]. Average annual air temperatures within the southern Great Basin valleys are about 15 °C, which is 3 °C warmer than those in the Salt Lake Valley (based on 18-yr average daily temperatures from Daymet data from Daymet web page, *http://www.daymet.org,* accessed on September 20, 2010). The atmospheric lapse rate, calculated using historical data from 36 meteorological stations located within the southern Great Basin (data from Western Regional Climate Center web page, *http://www.wrcc.dri.edu*, accessed on September 20, 2010) is -8.0 °C km^{-1}. The main groundwater discharge mechanism is evapotranspiration.

2.4 Modeling Approach

Groundwater flow and energy (thermal) transport were modeled using the U.S. Geological Survey code, SUTRA [*Voss and Provost*, 2002]. SUTRA is a two-dimensional/three-dimensional, finite-element/finite-difference, saturated/unsaturated code that simulates both flow and either solute transport or thermal energy transport in porous media. A beta version of SUTRA that includes drains [*A. Provost, U.S. Geological Survey, written commun.*, August 9, 2007] was used to allow for the simulation of evapotranspiration as a head-dependent process. A two-dimensional, cross-sectional model based on a topographic basin typical of the Basin and Range was developed and executed using the pre- and postprocessor graphical user interface, Argus ONE (Argus Holdings, Ltd.).

2.4.1 Mesh Design

The two-dimensional, cross-sectional mesh (Figure 2-3) was generated using the FishNet mesh (deformable grid of quadrilaterals) option in SUTRA. The mesh was constructed using six superblocks to account for changes in slope as one moves from the valley to the mountain block. The mesh is 25 km long, and the top surface (land surface) ranges in elevation from 1,000 m to 2,700 m. Each superblock was divided into 20 elements in the z-direction, while the number of elements in the x-direction for each superblock was chosen so that the elements were ~250 m long (Figure 2-3). The mesh is 1 m thick in the y-direction. The modeled topographic basin was assumed to be symmetrical; only half of the basin, therefore, was modeled.

2.4.2 Boundary Conditions

The bottom and sides of the model domain are no-flow boundaries with respect to groundwater flow. The top boundary is a mix of a specified-flux boundary, allowing for recharge over the mountain block, and a head-dependent flux boundary, allowing for discharge in the valley through evapotranspiration (Figure 2-3).

With respect to thermal energy, the sides of the model domain are no-flux boundaries as heat flow is assumed to parallel these boundaries. The bottom boundary is a specified-flux boundary to allow basal heat flow to enter the model, while the top boundary is a specified-temperature boundary. Temperatures along the top boundary range between 15 °C on the left hand side of the model to 1.4 °C on the right hand side of the model, and are defined on the basis of elevation using an atmospheric lapse rate of -8 °C km^{-1} with a valley reference temperature of 15 °C. The temperature of the recharging water was assumed to equal the temperatures of the top boundary of the model where the

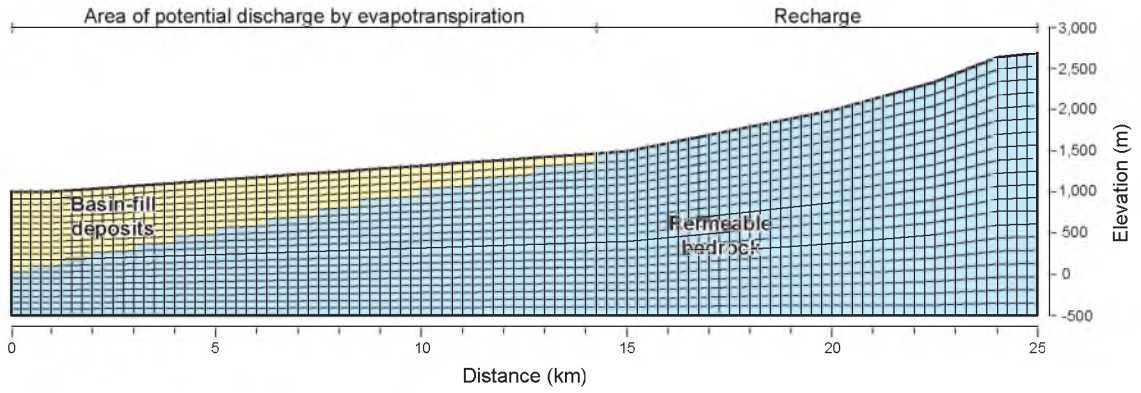

Figure 2-3. Two-dimensional model grid used for simulations.

recharge is being applied.

2.4.3 Model Parameters

Model parameters of bedrock permeability, basal heat flux, thermal conductivity of solids, and recharge rates were varied throughout the modeling process to investigate the sensitivity of groundwater thermal perturbations to each of these parameters. Table 2-1 lists these and other model parameters, the range over which the parameters were varied, and the references used to define these parameters. The ranges of the parameters are considered typical of those of groundwater aquifers in the Great Basin.

2.5 Model Results and Discussion

Initial sensitivity analyses showed that the two parameters that had the greatest effect in producing a hydrologic disturbance to the conductive thermal regime were recharge rate and bedrock permeability. This is highly similar to hydrologic studies that have determined that the position of the water table is either topographically controlled or recharge controlled [*Haitjema and Mitchell-Bruker*, 2005; *Gleeson and Manning*, 2008], especially in mountainous terrain. The thermal parameters of basal heat flux and thermal conductivity of aquifer solids, while affecting the absolute temperatures, had little effect on changing temperatures relative to the conductive case. Thermal parameters were only important in simulations with very low recharge rates (less than 5 mm yr^{-1}) compared to effects produced by greater groundwater flow due to recharge rates higher than this. It is likely that at lower permeabilities than were investigated in this study, thermal parameters would also have a larger effect [*Smith and Chapman*, 1983]. This study, however, was focused on determining the hydrologic disturbance of the thermal regime

Table 2-1. Parameter values used for fluid and thermal properties.

Model parameter	Parameter values	Source
Permeability of bedrock[1]	10^{-13}–10^{-11} m^2	*Belcher et al.* [2001, 2002]; *San Juan et al.* [2004]
Permeability of basin-fill deposits[2]	1.7×10^{-12} m^2	*Belcher et al.* [2001, 2002]; *San Juan et al.* [2004]
Porosity of bedrock[1]	0.05	*Harrill and Prudic* [1998]
Porosity of basin-fill deposits[2]	0.3	*Domenico and Schwartz* [1990]
Thermal conductivity of aquifer solids[1]	2–4W m^{-1} K^{-1}	*Langevin et al.* [2008]
Thermal conductivity of fluid[2]	0.6 W m^{-1} K^{-1}	*Langevin et al.* [2008]
Reference density of fluid[2]	1,000 kg m^{-3}	*Domenico and Schwartz* [1990]
Specific heat of fluid[2]	4,186 J kg^{-1} K^{-1}	*Smith and Chapman* [1983]
Basal heat flux[1]	60–100 mW m^{-2}	*Sass et al.* [2005]

[1]Varied through range for sensitivity analyses

[2]Held constant for all simulations

in aquifers within the Great Basin, which generally have moderate to high permeability.

The discussion below focuses on how the recharge rate and bedrock permeability influence the hydrologic disturbance to conductive heat flow. Thermal parameter values used in the following simulations were 80 mW m^{-2} for the basal heat flux (middle of the range typical for the Basin and Range [*Sass et al.*, 2005]), and 3 W m^{-1} K^{-1} for the thermal conductivity of the aquifer solids (middle of the range typical for thermal conductivity of rocks [*Langevin et al.*, 2008]).

2.5.1 Purely Conductive Case

Figure 2-4 shows the simulated surface heat flow and temperature distribution for the purely conductive case in the absence of groundwater flow. Surface heat flow across the top boundary of the model was computed using temperatures at the top two nodes of the model grid, and is the same as the basal heat flux (80 mW m^{-2}). Due to the topography and application of the lapse rate temperatures across the top boundary of the model, the simulated temperature contours are subparallel to the ground surface. Temperatures in this simulation range between 1.4 °C and 84.6 °C.

2.5.2 Influence of Bedrock Permeability and Recharge Rate

The influence of bedrock permeability and recharge rate on the hydrologic disturbance to the conductive heat flow field is shown in Figure 2-5. Recharge rates were varied between 1 and 100 mm yr^{-1} and bedrock permeabilities were varied between $1x10^{-13}$ and $1x10^{-11}$ m^2, typical of carbonate rock aquifers in the Basin and Range (Table 2-1). The contours in Figure 2-5 represent the root mean square deviation of temperatures from the purely conductive case calculated at all model grid nodes, expressed in percent.

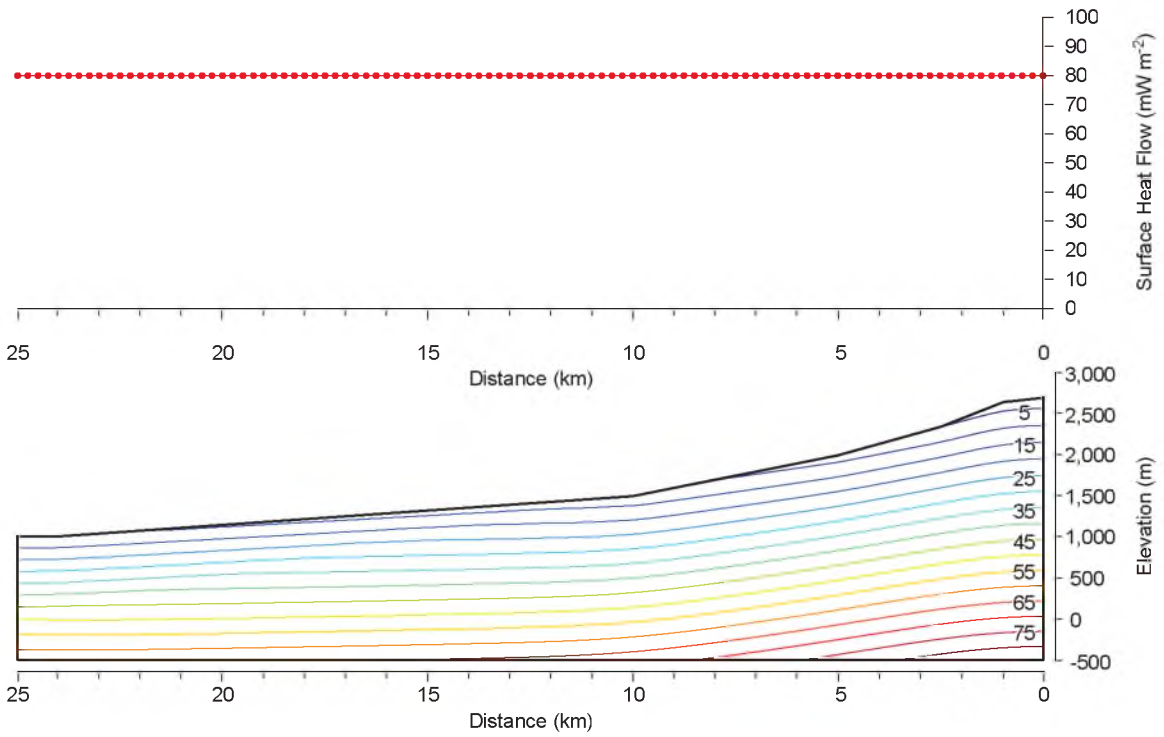

Figure 2-4. Top panel: Simulated surface heat flow for the purely conductive case (no groundwater flow). Heat flow profile calculated by using the upper two nodes in the model grid. Bottom panel: Simulated temperature distribution for the purely conductive case. Contours are in degrees Celsius.

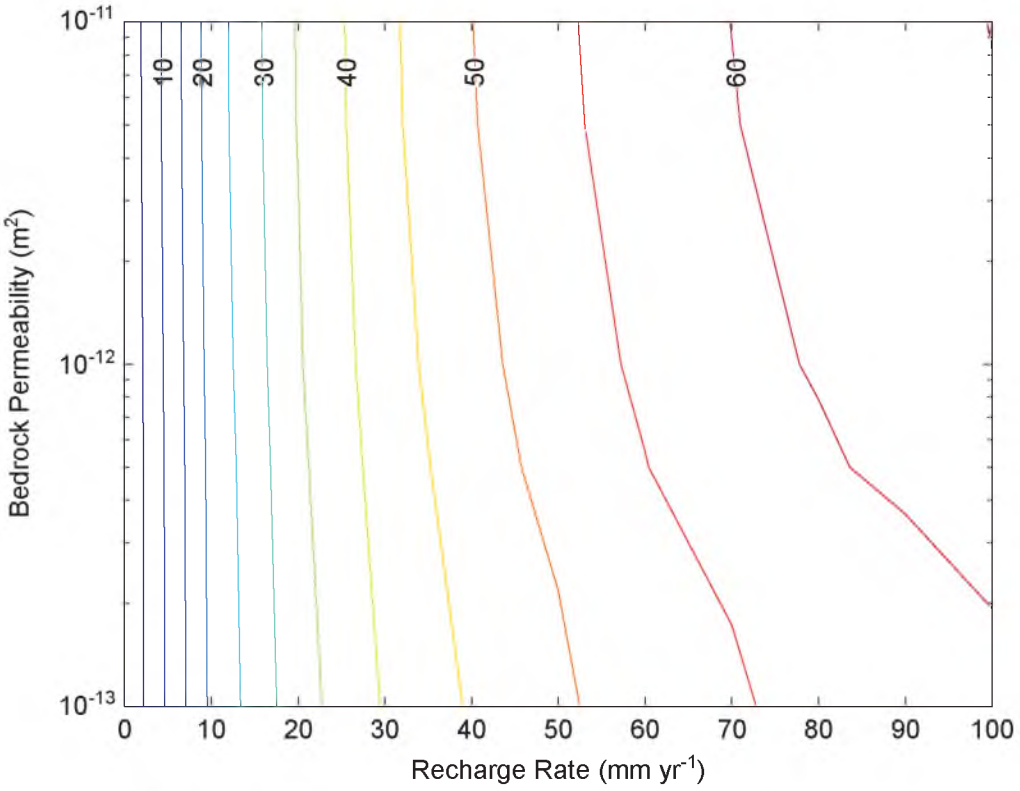

Figure 2-5. Influence of bedrock permeability and recharge rate on the hydrologic disturbance to conductive heat flow. Contours are the root mean square deviation of temperatures from the purely conductive case calculated at all model grid nodes, expressed in percent.

At recharge rates of 10 mm yr^{-1} or less, the hydrologic disturbance is almost completely dependent on the recharge rate. Figures 2-6 and 2-7 show the results of simulations with recharge rates of 10 mm yr^{-1}, and bedrock permeabilities of $5x10^{-13}$ and $5x10^{-12}$ m^2, respectively. Temperatures in the lower permeability simulation range between 1.4 °C and 75.1 °C, and temperatures in the higher permeability simulation range between 1.4 °C and 76.8 °C. At this recharge rate, the largest temperature perturbations occur in the deepest portions of the recharge area, and directly beneath the nodes where discharge is occurring. The temperature difference is near zero for the majority of the area within and beneath the basin fill. Surface heat flow rates are approximately 25 mW m^{-2} in the recharge area, and rapidly approach basal heat flux rates within 2 to 3 km of the recharge area. Surface heat flow rates in the discharge area are much higher, with values ranging between about 400 and 500 mW m^{-2}. At recharge rates of 10 mm yr^{-1} groundwater temperatures would be need to be measured in very specific locations in the recharge or discharge areas to detect these thermal anomalies.

Figures 2-8 and 2-9 show the results of simulations with recharge rates of 50 mm yr^{-1}, and bedrock permeabilities of $5x10^{-13}$ and $5x10^{-12}$ m^2, respectively. Temperatures in the lower permeability simulation range between 1.4 °C and 62.9 °C, and temperatures in the higher permeability simulation range between 1.4 °C and 51.0 °C. At this recharge rate, the largest temperature perturbations are in the deeper portions of the recharge area. This plume of cooler water, however, persists throughout and under the basin-fill deposits towards the discharge area, and at fairly shallow (less than 500 m) depths unlike simulations with recharge rates of less than 50 mm yr^{-1}. Likewise, the surface heat flux also follows this pattern. Surface heat flow rates are approximately 5 mW m^{-2} or less in

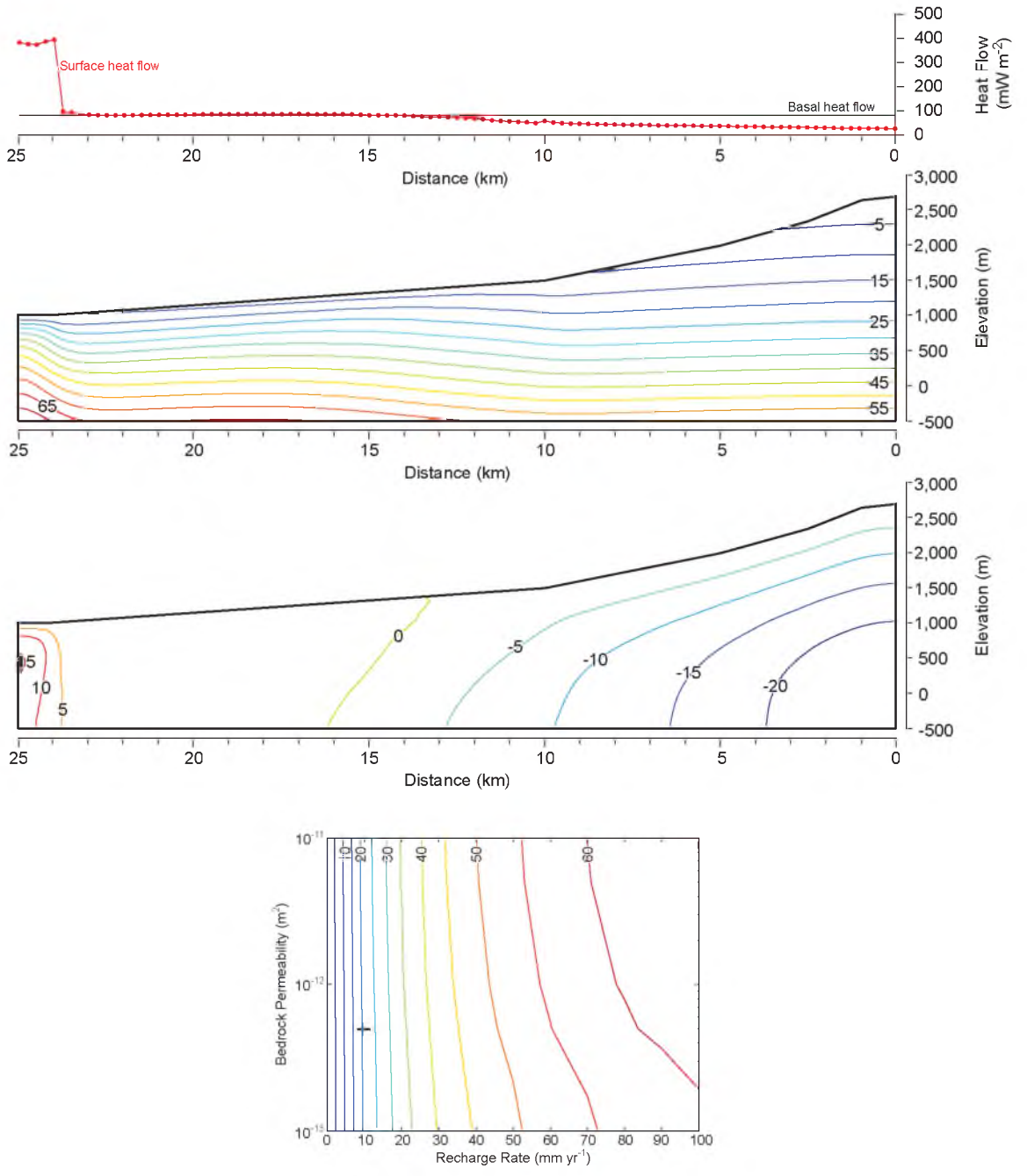

Figure 2-6. Thermal effects of groundwater flow in a basin with bedrock permeability of $5x10^{-13}$ m^2 and recharge rate of 10 mm yr^{-1}. Top panel: Simulated surface heat flow. Top middle panel: Simulated temperature distribution across the model domain (contours are in degrees Celsius). Bottom middle panel: Temperature difference distribution from the purely conductive case across the model domain (contours are in degrees Celsius). Bottom panel: Contours are the root mean square deviation of temperatures from the purely conductive case calculated at all model grid nodes, expressed in percent; cross represents the location of the simulation in bedrock permeability-recharge rate space.

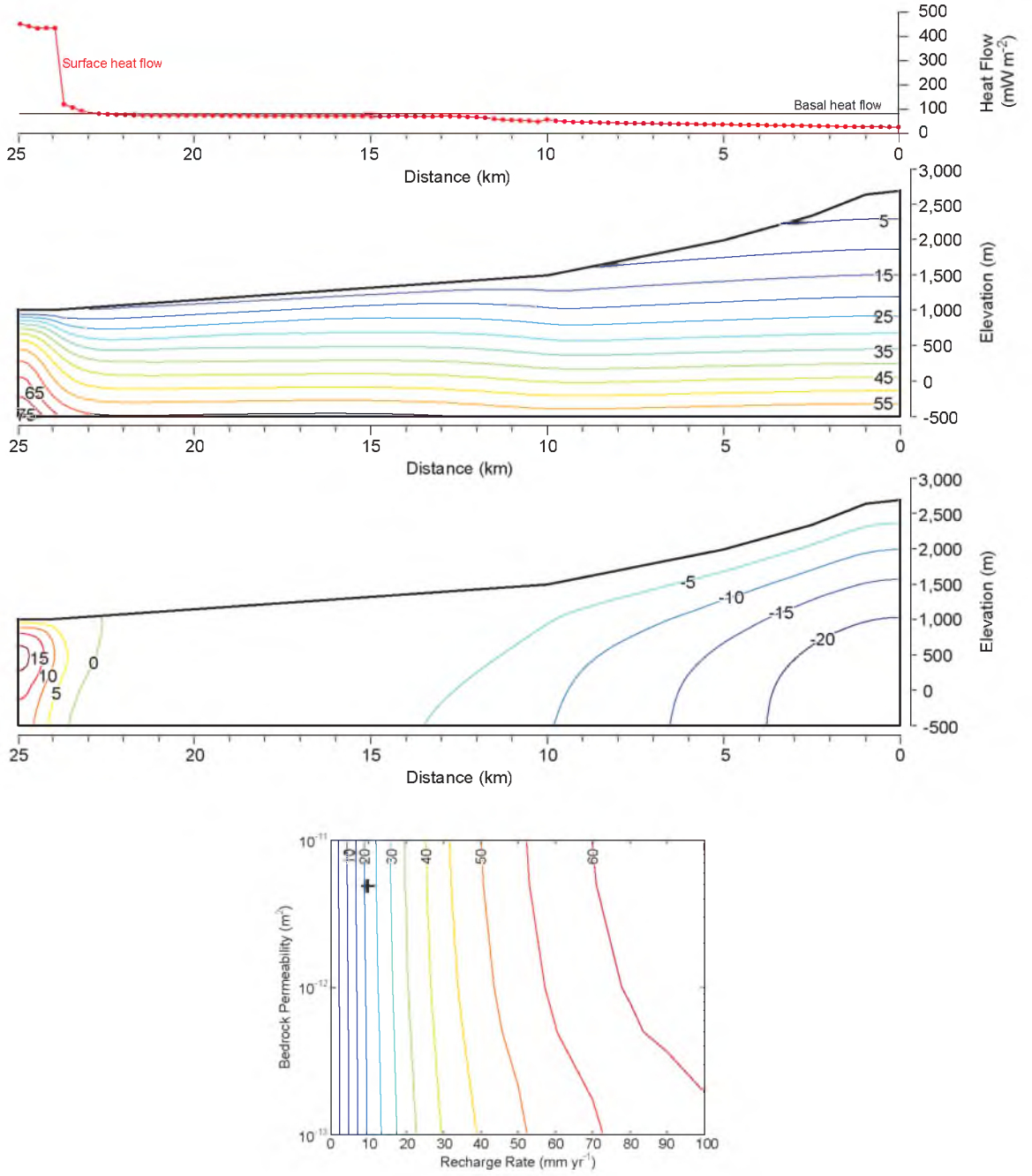

Figure 2-7. Thermal effects of groundwater flow in a basin with bedrock permeability of 5×10^{-12} m^2 and recharge rate of 10 mm yr^{-1}. Top panel: Simulated surface heat flow. Top middle panel: Simulated temperature distribution across the model domain (contours are in degrees Celsius). Bottom middle panel: Temperature difference distribution from the purely conductive case across the model domain (contours are in degrees Celsius). Bottom panel: Contours are the root mean square deviation of temperatures from the purely conductive case calculated at all model grid nodes, expressed in percent; cross represents the location of the simulation in bedrock permeability-recharge rate space.

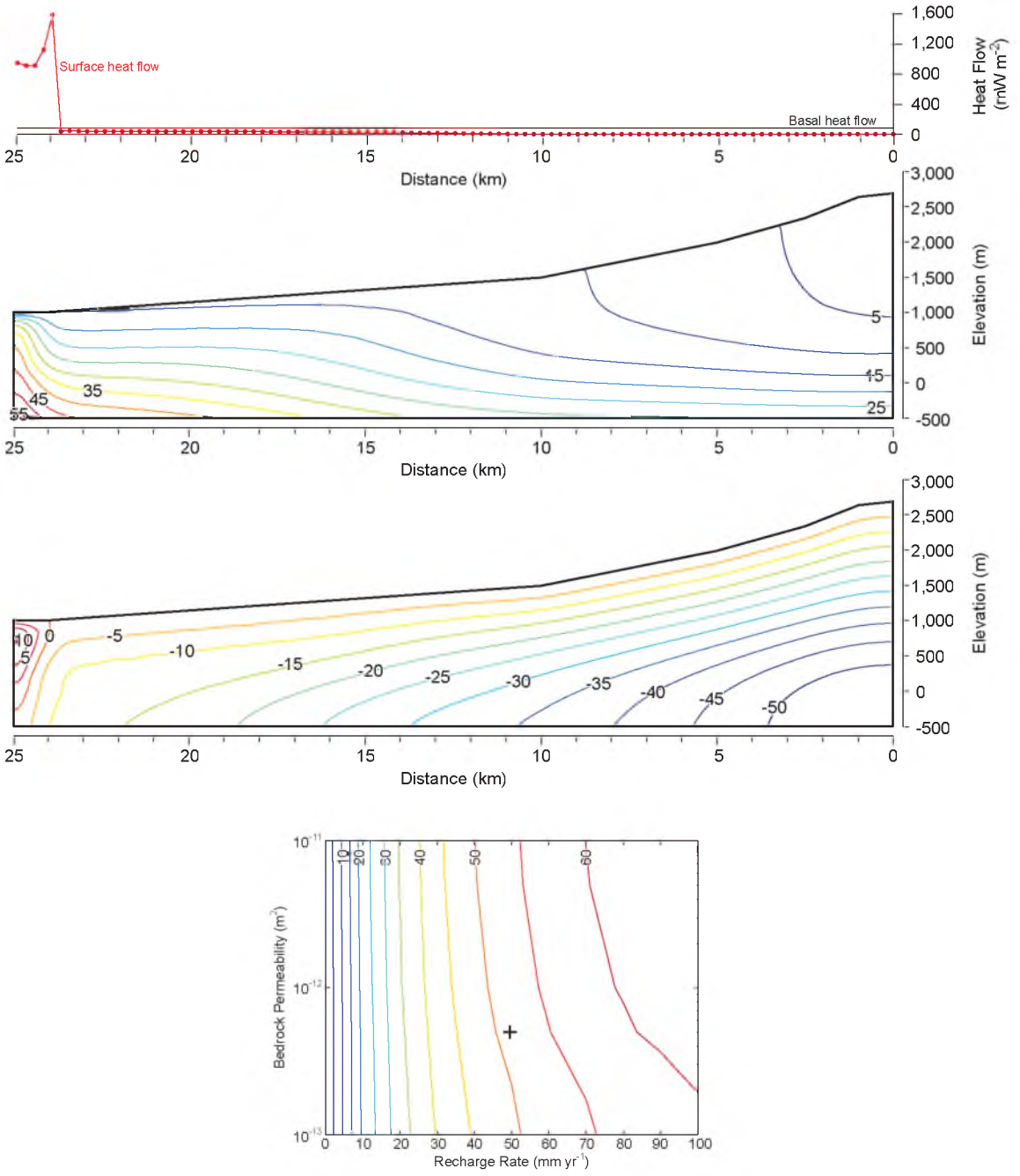

Figure 2-8. Thermal effects of groundwater flow in a basin with bedrock permeability of $5x10^{-13}$ m^2 and recharge rate of 50 mm yr^{-1}. Top panel: Simulated surface heat flow. Top middle panel: Simulated temperature distribution across the model domain (contours are in degrees Celsius). Bottom middle panel: Temperature difference distribution from the purely conductive case across the model domain (contours are in degrees Celsius). Bottom panel: Contours are the root mean square deviation of temperatures from the purely conductive case calculated at all model grid nodes, expressed in percent; cross represents the location of the simulation in bedrock permeability-recharge rate space.

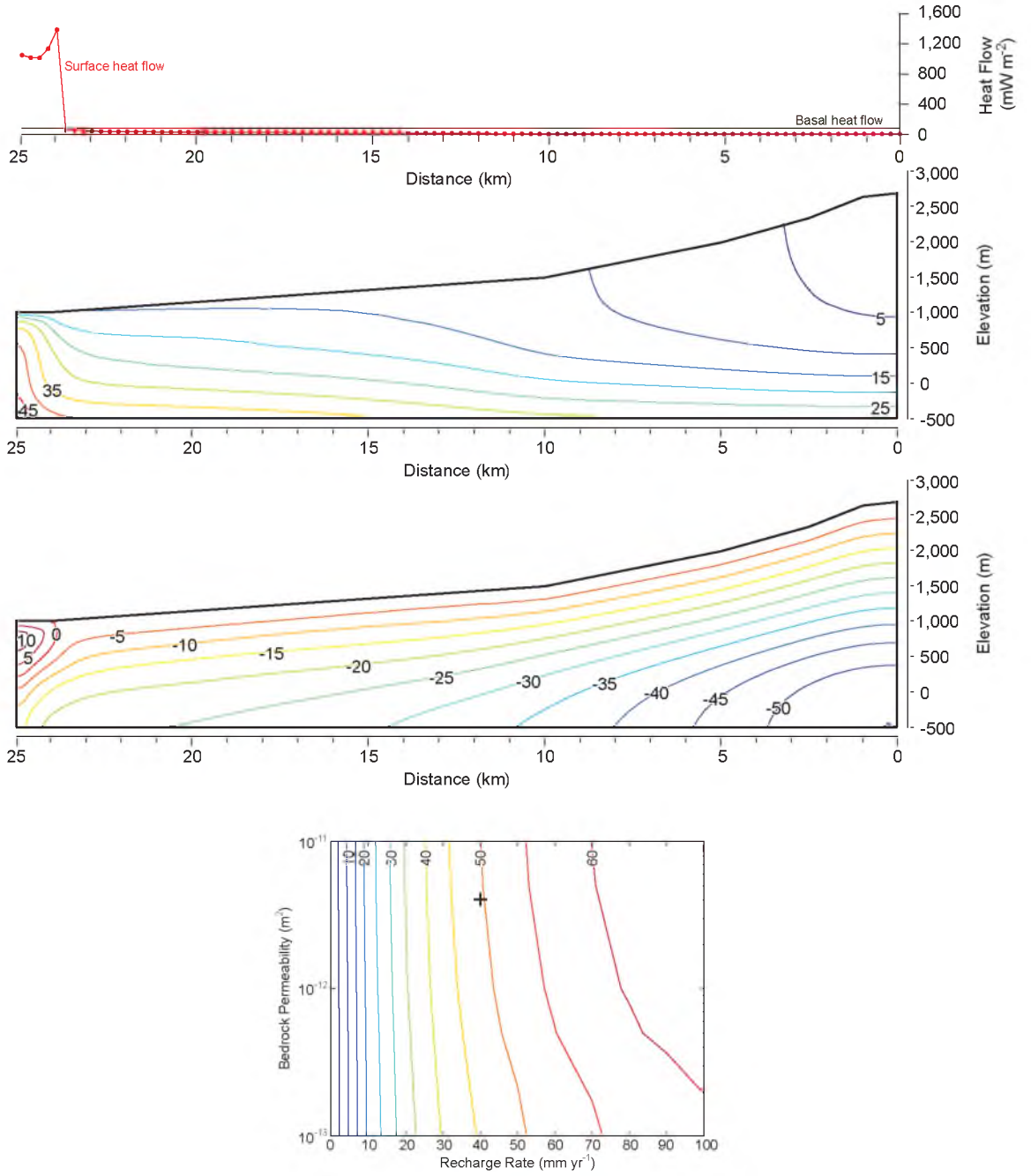

Figure 2-9. Thermal effects of groundwater flow in a basin with bedrock permeability of $5x10^{-12}$ m^2 and recharge rate of 50 mm yr^{-1}. Top panel: Simulated surface heat flow. Top middle panel: Simulated temperature distribution across the model domain (contours are in degrees Celsius). Bottom middle panel: Temperature difference distribution from the purely conductive case across the model domain (contours are in degrees Celsius). Bottom panel: Contours are the root mean square deviation of temperatures from the purely conductive case calculated at all model grid nodes, expressed in percent; cross represents the location of the simulation in bedrock permeability-recharge rate space.

the recharge area, and only reach values of 50 to 55 mW m^{-2} away from the recharge area before reaching the discharge area. Surface heat flow rates in the discharge area are much higher, with values ranging between about 1,000 and 1,600 mW m^{-2}. This plume of cooler water, therefore, could be easily measured using wells placed in the basin-fill deposits and used to constrain recharge rates to the system as a whole. Under these conditions the root mean difference in temperatures from the conductive case is slightly more dependent on bedrock permeability. Differences in the bedrock permeability at this recharge rate, however, produce only very slight differences in the distribution of the simulated temperatures and temperature perturbations. In the higher permeability simulation, temperature perturbations persist about 3 to 5 km further away from the recharge area than in the lower permeability simulation. It appears, therefore, that the permeability controls how far the perturbation will extend from the recharge area.

Figures 2-10 and 2-11 show the results of simulations with recharge rates of 90 mm yr^{-1}, and bedrock permeabilities of $5x10^{-13}$ and $5x10^{-12}$ m^2, respectively. Temperatures in the lower permeability simulation range between 1.4 °C and 51.8 °C, and temperatures in the higher permeability simulation range between 1.4 °C and 38.8 °C. Similarly to the other simulations, the largest temperature perturbations are in the deeper portions of the recharge area. Also similarly to the simulations with a recharge rate of 50 mm yr^{-1}, the plume of cooler water persists throughout and under the basin-fill deposits towards the discharge area, and at even shallower depths than the simulations using a recharge rate of 50 mm yr^{-1}. Surface heat flow values range between about 0 and 20 mW m^{-2} everywhere except the discharge area, where surface heat flow values range between about 1,500 and 3,000 mW m^{-2}. Under these conditions the root mean difference

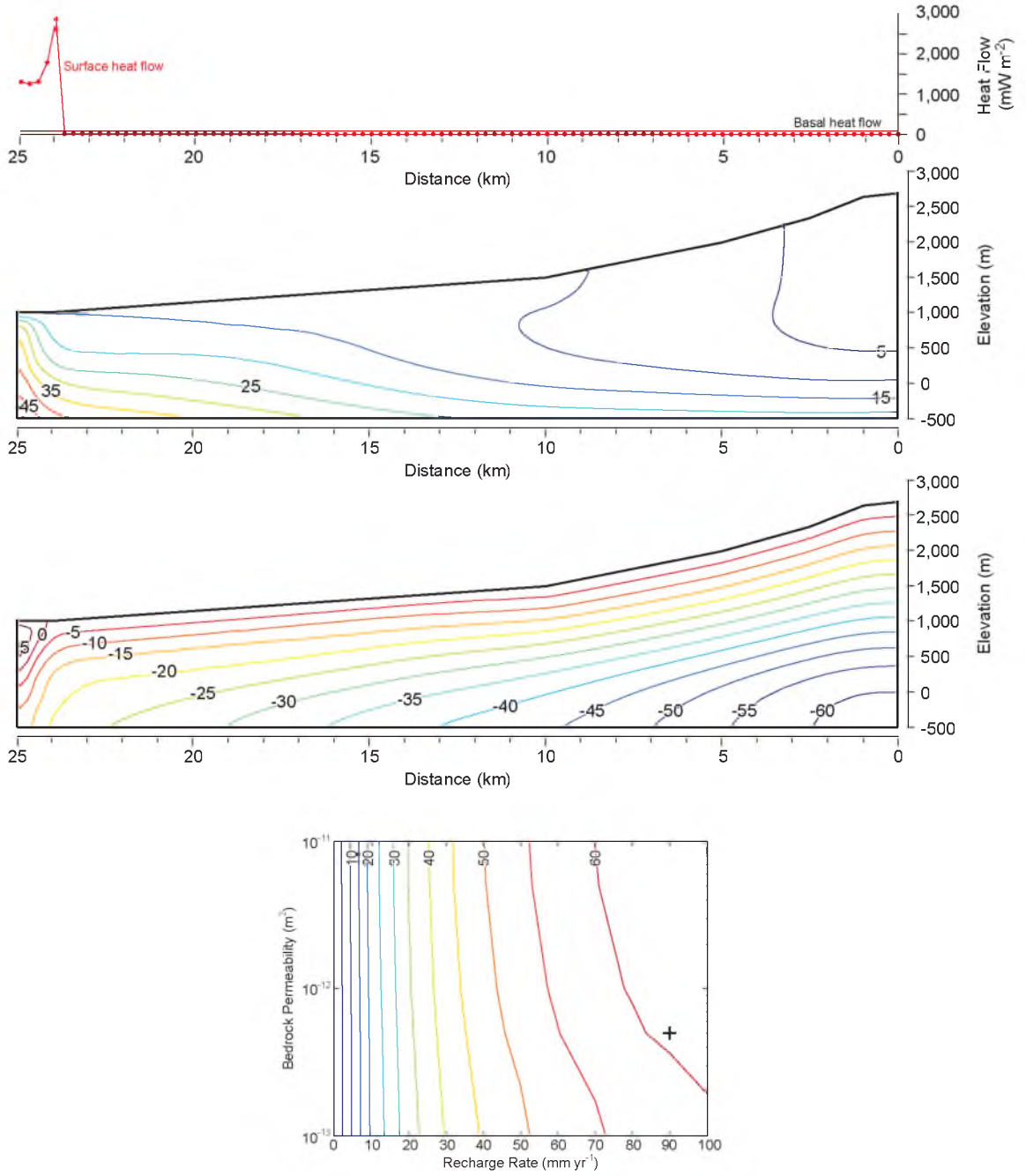

Figure 2-10. Thermal effects of groundwater flow in a basin with bedrock permeability of 5×10^{-13} m^2 and recharge rate of 90 mm yr^{-1}. Top panel: Simulated surface heat flow. Top middle panel: Simulated temperature distribution across the model domain (contours are in degrees Celsius). Bottom middle panel: Temperature difference distribution from the purely conductive case across the model domain (contours are in degrees Celsius). Bottom panel: Contours are the root mean square deviation of temperatures from the purely conductive case calculated at all model grid nodes, expressed in percent; cross represents the location of the simulation in bedrock permeability-recharge rate space.

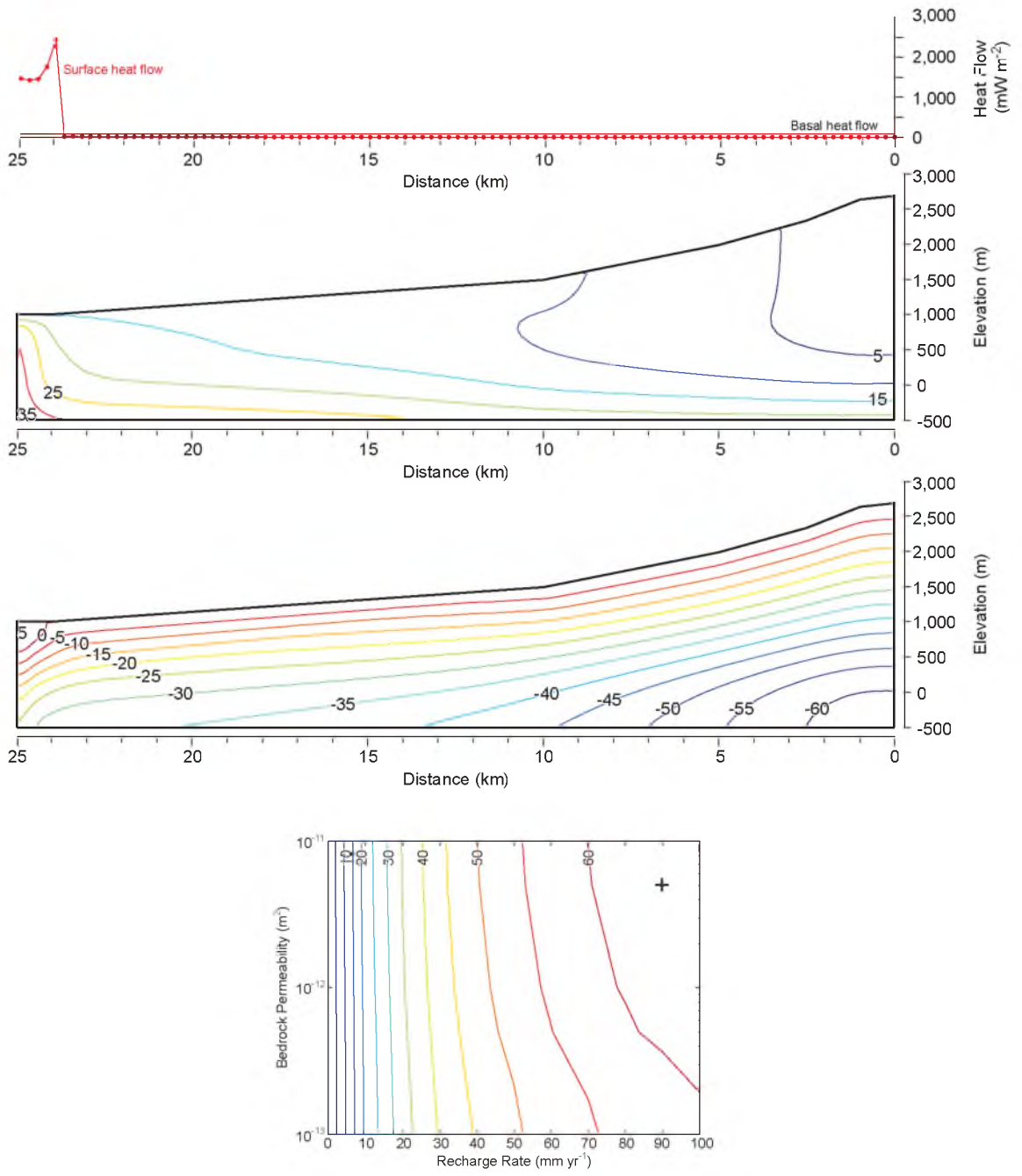

Figure 2-11. Thermal effects of groundwater flow in a basin with bedrock permeability of $5x10^{-12}$ m^2 and recharge rate of 90 mm yr^{-1}. Top panel: Simulated surface heat flow. Top middle panel: Simulated temperature distribution across the model domain (contours are in degrees Celsius). Bottom middle panel: Temperature difference distribution from the purely conductive case across the model domain (contours are in degrees Celsius). Bottom panel: Contours are the root mean square deviation of temperatures from the purely conductive case calculated at all model grid nodes, expressed in percent; cross represents the location of the simulation in bedrock permeability-recharge rate space.

in temperatures from the conductive case is even more dependent on bedrock permeability than the previous simulations at lower recharge rates. Differences in the bedrock permeability at this recharge rate produce a greater difference in the distribution of the simulated temperatures and temperature perturbations than the previous simulations. In the higher permeability simulation, temperature perturbations persist at least 5 km further away from the recharge area than in the lower permeability simulation. These simulations definitely show that the permeability controls how far the temperature perturbation will extend from the recharge area. Additionally, groundwater temperatures are as much as 10 °C cooler in the discharge area in the higher permeability simulation versus the lower permeability simulation. Surface heat flow values are also slightly lower at the discharge area for the higher permeability simulation versus the lower permeability simulation.

2.6 Conclusions

Two-dimensional numerical modeling of the combined effects of fluid flow and heat transport were used to quantify the effects of groundwater flow on the subsurface thermal regime. The numerical simulations could also be used to determine the lower limit of recharge rate that will produce an observable perturbation such that groundwater temperatures can be used to constrain recharge rates. Simulations of a basin 25 km wide to a depth of -500 m with 1,700 m of topographical relief, representative of basins within the Great Basin, and with moderate to high permeabilities representative of aquifers within the Great Basin, lead to the following conclusions:

1. Higher recharge rates and bedrock permeabilities produce greater thermal perturbations than lower recharge rates and permeabilities.

2. For all recharge rates and bedrock permeabilities, the greatest temperature perturbations occur in the deepest portion of the recharge area.
3. At lower recharge rates (10 mm yr^{-1} or less) the hydrologic disturbance is almost completely dependent on the recharge rate. At these recharge rates the temperature perturbation throughout the majority of the simulated area is nearly undetectable. Groundwater temperatures would need to be measured in very specific locations in the recharge or discharge areas to detect the hydrologic disturbance.
4. At more moderate recharge rates (50 mm yr^{-1}) the hydrologic disturbance is slightly more dependent on the bedrock permeability. Differences in the bedrock permeability at this recharge rate, however, produce only very slight differences in the distribution of the simulated temperatures and temperature perturbations.
5. At high recharge rates (90 mm yr^{-1}) the hydrologic disturbance is even more dependent on the bedrock permeability. Differences in the bedrock permeability at this recharge rate produce a greater difference in the distribution of the simulated temperatures and temperature perturbations versus simulations at lower recharge rates. Groundwater temperatures are as much as 10 °C cooler in the discharge area in the higher permeability simulation versus the lower permeability simulation.
6. Bedrock permeabilities appear to control the distance to which the temperature perturbation will extend from the recharge area. For moderate recharge rates (around 50 mm yr^{-1}) temperature perturbations at the higher permeabilities extend at least 3 km further from the recharge area than the perturbations at lower

permeabilities; at higher recharge rates (around 90 mm yr^{-1}) the temperature perturbations at higher permeabilities extend at least 5 km further from the recharge area.

7. Variations in the surface heat flux are quite different depending on the recharge rate. At low recharge rates, the highest variations only exist in the recharge and discharge areas. At higher recharge rates, the differences are larger in the recharge and discharge areas, and also persist in areas away from the recharge and discharge areas. Measurement of the surface heat flux is a robust indicator of the hydrologic disturbance caused by a specific recharge rate.
8. At recharge rates of 50 mm yr^{-1} and above, the plume of colder water extends past the recharge area and persists throughout and under the basin-fill deposits towards the discharge area, at fairly shallow (less than 500 m) depths and can be detected by measuring surface heat flux unlike simulations with recharge rates of less than 50 mm yr^{-1}. This plume of cooler water could be easily measured using wells placed in the basin-fill deposits and used to constrain recharge rates to the system as a whole. The lower limit of recharge rates needed to produce a thermal perturbation large enough such that groundwater temperatures can be used to constrain recharge rates, therefore, is 50 mm yr^{-1}.

2.7 References

Belcher, W.R., P.E. Elliott, and A.L. Geldon (2001), Hydraulic-property estimates for use with a transient ground-water flow model of the Death Valley regional ground-water flow system, Nevada and California, *US Geol. Surv. Water-Resour. Invest. Rep. 01–4120*, 33 pp.

Belcher, W.R., D.S. Sweetkind, and P.E. Elliott (2002), Probability distributions of hydraulic conductivity for the hydrogeologic units of the Death Valley regional ground-water flow system, Nevada and California, *US Geol. Surv. Water-Resour. Invest. Rep. 02–4212*, 24 pp.

Bredehoeft, J.D., and I.S. Papadopulos (1965), Rates of vertical groundwater movement estimated for the Earth's thermal profile, *Water Resour. Res.*, *1*, 325–328.

Cartwright, K. (1970), Groundwater discharge in the Illinois Basin as suggested by temperature anomalies, *Water Resour. Res.*, *6*, 912–918.

Cartwright, K. (1971), Redistribution of geothermal heat by a shallow aquifer, *Geol. Soc. of Am. Bull.*, *82*, 3197–3200.

Domenico, P.A., and V.V. Palciauskas (1973), Theoretical analysis of forced convective heat transfer in regional ground-water flow, *Geol. Soc. of Am. Bull.*, *84*, 3803–3814.

Domenico, P.A., and F.W. Schwartz, (1990), *Physical and Chemical Hydrogeology*, John Wiley and Sons, Inc., New York.

Donaldson, J.G. (1962), Temperature gradients in the upper layers of the earth's crust due to convective water flows, *J. Geophys. Res.*, *76*, 3449–3459.

Flint, A.L., and L.E. Flint, (2007a), Application of the Basin Characterization Model to estimate in-place recharge and runoff potential in the Basin and Range carbonate-rock aquifer system, White Pine County, Nevada, and adjacent areas in Nevada and Utah, *US Geol. Surv. Scien. Invest. Rep. 2007–5099*, 20 pp.

Flint, A.L., L.E. Flint, and M.D. Masbruch (2011), Input, calibration, uncertainty, and limitations of the Basin Characterization Model, Appendix 3 in Conceptual model of the Great Basin carbonate and alluvial aquifer system, edited by V.M. Heilweil and L.E. Brooks, *US Geol. Surv. Scien. Invest. Rep. 2010–5193*, 149–164.

Flint, L.E., and A.L. Flint (2007b), Regional analysis of ground-water recharge, in Ground-water recharge in the arid and semiarid southwestern United States edited by D.A. Stonestrom, J. Constantz, T.P.A. Ferre, and S.A. Leake, *US Geol. Surv. Prof Pap. 1703*, 29–59.

Forster, C., and L. Smith (1988), Groundwater flow systems in mountainous terrain, 1. Numerical modeling technique, *Water Resour. Res.*, *24*, 999–1010.

Forster, C., and L. Smith (1989), The influence of groundwater flow on thermal regimes in mountainous terrain: A model study, *J. Geophys. Res.*, *94*, 9439–9451.

Gleeson, T., and A.H. Manning (2008), Regional groundwater flow in mountainous terrain: Three-dimensional simulations of topographic and hydrogeologic controls, *Water Resour. Res.*, *44*, W10403, doi:10.1029/2008WR006848.

Haitjema, H.M., and S. Mitchell-Bruker, (2005), Are water tables a subdued replica of the topography?, *Ground Water*, *43*, 781–786.

Harrill, J.R., and D.E. Prudic (1998), Aquifer systems in the Great Basin region of Nevada, Utah, and adjacent states—Summary report, *US Geol. Surv. Prof. Pap. 1409–A*, 66 pp.

Heilweil, V.M., and L.E. Brooks, eds. (2011), Conceptual model of the Great Basin carbonate and alluvial aquifer system, *US Geol. Surv. Scien. Invest. Rep. 2010–5193*, 191 pp.

Hevesi, J.A., A.L. Flint, and L.E. Flint (2003), Simulation of net infiltration and potential recharge using a distributed-parameter watershed model of the Death Valley region, Nevada and California, *US Geol. Surv. Water-Resour. Invest. Rep. 2003–4090*, 161 pp.

Keys, W.S., and R.F. Brown (1978), The use of temperature logs to trace the movement of injected water, *Ground Water*, *16*, 32–48.

Lachenbruch, A.H., and J.H. Sass (1977), Heat flow in the United States, in The Earth's Crust edited by J.G. Heacock, *Geophys. Mono. Ser.*, AGU, Washington, D.C., 626–675.

Langevin, C.D., D.T. Thorne, Jr., A.M. Dausman, M.C. Sukop, and W. Guo (2008), SEAWAT version 4: A Computer program for simulation of multi-species solute and heat transport, *US Geol. Surv. Tech. and Meth. Book 6, Chapter A22*, 39 pp.

Leavesley, G.H., R.W. Lichty, B.M. Troutman, and L.G. Saindon, (1983), Precipitation-runoff modeling system: User's manual, *US Geol. Surv. Water-Resour. Invest. Rep. 83–4238*, 207 pp.

Manning, A.H., and D.K. Solomon (2005), An integrated environmental tracer approach to characterizing groundwater circulation in a mountain block, *Water Resour. Res.*, *41*, W12412, doi:10.1029/2005WR004178.

Markstrom, S.L., R.G. Niswonger, R.S. Regan, D.E. Prudic, and P.M. Barlow (2008), GSFLOW—Coupled ground-water land surface-water flow model based on the integration of the precipitation-runoff modeling system (PRMS) and the modular ground-water flow model (MODFLOW-2005), *US Geol. Surv. Tech. and Meth. 6-D1*, 240 pp.

Masbruch, M.D., V.M. Heilweil, S.G. Buto, L.E. Brooks, D.S. Susong, A.L. Flint, L.E. Flint, and P.M. Gardner (2011), Groundwater budgets, chap. D in Conceptual model of the Great Basin carbonate and alluvial aquifer system, edited by V.M. Heilweil, and L.E. Brooks, *US Geol. Surv. Scien. Invest. Rep. 2010–5193*, 73–126.

Maxey, G.B., and T.E. Eakin (1949), Ground water in White River Valley, White Pine, Nye, and Lincoln Counties, Nevada, *Nev. Off. St. Eng. Water Resour. Bull. no. 8*, 59 pp.

Parsons, M.L. (1970), Groundwater thermal regime in a glacial complex, *Water Resour. Res.*, *6*, 1701–1720.

Prudic, D.E., J.R. Harrill, and T.J. Burbey (1995), Conceptual evaluation of regional ground-water flow in the Carbonate-Rock Province of the Great Basin, Nevada, Utah, and adjacent states, *US Geol. Surv. Prof. Pap. 1409–D*, 102 pp.

Salem, Z.E., M. Taniguchi and Y. Sakura (2004), Use of temperature profiles and stable isotopes to trace flow lines: Nagaoka area, Japan, *Ground Water*, *42*, 83–91.

San Juan, C.A., W.R. Belcher, R.J. Laczniak, and H.M. Putnam (2004), Hydrologic components for model development, chap. C in Death Valley regional ground-water flow system, Nevada and California—Hydrogeologic framework and transient ground-water flow model, edited by W.R. Belcher, *US Geol. Surv. Scien. Invest. Rep. 2004–5205*, 103–136.

Sass, J.H., S.S. Priest, A.H. Lachenbruch, S.P. Galanis, Jr., T.H. Moses, Jr., J.P. Kennelly, Jr., R.J. Munroe, E.P. Smith, F.V. Grubb, R.H. Husk, Jr., and C.W. Mase (2005), Summary of supporting data for USGS regional heat-flow studies of the Great Basin, 1970-1990, *US Geol. Surv. Open-File Rep. 2005–1207*, online version 1.0, URL: *http://pubs.er.usgs.gov/publication/*ofr20051207, accessed on July 10, 2007.

Smith, L.S., and D.S. Chapman (1983), On the thermal effects of groundwater flow, 1. Regional scale systems, *J. Geophys. Res.*, *88*, 593–608.

Sorey, M.L. (1971), Measurement of vertical groundwater velocity from temperature profiles in wells, *Water Resour. Res.*, *7*, 963–970.

Stallman, R.W (1963), Computation of groundwater velocity from temperature data, *US Geol. Surv. Water Supp. Pap. 1554–H*, 36–46.

Stallman, R.W. (1965), Steady one-dimensional fluid flow in a semi-finite porous medium with sinusoidal surface temperature, *J. Geophys. Res.*, *70*, 2821–2827.

U.S. Census Bureau (2000), Pre-2010 cartographic boundary file naming conventions and download access, accessed April 21, 2005 at *http://www.census.gov/geo/maps-data/data/prev_cartbndry_names.html*.

Voss, C.I., and A.M. Provost (2002), SUTRA, a model for saturated-unsaturated variable-density ground-water flow with solute or energy transport, *US Geol. Surv. Water-Resour. Invest. Rep. 2002–4231*, 250 pp.

CHAPTER 3

HYDROLOGY AND NUMERICAL SIMULATION OF GROUNDWATER MOVEMENT AND HEAT TRANSPORT IN SNAKE VALLEY AND SURROUNDING AREAS, JUAB, MILLARD, AND BEAVER COUNTIES, UTAH, AND WHITE PINE AND LINCOLN COUNTIES, NEVADA

3.1 Abstract

The Snake Valley and surrounding area, along the Utah-Nevada state border, is part of the Great Basin carbonate and alluvial aquifer system. The groundwater system in the study area consists of water in unconsolidated deposits in basins and water in consolidated rock underlying the basins and in the adjacent mountain blocks. Most recharge occurs from precipitation on the mountain blocks and most discharge occurs from the lower altitude basin-fill deposits mainly as evapotranspiration, spring flow, and well withdrawals.

The Snake Valley area regional groundwater flow system was simulated using a three-dimensional model incorporating both groundwater flow and heat transport. The model was constructed with MODFLOW-2000, a version of the U.S. Geological Survey's groundwater flow model, and MT3DMS, a transport model that simulates advection, dispersion, and chemical reactions of solutes or heat in groundwater systems. Observations of groundwater discharge by evapotranspiration, spring flow, mountain

stream baseflow, and well withdrawals; groundwater-level altitudes; and groundwater temperatures were used to calibrate the model. Parameter values estimated by regression analyses were reasonable and within the range of expected values.

This study represents one of the first regional modeling efforts to include calibration to groundwater temperature data. The inclusion of temperature observations reduced parameter uncertainty, in some cases quite significantly, over using just water-level altitude and discharge observations. Of the 39 parameters used to simulate horizontal-hydraulic conductivity, uncertainty on 11 of these parameters was reduced to one order of magnitude or less. Other significant reductions in parameter uncertainty occurred in parameters representing the vertical anisotropy ratio, drain and river conductance, recharge rates, and well withdrawal rates.

The model provides a good representation of the groundwater system; simulated water-level altitudes range over almost 2,000 m, and 98 percent of the simulated values of water-level altitudes in wells are within 30 m of observed water-level altitudes, and 58 percent of them are within 12 m. Nineteen of 20 discharge observations are within 30 percent of observed discharge. Eighty-one percent of the simulated values of temperatures in wells are within 2 °C of the observed values, and 55 percent of them are within 0.75 °C. The numerical model represents a more robust quantification of groundwater budget components than previous studies because the model integrates all components of the groundwater budget. The model also incorporates several new data including (1) a detailed hydrogeologic framework; and (2) more observations including several new water-level altitudes throughout the study area, several new measurements of spring discharge within Snake Valley which had not previously been monitored, and

groundwater temperature data. Uncertainty in the estimates of subsurface flow are less than those of previous studies because the model balanced recharge and discharge across the entire simulated area, not just in each hydrographic area (HA), and because of the large dataset of observations (water-level altitudes, discharge, and temperatures) used to calibrate the model and the resulting transmissivity distribution.

Groundwater recharge from precipitation and unconsumed irrigation in Snake Valley is 160,000 acre-ft/yr, which is within the range of previous estimates. Subsurface inflow from southern Spring Valley to southern Snake Valley is 13,000 acre-ft/yr and is within the range of previous estimates; subsurface inflow from Spring Valley to Snake Valley north of the Snake Range, however, is only 2,200 acre-ft/yr, which is much less than has been previously estimated. Groundwater discharge from groundwater evapotranspiration and springs is 100,000 acre-ft/yr, and discharge to mountain streams is 3,300 acre-ft/yr; these are within the range of previous estimates. Current well withdrawals are 28,000 acre-ft/yr. Subsurface outflow from Snake Valley occurs to Pine Valley (2,000 acre-ft/yr), Wah Wah Valley (23 acre-ft/yr), Tule Valley (31,000 acre-ft/yr), Fish Springs Flat (790 acre-ft/yr), and outside of the study area towards Great Salt Lake Desert (8,400 acre-ft/yr), totaling 44,000 acre-ft/yr and is within the range of previous estimates.

The subsurface flow amounts indicate the degree of connectivity between HAs within the study area. The simulated transmissivity and locations of natural discharge, however, provide a better estimate of the effect of groundwater withdrawals on groundwater resources than does the amount and direction of subsurface flow between hydrographic areas. The distribution of simulated transmissivity throughout the study

area includes many areas of high transmissivity within and between HAs. Increased well withdrawals within these high transmissivity areas will likely affect a large part of the study area, resulting in decreasing groundwater levels, as well as leading to a decrease in natural discharge to springs and evapotranspiration.

3.2 Introduction

Snake Valley is a sparsely populated basin located along the Utah-Nevada border in the eastern Great Basin physiographic province described by *Fenneman* [1931]. The study area (Figure 3-1), which covers approximately 21,000 km^2 (8,100 mi^2), is part of the Great Basin carbonate and alluvial aquifer system (GBCAAS) which comprises aquifers and confining units in unconsolidated basin-fill and volcanic deposits, carbonate, and other bedrock units [*Heilweil et al.*, 2011]. In some areas of the GBCAAS, aquifers are hydraulically connected between basins. In other areas, interbasin groundwater flow is impeded by mountain ranges that consist of less permeable rock. The basins in this study area approximately coincide with the southern half of the Great Salt Lake Desert regional groundwater flow system as defined by *Harrill et al.* [1988]. These basins are divided on the basis of hydrographic area (HA) boundaries [*Harrill et al.*, 1988] which generally coincide with topographic basin divides. The study area consists of three partial HAs: Spring Valley, Dugway-Government Creek Valley, and Sevier Desert; and five complete HAs: Snake Valley, Fish Springs Flat, Tule Valley, Pine Valley, and Wah Wah Valley (Figure 3-1).

The study area is characterized by north-south trending mountain ranges and basins that range in altitude from over 3,950 m (13,000 ft) in the highest peaks of the Snake Range to less than 1,350 m (4,400 ft) in the basin bottoms at the southern end of

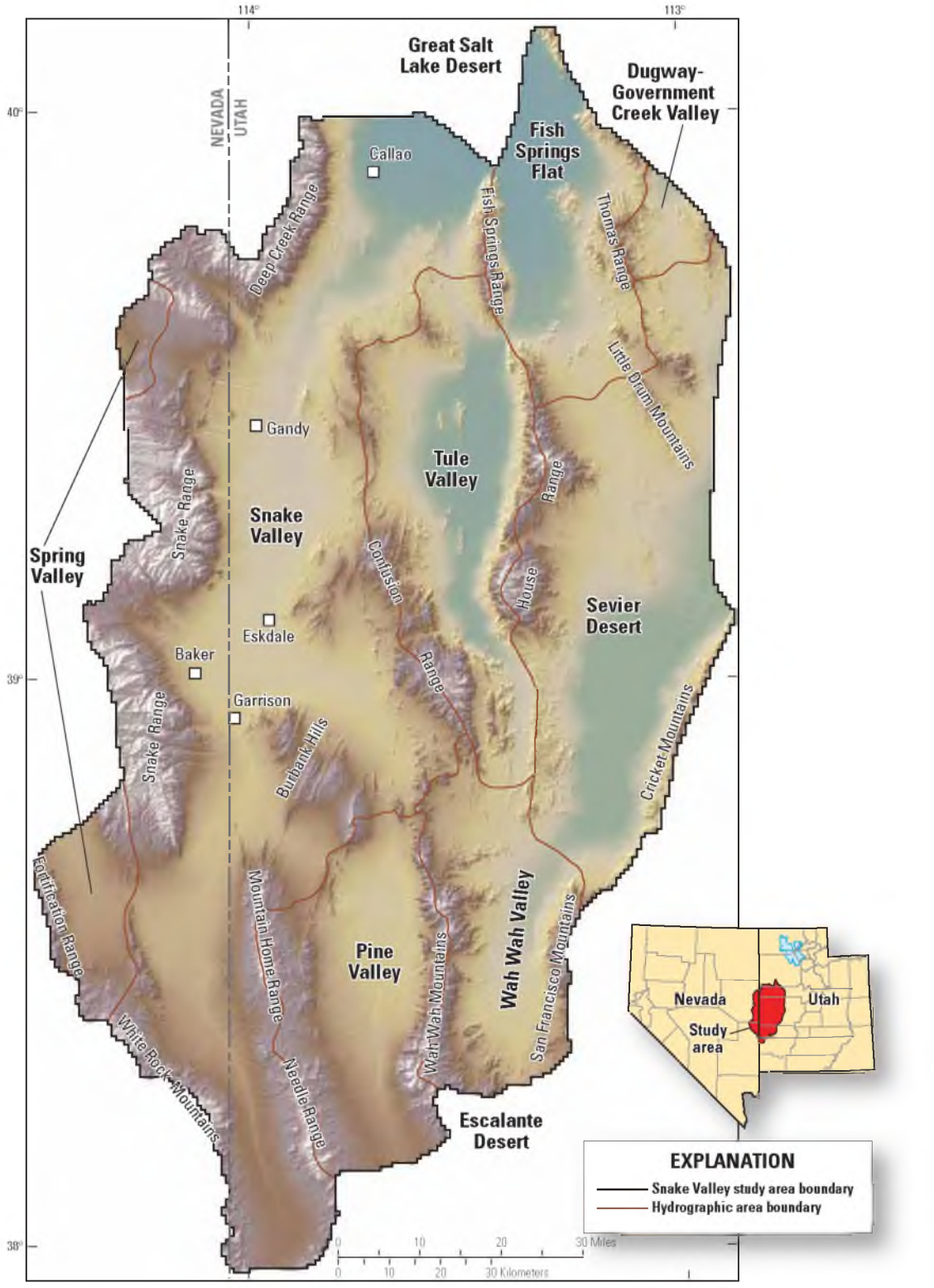

Figure 3-1. Location of the Snake Valley study area, Utah and Nevada. State and county boundary data from: *U.S. Census Bureau* [2000]. Modified from: *Masbruch et al.* [201X], in review.

the Great Salt Lake Desert (Figure 3-1). Climatic conditions range from temperate in the high-altitude Snake and Deep Creek Ranges to semiarid and arid across much of the rest of the study area. Annual precipitation varies from about 150 mm (6 in) in the low altitudes of northernmost Snake Valley to about 760 mm (30 in) in the highest altitudes of the Snake and Deep Creek Ranges based on 30-yr average PRISM (Parameter-Elevation Regressions on Independent Slopes Model) precipitation data [*Daly et al.*, 1994; 2008]. The majority of precipitation occurs during the winter months, often as snow that accumulates in the mountains. Most groundwater in the valleys in the study area is derived from snowmelt and rainfall above altitudes of 1,800 m (6,000 ft) where precipitation amounts generally exceed losses from evapotranspiration [*Hood and Rush*, 1965].

The local economy is dominated by irrigated agriculture and ranching. Very few perennial streams flow into the basins and those that do are fully appropriated. Total annual withdrawal of groundwater in Snake Valley was approximately 17,500 acre-ft/yr in 2010 [*Burden et al.*, 2011], nearly all of which was used to irrigate approximately 37 km^2 (9,200 acres) of land [*Welch et al.*, 2007].

The Southern Nevada Water Authority (SNWA) has proposed developing unappropriated groundwater resources in Snake Valley and adjacent basins in eastern Nevada in order to supply the growing urban population of Las Vegas, Nevada. SNWA proposes to pump groundwater from five valleys in eastern Nevada using a network of 144 to 174 wells, up to 680 km (430 mi) of collector pipelines, and approximately 500 km (300 mi) of main and lateral pipeline to deliver water to Las Vegas located more than 400 km (250 mi) to the south of Baker, Nevada (SNWA, 2011). SNWA plans to develop

up to 185,000 acre-ft/yr of its existing water rights and applications in Spring, Snake, Cave, Dry Lake, and Delamar Valleys of eastern Nevada. A ruling was issued on March 22, 2012, granting SNWA water rights for 61,127 acre-ft/yr of groundwater from Spring Valley, located immediately to the west of Snake Valley (Figure 3-1). Furthermore, SNWA holds applications for approximately 50,700 acre-ft/yr of groundwater in Snake Valley.

Because of the magnitude of the SNWA groundwater development project and the possible interconnected nature of groundwater basins in the region, groundwater users and managers in Utah are concerned about declining groundwater levels and spring flows in western Utah which could result from the proposed groundwater withdrawals. The objectives of this study are (1) understanding the links between basin-fill and carbonate aquifer systems, and the movement of groundwater within and between basins in the Snake Valley and surrounding area; (2) to quantify uncertainties in key components of the regional flow system, including aquifer properties, interbasin flow rates, and recharge rates and locations; and (3) to evaluate the value of subsurface temperature data in constraining regional groundwater flow models. This study lays the foundation for future studies, and will provide a baseline that can be used to assess the effects of future groundwater withdrawals on groundwater resources in the Snake Valley area.

The purpose of this report is to describe the groundwater hydrology of the Snake Valley area and to present the construction, calibration, and results of a numerical simulation of the groundwater system. A numerical groundwater flow and heat transport model was developed to simulate groundwater flow and heat transport in the Snake Valley area, and to test the conceptual understanding of the groundwater system. A more

complete understanding of the groundwater system and groundwater budget can aid in effective management of groundwater resources. Information from a number of previous and current investigations was compiled to conceptualize and quantify hydrologic and thermal components of the groundwater system, and to provide hydraulic and thermal properties and observation data used in the calibration of the numerical groundwater model. It was beyond the scope of the current study to develop a transient groundwater model to simulate increased groundwater withdrawals. The groundwater model developed in this study, however, can be used as a tool in future studies to assess long-term effects of groundwater withdrawals and to guide the collection of further data that will lead to better predictions of the reduction of groundwater discharge to springs and declining water levels if increased well withdrawals occurr. This study is a cooperative effort between the U.S. Geological Survey (USGS) and Millard, Juab, Tooele, Salt Lake, and Utah Counties.

3.3 Previous Studies

Early evaluations of groundwater in the study area were published by *Bolke and Sumsion* [1978], *Hood and Rush* [1965], *Stephens* [1974; 1976; 1977], *Stephens and Sumsion* [1978], and *Wilberg* [1991]. These reconnaissance studies provide general descriptions of groundwater resources and chemical quality. *Gates and Kruer* [1981] summarized some of these earlier studies and compiled their data to better evaluate the southern Great Salt Lake Desert as an integrated groundwater flow system. *Gates and Kruer* [1981] looked at potential pathways for interbasin groundwater flow and at the source of water discharging from the Fish Springs complex. Although *Gates and Kruer* [1981] provided interpretations on the locations and amounts of interbasin flow from a

thorough assessment of existing and new information, these estimates were based on sparse hydrologic data.

During the 1980s, the USGS Regional Aquifer System Analysis (RASA) program assessed the nation's major aquifer systems and, as part of this effort, delineated major aquifer systems in the Great Basin (GB) and evaluated regional flow in the Carbonate-Rock Province of the Great Basin [*Harrill and Prudic*, 1998]. The RASA-GB study included hydrogeology [*Plume and Carlton*, 1988], geochemistry [*Thomas et al.*, 1996], hydrology [*Harrill et al.*, 1988; *Thomas et al.*, 1986] and a numerical groundwater flow model [*Prudic et al.*, 1995] for a large geographic area that encompasses the Snake Valley study area. The results of the RASA studies form the basis of most subsequent conceptualizations of groundwater flow in the Great Basin.

Kirby and Hurlow [2005] revisited the hydrogeology of the Snake Valley area with the goal of assessing the potential impacts of the proposed SNWA groundwater development project on groundwater resources in Utah using an existing, basin-scale geologic framework and numerical groundwater flow model. Their conclusion, that the current understanding of geology and hydrology for the area was insufficient, prompted the Utah State Legislature to fund the establishment of a long-term groundwater monitoring network in the Snake Valley area. This network includes wells and spring gages in Snake Valley, and wells in Tule Valley and Fish Springs Flat where water levels and discharge are monitored continuously [*Utah Geological Survey*, 2009].

A more recent regional investigation, the Basin and Range carbonate-rock aquifer system study (BARCAS) was completed by the USGS and the Desert Research Institute in support of federal legislation to investigate the groundwater flow system underlying

White Pine County and adjacent counties in Nevada and Utah. The BARCAS study developed potentiometric-surface maps showing groundwater flow directions in both alluvial and carbonate aquifers, derived new groundwater budget estimates, and assessed interbasin groundwater flow using a combination of basin-boundary geology, hydraulic head data, and geochemistry. The results of the BARCAS study are available in a summary report ([*Welch et al.*, 2007] and references therein).

A comprehensive summary of hydrologic data for the entire Great Basin carbonate and alluvial aquifer system (GBCAAS) was recently published and presents an updated conceptual model of groundwater flow for a 285,000 km^2 (110,000 mi^2) area predominantly in eastern Nevada and western Utah [*Heilweil and Brooks*, 2011]. This study was part of a national water census program summarizing groundwater availability on regional scales across the U.S. The large area of the GBCAAS study completely encompasses Snake Valley and the surrounding areas investigated in the present study. In addition to providing a summary and compilation of data collected from numerous sources, the GBCAAS report also includes: a new hydrogeologic framework created by extracting and combining information from a variety of datasets; a regional potentiometric-surface map for the entire study area; and groundwater budget estimates compiled for 165 individual HAs and 17 regional groundwater flow systems.

To assess the hydrologic effects of developing groundwater in Snake Valley, *Halford and Plume* [2011], in cooperation with the National Park Service, refined and recalibrated the RASA-GB numerical model [*Prudic et al.*, 1995] in Spring and Snake Valleys. A variant of this model was used to estimate potential effects of groundwater development on water levels, groundwater evapotranspiration, and spring discharges

around the southern Snake Range. Four development scenarios were investigated and results are presented as maps of drawdown and groundwater capture, and time series of drawdowns and discharges from selected wells, springs, and control volumes. Results of the study show that (1) simulated drawdown was attenuated where groundwater discharge could be captured; (2) capture rates of groundwater discharge in Snake Valley were generally less than 1 ft/yr, but locally could be as great as 3 ft/yr; and (3) simulated drawdowns of greater than 1 ft propagated outside of Spring and Snake Valleys after 200 years of pumping in all scenarios.

3.4 Hydrogeologic Setting

The groundwater system in the study area consists of water in unconsolidated deposits in the basins as well as water in consolidated rock underlying the basins and in the adjacent mountain blocks. The consolidated rock and basin-fill aquifers are well connected hydraulically [*Gardner et al.*, 2011; *Sweetkind et al.*, 2011b], with most of the recharge occurring in the consolidated rock mountain blocks and most of the discharge occurring within the lower altitude basin-fill deposits.

Within the study area, groundwater divides do not coincide with surface-water divides in many areas. For example, along the western boundary, the groundwater divide diverges from the topographic/surface-water divide in the southern Snake Range, and actually occurs within the basin in southern Spring Valley [*Gardner et al.*, 2011]. Similarly, along the eastern portion of the study area, groundwater flow from the east, west, and south converges in the Tule Valley and Sevier Desert HAs, and flows north towards Fish Springs [*Gardner et al.*, 2011; *Gates*, 1987; *Prudic et al.*, 1995]. This is

characteristic of many areas within the Great Basin, where interbasin groundwater flow can occur between basins.

3.4.1 Hydrogeologic Framework

As part of the GBCAAS study, a three-dimensional hydrogeologic framework of the eastern Great Basin was constructed [*Cederberg et al.*, 2011; *Sweetkind et al.*, 2011a]. The GBCAAS study area is inclusive of the current study area; therefore, this same hydrogeologic framework, with a few refinements (discussed below) was used in the current study. The framework was constructed using data from a variety of sources, including geologic maps and cross-sections, drill-hole data, geophysical models, and stratigraphic surfaces created for other three-dimensional hydrogeologic frameworks within the GBCAAS study area. The framework was developed using a 1-mi^2 grid cell size.

In the hydrogeologic framework developed for the GBCAAS, the consolidated pre-Cenozoic rocks, Cenozoic sediments, and igneous rocks of the study area were subdivided into nine hydrogeologic units (HGUs) [*Sweetkind et al.*, 2011a]. An HGU has considerable lateral extent and reasonably distinct physical characteristics that may be used to infer the capacity of a sediment or rock to transmit water. The definition of HGUs is important in conceptualizing the hydrogeologic system, construction of a geologic framework for describing the groundwater-flow system, and use in numerical groundwater-flow models.

Of the nine HGUs defined in the hydrogeologic framework developed for the GBCAAS, seven exist in the current study area (Figures 3-2 and 3-3). The HGUs that exist in the current study area are: (1) a non-carbonate confining unit (NCCU)

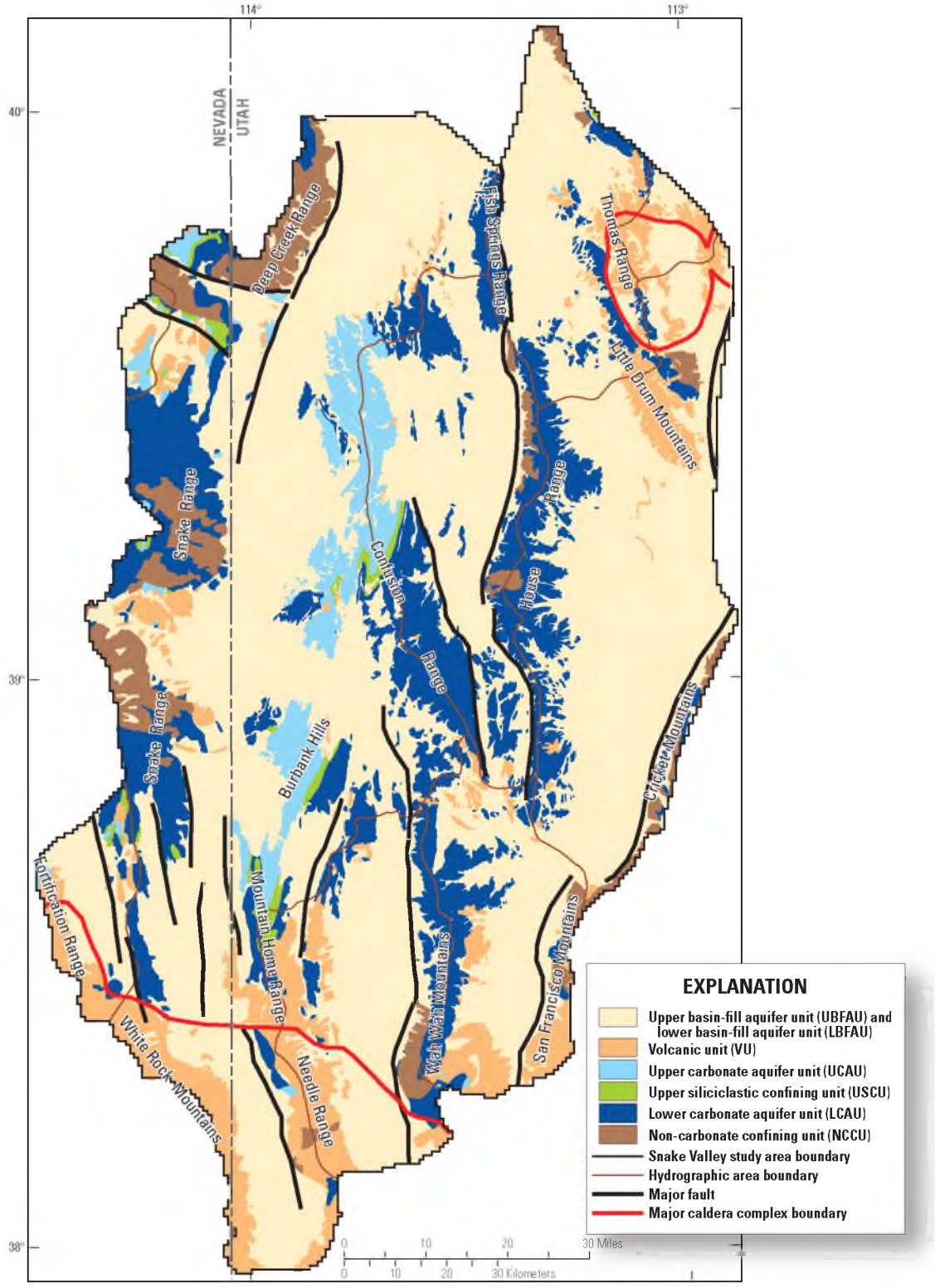

Figure 3-2. Surficial extent of hydrogeologic units and prominent structural geologic features in the Snake Valley study area. State boundary data from: *U.S. Census Bureau* [2000]. Modified from: *Sweetkind et al.* [2011a] and *Masbruch et al.* [201X], in review.

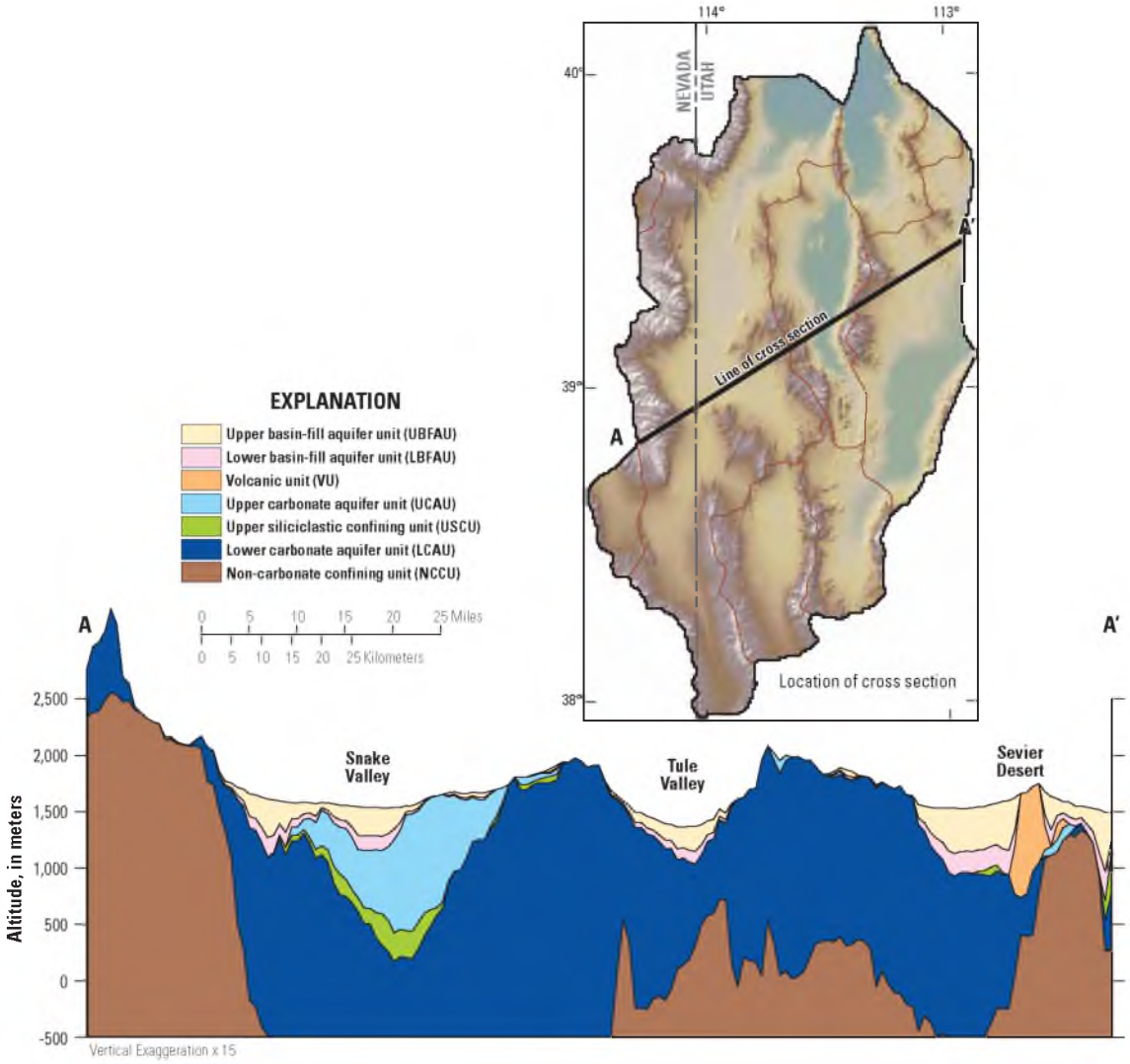

Figure 3-3. Example cross section across the study area showing hydrogeologic units. Data from: *Sweetkind et al.* [2011a]. Modified from: *Masbruch et al.* [201X], in review.

representing low- to moderate-permeability Precambrian siliciclastic formations as well as intrusive igneous rocks that are locally exposed in mountain ranges, and underlies portions of the study area; (2) a lower carbonate aquifer unit (LCAU) representing a thick succession of predominantly high- to moderate-permeability Cambrian through Devonian carbonate rocks that are locally exposed in the mountain ranges, and present beneath most of the valleys within the study area; (3) an upper siliciclastic confining unit (USCU) representing low-permeability Mississippian siliciclastic rocks, predominantly shales, that are limited in extent; (4) an upper carbonate aquifer unit (UCAU) representing a thick succession of low- to high-permeability Pennsylvanian and Permian carbonate rocks that are locally exposed in the mountain ranges and exist beneath some of the valleys within the study; (5) a volcanic unit (VU) representing large volumes of low- to high-permeability Cenozoic volcanic rocks that are locally exposed in the mountain ranges and exist beneath some of the valleys within the study; (6) a lower basin-fill aquifer unit (LBFAU) representing the deepest one-third of the Cenozoic basin fill and consists of moderate- to high-permeability volcanic rocks buried within the basin fill and consolidated older basin-fill sediments; and (7) an upper basin-fill aquifer unit (UBFAU) representing the shallowest two-thirds of the Cenozoic basin fill and includes a wide variety of low- to moderate-permeability basin-fill sediments [*Sweetkind et al.*, 2011a].

After the construction of the GBCAAS hydrogeologic framework, lithologic information from newly installed wells in Snake Valley and adjacent areas, as part of the Utah Geological Survey's (UGS) Snake Valley groundwater monitoring-well project, was used to refine the hydrogeologic framework in the study area. The following changes were made to the GBCAAS framework (*D. Sweetkind, USGS, written commun.*, July,

2010).

1. At UGS well PW04B (USGS site number: 383452114023402), located in volcanics on the east side of Hamlin (southern Snake) Valley, the UGS well intercepted the volcanics (VU) at a depth consistent with the GBCAAS framework altitude. The UGS well, however, was still in volcanics at a depth of 299 m (980 ft), whereas in the GBCAAS framework, the altitude of the contact between VU and UCAU was at a depth of only 97 m (318 ft). The top altitude of all Paleozoic units (UCAU, USCU, LCAU, and NCCU), therefore, was adjusted down by approximately 250 m (820 ft) in this area; for example, the top of UCAU was adjusted from an altitude of 1,793 m (5,883 ft) to 1,543 m (5,063 ft). Altitudes for all HGUs in a 3-by-5 grid cell area around the well bore were adjusted by hand to smooth out this correction.
2. At UGS well PW02B (USGS site number: 384651114025102), located in carbonates (UCAU) just north of Needle Point Spring in southern Snake Valley, the UGS well hit UCAU at 6.7 m (22 ft) depth. The GBCAAS framework, however, had the top of UCAU at 181 m (594 ft) depth. The framework in this area was adjusted by raising the top of UCAU by 175 m (574 ft), thereby thickening the unit. This adjustment was carried northward in three grid cells, which essentially defines the structural culmination of the Needle Point Anticline in this area.
3. At UGS well PW07B (USGS site number: 390143113533002), located in basin-fill deposits south of Eskdale in Snake Valley, the UGS well bottomed in basin-fill (UBFAU/LBFAU) at an elevation of 1,105 m (3,625 ft). The

GBCAAS framework, however, had the base of the basin-fill units at an altitude of 1,254 m (4,114 ft). The framework in this area was adjusted by lowering the bottom of the basin-fill units (LBFAU) by 200 m (656 ft). The tops of the underlying Paleozoic carbonate units (UCAU, USCU, LCAU, and NCCU) were not adjusted; therefore, the UCAU in this area was thinned by 200 m (656 ft). This adjustment was made for three grid cells in this area.

4. At UGS well PW19C (USGS site number: 393803113161602), located in carbonates in southern Fish Springs Flat, the UGS well intercepted Cambrian limestone (LCAU) at a depth consistent with the GBCAAS framework altitude. The GBCAAS framework, however, had a relatively broad area in northeastern Tule Valley and in southwestern Fish Springs Flat where LCAU had zero thickness. The framework in this area was adjusted by lowering the altitude of the top of the NCCU by 500 m (1,640 ft), thereby increasing the thickness of LCAU to 500 m (1,640 ft). This increased thickness of LCAU is based on the exposed thickness of Cambrian limestone in the House Range between Fish Springs Flat and Tule Valley.

3.4.2 Hydrogeologic Unit Hydraulic Properties

Hydraulic properties describe the ability of a groundwater system to transmit and store water. The distribution of these properties in the study area is variable and depends on the depositional environment of sediments in the basin-fill aquifer and confining units and on the degree of structural deformation, fracturing, and/or chemical dissolution in the bedrock aquifers and confining units.

Sweetkind et al. [2011a] estimated thickness and hydraulic properties of the HGUs in the GBCAAS study area (Table 3-1). These were taken from studies by *Belcher et al.* [2001; 2002] that analyzed and compiled estimates of transmissivity, hydraulic conductivity, storage coefficients, and anisotropy ratios for HGUs within the Death Valley regional groundwater flow system.

Additionally, the USGS Nevada Water Science Center (NVWSC) has conducted seven recent aquifer tests in Snake and Spring Valleys. These include both single and multiple pumping well tests, in the basin-fill and carbonate aquifers. The tests were also analyzed by a variety of methods including Cooper-Jacob analysis and three-dimensional numerical simulations (*http://nevada.usgs.gov/water/AquiferTests/aqtests.htm*, accessed on 9/4/2012). Results from these aquifer tests are summarized in Table 3-2.

3.4.3 Occurrence and Movement of Groundwater

Groundwater recharge occurs mostly from the infiltration of precipitation at higher altitudes [*Masbruch et al.*, 2011; *San Juan et al.*, 2010; *Welch et al.*, 2007]. Much of this recharge occurs in the form of snowmelt. Additional, but limited recharge occurs from the infiltration of runoff from precipitation near the mountain front, and infiltration along stream channels [*Flint and Flint*, 2007a; 2007b; *Flint et al.*, 2011; *Hevesi et al.*, 2003; *Masbruch et al.*, 2011]. There may also be recharge from applied irrigation; it is believed, however, that most of this applied water evaporates or is consumptively used by crops before reaching the water table. Groundwater moves from areas of recharge to springs and streams in the mountains; and to evapotranspiration areas, springs, and wells in the basins.

Table 3-1. Hydraulic properties of hydrogeologic units from the Great Basin carbonate and alluvial aquifer system study area. Data from: *Belcher et al.* [2001, 2002] and *Sweetkind et al.* [2011a]. Modified from: *Masbruch et al.* [201X], in review.

[**Abbreviations:** >, greater than; NC, not calculated; UBFAU, upper basin-fill aquifer unit; LBFAU, lower basin-fill aquifer unit; LCAU, lower carbonate aquifer unit; NCCU, non-carbonate confining unit; UCAU, upper carbonate aquifer unit; USCU, upper siliciclastic confining unit; VU, volcanic unit]

Major hydrogeologic unit	Hydrogeologic unit abbreviation	Maximum unit thickness (meters)	Hydraulic conductivity (meters per day)			
			Arithmetic mean	Geometric mean	Minimum	Maximum
Cenozoic basin-fill sediments	UBFAU and LBFAU	11,000	9	1	0.00003	131
Cenozoic volcanic rock	VU	1,000 (>3,900 in calderas)	6	0.9	0.01	55
Upper Paleozoic carbonate rock	UCAU	7,300	19	0.1	0.00009	319
Upper Paleozoic siliciclastic confining rock	USCU	>1,500	0.1	0.02	0.00003	0.9
Lower Paleozoic carbonate rock	LCAU	5,000	52	1	0.003	824
Non-carbonate confining rock	NCCU	NC	0.2	0.002	0.00000002	5

Table 3-2. Summary of estimates of aquifer properties from results of aquifer tests in Spring and Snake Valleys. Modified from: *Masbruch et al.* [201X], in review.

[Data from *http://nevada.usgs.gov/water/AquiferTests/aqtests.htm* accessed on 9/4/2012. **Abbreviations:** NR, not reported; NC, not calculated; 3-D, three-dimensional]

Well	Primary Aquifer	Thickness (meters)	Average hydraulic conductivity (meters per day)	Average transmissivity (square meters per day)	Type	Analysis method
(C-20-19)19dcd-1	Alluvial fill	610	0.6	680	Multiple-well pumping	3-D, numerical model
NDOW Well	Alluvial fill	NR	NC	28	Single-well pumping	Cooper-Jacob
Baker Creek	Alluvial fill	NR	8.1	84	Multiple-well pumping	3-D, numerical model
Big Springs NW	Alluvial fill	NR	NC	930	Single-well pumping	Cooper-Jacob
Big Springs SW	Carbonate rocks	NR	NC	370	Single-well pumping	Cooper-Jacob
Needle Point	Carbonate rocks	305	11.0	1,070	Multiple-well pumping	3-D, numerical model
184W101	Carbonate rocks	610	1.6	970	Multiple-well pumping	3-D, numerical model

As part of this study, *Gardner et al.* [2011] published a potentiometric map of Snake Valley and the surrounding areas in the southern Great Salt Lake Desert groundwater flow system. This map presents contours based on water levels measured during the spring of 2010 from 190 wells finished in consolidated rock and basin fill. The water-level contours are used to refine conceptual pathways of intrabasin and interbasin groundwater flow. Evaluation of vertical and horizontal hydraulic gradients indicates that: (1) aquifers within the consolidated rock and unconsolidated basin fill are generally hydraulically well connected, and often act as a single aquifer unit; (2) a groundwater divide exists in southern Spring Valley where groundwater moving from the mountainous recharge areas on both sides of the valley diverges toward the north and south; (3) groundwater flow in Snake Valley is primarily north-northeastward, and eastward interbasin flow out of Snake Valley may be restricted by steeply dipping, northeast trending, siliciclastic rocks extending from the Mountain Home Range as far north as the Confusion Range (Figure 3-2); (4) groundwater flow is generally northward through Pine and Wah Wah Valleys, and westward through Sevier Desert toward Tule Valley where a nearly flat hydraulic gradient exists for more than 80 km (50 miles) from south to north; more recently collected water-level data in Pine Valley, however, indicates that groundwater in Pine Valley may follow a more easterly direction (*P. Gardner, oral commun.*, March 2012); and (5) there is some groundwater flow out of the study area towards the Great Salt Lake Desert to the north and west from Snake Valley and Fish Springs Flat.

3.4.4 Conceptual Groundwater Budget

Development of a groundwater budget is important in understanding the occurrence and movement of groundwater in the flow system, and in evaluating the balance between flow into and flow out of the system. The primary components of the groundwater budget are: recharge from precipitation (including direct infiltration and infiltration of runoff at lower elevations), infiltration of mountain stream baseflow, and infiltration of unconsumed irrigation; and discharge to evapotranspiration (ETg), springs, mountain streams, and well withdrawals. Recharge or discharge as subsurface (lateral) flow into or out of an HA or the study area across its boundary may also be occurring.

The current study considers all forms of recharge to and discharge from the groundwater system, including the surrounding mountains. This is illustrated by considering the fate of recharge from direct infiltration of mountain precipitation and subsurface inflow from adjacent areas to permeable consolidated rock of the mountain block (R1 and R3 of Figure 3-4). Part of this recharge moves directly through the subsurface from the mountain block into the adjacent unconsolidated basin fill. Another part of this recharge becomes groundwater discharge to mountain streams and springs (D1 of Figure 3-4). A fraction of this mountain-block groundwater discharge is consumptively lost as evapotranspiration, both in the mountains and as this water enters the valley in streams; a fraction of the remaining water in the streams, combined with surface-water runoff becomes recharge to the unconsolidated basin fill (R2 of Figure 3-4). This water ultimately discharges in the valley lowlands as evapotranspiration or to basin-fill springs (D2 and D3 of Figure 3-4), well withdrawals (D4 of Figure 3-4) or subsurface outflow (D5 of Figure 3-4).

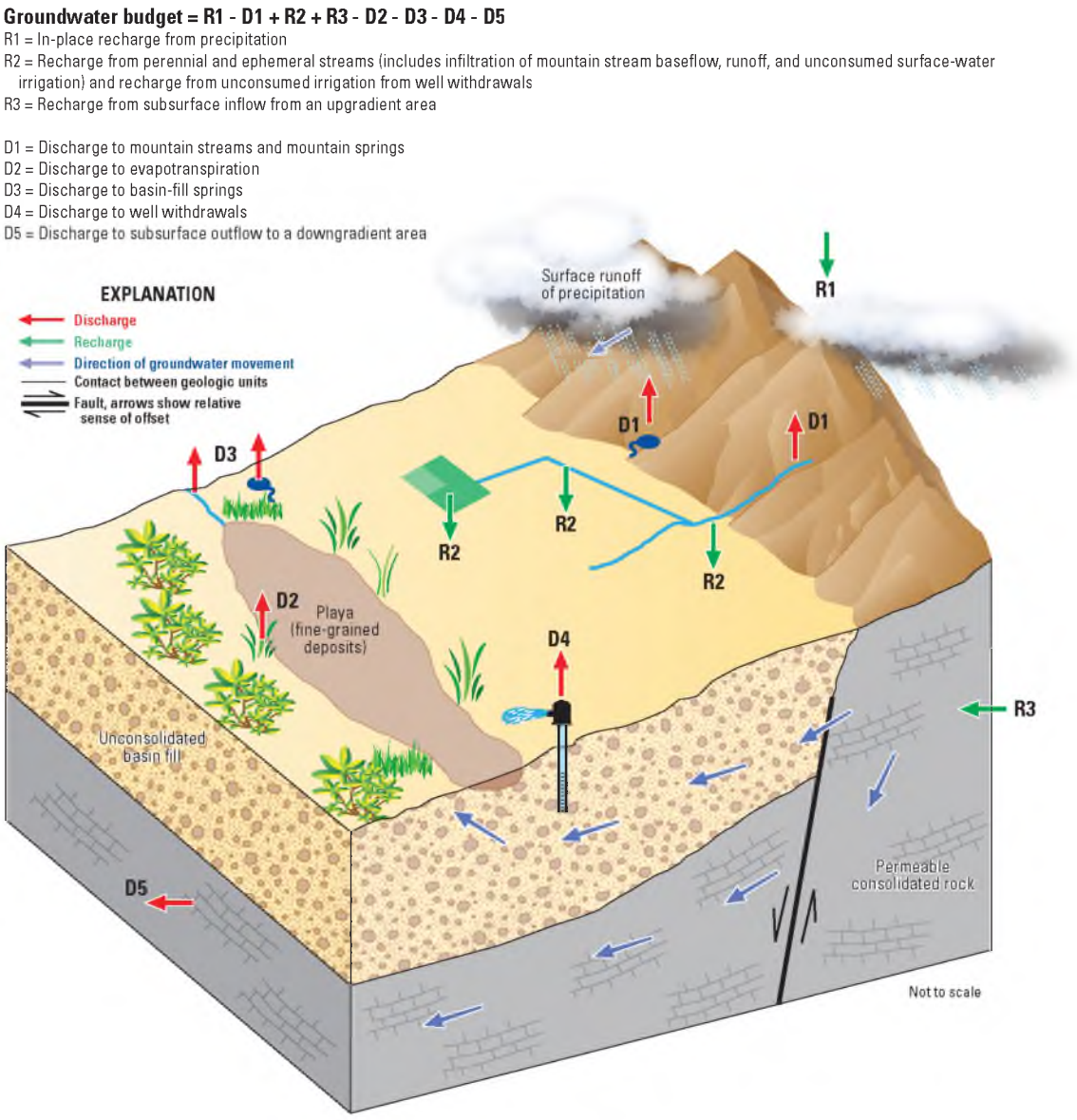

Figure 3-4. Schematic diagram showing conceptualization of groundwater-budget components and budget calculation for the Snake Valley study area. Modified from: *Masbruch et al.* [2011] and *Masbruch et al.* [201X], in review.

A conceptual groundwater budget for the current study was developed using estimates compiled from previous studies, as well as newer data that has been collected in the study area. Annual recharge and discharge have been previously estimated for portions of the study area and published in numerous reports (Table 3-3). Each of these reports provide estimates for some or all water-budget components within a portion of an HA, an entire HA, or multiple HAs. Many of these previous estimates were used in the current study groundwater budget as it was beyond the scope of the current study to make updated measurements of all of the primary components of the groundwater budget. This conceptual groundwater budget was then further tested using a numerical groundwater flow model (see "Regional Groundwater Budget" section under "Model Evaluation" in this chapter). Groundwater budgets for this study were developed at the HA and study area scales.

3.4.4.1 Recharge

Precipitation within the study area is the primary source of groundwater recharge. The majority of precipitation comes as winter snowfall on the mountain ranges, with lesser amounts falling as rain. Infiltration of precipitation and snowmelt within the mountain block provides (1) discharge to mountain springs and baseflow to mountain streams; (2) discharge to ETg, springs, and wells in the adjacent basin; and (3) flow which follows deeper and longer flow paths to regional discharge locations, including large springs and areas of ETg, in basins not adjacent to the mountain block. The majority of groundwater recharge within the study area occurs in the higher altitude mountain ranges as direct infiltration of precipitation (in-place recharge).

Table 3-3. Current study conceptual and ranges of previously reported groundwater budget estimates for hydrographic areas and the Snake Valley study area. Modified from: *Masbruch et al.* [201X], in review.

[All estimates in acre-feet per year rounded to two significant figures.
Abbreviations: HA, hydrographic area; —, no data; NE, not estimated]

	Conceptual	Previous studies
Spring Valley (HA 184)[1]		
Recharge		
Direct infiltraion of precipitation (in-place recharge)	15,000	
Infiltration of runoff (includes unconsumed surface-water irrigation)	930	—
Mountain stream baseflow	0	
Unconsumed irrigation from well withdrawals	0	—
Subsurface inflow	NE	—
Discharge		
Groundwater evapotranspiration + springs	0	—
Mountain streams	0	—
Well withdrawals	0	—
Subsurface outflow	NE	4,000 to 49,000[2,3,4,5,6,7,8]
Northern Spring Valley to Snake Valley	NE	16,000[5]
Southern Spring Valley to Snake Valley	NE	4,000 to 33,000[2,3,4,5,6,7,8]
Snake Valley (HA 254)		
Recharge		
Direct infiltraion of precipitation (in-place recharge)	150,000	
Infiltration of runoff (includes unconsumed surface-water irrigation)	6,900	99,000 to 160,000[2,3,5,9,10]
Mountain stream baseflow	360	
Unconsumed irrigation from well withdrawals	2,200[11]	3,300[12,13]
Subsurface inflow	NE	4,000 to 49,000[2,3,4,5,6,7,8]
From Northern Spring Valley	NE	16,000[5]
From Southern Spring Valley	NE	4,000 to 33,000[2,3,4,5,6,7,8]
Discharge		
Groundwater evapotranspiration + springs	120,000	64,000 to 130,000[2,3,5,14]
Mountain streams	3,600	2,800[14]
Well withdrawals	22,000[11]	11, 000[12,13]
Subsurface outflow	NE	25,000 to 43,000[2,3,4,5,7]
To Tule Valley	NE	15,000 to 42,000[2,3,4]
To Fish Springs Flat	NE	0[4]
To outside study area	NE	10,000 to 29,000[2,4,5]

Table 3-3. Continued

[All estimates in acre-feet per year rounded to two significant figures.
Abbreviations: HA, hydrographic area; —, no data; NE, not estimated]

	Conceptual	Previous studies
Pine Valley (HA 255)		
Recharge		
Direct infiltraion of precipitation (in-place recharge)	26,000	21,000 to 27,000[3,9,10,15]
Infiltration of runoff (includes unconsumed surface-water irrigation)	960	
Mountain stream baseflow	0	
Unconsumed irrigation from well withdrawals	0	—
Subsurface inflow	NE	—
Discharge		
Groundwater evapotranspiration + springs	0	0[3,14,15]
Mountain streams	0	0[3,14,15]
Well withdrawals	0	5[15]
Subsurface outflow	NE	3,000 to 14,000[3,4,15,17]
To Wah Wah Valley	NE	3,000 to 14,000[4,15,17]
To Tule Valley	NE	14,000[3]
Wah Wah Valley (HA 256)		
Recharge		
Direct infiltraion of precipitation (in-place recharge)	5,500	6,000 to 7,000[3,9,10,18]
Infiltration of runoff (includes unconsumed surface-water irrigation)	450	
Mountain stream baseflow	0	
Unconsumed irrigation from well withdrawals	0	—
Subsurface inflow	NE	3,000 to 14,000[4,15,17]
From Snake Valley	NE	—
From Pine Valley	NE	3,000 to 14,000[4,15,17]
Discharge		
Groundwater evapotranspiration + springs	740	1,400 to 1,500[3,14,17]
Mountain streams	0	0[3,14,17]
Well withdrawals	0	110[19]
Subsurface outflow	NE	8,500[3,4]
To Tule Valley	NE	8,500[3,4]

Table 3-3. Continued

[All estimates in acre-feet per year rounded to two significant figures.
Abbreviations: HA, hydrographic area; —, no data; NE, not estimated]

	Conceptual	Previous studies
Tule Valley (HA 257)		
Recharge		
Direct infiltraion of precipitation (in-place recharge)	13,000	7,600 to 13,000[3,9,10,18]
Infiltration of runoff (includes unconsumed surface-water irrigation)	320	
Mountain stream baseflow	0	
Unconsumed irrigation from well withdrawals	0	—
Subsurface inflow	NE	15,000 to 50,000[2,3,4,18,20]
From Snake Valley	NE	15,000 to 42,000[2,3,4]
From Wah Wah Valley	NE	8,500 to 32,000[3,4,18]
From Sevier Desert	NE	9,000[4]
Discharge		
Groundwater evapotranspiration + springs	39,000	24,000 to 56,000[3,14,18]
Mountain streams	0	0[3,14,18]
Well withdrawals	0	—
Subsurface outflow	NE	27,000 to 31,000[4,21]
To Fish Springs Flat	NE	27,000[4]
Fish Springs Flat (HA 258)		
Recharge		
Direct infiltraion of precipitation (in-place recharge)	1,500	1,600 to 4,000[3,9,10,21]
Infiltration of runoff (includes unconsumed surface-water irrigation)	150	
Mountain stream baseflow	0	
Unconsumed irrigation from well withdrawals	0	—
Subsurface inflow	NE	27,000 to 31,000[3,4,21]
From Snake Valley	NE	0[4]
From Tule Valley	NE	27,000[4]
From Sevier Desert	NE	0[4]
Discharge		
Groundwater evapotranspiration + springs	34,000	34,000 to 35,000[3,14,21]
Mountain streams	0	0[3,14,21]
Well withdrawals	0	—
Subsurface outflow	NE	100 to 1,000[3,4]
To outside study area	NE	1,000[4]

Table 3-3. Continued

[All estimates in acre-feet per year rounded to two significant figures.
Abbreviations: HA, hydrographic area; —, no data; NE, not estimated]

	Conceptual	Previous studies
Dugway-Government Creek Valley (HA 259)[1]		
Recharge		
Direct infiltraion of precipitation (in-place recharge)	200	—
Infiltration of runoff (includes unconsumed surface-water irrigation)	110	
Mountain stream baseflow	0	
Unconsumed irrigation from well withdrawals	0	—
Subsurface inflow	NE	—
Discharge		
Groundwater evapotranspiration + springs	0	—
Mountain streams	0	—
Well withdrawals	0	—
Subsurface outflow	NE	—
Sevier Desert (HA 287)[1]		
Recharge		
Direct infiltraion of precipitation (in-place recharge)	8,500	—
Infiltration of runoff (includes unconsumed surface-water irrigation)	1,600	
Mountain stream baseflow	0	
Unconsumed irrigation from well withdrawals	0	—
Subsurface inflow	NE	—
Discharge		
Groundwater evapotranspiration + springs	8,600	8,600[22]
Mountain streams	0	—
Well withdrawals	0	—
Subsurface outflow	NE	8,800 to 9,000[4,20]
To Tule Valley	NE	9,000[4]
To Fish Srings Flat	NE	0[4]

Table 3-3. Continued

[All estimates in acre-feet per year rounded to two significant figures.
Abbreviations: HA, hydrographic area; —, no data; NE, not estimated]

	Conceptual	Previous studies
Study area total		
Recharge		
Direct infiltraion of precipitation (in-place recharge)	220,000	—
Infiltration of runoff (includes unconsumed surface-water irrigation)	11,000	
Mountain stream baseflow	360	
Unconsumed irrigation from well withdrawals	2,200	—
Subsurface inflow	NE	—
Discharge		
Groundwater evapotranspiration + springs	200,000	—
Mountain streams	3,600	—
Well withdrawals	22,000	—
Subsurface outflow	NE	—

[1]Partial HA; estimates only for portion of HA within study area.
[2]*Hood and Rush* [1965].
[3]*Gates and Kruer* [1981].
[4]*Harrill et al.* [1988].
[5]*Welch et al.* [2007].
[6]*Rush and Kazmi* [1965].
[7]*Scott et al.* [1971].
[8]*Nichols* [2000].
[9]*Harrill and Prudic* [1998].
[10]*Masbruch* [2011a].
[11]Estimate for the year 2009.
[12]*Masbruch* [2011b].
[13]Estimate for the year 2000.
[14]*Masbruch* [2011c].
[15]*Stephens* [1976].
[16]Estimate for the year 1976.
[17]*Stephens* [1974].
[18]*Stephens* [1977].
[19]Estimate for the year 1974.
[20]*Holmes* [1984].
[21]*Bolke and Sumsion* [1978].
[22]*Wilberg* [1991].

During the 1960s and 1970s, the USGS, in cooperation with the States of Utah and Nevada, completed a series of reconnaissance studies to evaluate the groundwater resources in these states. Generally, these studies developed groundwater budgets focused on the basin-fill (valley) portion of each HA, where groundwater was being developed as a resource. Estimates of recharge from precipitation presented in these reports were based on a method developed by *Maxey and Eakin* [1949], which was calibrated to estimate groundwater discharge in the valleys, and provided estimates of "net" recharge to the unconsolidated basin-fill aquifer based on precipitation zones. These earlier methods did not consider groundwater discharge within the mountain block such as stream baseflow and spring discharge, nor the subsequent recharge of a portion of this water as infiltration of runoff to unconsolidated basin-fill deposits.

In recent years, a new class of spatially distributed recharge estimation techniques utilizing water-balance methods has been developed that provide estimates for "total" recharge from precipitation in a watershed or HA [*Flint and Flint*, 2007a; 2007b; *Flint et al.*, 2011; *Hevesi et al.*, 2003; *Leavesley et al.*, 1983; *Masbruch et al.*, 2011]. Since these newer estimates include the partial loss of in-place recharge as groundwater discharge in the mountains to streams and springs, not considered in the earlier Maxey-Eakin method of estimating recharge, these newer spatially distributed recharge methods often yield higher recharge estimates than the previous Maxey-Eakin type of recharge estimates. Consequently, these newer spatially distributed recharge estimates may cause over-appropriations of water rights if the consumptive losses of groundwater discharge in the mountains are not also considered.

3.4.4.1.1 Precipitation

A regional-scale water-balance method, known as the Basin Characterization Model (BCM) [*Flint and Flint*, 2007a] developed for the GBCAAS study, was used to provide estimates of annual recharge from direct infiltration of precipitation (in-place recharge) and runoff. The BCM is a distributed-parameter water-balance accounting model used to identify areas having climatic and geologic conditions that allow for precipitation to become potential in-place recharge or runoff, and to provide estimates of each [*Flint et al.*, 2011; *Masbruch et al.*, 2011]. BCM in-place recharge is calculated as the volume of water per time that percolates through the soil zone past the root zone and becomes net infiltration to consolidated rock or unconsolidated deposits. Runoff is the volume of water per time that runs off the surface, and may infiltrate the subsurface, undergo evapotranspiration further downslope, or becomes streamflow which can, in turn, recharge the unconsolidated deposits from infiltration beneath the stream channels, irrigation canals, and/or fields irrigated with surface water [*Masbruch et al.*, 2011]. The BCM does not track or route runoff. For a more complete description of the BCM developed for the GBCAAS study see *Flint et al.* [2011] and *Masbruch et al.* [2011].

Streamflow at the mountain front also includes baseflow. This water originates as in-place recharge in the mountains and then discharges to mountain streams. Similar to runoff, a portion of this baseflow subsequently recharges the basin-fill deposits as infiltration beneath stream channels, irrigation canals, or fields irrigated with surface water [*Masbruch et al.*, 2011].

Total groundwater recharge from precipitation is calculated as the sum of the BCM in-place recharge, recharge from runoff that infiltrates the subsurface, and a

fraction of mountain stream baseflow that also infiltrates the subsurface. In-place recharge is calculated at the the location as it occurs in the BCM. Because BCM does not route runoff, runoff that originates at higher altitudes was redistributed to areas along the mountain front that contain unconsolidated basin fill material with a slope of 5 to 10 percent; in this way, recharge from upland runoff was accounted for where the streams enter the valleys. The amount of runoff that infiltrates the subsurface is typically calculated as a percentage of the total BCM runoff. For this study, it was assumed that 10 percent of the total runoff infiltrates the subsurface [*Masbruch et al.*, 2011]; this includes recharge from the infiltration of unconsumed surface-water irrigation. Likewise, it was also assumed that 10 percent of the mountain stream baseflow infiltrates the subsurface and becomes recharge [*Masbruch et al.*, 2011] and this recharge is also distributed in areas along the mountain front that contain unconsolidated basin fill material with a slope of 5 to 10 percent. The other 90 percent of runoff and mountain stream baseflow is assumed to be consumptively lost to evapotranspiration before it can infiltrate into the aquifer [*Hevesi et al.*, 2003; *Masbruch et al.*, 2011; *San Juan et al.*, 2010]. Estimates of recharge from precipitation (in-place recharge+recharge from runoff (including unconsumed surface-water irrigation)+recharge from mountain stream baseflow) for each HA and the study area are given in Table 3-3 and conceptual recharge rates area shown in Figure 3-5.

3.4.4.1.2 Unconsumed Irrigation From Well Withdrawals

Most well withdrawals in the study area are used for irrigation, and these wells are located exclusively within Snake Valley. It is assumed that part of this groundwater recharges the aquifer system as infiltration of unconsumed irrigation water applied to

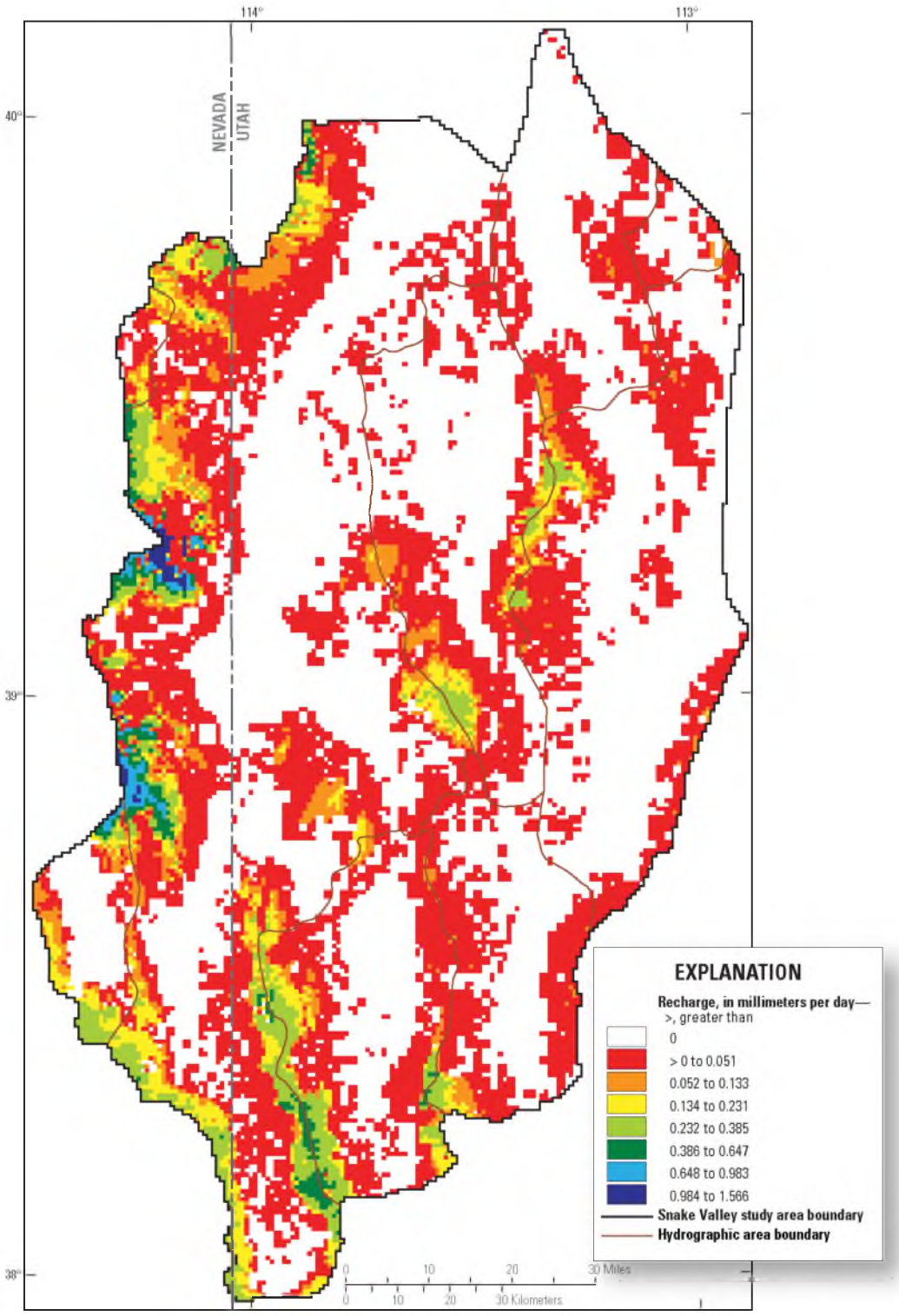

Figure 3-5. Conceptual rate of recharge from precipitation (in-place recharge+recharge from runoff (including unconsumed surface-water irrigation)+recharge from mountain stream baseflow) in the Snake Valley study area. State boundary data from: *U.S. Census Bureau* [2000]. Modified from: *Masbruch et al.* [201X], in review.

fields. Irrigation return flow studies in the Amargosa Desert, CA [*Stonestrom et al.*, 2003] and the Milford Area, UT [*Susong*, 1995] show that recharge from irrigation on sprinkler-irrigated fields ranges from 8 to 16 percent of the applied irrigation. Because most of the fields in Snake Valley are sprinkler irrigated, it was assumed that 10 percent of the applied irrigation groundwater recharged back into the aquifer system (Table 3-3).

3.4.4.1.3 Subsurface Inflow

The potentiometric-surface map for the study area [*Gardner et al.*, 2011] indicates that groundwater may enter and leave the study area via subsurface inflow and outflow along some parts of the study-area boundary. Subsurface flow may also occur between HAs within the study area. Previous studies have estimated subsurface flow by a variety of methods, and with little to no indication of the uncertainties on these estimates. These estimates can vary widely due to the differences in the methods used to calculate them (Table 3-3). Rather than predefining a conceptual estimate of subsurface flow, the calibrated groundwater flow model developed in this study was used to estimate subsurface inflow into the study area and between HAs within the study area. By allowing the groundwater model to predict estimates of subsurface flow, uncertainties on this estimate could be calculated. These estimates and associated uncertainties are discussed in the "Regional Groundwater Budget" section under "Model Evaluation" in this chapter.

3.4.4.2 Discharge

Discharge from the groundwater system occurs by evapotranspiration (ETg), as discharge to springs, as discharge to mountain streams (baseflow), as well withdrawals,

and subsurface outflow to neighboring basins (Figure 3-6). The majority of discharge within the study area occurs as ETg.

3.4.4.2.1 Groundwater Evapotranspiration

Discharge to ETg (Table 3-3) is based on estimates from previous studies [*Bolke and Sumsion*, 1978; *Gates and Kruer*, 1981; *Stephens*, 1977; *Welch et al.*, 2007; *Wilberg*, 1991]. In these studies, ETg was estimated using a volumetric calculation of ETg from major areas of phreatophytic vegetation. In some studies, discharge to springs was indirectly accounted for in the ETg estimate as these studies assumed that all spring discharge from the basin fill was ultimately consumed through evapotranspiration.

For Snake Valley, the previously reported ETg [*Welch et al.*, 2007] was estimated for predevelopment conditions and includes discharge to springs; these contributing springs, however, were not identified in the report. In the current study, it was assumed that springs within 1 mile of an ETg area contributed to this previous ETg estimate. The previous ETg estimate for Snake Valley, therefore, was reduced by the amount of estimated spring discharge located within 1 mile of the ETg areas and this spring discharge was accounted for separately (see "Spring Discharge" section of this chapter). Additionally, in the current study, representative long-term well withdrawals within Snake Valley are also being simulated, so the amount of groundwater available for ETg is reduced compared to predevelopment conditions. Previously reported ETg for Snake Valley, therefore, was further reduced by an amount equaling 90 percent of the total well withdrawals within each area (excluding the 10 percent that is assumed to recharge the aquifer from irrigation return flow).

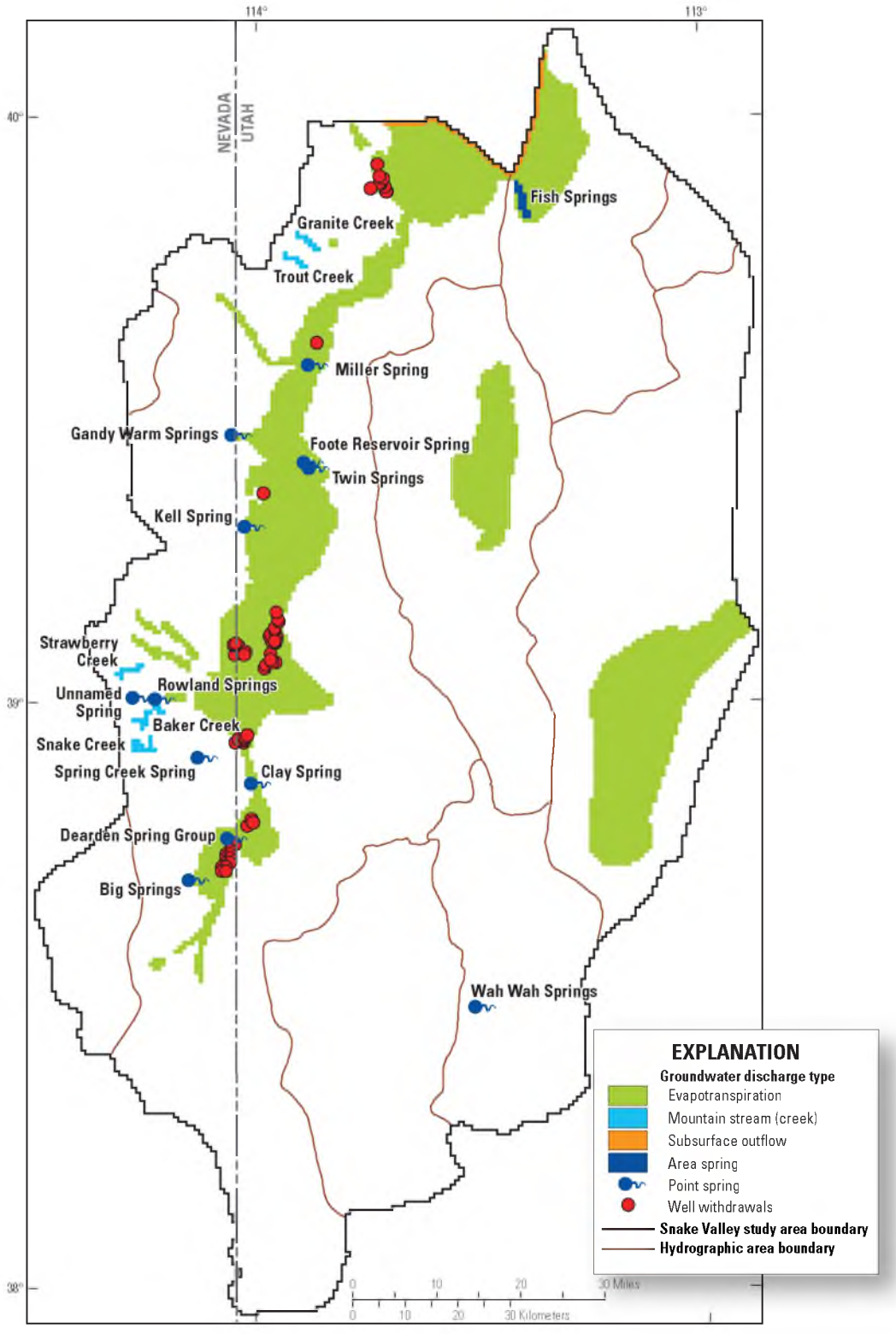

Figure 3-6. Locations and types of discharge in the Snake Valley study area. State boundary data from: *U.S. Census Bureau* [2000]. Modified from: *Masbruch et al.* [201X], in review.

3.4.4.2.2 Spring Discharge

Groundwater discharge to springs (Table 3-3) is based on estimates from previous studies [*Bolke and Sumsion*, 1978; *Elliott et al.*, 2006; *Hood and Rush*, 1965; *Stephens*, 1974], data from the USGS's National Water Information Systems (NWIS) database [*Mathey*, 1998], or data collected by the UGS as part of their Snake Valley groundwater monitoring project [*L. Jordan, Utah Geological Survey, written commun.*, August, 2010]. The majority of these springs are located in Snake Valley except for Wah Wah Springs, which is located in Wah Wah Valley, and Fish Springs, an area spring which is located in Fish Springs Flat (Figure 3-6).

3.4.4.2.3 Baseflow to Mountain Streams

Groundwater discharge that provides baseflow to mountain streams (Table 3-3) is based on estimates from previous studies [*Elliott et al.*, 2006; *Masbruch et al.*, 2011]. There are five perennial mountain streams within the study area that had been previously measured: Granite and Trout Creeks on the east side of the Deep Creek Range; and Strawberry, Baker, and Snake Creek on the east side of the southern Snake Range (Figure 3-6). These measurements are based on the minimum mean daily discharge or are instantaneous low-flow measurements and, therefore, represent the minimum amount of groundwater discharge to mountain streams. *Elliott et al.* [2006] also measured discharge in Lehman Creek and these measurements indicated that the majority of baseflow in Lehman Creek is supplied by Unnamed Spring and Rowland Spring. Because discharge to these springs is already accounted for in this study (see "Spring Discharge" section above) groundwater discharge to Lehman Creek, therefore, is not included in this estimate.

3.4.4.2.4 Well Withdrawals

Groundwater withdrawals in the study area are used for irrigation, industrial use, public and domestic supply, and stock watering. Significant groundwater withdrawal from wells only occurs in Snake Valley (Table 3-3). Annual withdrawals from pumped irrigation wells in the Utah portion of the valley (Figure 3-7) were estimated from flow measurements and corresponding power-consumption records for individual wells for the year 2009 as part of the state-wide groundwater use monitoring program [*Burden et al.*, 2010].

There are no historical estimates of well withdrawals for the Nevada side of the HA. Well withdrawals for a large number of center pivots just to the east of Big Spring in Nevada, therefore, were estimated by assuming one well per pivot (for a total of 11 wells), and withdrawals equaling an average irrigation application rate of 3 ft/yr [*Welch et al.*, 2007] applied over the surface area supplied by each pivot [*Welborn and Moreo*, 2007].

In recent years, well withdrawals for irrigation in the unconsolidated basin fill have increased, especially in the southern portion of Snake Valley. The source of water for these well withdrawals is partially from groundwater in storage, but is also from capturing of natural discharge. One such example of this is Needle Point Springs in southern Snake Valley, which was a watering source for stock and wild horses; water levels in the vicinity of the spring, however, have declined so that the spring is no longer flowing [*P. Summers, Bureau of Land Management, written commun.*, March 2013]. Increasing well withdrawals within Snake Valley will likely continue to affect the groundwater system by removing more groundwater from storage, resulting in decreasing

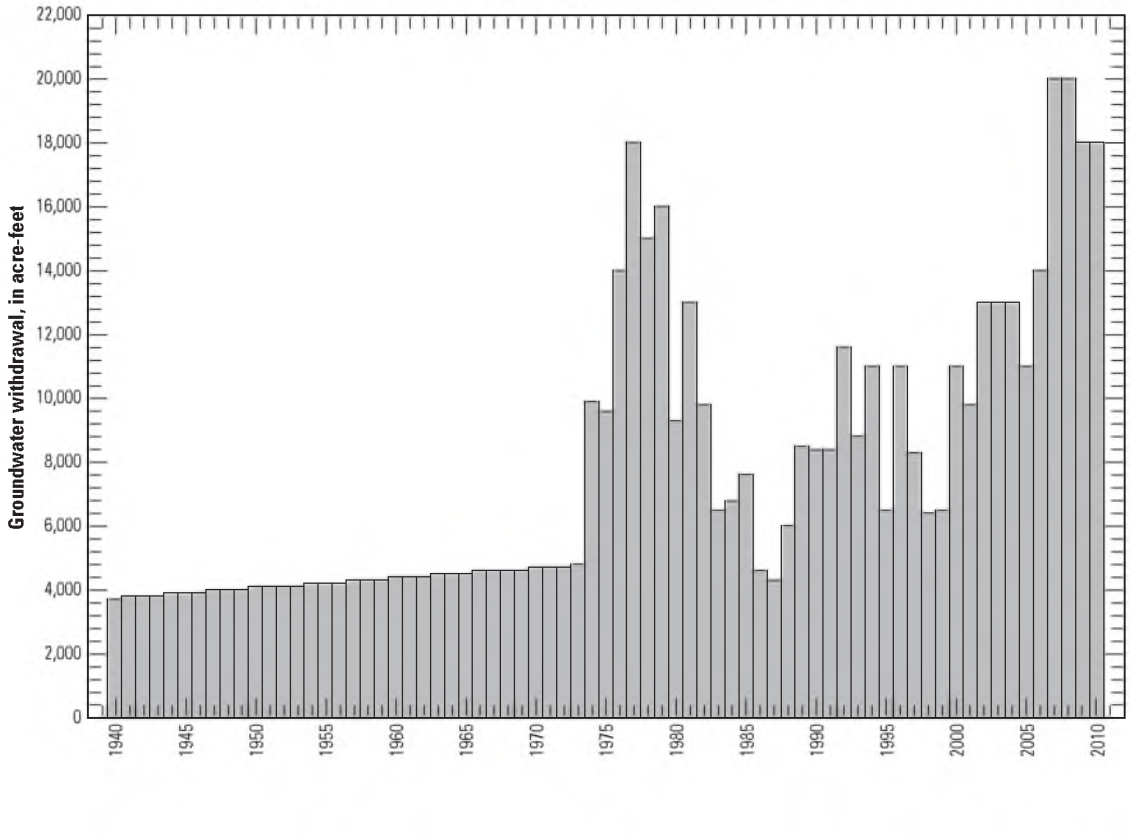

Figure 3-7. Estimated total annual groundwater withdrawals from wells in Snake Valley (Utah side only), 1940−2010. Data from: *Burden et al.* [2011] and *Heilweil and Brooks* [2011]. Modified from: *Masbruch et al.* [201X], in review.

groundwater levels, as well as leading to a decrease in natural discharge to springs and evapotranspiration within the basin.

3.4.4.2.5 Subsurface Outflow

Similar to subsurface inflow, subsurface outflow from the study area and between HAs within the study area was estimated using the calibrated groundwater flow model (see the "Subsurface Inflow" section). These estimates and associated uncertainties are discussed in the "Regional Groundwater Budget" section under "Model Evaluation" in this chapter.

3.4.5 Water-Level Fluctuations

Water levels in wells fluctuate in response to imbalances between groundwater recharge and discharge and are driven by both natural and anthropogenic processes. *Gardner et al.* [2011] present multiple-year water-level hydrographs for 32 wells completed in the basin fill in Snake Valley and the surrounding valleys showing that patterns of water-level fluctuation are distinctly different across the study area. Hydrographs from three of these wells (Figures 3-8 and 3-9) illustrates three types of water-level fluctuations that are characteristic of Snake Valley and the surrounding areas.

In the eastern half of the study area, including Tule Valley, Pine Valley, Wah Wah Valley, Fish Springs Flat, and Sevier Desert, water-level fluctuations are minimal, varying by less than about 2 ft over the period of record (for example, Figure 3-9, USGS site number 393933113214801). These steady water levels are likely due to a combination of low recharge rates in the nearby mountains and negligible groundwater pumping in these valleys.

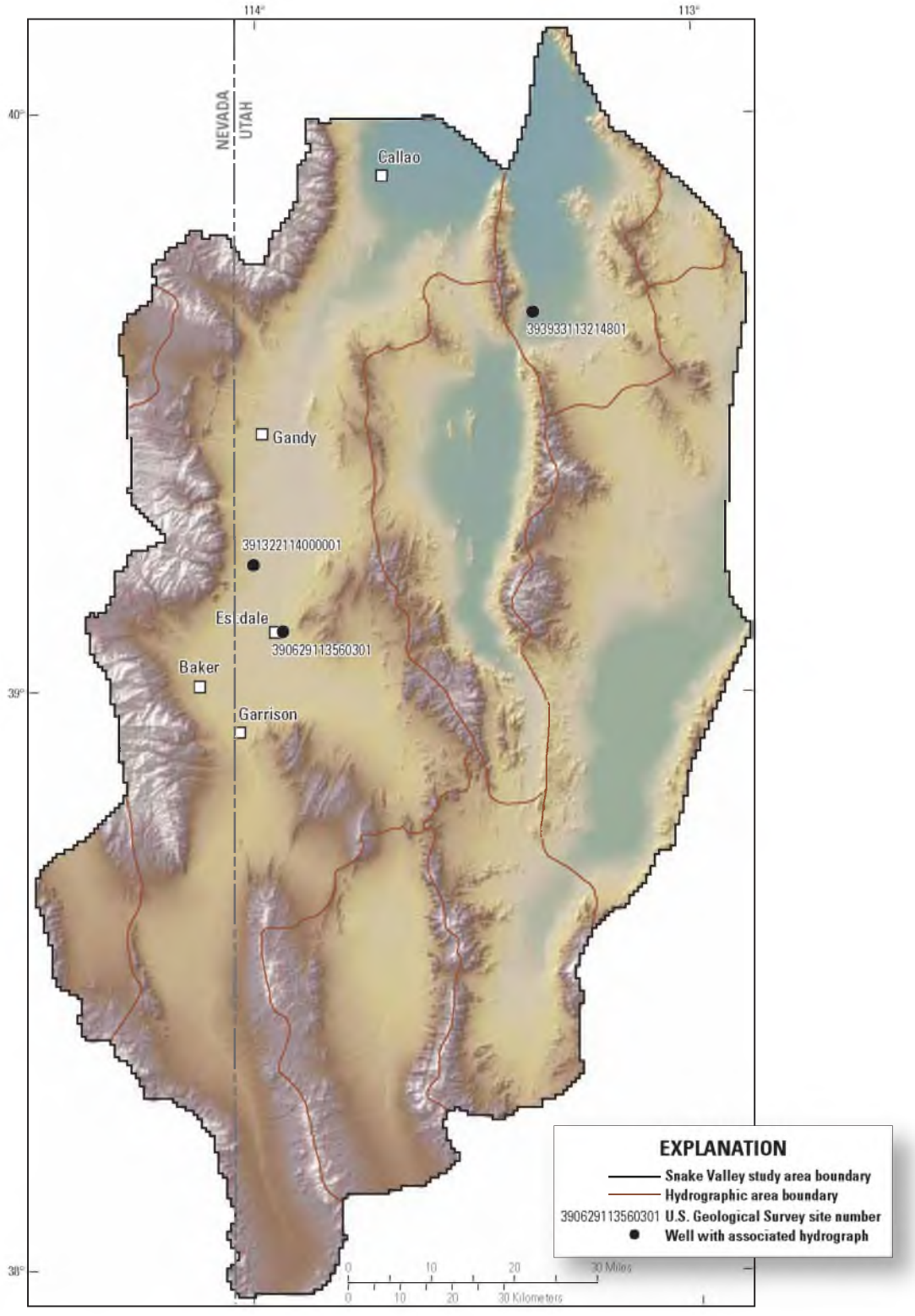

Figure 3-8. Location of three wells with multiple-year water-level records in the Snake Valley study area. State boundary data from: *U.S. Census Bureau* [2000]. Modified from: *Masbruch et al.* [201X], in review.

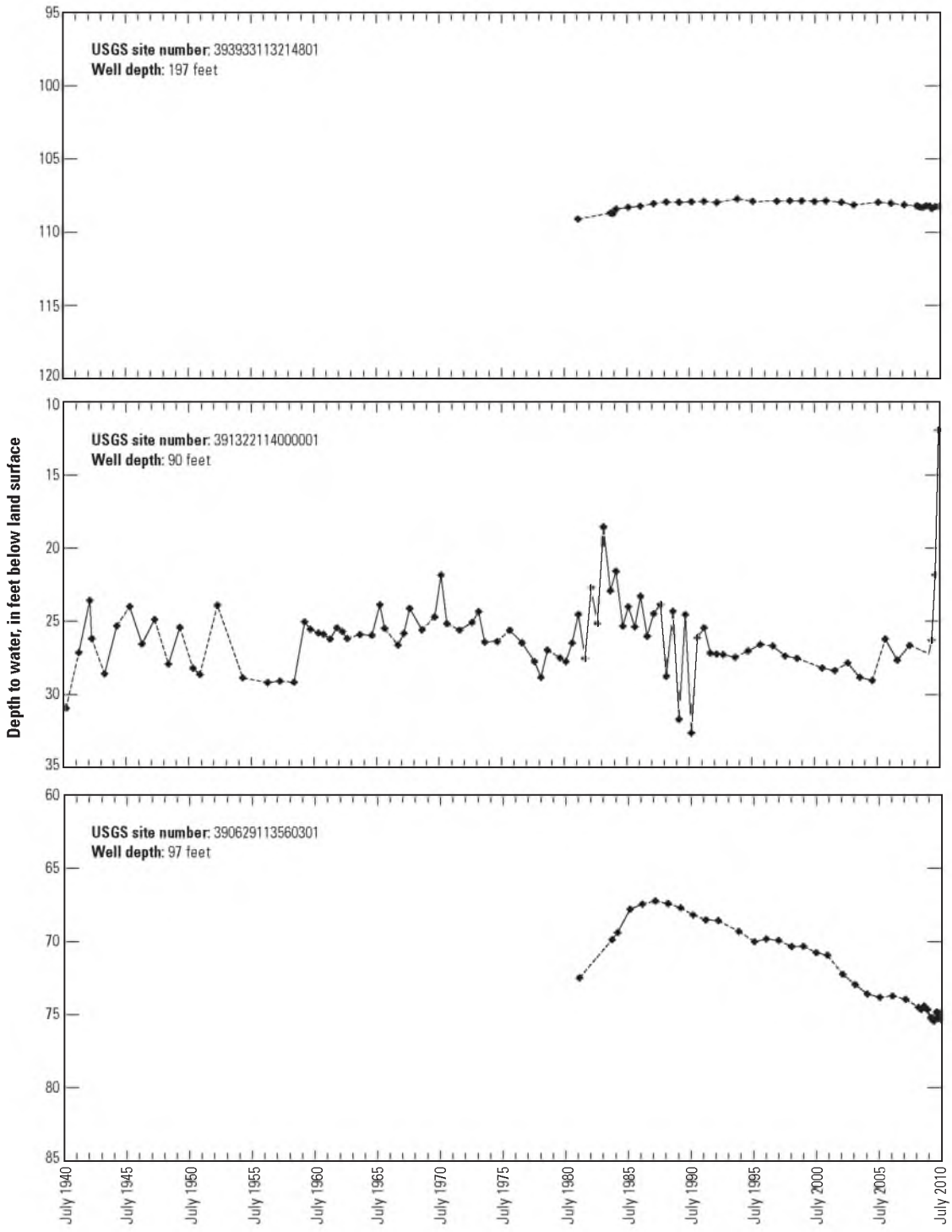

Figure 3-9. Multiple-year water-level hydrographs from three wells in the Snake Valley study area. Data available at: *http://nwis.usgs.gov*. Modified from: *Masbruch et al.* [201X], in review.

Conversely, water levels in wells in the western part of the study area, namely Spring Valley and Snake Valley, experience notably more fluctuation. Many of the wells in these valleys are located close to high-altitude mountain areas that receive substantial winter precipitation and groundwater recharge. Water levels in these wells clearly respond to annual recharge or to multiple-year periods of above- or below-average precipitation. Wells located close to the Snake and Deep Creek Ranges (for example, Figure 3-9, USGS site number 391322114000001) show water-level fluctuations of 10 to 20 ft over periods of only a few years. The sudden water level rise of nearly 15 ft seen at the end of the record in USGS site number 391322114000001 occurred between March and June of 2010, coincident with the timing of snowmelt.

Water levels in several wells located near agricultural pumping centers (for example, Figure 3-9, USGS site number 390629113560301) appear to be influenced by pumping. Water levels in these areas rose in response to a period of above-average precipitation during the mid-1980s [*Wilkowske et al.*, 2003] and most reached a maximum around the late 1980s to early 1990s. Since that time, water levels in these areas have fallen steadily and show little to no recovery during subsequent periods of above-average precipitation (for example, 1996–98 and 2004–05). These declines are most likely caused by groundwater withdrawal used for irrigation.

3.4.6 Groundwater Temperatures and Heat Flow

Within the Earth's crust, temperatures generally increase with depth (geothermal gradient). If groundwater flows are large enough, they will redistribute heat within the subsurface both vertically and laterally and alter the natural, conductive geothermal gradient of the area. These changes in the geothermal gradient and distribution of heat

flow, and associated groundwater temperatures, can be used to assess the magnitude of groundwater flow in an area [*Bredehoeft and Papadopulos*, 1965; *Cartwright*, 1970; *Manning and Solomon*, 2005; *Smith and Chapman*, 1983].

Figure 3-10 shows a conceptualization of how groundwater flow may perturb the conductive geothermal gradient and laterally redistribute heat in terrain with high topographic relief. In areas of groundwater recharge (A on Figure 3-10), groundwater temperatures tend to be cooler and will depress the natural (conductive) geothermal gradient as this cold water enters the subsurface. The amount of depression of the geothermal gradient is proportional to the velocity at which the groundwater is flowing. This produces an area of lower than expected heat flow at the surface. Essentially, in these areas, the groundwater is removing heat from the subsurface. As the groundwater moves laterally away from the recharge area, it carries this extra heat energy with it and begins to warm as it moves towards the discharge area (B on Figure 3-10). In areas of groundwater discharge (C on Figure 3-10), groundwater temperatures tend to be warmer and will raise the natural (conductive) geothermal gradient as warm water at depth is brought to the surface or as any heat that was removed in the recharge area is delivered to the discharge location. This produces an area of higher than expected heat flow at the surface.

Vertical temperature logs (temperature vs. depth) have recently been collected from 23 wells in the Snake Valley area [*Blackett*, 2011] as part of the UGS Snake Valley groundwater monitoring project. Temperatures in these wells were sampled at depths up to 500 m at intervals of 5 to 20 m using a high-precision thermistor probe and temperature-logging equipment [*Blackett*, 2011]. The thermistor was lowered into the

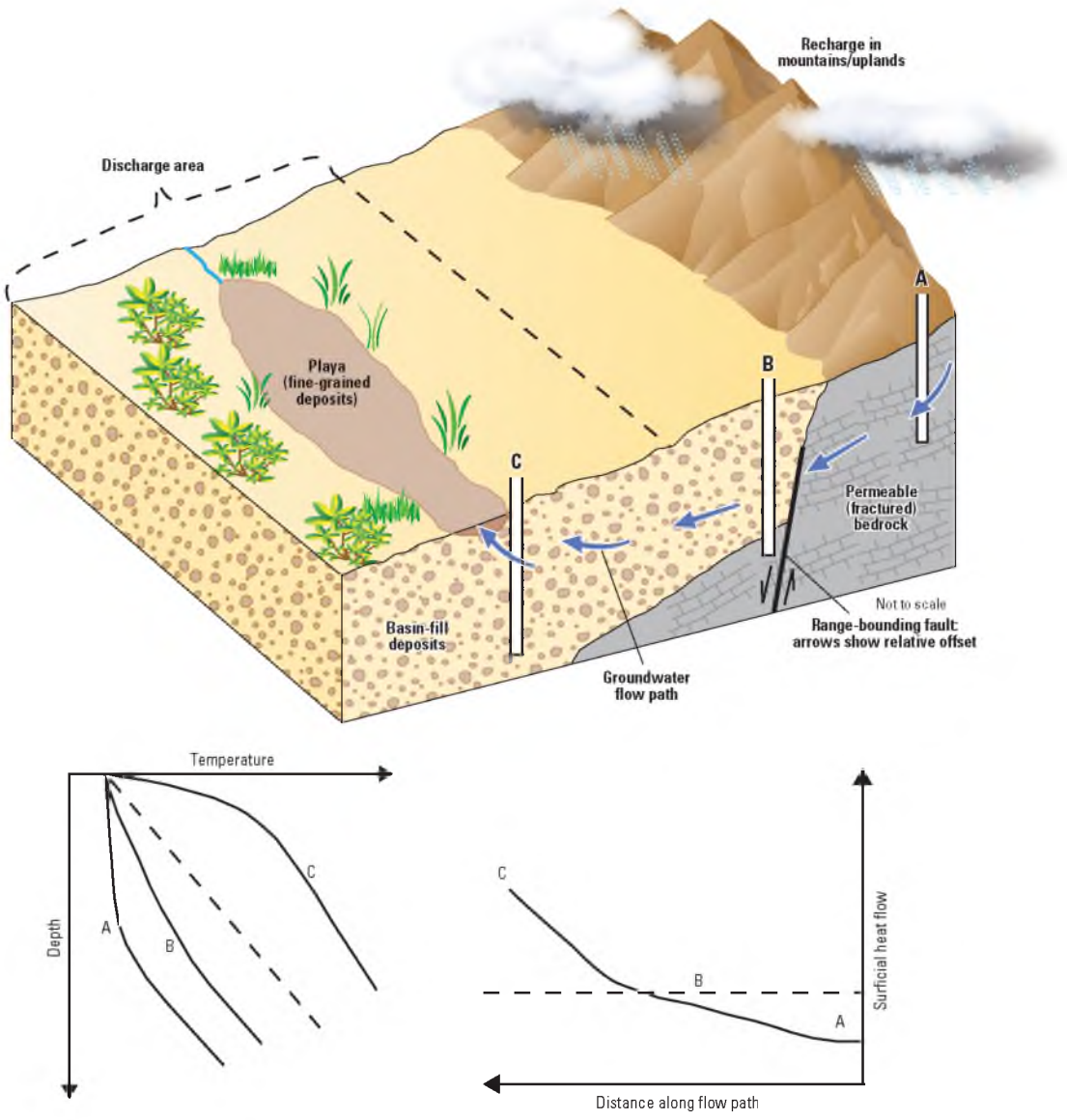

Figure 3-10. Schematic diagram showing conceptualization of how geothermal gradients and surficial-heat flow are affected by groundwater flow. Letters in bottom figures correspond to wells A, B, and C in top figure. Background Basin and Range geothermal gradients (30 °C/km) and heat flow (90 mW/m^2) are shown by dashed lines. Modified from: *Masbruch et al.* [2011] and *Masbruch et al.* [201X], in review.

well at regular depth intervals and temperature measurements at each depth were recorded once thermal equilibration was reached (typically 12 min for air, and less than 1 min for water). To ensure that temperatures were not being affected by local perturbations of flow due to well withdrawals, logs were only collected within wells that were not being actively pumped.

The temperature log data [*Blackett*, 2011] indicates an active groundwater flow system that is removing heat from the southern portion of the study area and potentially redistributing it to the northern portion of the study area. Typical conductive geothermal gradients for the Great Basin are approximately 30 °C/km, which correspond to heat flow values of approximately 90 mW/m^2. Figure 3-11 shows the distribution of thermal gradients [*Blackett*, 2011] below the water table calculated from the logged wells within the Snake Valley study area. Thermal gradients in the southern portion of Snake Valley are lower than typical Basin and Range geothermal gradients, with the majority ranging between 10 and 20° C/km, corresponding to heat flow values of 30 to 60 mW/m^2. In the northern portion of the study area thermal gradients are generally higher than typical Basin and Range geothermal gradients, with temperature logs from three wells indicating gradients between 44 and 86 °C/km, corresponding to heat flow values ranging between 132 and 258 mW/m^2. Shallow thermal gradients in a well near Fish Springs, a regional discharge location in the northern portion of the study area, are as high as 320 °C/km. Additionally, spring temperatures in the northern portion of Snake Valley and at Fish Springs are much higher than ambient surface temperatures of approximately 12 to 13 °C, suggesting that heat is being redistributed laterally or vertically to these discharge points as well.

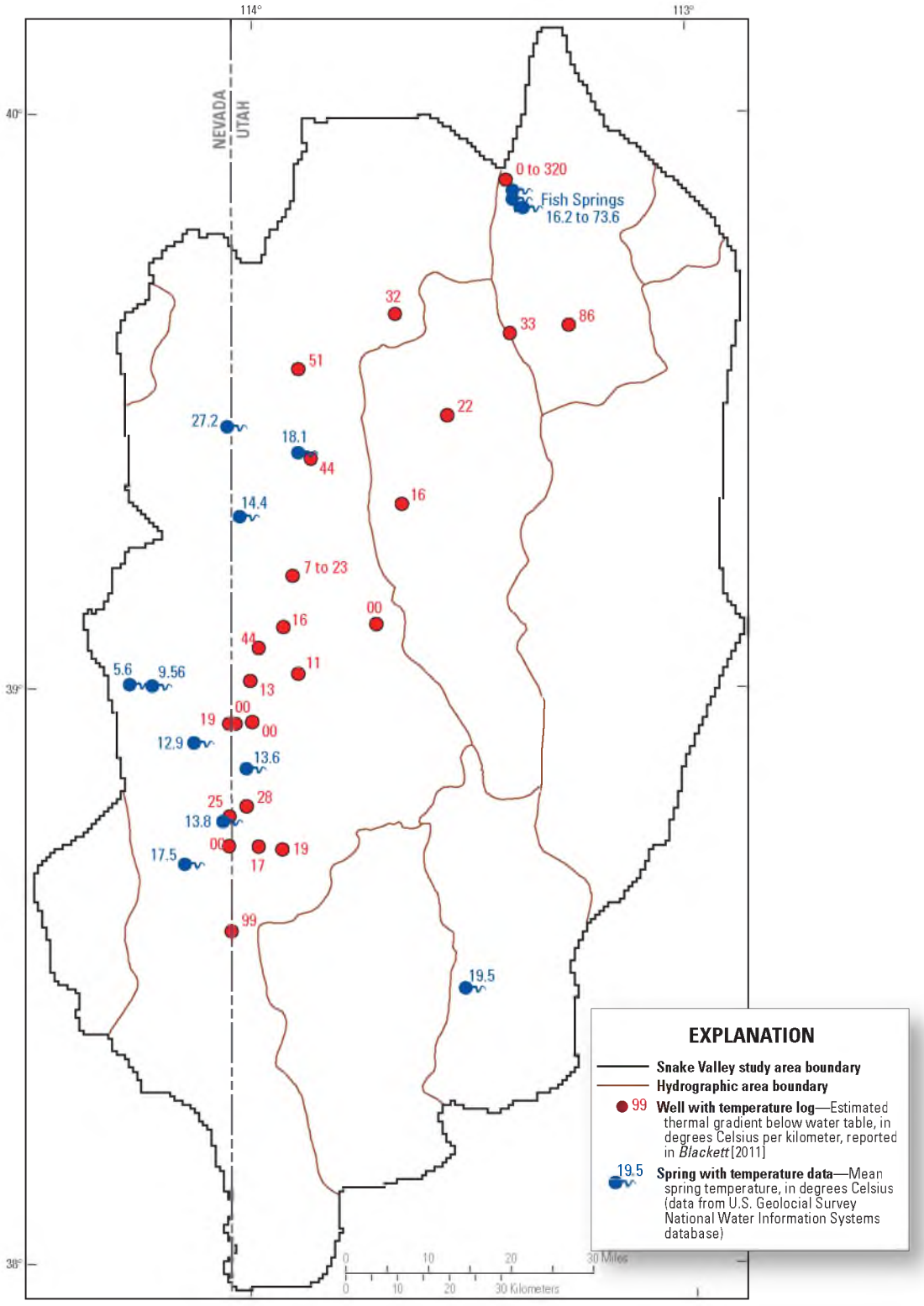

Figure 3-11. Location of wells with thermal logs and associated estimated thermal gradients, and springs with temperature data in the Snake Valley study area. State boundary data from: *U.S. Census Bureau* [2000]. Modified from: *Masbruch et al.* [201X], in review.

3.5 Numerical Simulation of Groundwater Flow and Heat Transport

A steady-state numerical groundwater flow and heat transport model was developed to simulate groundwater flow and heat transport in the Snake Valley area, with the specific purpose of testing the conceptual model and groundwater budget and understanding of the groundwater system. The model allows for the simulation of groundwater flow and heat transport through the groundwater system in consolidated rock and unconsolidated basin-fill. The advantage of simulating both groundwater flow and heat transport is that the groundwater temperatures are additional observations besides water levels and discharge that can be used to assess model performance and constrain model parameters, thereby improving how the model represents the groundwater flow system. Development of the model included compilation and examination of water-level, streamflow, springflow, evapotranspiration, groundwater withdrawal, and temperature data, and estimation of the spatial distribution of recharge, discharge, hydraulic conductivity, and thermal properties. The "Model Construction" section discusses the details of discretization, boundary conditions, and model parameters. The "Model Calibration" section discusses how the model was changed to match observed data and the "Model Evaluation" section discusses how adequately the model simulates the groundwater system.

3.5.1 Model Construction

Construction of the groundwater flow and heat transport model required (1) discretization of the of the groundwater system, including the establishment of the model grid and boundaries; (2) assignment of boundary conditions including recharge and

discharge, water-table temperatures, and basal heat flux; and (3) assignment of material properties such as hydraulic conductivity and thermal conductivity. Given the amount and complexity of the input data, it is impractical to present or reference all required information to reconstruct the model from the information presented in this chapter. A copy of the model and associated data sets can be obtained from the USGS Utah Water Science Center, Salt Lake City, Utah.

The model described in this report uses parameters [*Harbaugh et al.*, 2000] to define much of the input data. A parameter is a single value that is given a name and determines the value of a variable in the finite-difference groundwater flow or heat transport equations [*Harbaugh et al.*, 2000]. When parameters are used, the data value for a cell is calculated as the product of the parameter value, which might apply to many cells and can be described using zones, and a cell multiplier defined using multiplier arrays, which applies only to that cell [*Harbaugh et al.*, 2000]. Sensitivity analysis [*Hill et al.*, 2000] was used to assess the relative importance of various parameters in the model and guide model construction and calibration.

3.5.1.1 Numerical Model Selection

The USGS three-dimensional groundwater flow model program MODFLOW-2000 was used to simulate groundwater flow in the Snake Valley study area [*Harbaugh et al.*, 2000; *Hill et al.*, 2000]. MODFLOW-2000 is a block-centered finite-difference code that solves the groundwater flow equation at the center of each model cell. Flow area and gradient through the cell represent the average area and gradient of groundwater flow through the cell.

The transport code MT3DMS, developed by *Zheng and Wang* [1999] and *Zheng* [2010], was used to simulate heat transport in the Snake Valley area. MT3DMS is a three-dimensional, finite-difference, multispecies transport model that simulates advection, dispersion, and chemical reactions of solutes in groundwater systems. For the advective component, MT3DMS uses the cell-by-cell flows computed by MODFLOW as input to determine advective transport through the model. Because the advection-dispersion equation governing solute transport and the conduction-advection equation governing heat transport have fundamentally the same form, heat can be treated as a solute. Modifications of inputs to the transport equation to simulate heat follow those suggested by *Langevin et al.* [2008; pp. 7–11].

The modeling codes used in this study to simulate groundwater flow and heat transport are not fully coupled; that is, the flow model does not take into account density and viscosity changes due to changes in groundwater temperature. Preliminary simulations of viscosity effects due to groundwater temperature showed that these effects were equivalent to changing the hydraulic conductivity of the hydrogeologic units used in the model by a factor of only 2 or 3. This is well within the uncertainty in hydraulic conductivity, which spans at least 1 to 2 orders of magnitude. Additionally, the density of the groundwater would only vary up to 4 percent over the expected range of simulated temperatures. It was concluded, therefore, that a fully coupled groundwater flow and heat transport model likely would not simulate groundwater flow and heat transport with any additional accuracy, and a fully-coupled model was not required.

UCODE-2005 [*Poeter et al.*, 2005] was used to perform sensitivity analysis, calibration (including parameter estimation through nonlinear regression), and

uncertainty evaluation. While MODFLOW-2000 contains the methods for these analyses [*Hill et al.*, 2000], UCODE-2005 has the ability to handle parameters for multiple process input models (e.g., MODFLOW-2000 and MT3DMS), and runs the necessary sensitivity, calibration, and uncertainty analyses using all parameters for each input model simultaneously.

3.5.1.2 Grid Definition

The north-south-oriented grid for the model consists of 310 rows, 175 columns, and 7 layers, for a total of 379,750 cells with a constant grid-cell spacing of 804.65 m (0.5 mi). Finite-difference methods require that the model grid be constructed for the bounding rectangle of the model domain (Figure 3-12). The boundary of active cells delineates the lateral boundaries of the simulated groundwater system. This boundary generally coincides with a groundwater divide along the western boundary, and surface-water divides on the southern and northern boundaries

The model uses seven layers to simulate groundwater flow and heat transport in the Snake Valley study area (Figure 3-13). The layers range in thickness from 5 m to more than 2,750 m (Table 3-4 and Figure 3-13) and layer 7 extends to a depth of 500 m below sea level. Model layer thicknesses generally increase with depth, allowing for greater resolution at the top of the model where more hydrologic, geologic, and thermal data are available.

All model layers were assigned as confined layers in MODFLOW-2000. The top of the groundwater system is actually unconfined, but simulating layer 1 as unconfined caused numerical instability. Simulating layer 1 as confined is a reasonable approximation if the top of the model is close to the simulated water levels in layer 1

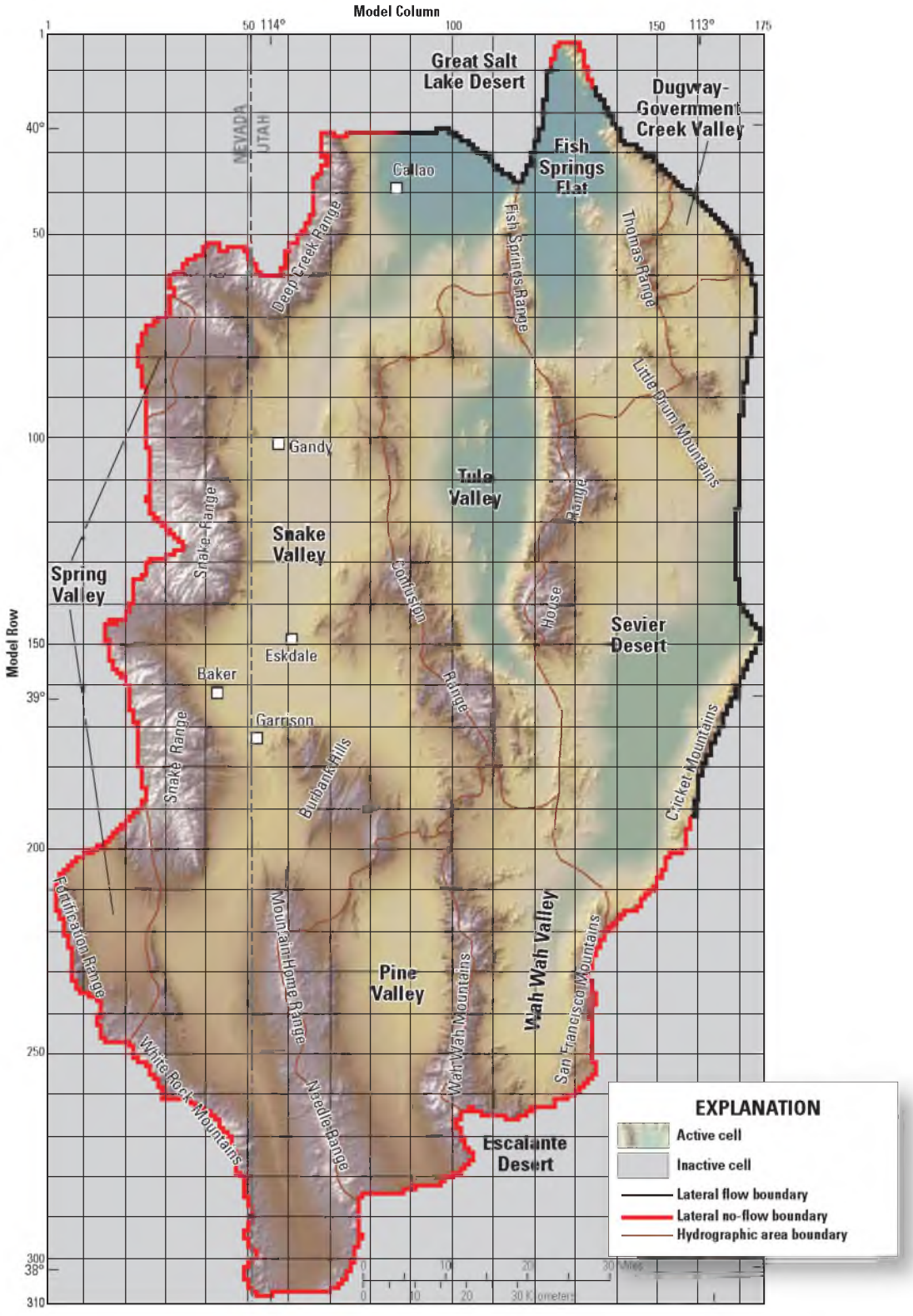

Figure 3-12. Location of the model grid for the Snake Valley study area. State boundary data from: *U.S. Census Bureau* [2000]. Modified from: *Masbruch et al.* [201X], in review.

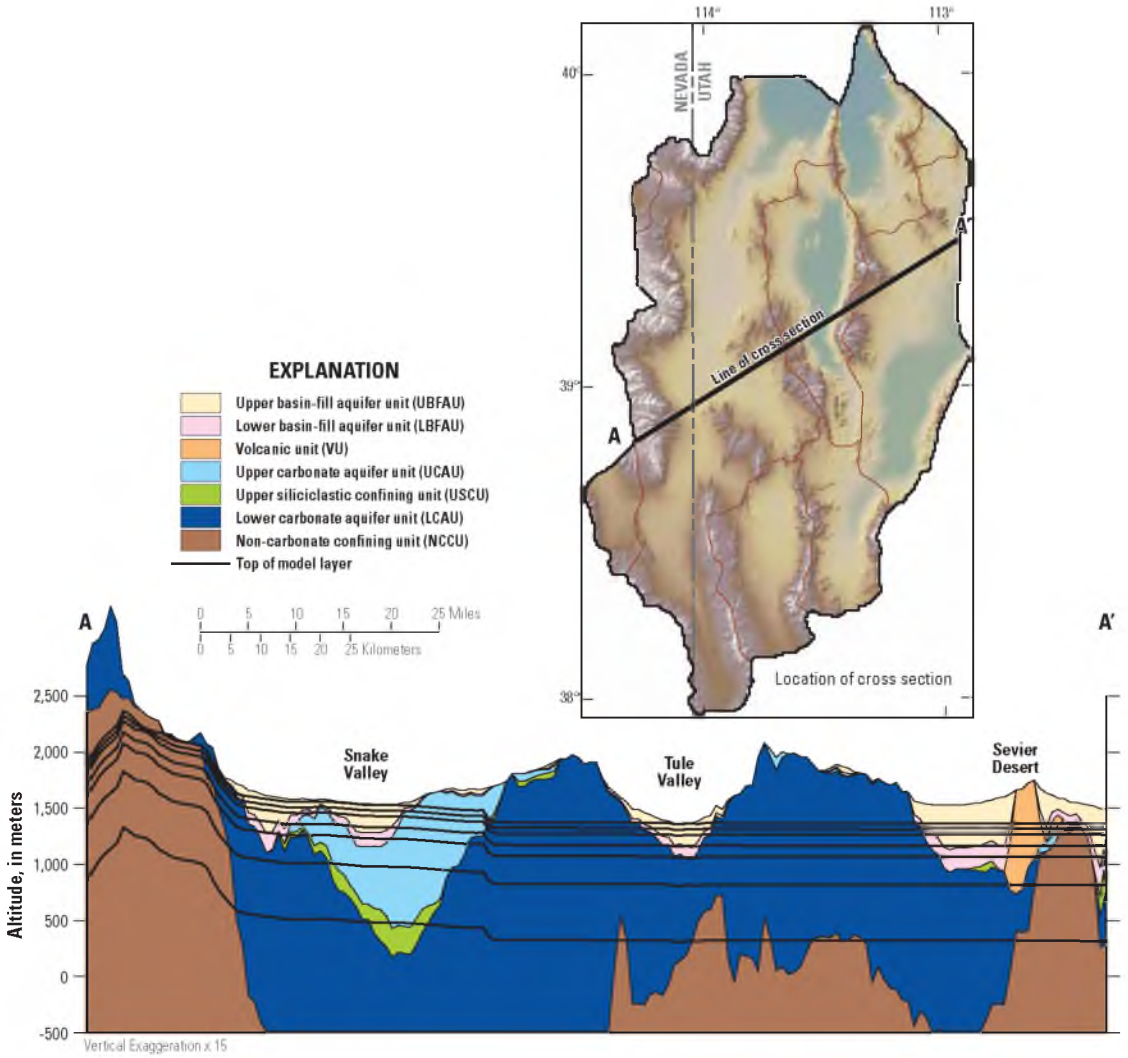

Figure 3-13. Example cross section across the model domain showing hydrogeologic units and subsurface configuration of model layers. Data from: *Sweetkind et al.* [2011a]. Modified from: *Masbruch et al.* [201X], in review.

Table 3-4. Thickness and depth to top of each layer in the Snake Valley area groundwater model. Modified from: *Masbruch et al.* [201X], in review.

Model layer	Layer thickness (meters)	Minimum depth to top of layer (meters)
1	5 to 349	—
2	5 to 50	5
3	5 to 100	10
4	5 to 100	15
5	195 to 250	20
6	500	215
7	746 to 2,754	715

[*Faunt et al.*, 2011]. The top of layer 1 was originally set at land surface (USGS's National Elevation Dataset (NED), *U.S. Geological Survey EROS Data Center* [1999]); during calibration, however, it was updated to be closer to the simulated heads in layer 1. In a few isolated areas, the simulated heads in layer 1 are above land surface. These areas are generally in mountain ranges with low-permeability rocks and discharge areas. This is expected for discharge areas, as the driving head for groundwater to discharge in ETg areas and at springs would need to be above land surface; in the mountain ranges, however, this is not a realistic condition and most likely is a result of inaccuracies produced by grid discretization and/or uncertainties in hydrologic parameters within the mountain block. A number of these grid cells where water levels are above land surface in the mountains occur adjacent to, or within, stream channels that are not captured with the large grid cell size, or were not identified in previous studies as measured river channels. Discharge within these cells, therefore, is not simulated in the model, resulting in higher water-level altitudes within these cells.

3.5.1.3 Flow Model Boundary Conditions

The boundaries chosen for the groundwater flow model mathematically describe how the simulated groundwater system interacts with the surrounding hydrologic system [*Anderson and Woessner*, 2002]. Mathematical boundaries that are used to represent hydrologic boundaries include no-flow boundaries, specified-flux boundaries, and head-dependent flux boundaries. These boundaries define the physical limits of the simulated groundwater system and are also used to simulate recharge and discharge. No-flow boundaries are considered impermeable and no groundwater flow is simulated across them. Specified-flux boundaries allow a specified rate of water through the cell and are

used to simulate all recharge, lateral inflow, and well withdrawals in this model. Head-dependent flux boundaries simulate flow across the boundary proportional to the difference in heads across the boundary and are used to simulate all discharge, except well withdrawals, in this model.

3.5.1.3.1 No-Flow Boundaries

Lateral no-flow boundaries (Figure 3-12) were defined based on water-level data [*Gardner et al.*, 2011], geologic data [*Sweetkind et al.*, 2011b], and a larger numerical groundwater flow model developed for the eastern Great Basin [*L.E. Brooks, USGS, written commun.*, August 2010]. No-flow boundaries simulated in the model include (1) the top of the Deep Creek, Snake, and Fortification Ranges, the top of the San Francisco and Cricket Mountains, and the southern boundaries of Snake, Pine and Wah Wah Valleys where potentiometric contours indicate groundwater divides [*Heilweil and Brooks*, 2011] or where the relative likelihood of connection across the boundary is low based on geology [*Sweetkind et al.*, 2011b]; (2) portions of the western boundary in northern and southern Spring Valley where potentiometric contours indicate groundwater divides [*Gardner et al.*, 2011; *Heilweil and Brooks*, 2011] and/or where the larger numerical groundwater flow model indicated divergent flow [*L.E. Brooks, USGS, written commun.*, August 2010]; and (3) the western and eastern portions of the northern boundary dividing Snake Valley and Fish Springs Flat from the Great Salt Lake Desert where either potentiometric contours indicate groundwater flow parallel to the boundary [*Heilweil and Brooks*, 2011] or the relative likelihood of connection across the boundary is low based on geology [*Sweetkind et al.*, 2011b].

3.5.1.3.2 Recharge Boundaries

Recharge from infiltration of precipitation (including in-place recharge, recharge from runoff, infiltration of mountain stream baseflow, and infiltration of unconsumed surface-water irrigation) and unconsumed irrigation from well withdrawals is simulated as a specified-flux boundary with the Recharge (RCH) Package [*Harbaugh et al.*, 2000]. Recharge is applied to the highest active cell (model layer 1) and defined using a multiplier array. The multiplier array represents the conceptual recharge rate at each cell in m/day (Figures 3-5 and 3-14). Parameters and zones were used to multiply the conceptual recharge rates by a constant value and were allowed to vary during calibration and parameter estimation.

In this model, BCM in-place recharge is simulated at the same location as it occurs in the BCM. The BCM, however, does not route runoff, so in this groundwater flow model, runoff that originated at higher altitudes was redistributed to cells along the mountain front that contained unconsolidated basin fill material with a slope of 5 to 10 percent; in this way, recharge from upland runoff was accounted for where the streams enter the valleys. Recharge from mountain stream baseflow was distributed to these same cells. Areal recharge from unconsumed irrigation from well withdrawals was distributed using an irrigated acreage database [*Welborn and Moreo*, 2007] to determine the area (or model cells) over which irrigation was applied. If there was no clear associated irrigated area for a specific well withdrawal indicated in the database, the recharge was applied to the cell in which the well was located.

Additionally, recharge from subsurface inflow is simulated across a portion of the eastern boundary using a specified-flux boundary by placing injection wells in all seven

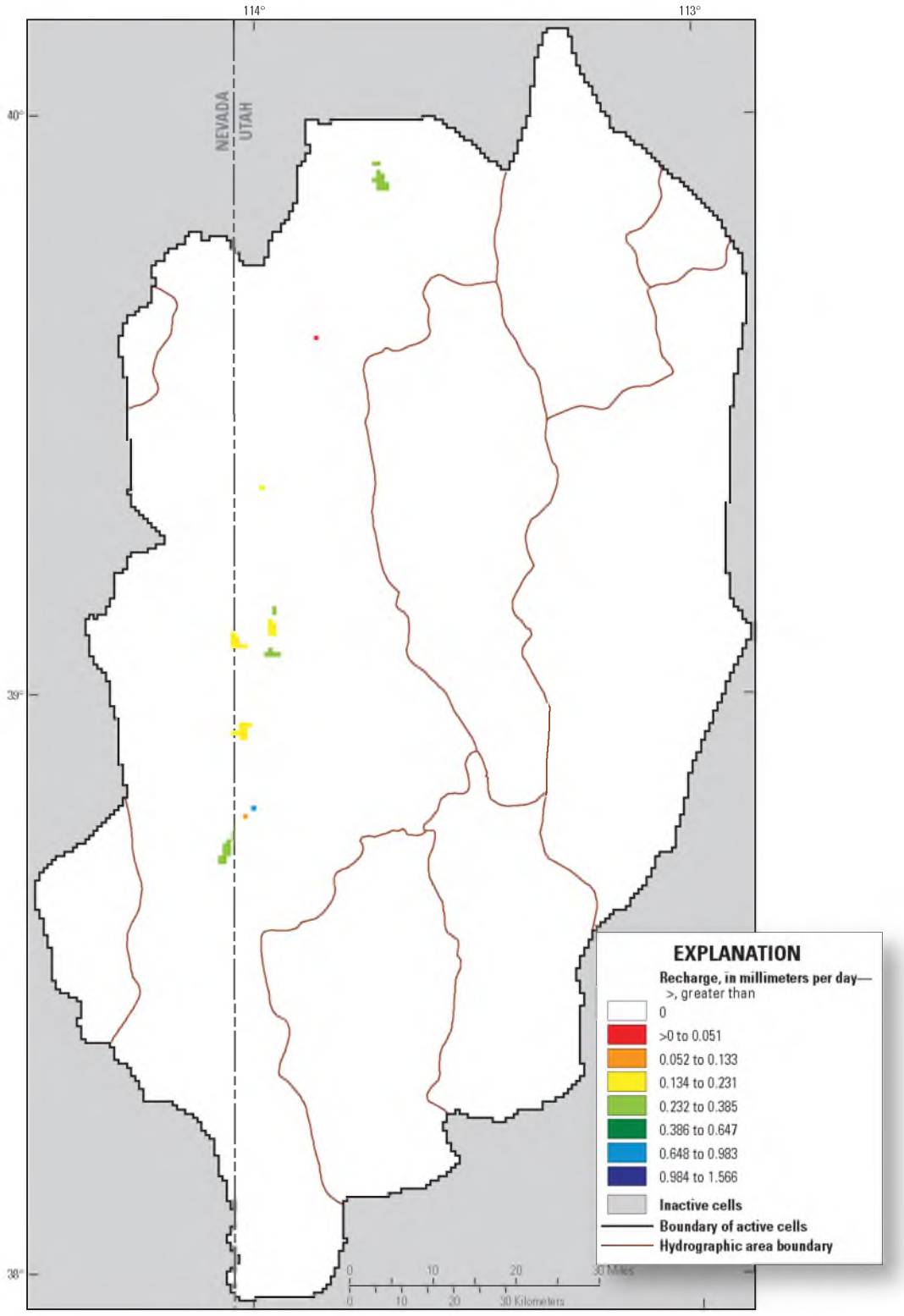

Figure 3-14. Conceptual rate and distribution of recharge from unconsumed irrigation from well withdrawals simulated in the Snake Valley area groundwater model. State boundary data from: *U.S. Census Bureau* [2000]. Modified from: *Masbruch et al.* [201X], in review.

model layers along the boundary (Figure 3-15) using the Well (WEL) Package [*Harbaugh et al.*, 2000]. The specified flux applied to each of the wells was estimated using simulated groundwater flow amounts taken from a larger groundwater model that encompasses the Snake Valley area [*L.E. Brooks, USGS, written commun.*, August 2010]. A parameter was used to multiply the specified-flux rate by a constant value and was allowed to vary during calibration and parameter estimation.

3.5.1.3.3 Discharge Boundaries

Discharge is simulated to evapotranspiration, springs, mountain streams, wells, and as subsurface outflow to the north (Figure 3-6). Discharge to evapotranspiration, springs, mountain streams, and subsurface outflow is simulated using head-dependent flux boundaries, and well withdrawals are simulated using specified-flux boundaries.

3.5.1.3.3.1 Groundwater discharge to evapotranspiration (ETg) is simulated in layer 1 (Figure 3-6) with the Evapotranspiration (EVT) Package [*Harbaugh et al.*, 2000]. Data required for the EVT Package are the altitude of the ETg surface, the extinction depth, and the maximum ETg rate. The simulated ETg rate varies linearly between the extremes of no ETg when the simulated water-level is below the extinction depth, and the maximum ETg rate when the simulated water level is at or above the altitude of the ETg surface [*Anderson and Woessner*, 2002]. The altitude of the the ETg surface was estimated using the NED and was defined as the minimum land-surface altitude within each model cell. The minimum land-surface altitude was used to minimize vertical accuracy errors of the NED which average ± 7 m. ETg studies in the area have shown that the maximum rooting depth of certain phreatophytes can be as deep as 35 to 60 ft [*Moreo et al.*, 2007]. An extinction depth of 12 m (about 40 ft), therefore, was used

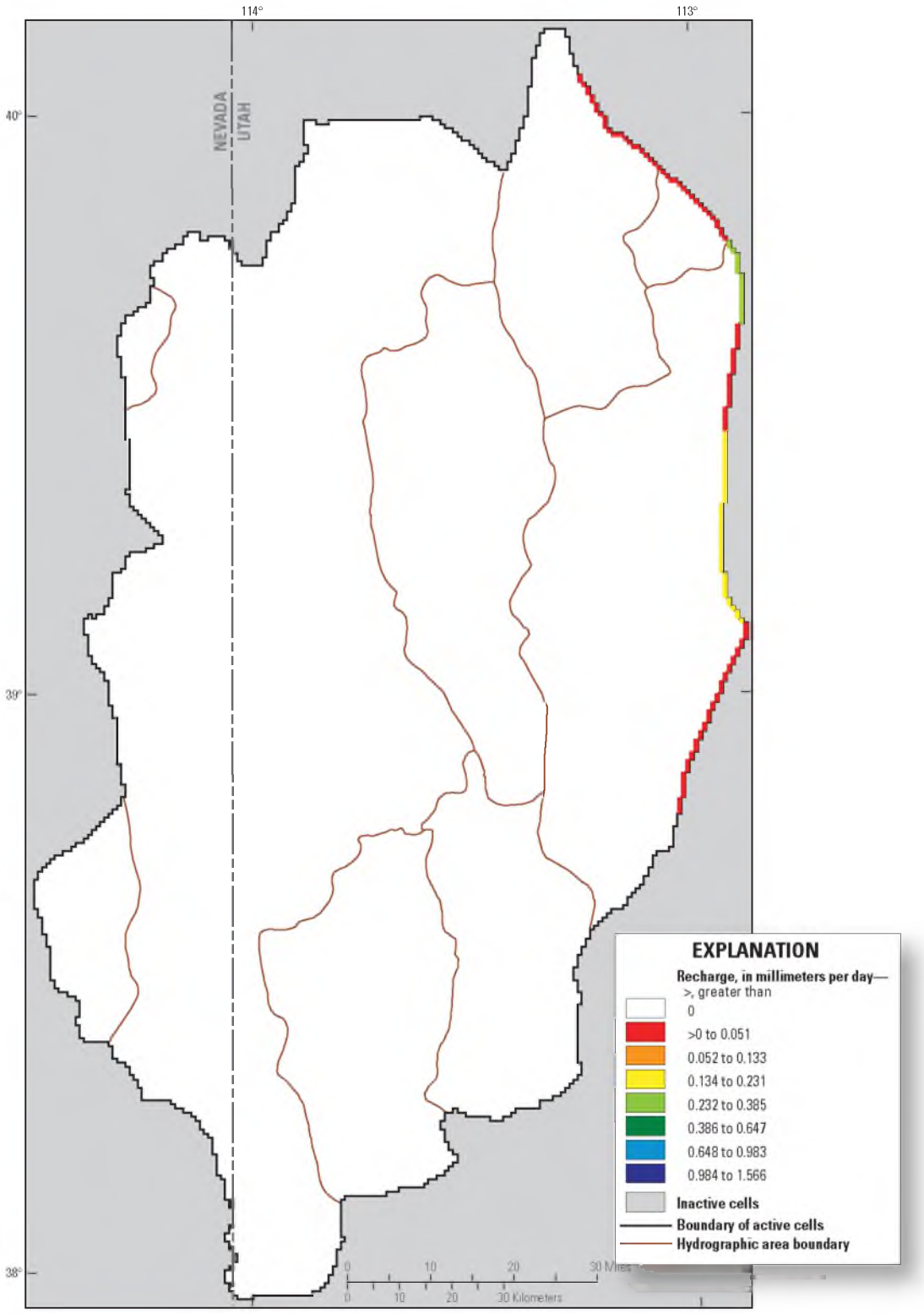

Figure 3-15. Conceptual rate of subsurface inflow simulated in the Snake Valley area groundwater model. State boundary data from: *U.S. Census Bureau* [2000]. Modified from: *Masbruch et al.* [201X], in review.

for all areas of evapotranspiration.

Simulated ETg areas were defined using digital data from two regional scale studies [*Buto*, 2011; *Masbruch et al.*, 2011; *Smith et al.*, 2007]. These studies used a combination of satellite and aerial photographic imagery, as well as field reconnaissance and mapping techniques, to define the outer extent of phreatophyte areas (based on plant species), including playas, where groundwater may be consumed by evapotranspiration [*Masbruch et al.*, 2011]. The maximum ETg rate for each area was calculated by dividing the estimated conceptual volumetric discharge of ETg by the size of the simulated ETg area, and, therefore, is constant across each area. The maximum rate of ETg was assigned to each model cell using a multiplier array (Figure 3-16). Parameters and zones were used to multiply the maximum rate of evapotranspiration by a constant value and were allowed to vary during calibration and parameter estimation.

3.5.1.3.3.2 Discharge to 12 point springs and one area spring (Figure 3-6) within the model domain was simulated using the Drain (DRN) Package [*Harbaugh et al.*, 2000]. The DRN Package simulates a head-dependent flux boundary for each cell to which it is assigned, and discharge is a function of the simulated water level and drain conductance [*McDonald and Harbaugh*, 1988]. Data required for the DRN Package are altitude and conductance of the drain. A parameter was used to define the conductance and was allowed to vary during model calibration and parameter estimation. The altitude of each drain was originally set at land surface, and was varied to no more than 10 m below the minimum land-surface altitude within each cell during calibration to account for springs being located in land-surface depressions that are lower than would be evident in the top surface of the model. Additionally, drains were originally inserted into all

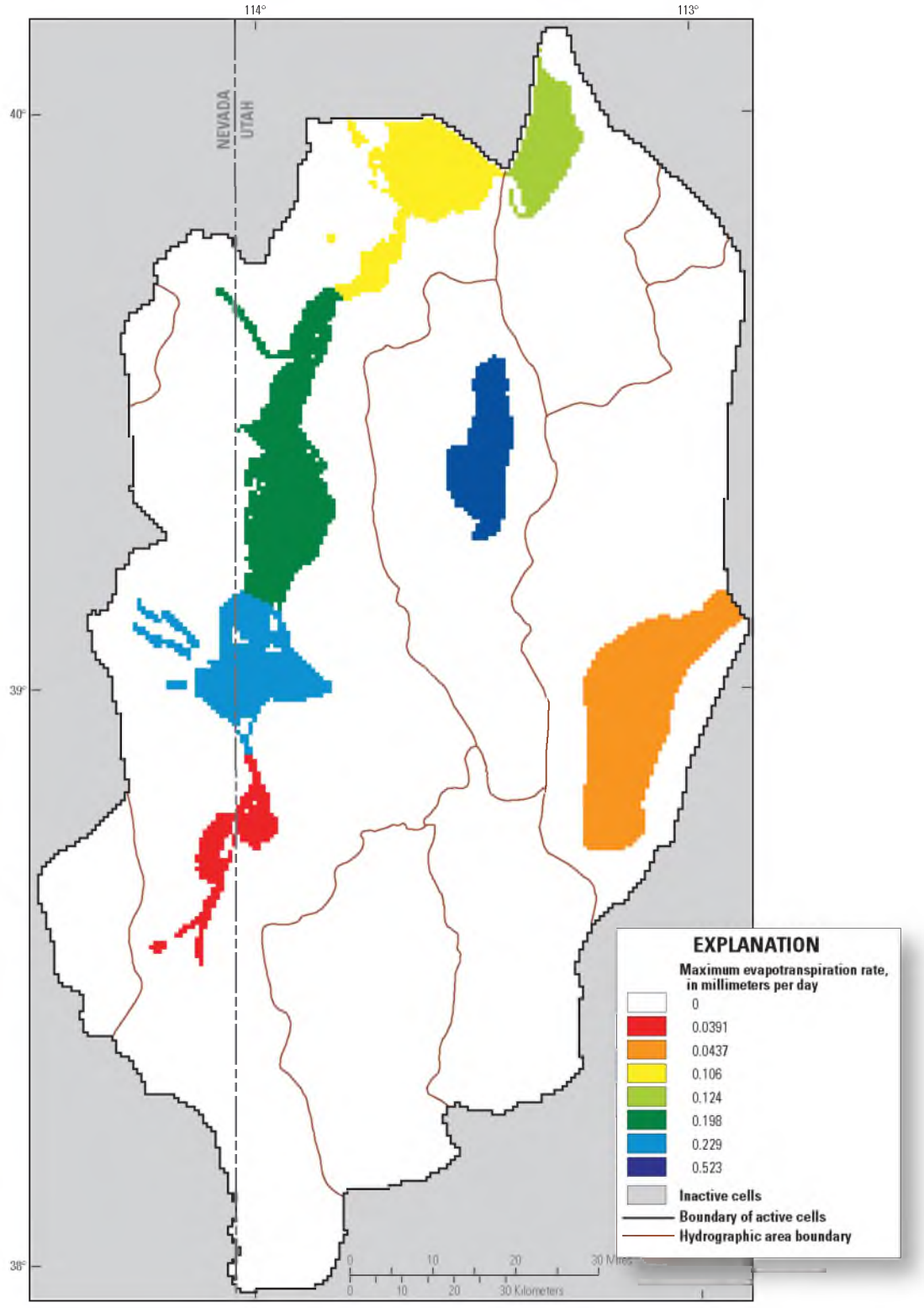

Figure 3-16. Maximum groundwater evapotranspiration rate simulated in the Snake Valley area groundwater model. State boundary data from: *U.S. Census Bureau* [2000]. Modified from: *Masbruch et al.* [201X], in review.

layers within the model and during calibration drains in the lower layers were removed at some of the springs.

This model simulates discharge to springs in the mountains. Previous studies have assumed that the regional water table is below the altitude of mountain springs and that discharge from those springs represents perched discharge from locally derived recharge [*Harrill and Bedinger*, 2004]. Discharge to mountain springs was simulated in the model for the following reasons: (1) BCM is used to estimate recharge, and ignoring the discharge of higher-altitude springs would require a reduction in recharge equal to the discharge from those springs; (2) although downward vertical gradients likely exist in mountain recharge areas, it is unlikely that all mountain springs are separate from the regional groundwater system; (3) ignoring discharge to mountain springs assumes that water levels in the mountains are about the same as water levels in the adjacent valleys and does not account for recharge mounds that probably occur beneath high-recharge areas in the mountains; and (4) simulating discharge to mountain springs provides sensitivity to model parameters within the mountain block.

3.5.1.3.3.3 Discharge representing baseflow to five mountain streams (Figure 3-6) in layer 1 was simulated using the River (RIV) Package [*Harbaugh et al.*, 2000]. Similar to mountain spring discharge, simulating streams in the mountains provides sensitivity to model parameters within the mountain block. Ignoring the groundwater discharge to mountain streams does not account for recharge mounds that probably occur beneath high-recharge areas in the mountains. The RIV Package simulates a head-dependent flux boundary for each cell to which it is assigned, and will allow recharge or discharge to a cell that is a function of the simulated water level and riverbed

conductance, which accounts for the geometry of the river channel [*Anderson and Woessner*, 2002]. Data required for the RIV Package are river stage, or hydraulic-head (water-level) altitude, conductivity of the riverbed, and the altitude of the bottom of the riverbed [*Harbaugh et al.*, 2000]. Only gaining portions of mountain streams are simulated in the model; losing portions of the streams contributing recharge to the aquifer were distributively simulated in cells along the mountain front that contained unconsolidated basin fill material with a slope of 5 to 10 percent (see "Recharge Boundaries" section of this chapter). Because only gaining portions were simulated, the river stage and river bottom were both set at the minimum land-surface altitude within each cell. A parameter was used to define the conductance and was allowed to vary during model calibration and parameter estimation.

3.5.1.3.3.4 Discharge to 63 irrigation wells (Figure 3-6) is simulated in layers 1 through 3 with the Well (WEL) Package [*Harbaugh et al.*, 2000]. The WEL Package simulates a specified-flux boundary in each cell to which a well is assigned. Data required for the WEL Package are the withdrawal rate in each layer. For the wells in which the withdrawals were estimated as part of the Utah state-wide groundwater use monitoring program [*Burden et al.*, 2011], the distribution of withdrawal among layers for each well was determined by multiplying the total withdrawal rate by the proportion of the open interval in each layer. For example, if 75 percent of the open interval of a well was in layer 1 and 25 percent of the open interval was in layer 2, the withdrawal rate assigned to the well in layer 1 was 75 percent of the total withdrawal for the well, with the remaining 25 percent of the withdrawal assigned as the withdrawal rate in layer 2. For the well withdrawals from the center pivots in the southern portion of the study area

east of Big Spring, 11 wells were inserted into layers 1 and 2 approximately at the center of each pivot, and the withdrawal rate for each well was split evenly between the two layers. A parameter was used to define a multiplier on the withdrawal rate for all of the wells and was allowed to vary during model calibration and parameter estimation.

3.5.1.3.3.5 Water levels and geology suggest that there may be some subsurface groundwater outflow from northern Snake Valley and eastern Fish Springs Flat towards the Great Salt Lake Desert [*Gardner et al.*, 2011; *Heilweil and Brooks*, 2011]. Previous estimates of this subsurface outflow, however, vary widely [*Harrill et al.*, 1988; *Hood and Rush*, 1965; *Welch et al.*, 2007]. Because of the uncertainty in the amount of outflow, the center portion of the northern boundary of the model was simulated as a head-dependent flux boundary (Figure 3-6) using the General-Head Boundary (GHB) Package [*Harbaugh et al.*, 2000]. The GHB was simulated where either potentiometric contours indicate groundwater flow perpendicular to the boundary [*Heilweil and Brooks*, 2011] or the relative likelihood of connection across the boundary was uncertain based on geology [*Sweetkind et al.*, 2011b]. The GHB Package takes as input the conductance between the aquifer cell and the boundary, and the water-level altitude at the boundary. The difference between this boundary water-level altitude and the simulated water-level altitude in the cell dictates whether water will enter or leave the model domain through this boundary. If the simulated water-level altitude is less than the boundary water-level altitude, water will enter the model through this boundary; if the simulated water-level altitude is greater than the boundary water-level altitude, water will leave the model through this boundary.

The conductance used in the GHB Package was based on the cross-sectional area

for each cell across all seven layers. A parameter was used to define the conductance and was allowed to vary throughout model calibration and parameter estimation. The head at the boundary was set at 1,305 m (4,300 ft [*Heilweil and Brooks*, 2011]).

3.5.1.4 Heat Transport Model Boundary Conditions

The boundaries chosen for the heat transport model mathematically describe how the simulated groundwater system interacts with the surrounding thermal system. Mathematical boundaries that are used to represent thermal boundaries include no-flux boundaries, specified-flux boundaries, and specified-temperature boundaries. No-flux boundaries were used to represent the lateral boundaries of the model as it was assumed that no additional heat was crossing these boundaries. Specified-flux boundaries allow a specified rate of heat flow through the cell and are used to simulate heat flux across the base of the model. Specified-temperature boundaries are used to simulate the temperature across the top of the water table, as well as recharge temperatures in the model.

3.5.1.4.1 Basal Heat Flux

Basal heat flux, the amount of heat that is transferred conductively from the interior of the Earth across the base of the model, was simulated using the Source/Sink Mixing (SSM) Package in MT3DMS [*Zheng and Wang*, 1999]. The SSM Package allows for point sources of heat to be defined that are independent of the flow solution by using the "mass-loading source" option, which was needed because the bottom boundary of the groundwater flow model was assigned as a no-flow boundary. The heat transport equivalent of this mass-loading source can be calculated using the following equation [*Langevin et al.*, 2008]:

$$\dot{M}_T = \frac{\dot{E}}{\rho_f c_{Pfluid}} \quad (3\text{-}1)$$

where

$\dot{M}_T$ is the mass-loading source for heat transport per model cell, in °Cm^3/s,

$\dot{E}$ is the heat flux per cell, in watts (W),

ρ_f is the fluid (groundwater) density, and is equal to 1,000 kg/m^3, and

c_{Pfluid} is the specific heat capacity of the fluid (groundwater), and is equal to 4,186 J/kg°C. The heat flux per each cell across the base of the model was defined as a parameter and was allowed to vary during model calibration and parameter estimation.

3.5.1.4.2 Specified Temperature

The top layer of the model was simulated using a specified-temperature boundary condition (Figure 3-17) to allow for conduction of heat out of the top of the model, except at all cells used to simulate spring discharge or the general-head boundary where advective heat loss through groundwater discharge dominates over conductive heat loss. In an early model simulation, groundwater temperatures in layer 1 were only specified in areas where no groundwater recharge or discharge occurred. This led to unreasonably warm simulated temperatures in both the recharge and discharge areas, by a factor of at least two and up to five, and resulted in model instability. A rough calculation showed that heat transport by groundwater advection through the top of the model in the groundwater recharge and ETg areas was diffuse enough to approximately equal heat transport by conduction calculated in adjacent areas with no advective flux out of the top of the model. By not specifying the temperature at the top of the model in the recharge

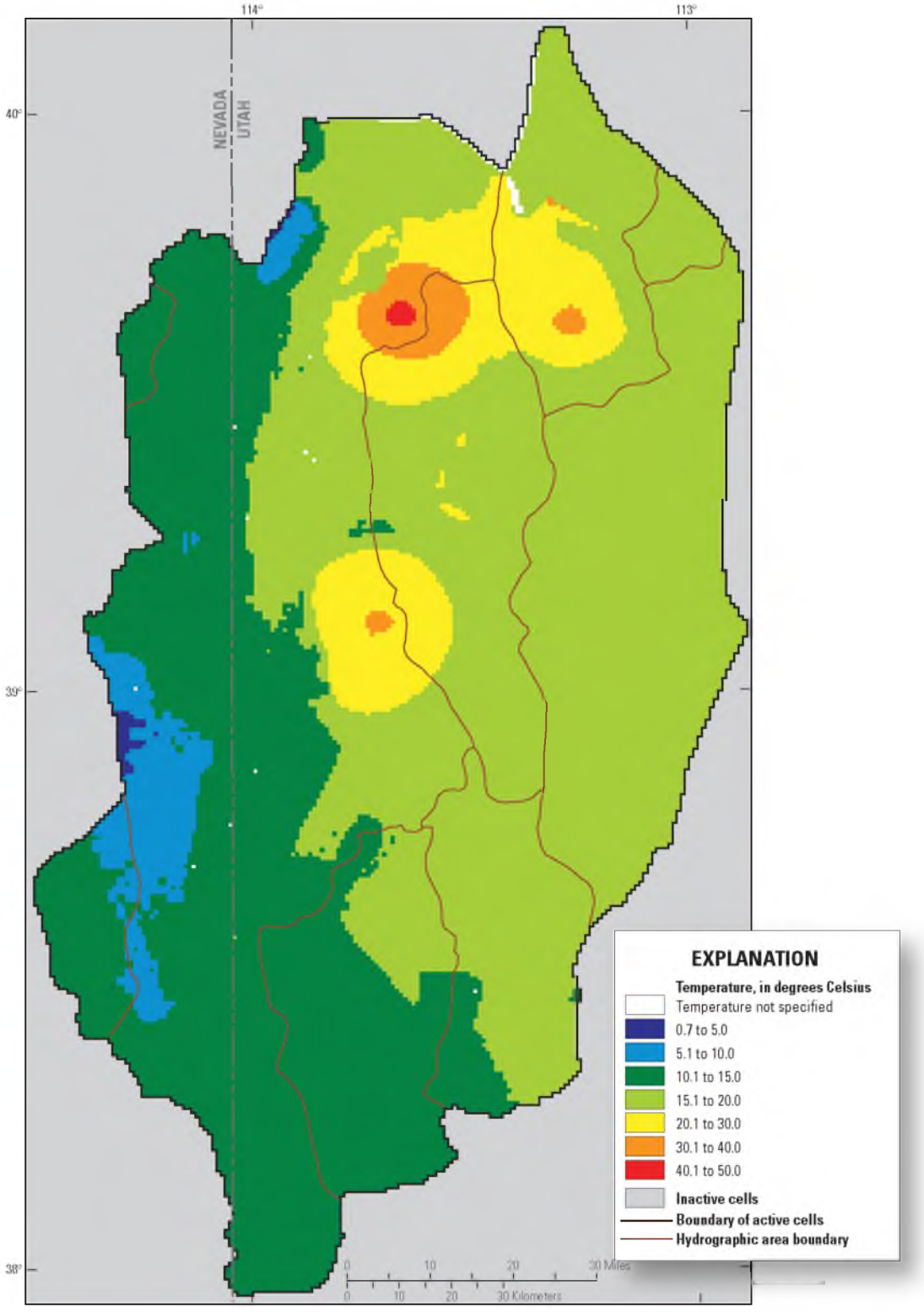

Figure 3-17. Distribution of specified temperatures assigned to layer 1 of the Snake Valley area groundwater model. State boundary data from: *U.S. Census Bureau* [2000]. Modified from: *Masbruch et al.* [201X], in review.

and ETg areas, and thereby not accounting for conductive heat transport through these cells, total heat transport across the top model boundary was not being correctly accounted for.

Because the top of the model represents the water table, three interpolated datasets were used to calculate the specified temperatures used to represent the water table. The first dataset is a natural neighbor interpolation (Figure 3-18) using 23 measured water-table temperatures [*Blackett*, 2011] from the newly installed UGS wells and 50 springs [*NWIS*, accessed on October 28, 2010]; this dataset was used to better represent the temperatures at the deeper water tables measured at a number of the UGS wells. The cooler temperatures from the springs in the House and Deep Creek Ranges were not used as it was assumed that these springs represent local, perched water tables based on noble gas recharge temperatures calculated for wells downgradient of these ranges [*P. Gardner, USGS, written commun.*, May 11, 2011] and do not represent the regional system. The second dataset is a lapse curve (Figure 3-19A) derived from temperatures measured in 95 springs and shallow (less than 30 m or 100 ft depth below land surface) wells [*Blackett*, 2011; *NWIS*, accessed on October 28, 2010; *Pavelko*, 2007] throughout the study area; this relationship was used to project water-table temperatures into the mountains. The third dataset is a lapse curve (Figure 3-19B) derived from noble gas recharge temperatures and altitudes calculated for several wells and springs in the study area [*P. Gardner, USGS, written commun.*, May 11, 2011]; this relationship was used for water-table temperatures in the carbonates in the southern portion of the Snake Range. Groundwater recharge temperatures were set equal to these same specified temperatures used in layer 1.

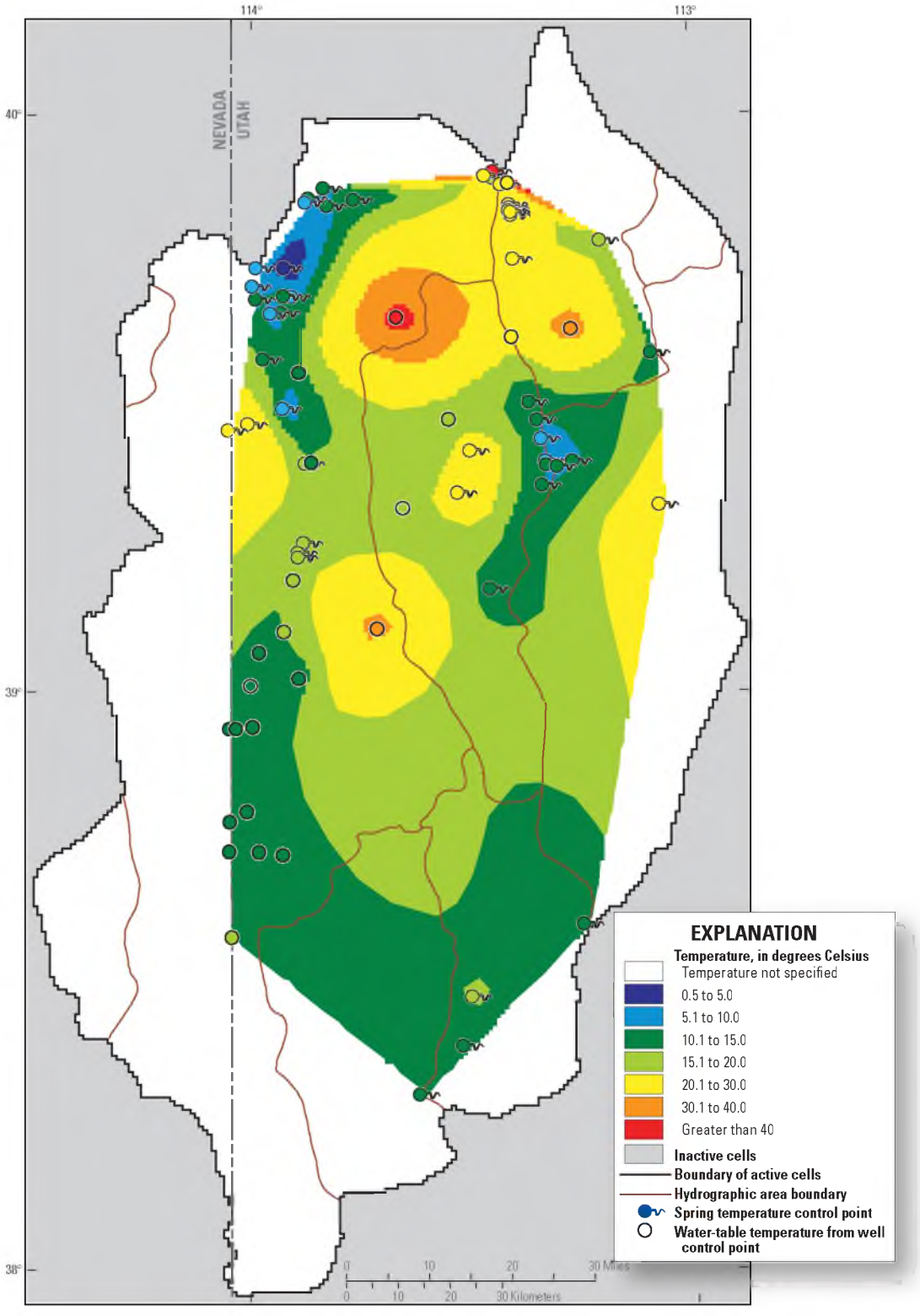

Figure 3-18. Water-table temperature control points and natural neighbor interpolation temperature results. State boundary data from: *U.S. Census Bureau* [2000]. Modified from: *Masbruch et al.* [201X], in review.

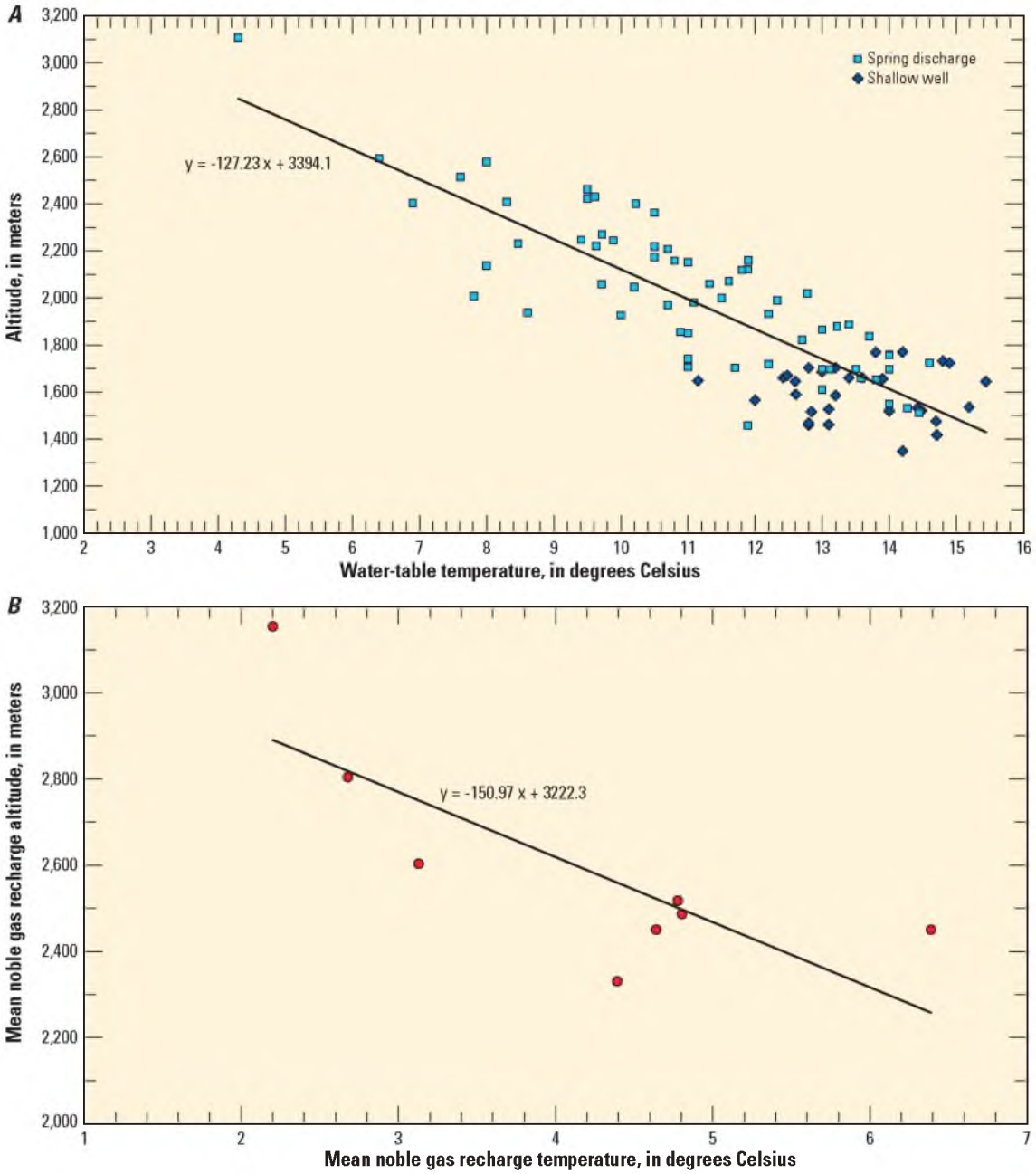

Figure 3-19. Derived lapse curves from (*A*) springs and shallow wells, and (*B*) noble gas recharge temperatures and altitudes from selected wells and springs in the Snake Valley study area. Modified from: *Masbruch et al.* [201X], in review.

3.5.1.5 Hydraulic Properties

The nine hydrogeologic units (HGUs) described in *Sweetkind et al.* [2011a] for the eastern Great Basin form the basis for assigning horizontal hydraulic conductivity and vertical anisotropy to the cells of the model grid using the Hydrogeologic-Unit Flow (HUF) Package [*Anderman and Hill*, 2000]. Zone arrays in MODFLOW-2000 were used to account for variations in hydraulic properties within an HGU. The HUF Package was chosen because it easily facilitates the discretization of the complicated geometry of the HGUs within the model [*Faunt et al.*, 2010]. Hydrogeologic structures that act as barriers to groundwater flow were simulated using the Horizontal-Flow Barrier (HFB) Package [*Harbaugh et al.*, 2000].

3.5.1.5.1 Hydrogeologic Units

The HUF Package [*Anderman and Hill*, 2000] takes as input the tops and thicknesses of each HGU and allows the hydraulic conductivity of the HGUs to be defined through zones and parameters. The HGUs are assigned to model cells in the HUF Package. Some model cells are filled by a single HGU, while other model cells may contain multiple HGUs. The HUF Package calculates the effective hydraulic conductivity in both the vertical and horizontal directions for each cell based on the hydraulic properties and thicknesses of the HGUs present within the cell [*Anderman and Hill*, 2000].

Of the nine HGUs defined in the hydrogeologic framework developed for the GBCAAS [*Sweetkind et al.*, 2011a], seven exist in the current study area and are defined in the HUF package. Each of these HGUs are stratigraphically and structurally heterogeneous, and all but USCU were further divided into a number of zones based on

depositional and structural characteristics (Figures 3-20 through 3-26) and are defined in Chapter B of the GBCAAS study [*Sweetkind et al.*, 2011a]. Many of these zones do not have independent measurements of hydraulic conductivity from aquifer tests, and the relative differences in hydraulic conductivity are defined based on other hydrogeologic information [*Sweetkind et al.*, 2011a]. Initial HGU parameters defined for the model were based on these zones and were allowed to vary during calibration and parameter estimation.

3.5.1.5.2 Vertical Anisotropy

Vertical anisotropy, which is the ratio of horizontal hydraulic conductivity to vertical hydraulic conductivity, was defined for each HGU parameter by using the HUF package. Because of their layered nature, and the existence of playa and prehistoric Lake Bonneville deposits [*Sweetkind et al.*, 2011a], the basin-fill HGUs are likely to have significant vertical anisotropy [*Domenico and Schwartz*, 1998]. The carbonate and other consolidated rock HGUs are likely to have relatively small vertical anisotropy due to the assumed presence of solution features and fractures, respectively [*Faunt et al.*, 2010]. Parameters were defined to represent vertical anisotropy for different HGUs and were allowed to vary during model calibration and parameter estimation.

3.5.1.5.3 Horizontal-Flow Barriers

Observed water levels and the existence of some springs in the study area indicate distinct variability in the hydraulic gradient. Areas where the gradient steepens abruptly or where discharge from a spring occurs could not always be simulated using only changes in the hydraulic conductivity within model cells. In these areas, simulated

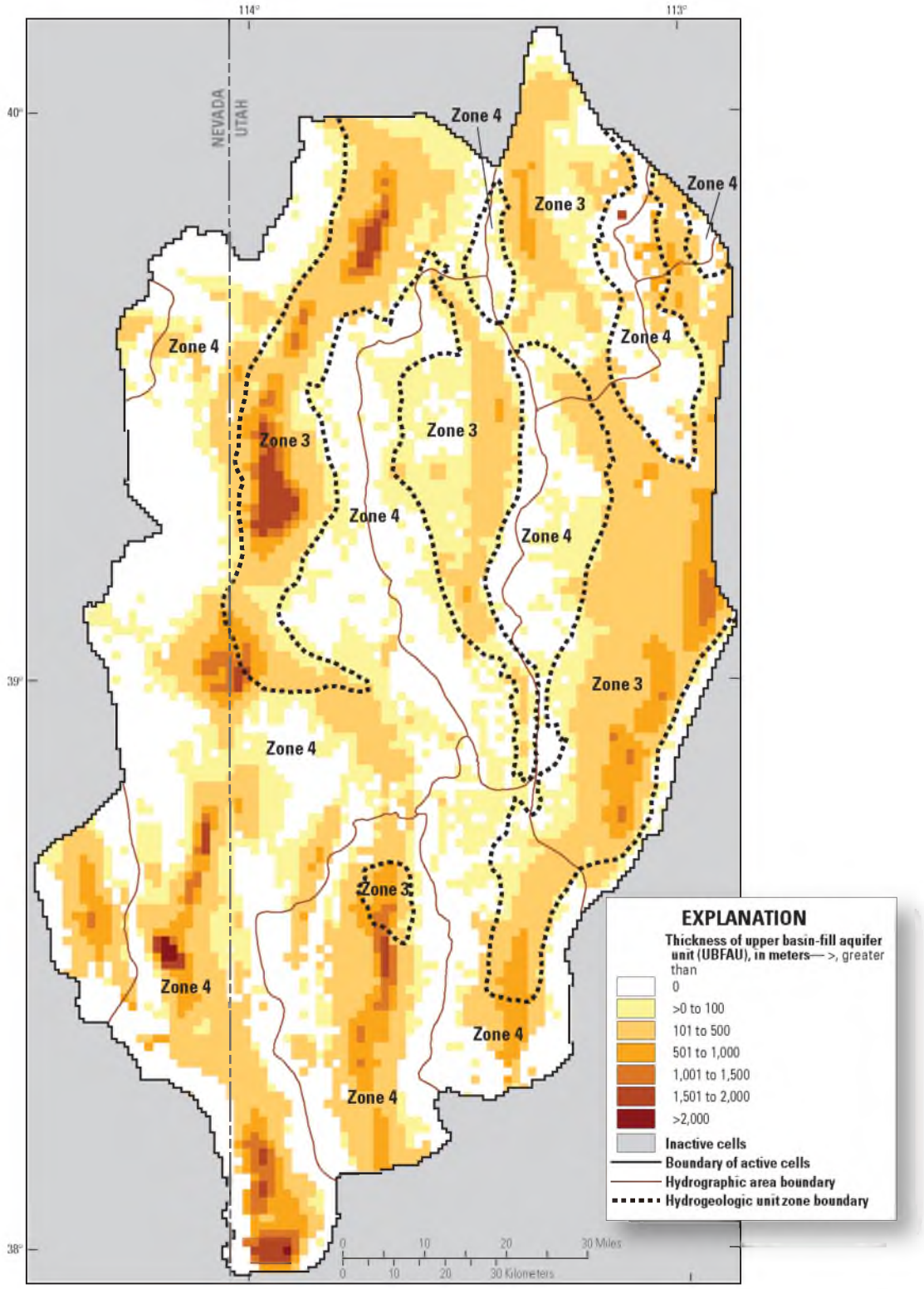

Figure 3-20. Simulated extent, thickness, and initial hydrogeologic unit zones of the upper basin-fill aquifer unit (UBFAU) in the Snake Valley area groundwater model. State boundary data from: *U.S. Census Bureau* [2000]. Modified from: *Masbruch et al.* [201X], in review.

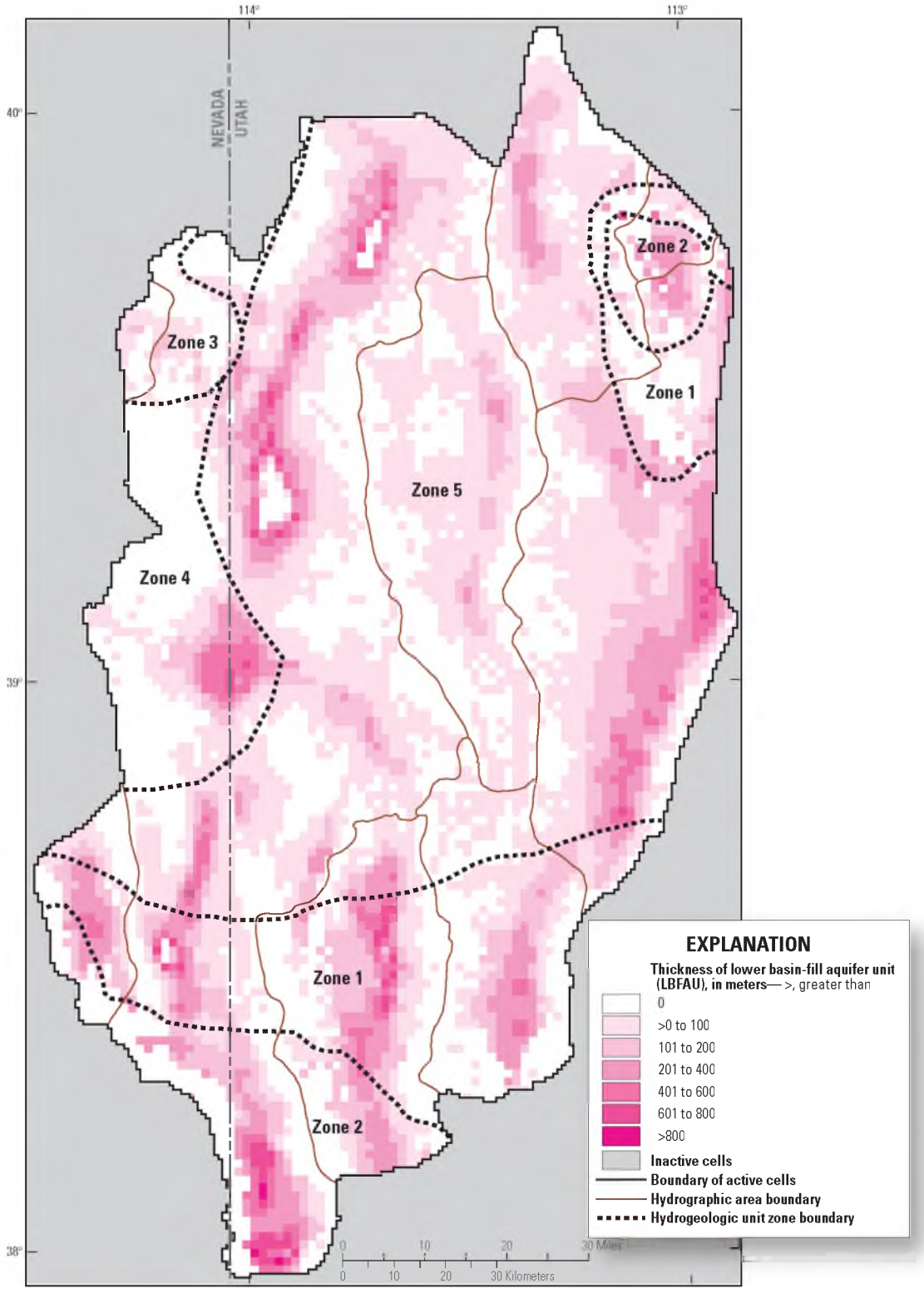

Figure 3-21. Simulated extent, thickness, and initial hydrogeologic unit zones of the lower basin-fill aquifer unit (LBFAU) in the Snake Valley area groundwater model. State boundary data from: *U.S. Census Bureau* [2000]. Modified from: *Masbruch et al.* [201X], in review.

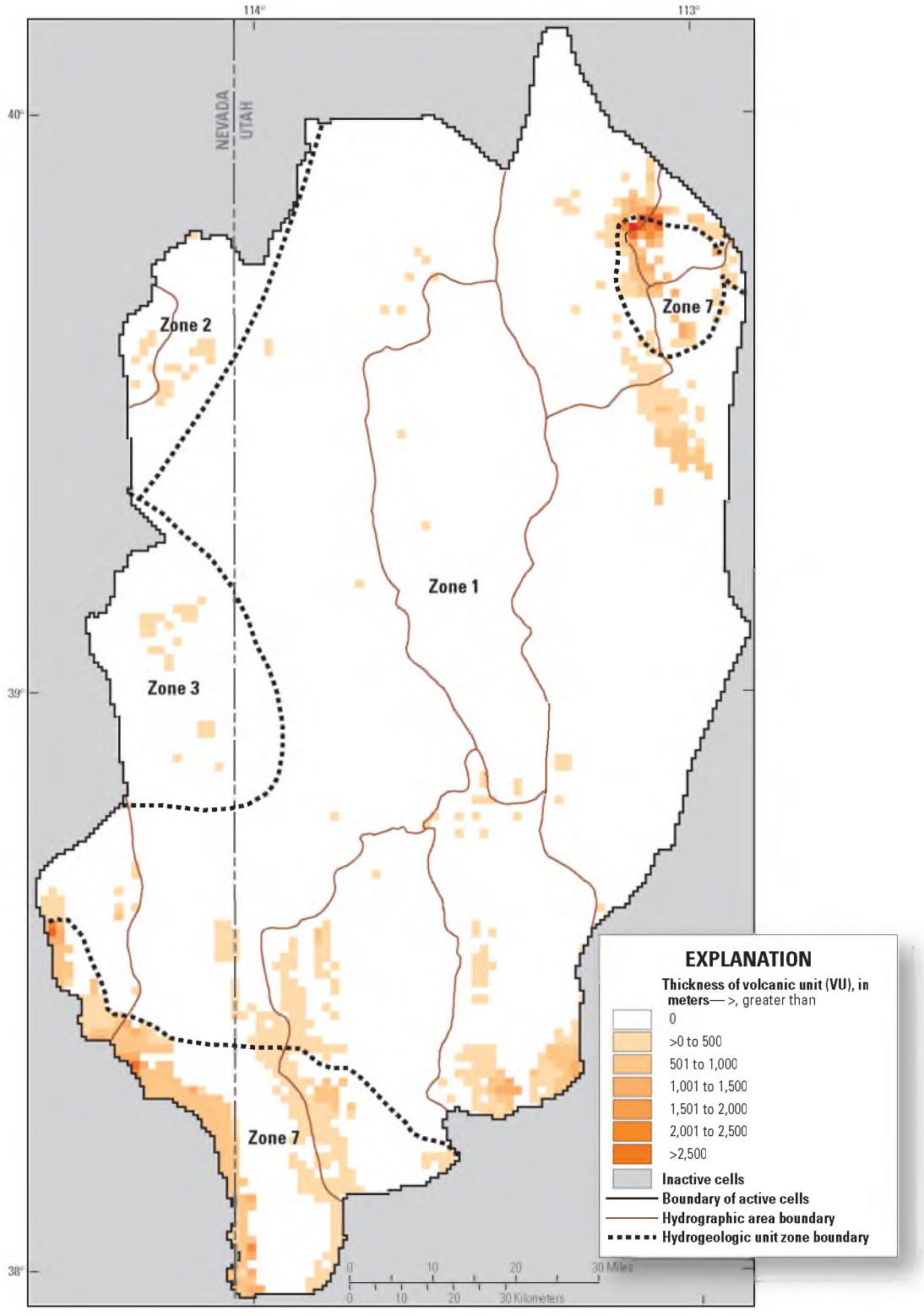

Figure 3-22. Simulated extent, thickness, and initial hydrogeologic unit zones of the volcanic unit (VU) in the Snake Valley area groundwater model. State boundary data from: *U.S. Census Bureau* [2000]. Modified from: *Masbruch et al.* [201X], in review.

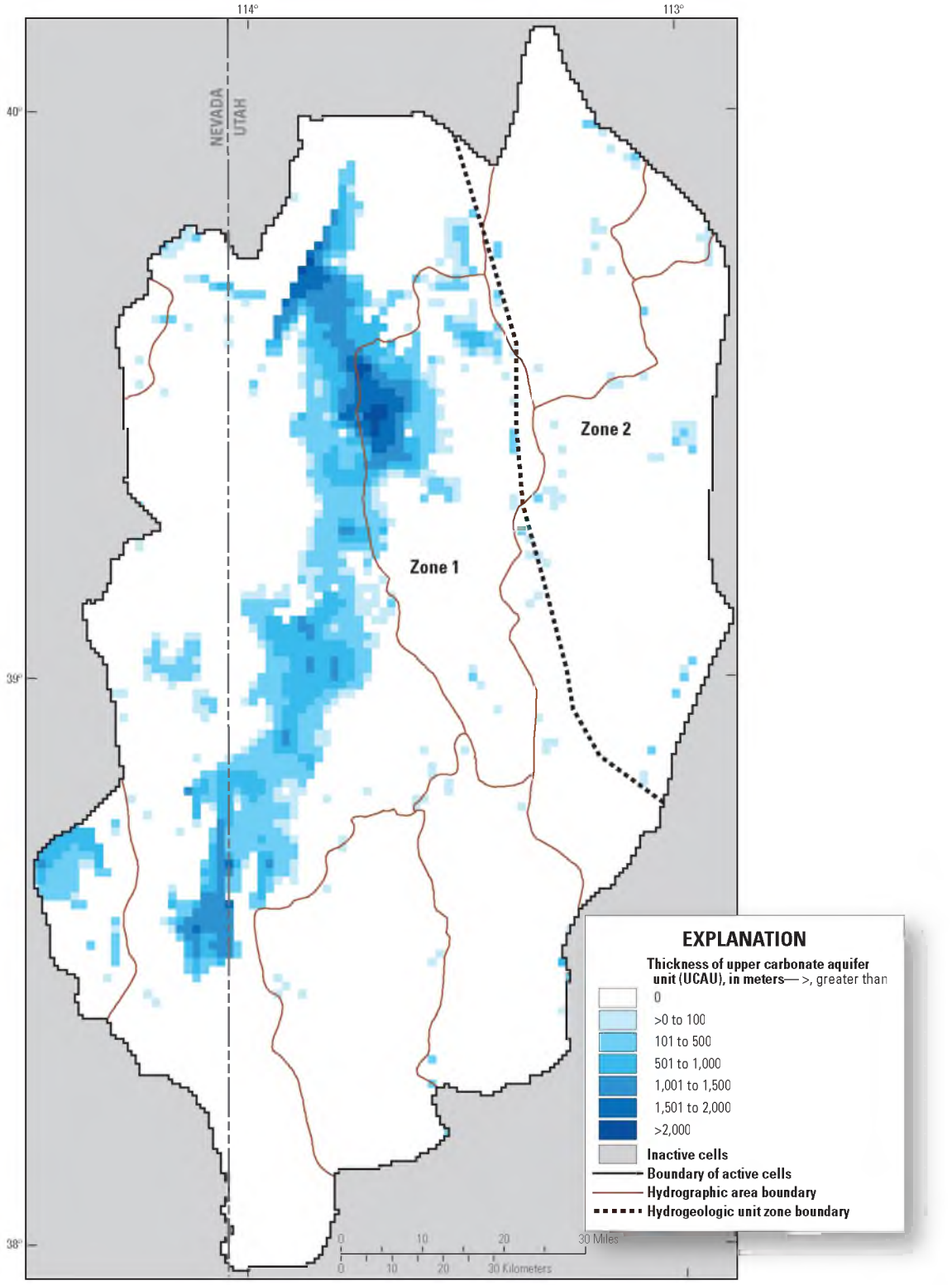

Figure 3-23. Simulated extent, thickness, and initial hydrogeologic unit zones of the upper carbonate aquifer unit (UCAU) in the Snake Valley area groundwater model. State boundary data from: *U.S. Census Bureau* [2000]. Modified from: *Masbruch et al.* [201X], in review.

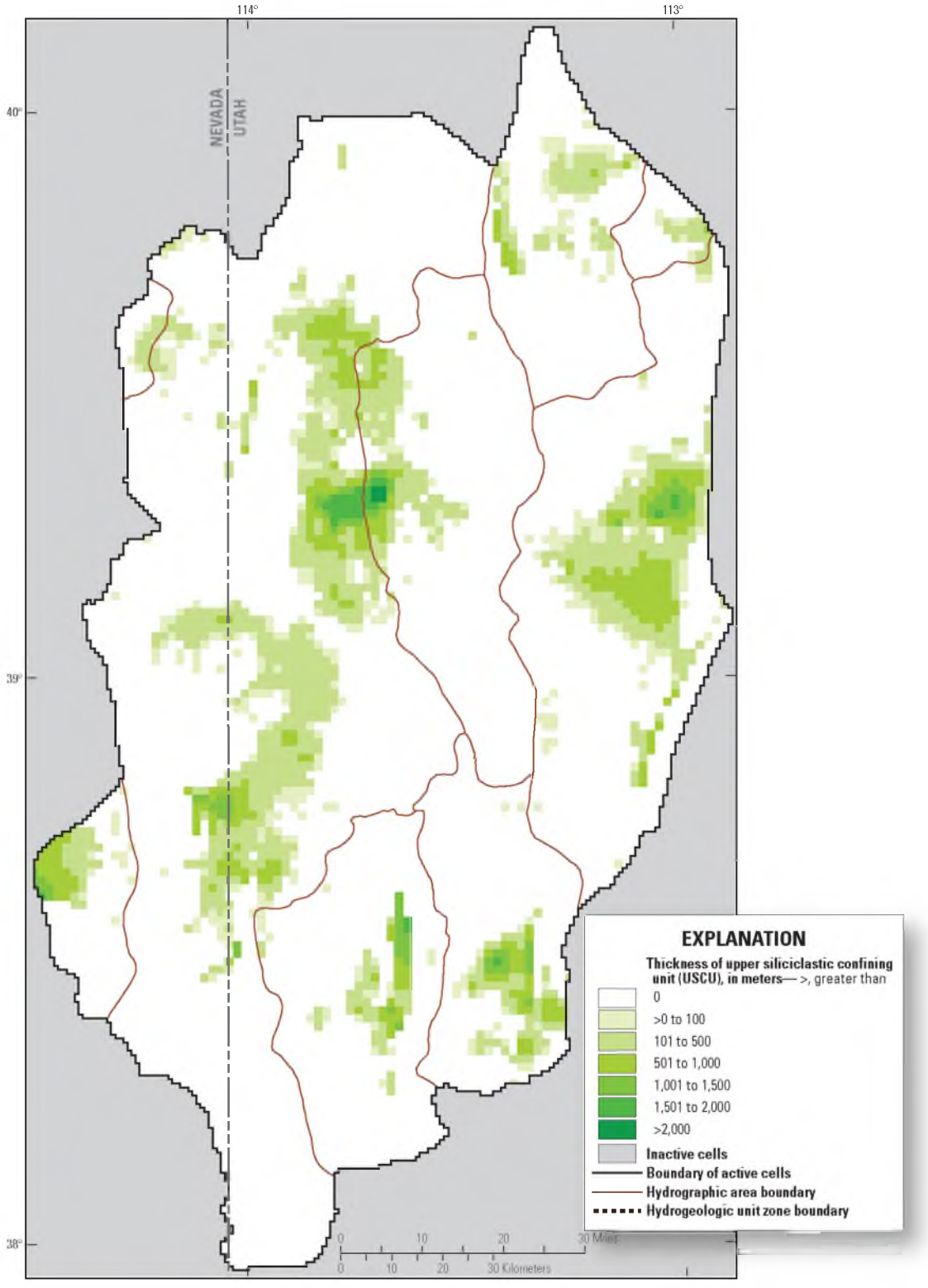

Figure 3-24. Simulated extent and thickness of the upper siliciclastic confining unit (USCU) in the Snake Valley area groundwater model. State boundary data from: *U.S. Census Bureau* [2000]. Modified from: *Masbruch et al.* [201X], in review.

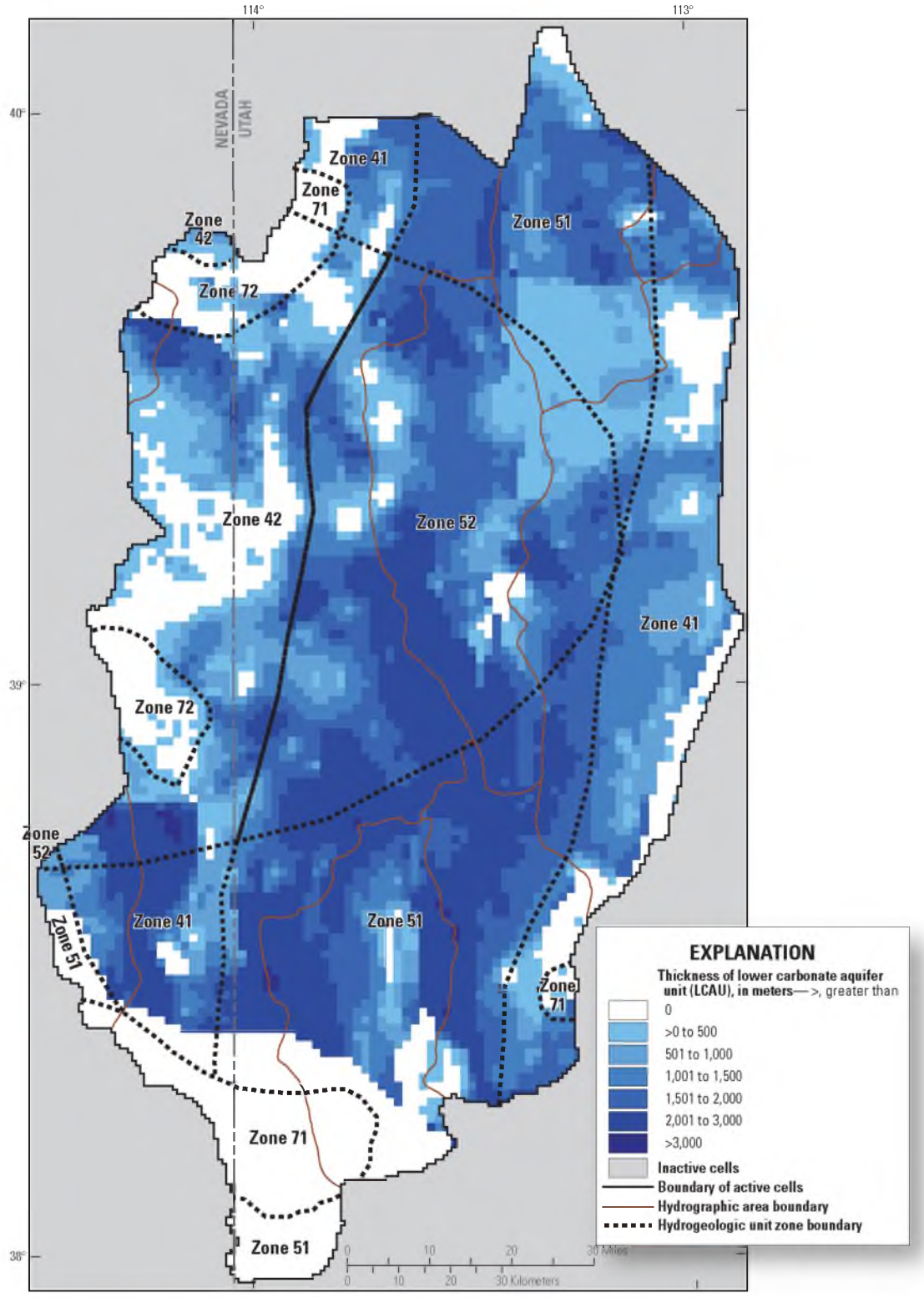

Figure 3-25. Simulated extent, thickness, and initial hydrogeologic unit zones of the lower carbonate aquifer unit (LCAU) in the Snake Valley area groundwater model. State boundary data from: *U.S. Census Bureau* [2000]. Modified from: *Masbruch et al.* [201X], in review.

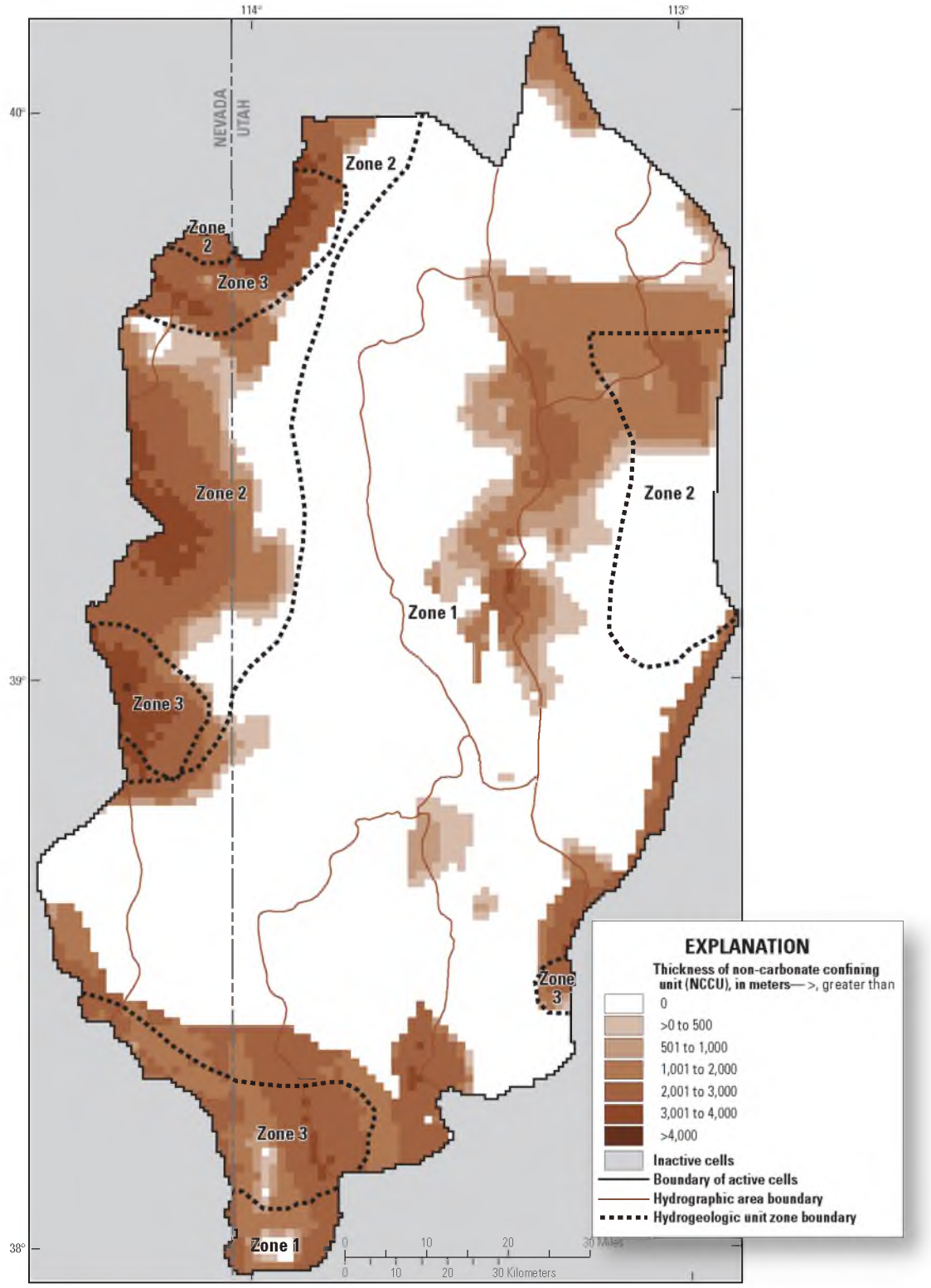

Figure 3-26. Simulated extent, thickness, and initial hydrogeologic unit zones of the non-carbonate confining unit (NCCU) in the Snake Valley area groundwater model. State boundary data from: *U.S. Census Bureau* [2000]. Modified from: *Masbruch et al.* [201X], in review.

horizontal-flow barriers using the HFB Package [*Harbaugh et al.*, 2000] were used to reduce the hydraulic conductivity between model cells. The HFB Package takes as input the location of the horizontal-flow barrier and the hydraulic characteristic of the barrier, which is the hydraulic conductivity of the barrier divided by the width of the barrier. The HFB Package allows the value of the hydraulic characteristic of the barrier to be defined as a parameter. Simulated horizontal-flow barriers in the model are located along cell boundaries to approximate the location of the features. The horizontal-flow barrier between Snake Valley and Pine and Tule Valleys (B_SV_NS1) corresponds with a steeply, almost vertically, dipping syncline limb of USCU (Figure 3-27); this HFB is simulated in all seven layers, except for a short section near the center of the length of the HFB where there is a slight break in the USCU. The horizontal-flow barriers near Gandy Springs in northern Snake Valley (B_SV_GWS) and Wah Wah Springs in Wah Wah Valley (B_SV_WWS) correspond to mapped faults in the study area (Figure 3-27); these HFBs are simulated in all seven layers in the model. Parameters representing the hydraulic characteristic of the horizontal-flow barriers were defined and allowed to vary during model calibration and parameter estimation.

3.5.1.6 Thermal Properties

Five additional thermal properties that were required for the heat transport model are porosity, thermal diffusivity, dispersivity, bulk density, and the thermal distribution factor. These are assigned in MT3DMS in arrays that represent each model layer [*Zheng and Wang*, 1999]. The equations that were used to calculate each of these parameters are given in Appendix A.

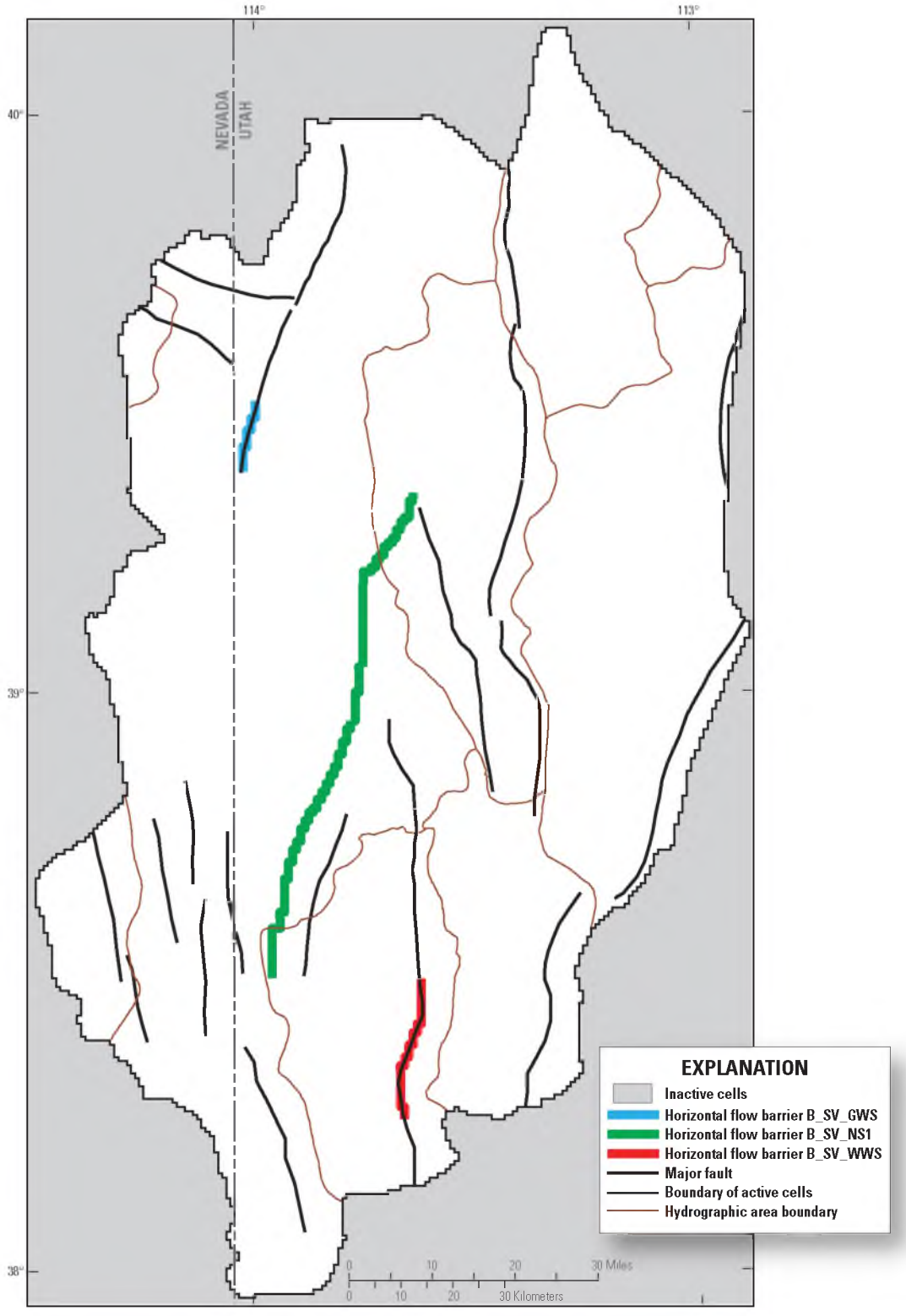

Figure 3-27. Map showing location of faults and simulated horizontal-flow barriers within the Snake Valley study area. State boundary data from: *U.S. Census Bureau* [2000]. Modified from: *Masbruch et al.* [201X], in review.

3.5.1.6.1 Porosity

Porosity is defined as the percentage of rock that is void space [*Domenico and Schwartz*, 1998]. It is needed in transport models to define the volume of water containing solute, in this case heat, in the bulk volume of the system. It is also needed to compute the bulk thermal conductivity and bulk density of the system (Appendix A).

Because a model cell may contain multiple HGUs, the porosity for each cell was calculated using a thickness weighted mean for each HGU within the cell (Appendix A). It was assumed that UBFAU, LBFAU, and VU have a porosity of 0.3 (middle of range of porosities for sediments and basalts reported in *Domenico and Schwartz* [1998]); UCAU and LCAU have a porosity of 0.1 on the basis of the reported range for carbonates in the Great Basin [*Harrill and Prudic*, 1998]; and that USCU and NCCU have a porosity of 0.01 on the basis of a model using similar rock types [*Manning and Solomon*, 2005]. Early simulations showed that the model was insensitive to porosity; these values were held constant and not included in sensitivity analysis or regression.

3.5.1.6.2 Thermal Diffusivity

Thermal diffusivity, which is analogous to the molecular diffusion term in solute transport [*Langevin et al.*, 2008], is used to define the heat transport process of thermal conduction within the system. The thermal diffusivity is dependent on the bulk thermal conductivity of the aquifer (includes both the solid aquifer material and the fluid in the pore spaces, in this case groundwater), the porosity of the aquifer, the density of the groundwater, and the heat capacity of the groundwater (Appendix A).

Thermal diffusivity was initially set up with a parameter that was allowed to vary and that defined a multiplier on the diffusivity (DMCOEF) array in the Dispersion

Package in MT3DMS where thermal diffusivity is assigned [*Langevin et al.*, 2008; *Zheng and Wang*, 1999]. This multiplier, however, was not allowed enough significant figures in MT3DMS for UCODE_2005 to determine any sensitivity on this parameter. Simple tests showed that small changes in thermal diffusivity had little effect on temperatures within the model. Thermal diffusivity, therefore, was held constant and not included in sensitivity analysis or regression.

3.5.1.6.3 Dispersivity

Dispersivity values are needed to calculate the dispersion coefficient term of the transport equation, which accounts for the apparent spreading of heat along flow paths due to small-scale variations in the groundwater velocity caused by small-scale heterogeneities in the aquifer. Values of dispersivity are highly scale dependent [*Gelhar et al.*, 1992]; dispersivity observed at a regional scale is much higher (up to several orders of magnitude) than dispersivity observed at a more local scale.

For a three-dimensional transport model, three types of dispersivity need to be considered: (1) longitudinal dispersivity, which describes the dispersive transport in the direction parallel to groundwater flow; (2) horizontal-transverse dispersivity, which describes the dispersive transport perpendicular to groundwater flow in the horizontal direction; and (3) vertical-transverse dispersivity, which describes the dispersive transport perpendicular to groundwater flow in the vertical direction [*Zheng and Bennet*, 2002]. Without field data, *Zheng and Bennett* [2002] suggest that horizontal-transverse dispersivity should be one order of magnitude less than longitudinal dispersivity, and vertical-transverse dispersivity should be two orders of magnitude smaller than longitudinal dispersivity.

Longitudinal dispersivity and the ratios of horizontal- and vertical-transverse dispersivity to longitudinal dispersivity are assigned in the Dispersion Package in MT3DMS. Longitudinal dispersivity can be defined as being 5 to 10 percent of the scale of the system or length of the flowpaths [*Gelhar et al.*, 1992]. In the current study area, possible flowpath lengths can vary over two orders of magnitude, from less than 10 km to more than 100 km. Longitudinal dispersivity, therefore, was defined as a parameter and allowed to vary during model calibration and parameter estimation.

3.5.1.6.4 Bulk Density and Thermal Distribution Factor

The bulk density and thermal distribution factor, assigned in the Chemical Reaction Package in MT3DMS, are used to compute the thermal equilibration between the aquifer solids and fluid (groundwater). The bulk density is dependent on the density of the aquifer solids and the porosity of the aquifer (Appendix A). The thermal distribution factor depends on both the heat capacity of the aquifer solids and fluid (groundwater), and the density of the groundwater (Appendix A). Early simulations showed that the model was insensitive to the bulk density and thermal distribution factor, so these values were held constant and not included in sensitivity analysis or regression.

3.5.2 Observations Used in Model Calibration

Model observations are measured values of water levels, spring discharge, gain and loss in streams, and other measurable indicators of the groundwater system. The term "observation" is used to denote that model output will be compared to the measured value, and this comparison is part of calibration, sensitivity analyses, and parameter estimation. Observations used in model calibration include water-level altitudes;

discharge measurements from springs, mountain streams, and evapotranspiration areas; and groundwater temperatures from wells. Additional measurements of spring and river water-level altitudes, and selected groundwater temperature measurements at springs were also included. For each set of observations, uncertainties, which are expressed as standard deviation (σ), variance (σ^2), or coefficient of variation (σ divided by the observation value), were calculated. These were then converted to variances which UCODE_2005 uses to define weights (which equal 1 divided by the variance) that are applied to the observations for sensitivity analyses and parameter estimation.

3.5.2.1 Water Levels

Water-level altitudes used for model calibration were collected in early spring 2009 from 123 wells in the Snake Valley study area (Figure 3-28). Only 27 wells within the study area had long-term records. At these wells the spring 2009 water-level measurements were found to be similar to long-term average water levels. Additionally, the spring 2009 water-levels measured in wells without long-term records were similar to those with long-term records. The spring 2009 water-level measurements used as observations in the model, therefore, were assumed to represent steady-state conditions. Most observations are from wells completed in the shallow part of the groundwater system. For wells open to more than one model layer, simulated water levels are a weighted average based on the proportion of the open interval of the well within each layer, which is calculated by the Hydraulic-Head Observation Process of MODFLOW-2000 [*Hill et al.*, 2000].

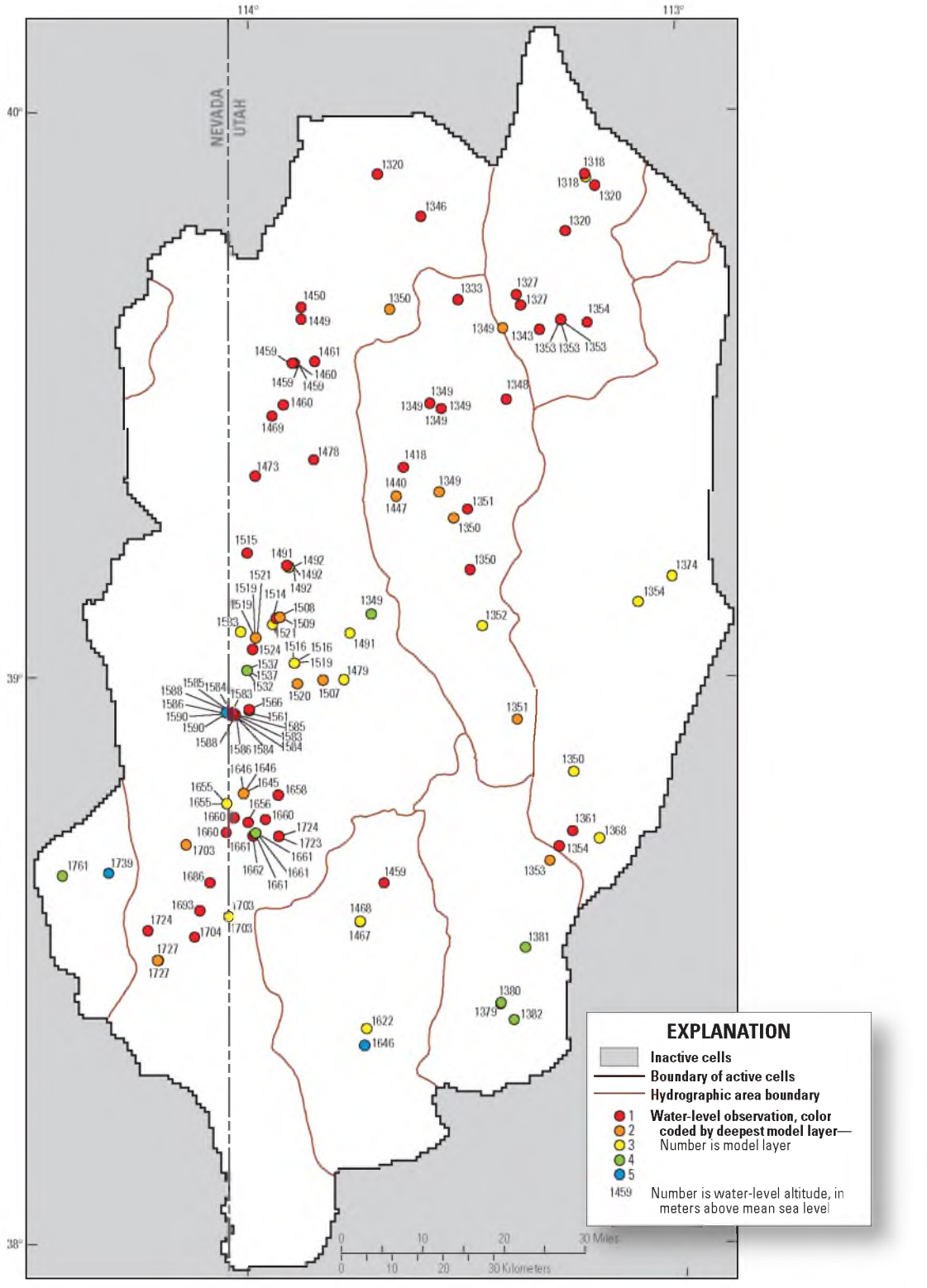

Figure 3-28. Spatial distribution of water-level observations used in calibration of the Snake Valley area groundwater model. State boundary data from: *U.S. Census Bureau* [2000]. Modified from: *Masbruch et al.* [201X], in review.

3.5.2.1.2 Water-Level Uncertainty

The uncertainty determined for each water-level observation includes uncertainties related to errors in the well altitude and location, water-level measurement error, nonsimulated transient error, and model discretization. The error for each of these components was calculated following the procedure outlined by *San Juan et al.* [2010] and *Faunt et al.* [2010] and is presented in Appendix B.

The standard deviations of water-level observations range from 1.2 m to 7.7 m, and average 2.3 m. About 98 percent of the water-level observations have a standard deviation of less than 5 m, and about 41 percent have a standard deviation of less than 2 m. The contribution of individual sources of uncertainty to total water-level observation uncertainty varies. In general, the smaller uncertainties are dominated by nonsimulated transient and model discretization error, while the larger uncertainties are dominated by well-altitude and model discretization error.

3.5.2.2 Water Levels at Discharge Locations

Water levels at selected discharge locations were also used as observations early in the process of model calibration because, if simulated discharge to a head-dependent boundary is zero, the sensitivity of the discharge observation to all parameters is also zero; therefore, this does not create a signal to regression to change parameters that will cause discharge to occur at this location. Water levels at these locations, however, were sensitive, and if the simulated water level was below the observed level, regression would change parameters that would increase the water level and cause discharge to occur.

The altitude used for water-level observations at the springs was set at the minimum of either the reported spring altitude or 10 m below the minimum land-surface

altitude within the cell. For mountain streams, two points were used as water-level observations: one representing stream altitude at the point midway between the gage and the upper end of the stream and one representing the stream altitude near the gage. The variance assigned to the altitude of the discharge points was 100 m^2. These water-level observations were removed from the model once discharge to the spring or stream began to occur, and the discharge observation became sensitive within the regression because the discharge observation may have a different sensitivity than the water level.

3.5.2.3 Water Levels Above Land Surface

During model calibration, the simulated water levels were frequently compared to land-surface altitude to ensure that abnormally high simulated water levels were not occurring. These comparisons were not formally included as observations and, therefore, did not influence the regressed values of parameters. Regressed values of the parameters, however, were modified manually if they created areas with water level altitudes of more than 50 m above the mean land-surface altitude within the cell. Given the large area of the model, the relatively large cell size, and simulated water-level altitudes ranging over almost 2,000 m, an error of 50 m (2.5 percent of simulated range) in simulated water levels was considered acceptable.

3.5.2.4 Groundwater Discharge Observations and Uncertainty

Groundwater discharge observations used for model calibration include discharge to ETg, springs, and mountain streams (Figures 3-6 and 3-29). Uncertainties were calculated depending on the type of data available for each discharge observation and are discussed below.

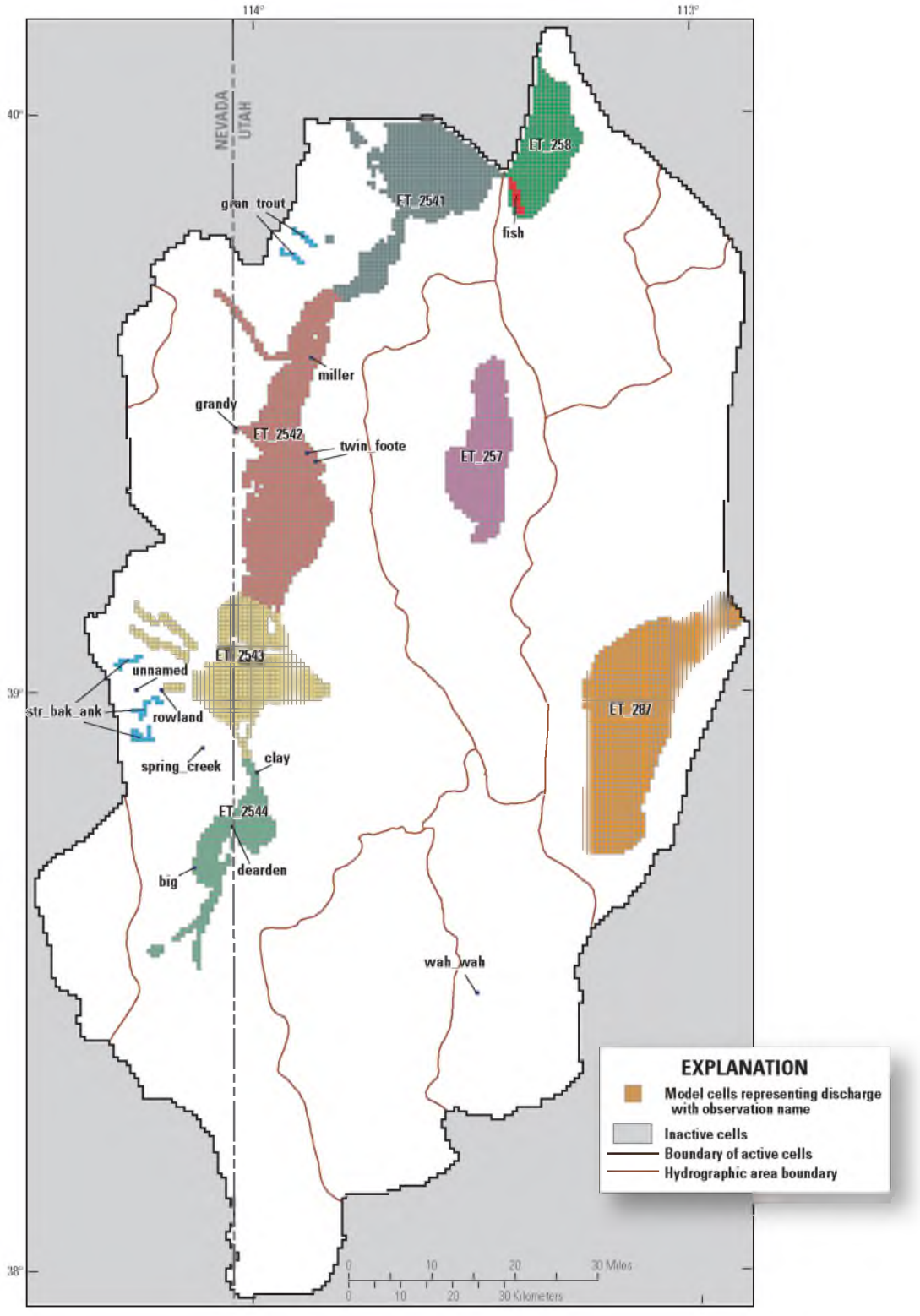

Figure 3-29. Spatial distribution of groundwater discharge observations used in calibration of the Snake Valley area groundwater model. State boundary data from: *U.S. Census Bureau* [2000]. Modified from: *Masbruch et al.* [201X], in review.

During early model calibration, regression would often match water-level observations while ignoring discharge observations when using error-based weights. This is due to observations being clustered in the model because of the high number of water-level observations in relation to the number of discharge observations [*Hill and Tiedeman*, 2007]. All discharge observations, therefore, were given a weight multiplier of 5.0 to force the regression not to ignore these observations [*Hill and Tiedeman*, 2007]. In UCODE_2005, weight is the inverse of the variance, and variance is proportional to the square of the coefficient of variation. Thus, the weight multiplier changes the coefficient of variation on discharge observations from an average of 0.26 to $[0.26/5^{1/2}]$ or 0.11.

3.5.2.4.1 Evapotranspiration

Uncertainties on estimates of groundwater discharge to ETg were determined by assuming a coefficient of variation (CV) of 0.3. This is similar to CVs in other areas of the Great Basin where ETg has been extensively studied. In the Death Valley region, CVs of ETg range between 0.1 and 0.71, and average about 0.31 [*Faunt et al.*, 2010]; in the BARCAS [*Welch et al.*, 2007] study area, CVs of ETg range between 0.13 and 1.5, and average about 0.24 [*Zhu et al.*, 2007].

3.5.2.4.2 Springs

Discharge observations and uncertainties for springs within the study area came from a variety of sources, and are summarized in Table 3-5. At springs with more than one measurement, the discharge and variance were calculated directly from the measurements. If the spring only had one discharge measurement, generally the variance was assumed to equal the average of the variances of springs with similar amounts of

Table 3-5. Summary of discharge data and uncertainty statistics for springs used as observations in the Snake Valley area groundwater model. Modified from: *Masbruch et al.* [201X], in review.

[**Abbreviations:** NWIS, National Water Information System; UGS, Utah Geological Survey; USGS, U.S. Geological Survey]

Spring name	Mean discharge (cubic meters per day)	Coefficient of variation	Period of record used	Discharge data source
Fish Springs	87,790	0.29	1970–1977	*Bolke and Sumsion* [1978]
Miller Spring	931	0.045	5/27/2010–8/2/2010	*L. Jordan, UGS, written commun.* [August, 2010]
Gandy Warm Springs	36,830	0.11	10/1/2005–7/25/2010	*NWIS*, USGS site 10172860
Foote Reservoir Spring	6,968	0.072	6/7/2005–7/6/2010	*L. Jordan, UGS, written commun.* [August, 2010]
Twin Springs (North and South)	6,274	0.017	1/2/2010–7/30/2010	*L. Jordan, UGS, written commun.* [August, 2010]
Unnamed Spring	4,906	0.21	9/7/2007	*NWIS*, USGS site 390042114152601
Rowland Springs	5,576	0.35	10/1/2002–9/30/2004	*NWIS*, USGS site 10243265
Spring Creek Spring	4,648	0.051	6/10/2003–10/7/2003	*Elliott et al.* [2006], Table 4, site Sn5
Clay Spring	868	0.023	9/21/2009–7/7/2010	*L. Jordan, UGS, written commun.* [August, 2010]
Dearden Spring Group	16,320	0.11	9/25/2009–7/26/2010	*L. Jordan, UGS, written commun.* [August, 2010]
Big Springs (North and South)	24,420	0.058	10/1/2005–7/26/2010	*NWIS*, USGS sites 102432241 and 10243224
Wah Wah Springs	2,725	0.37	10/12/1972	*Stephens* [1974]

discharge. Discharge observations from multiple springs were sometimes combined (summed) into one observation (Figure 3-29) because at the regional scale of the model minor variations of discharge in nearby cells is not as important as the total discharge in an area. When spring discharges were combined their variances were summed to determine the new total variance.

For springs monitored by the UGS (Clay, Dearden, Miller, Foote Reservoir, and Twin Springs; Figure 3-6), average discharge and variances were calculated directly from the discharge data [*L. Jordan, Utah Geological Survey, written commun.*, August, 2010]. For Twin Springs, the north pool was monitored slightly longer than the south pool, so the average discharge was calculated as the sum of the averages for each pool, and the total variance was the sum of the variances for each of the pools. Average discharge and variances for Gandy Warm Springs, Rowland Springs, and Big Springs (Figure 3-6) were calculated from discharge data from *NWIS* [accessed on July 26, 2010]. For Spring Creek Spring (Figure 3-6), data from *Elliott et al.* [2006] was used to determine the discharge and variance based on measurement uncertainty (± 8 percent) and seasonal fluctuations (difference between June and October measurements), and it was assumed that these represent with 95 percent confidence the error in the discharge measurement. Unnamed Spring and Wah Wah Springs (Figure 3-6) both only had one reported discharge measurement. Variances for these two springs were determined by taking the average variance for springs with similar discharge (1 to 3 ft^3/s). Discharge from Fish Springs (Figure 3-6) was taken from *Bolke and Sumsion* [1978], and was assumed to have a CV of 0.29 [*L.E. Brooks, USGS, written commun.*, August 2010].

3.5.2.4.3 Mountain Streams

Discharge of baseflow (groundwater) to mountain streams and associated uncertainties were determined using a variety of sources and are summarized in Table 3-6. Baseflow to Granite and Trout Creeks (Figure 3-6) was determined by using the estimates of groundwater discharge to baseflow given in *Heilweil and Brooks* [2011], whereby the annual groundwater discharge was estimated to be the minimum mean daily discharge at each gage for the period of record as reported in NWIS multiplied by 365 days per year. Uncertainty of groundwater discharge to these streams was assumed to have a CV of 0.25 [*L.E. Brooks, USGS, written commun.*, August 2010]. Baseflow to Strawberry, Baker, and Snake Creeks (Figure 3-6) was determined using data from *Elliott et al.* [2006] who performed seepage measurements on these creeks in 2003. The variances of these discharges were based on measurement uncertainty (± 8 percent) and seasonal fluctuations (difference between June and October measurements), and it was assumed that these represent with 95 percent confidence the error in the discharge measurement for Snake and Baker Creeks, and 90 percent confidence for Strawberry Creek. Because these measurements are based on the minimum mean daily discharge or are instantaneous low-flow measurements they are considered to represent the minimum amount of groundwater discharge to mountain streams.

Obersvations of discharge to mountain streams were combined into two groups; Granite and Trout Creeks were combined into one observation (observation name gran_trout), and Strawberry, Baker, and Snake Creeks were combined into another observation (observation name str_bak_snk; Figure 3-29). The variances for each stream were added to determine the total variance for each observation.

Table 3-6. Summary of discharge data and uncertainty statistics for streams used as observations in the Snake Valley area groundwater model. Modified from: *Masbruch et al.* [201X], in review.

Stream name	Mean discharge (cubic meters per day)	Coefficient of variation	Period of record used	Discharge data source
Granite Creek	709	0.25	6/21/2003–6/14/2007	*Heilweil and Brooks* [2011], Auxiliary 3J
Trout Creek	4,052	0.25	12/1/1958–6/14/2007	*Heilweil and Brooks* [2011], Auxiliary 3J
Strawberry Creek	612	5.9	6/10/2003–10/7/2003	*Elliott et al.* [2006], Table 4, site St4
Baker Creek	4,697	0.19	6/10/2003–10/7/2003	*Elliott et al.* [2006], Table 4, site B5
Snake Creek	2,251	3.5	6/10/2003–10/7/2003	*Elliott et al.* [2006], Table 4, site Sn3

3.5.2.5 Groundwater Temperature Observations and Uncertainty

Groundwater temperature observations from groundwater temperature logs collected from 16 wells in the Snake Valley area [*Blackett*, 2011] as part of the UGS Snake Valley ground-water monitoring project, and groundwater temperature data for five springs from NWIS (Figure 3-30), were used for model calibration. Temperatures in the UGS wells were sampled at depths up to 500 m using a high-precision thermistor probe and temperature-logging equipment [*Blackett*, 2011] at intervals of 5 to 20 m. Only temperatures that were taken at or below the water table were used as observations in the groundwater model, and temperature observations from layer 1 were not used because temperatures in layer 1 were assigned as a specified-temperature boundary in most cells (see "Thermal Model Boundary Conditions" section of this chapter). This resulted in a total of 36 temperature observations in different model layers at 21 sites that were used for model calibration.

Temperature observations per each model layer for the wells were calculated as the mean of all temperature measurements across each model layer. If a well did not penetrate the entire layer, then the temperature observation was calculated as either (1) the observation that was closest to the altitude of the middle of the model layer, for wells that reached the middle of the layer; or (2) the temperature observation at the lowest altitude within the layer, for wells that did not reach the middle of the layer. Temperature observations for the springs were calculated as the mean temperature for the period of record and applied to model layer 1.

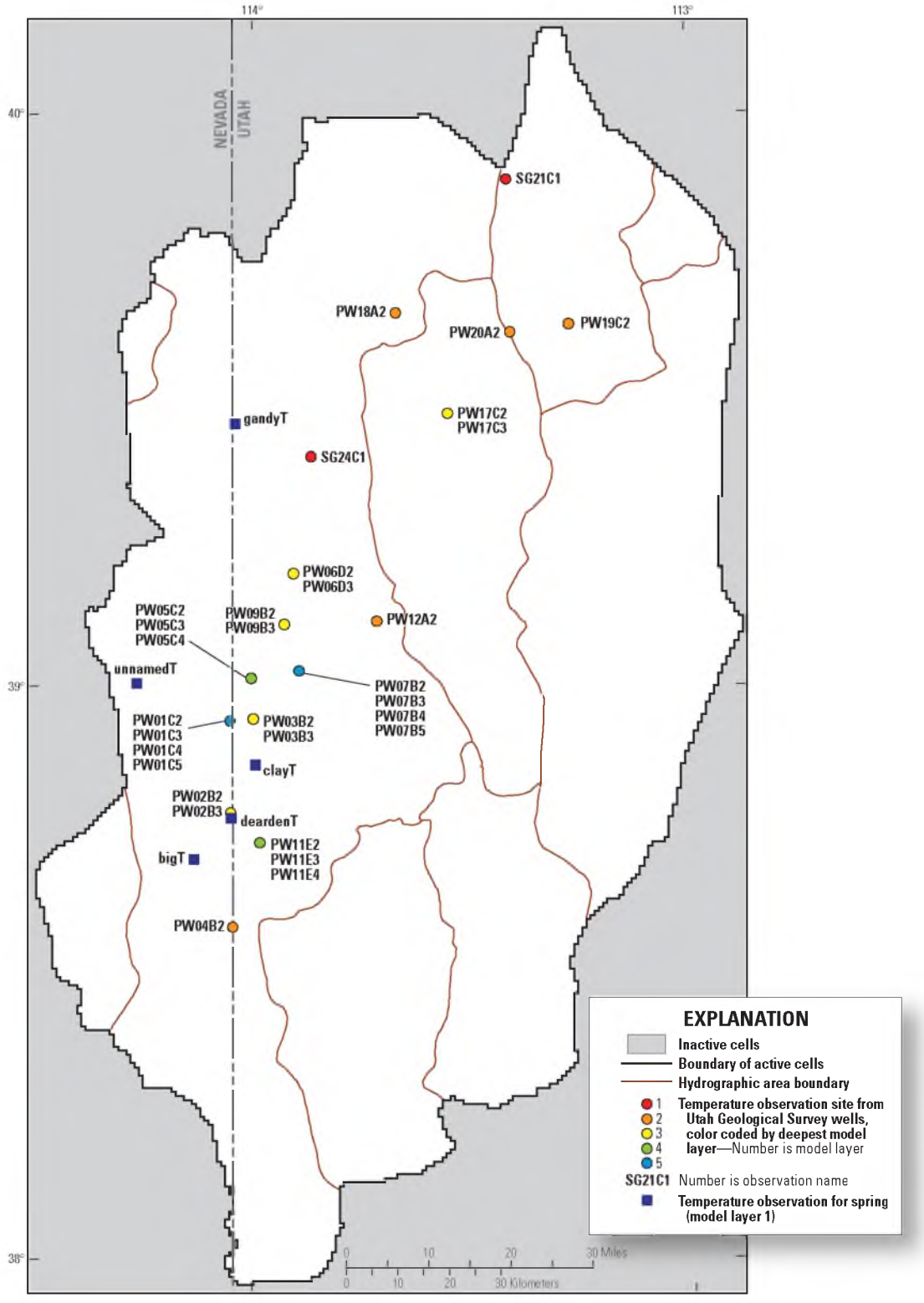

Figure 3-30. Spatial distribution of groundwater temperature observations used in calibration of the Snake Valley area groundwater model. State boundary data from: *U.S. Census Bureau* [2000]. Modified from: *Masbruch et al.* [201X], in review.

3.5.2.5.1 Temperature Observation Uncertainty

The uncertainty determined for each temperature observation includes uncertainties related to errors in the temperature measurement and model vertical discretization, which are discussed in Appendix C. The total standard deviations of temperature observations range from 0.0064 ºC to 1.8 ºC.

During early model calibration, regression would often match temperature observations while ignoring water-level and discharge observations. At the regional scale of the model, local processes that could affect temperature observations such as climatic effects, poor well construction, or local variations in geology or structures which can affect groundwater flow, could not be simulated and, therefore, were omitted. Because these errors cannot be quantified, they could not be directly included in the error-based weighting. The error-based weights on select temperature observations needed to be adjusted, therefore, to reflect the expected error introduced by the omission of these local processes [*Hill and Tiedeman*, 2007]. The temperature observations were split into three groups and given a weight multiplier of 1.0, 0.5, or 0.05 depending on their variance. This weighting changed the average standard deviation of temperatures from 0.33 ºC to 0.35 ºC.

3.5.3 Model Calibration

The objective of model calibration was to develop a model that reasonably represents groundwater recharge, movement, and discharge, and reasonably matches measured water levels and groundwater temperatures. Model calibration was accomplished by minimizing the sum of squared errors between simulated and observed data using UCODE-2005 [*Poeter et al.*, 2005]. During calibration, various aspects of the

model were changed to minimize differences between simulated results and associated observations in order to make differences between simulated and observed water levels, groundwater temperatures, and flows acceptable for the intended use of the model. This model was developed to simulate general groundwater flow and heat transport throughout the Snake Valley study area. It was not developed to simulate local effects of withdrawals, water budgets, or heat transport on a cell-by-cell basis. To determine the value and distribution of hydraulic conductivity, drain and river conductance, horizontal-flow barriers, and heat transport properties, model parameters were adjusted to cause simulated conditions to more closely match steady-state conditions. Calibration was achieved through formal parameter-estimation (nonlinear regression) methods using UCODE-2005 [*Poeter et al.*, 2005] and manual (trial and error) calibration.

3.5.3.1 Approach

Sensitivity analysis was used to evaluate the information provided by the observations for the estimation of all defined parameters, and nonlinear regression was used to estimate selected parameter values. For the Snake Valley area groundwater model, 47 parameters were used in sensitivity analyses and at least 43 were estimated at some point during the modeling process.

Uncertain aspects of the hydrogeology and thermal regime were evaluated by constructing models with different hydraulic-property distributions, and different methods to simulate recharge, discharge, and boundary conditions. These models were evaluated through the sensitivity analysis and nonlinear regression methods. These evaluation tools are discussed in the following sections, as well as how estimated

parameter values considered unreasonable were used to detect model error. The linear confidence intervals used to evaluate the estimated parameter values also are discussed.

3.5.3.1.1 Sensitivity Analysis

Sensitivity analysis was used to assess the effects of different conceptual models (different model designs and parameter values) including: (1) identifying and eliminating insensitive parameters from the regression and model, where possible; and (2) identifying areas where parameters could be further divided or combined. Changes in the conceptual model were assessed by evaluating the effect of parameter changes on model fit. Parameter sensitivities can be used to compare the importance of different observations to the estimation of a single parameter, or the importance of different parameters to the simulation of an observation [*Hill*, 1998].

3.5.3.1.1.1 Composite scaled sensitivity (CSS) is used to evaluate the overall sensitivity of a parameter and to evaluate whether available observations provide adequate information to estimate each parameter [*Hill et al.*, 2000]. CSS can also provide an overall view of the average amount that simulated values change given a 1-percent change in the parameter value [*Hill and Tiedeman*, 2007].

The relative size of CSS values can be used to assess whether additional parameters can be estimated. A relatively large CSS value indicates that observations contain enough information to represent that aspect of the system in more detail using additional parameters. A relatively small CSS value (about two orders of magnitude less than the largest CSS value) indicates that the observations provide insufficient information with which to estimate the parameter [*Faunt et al.*, 2010; *Poeter et al.*,

2005]. Parameters with small CSS values generally were either assigned a fixed value or were lumped with another parameter in this model.

3.5.3.1.1.2 Parameter correlation coefficients (PCC) indicate whether parameter values can be estimated uniquely and are calculated for each pair of parameters [*Hill and Tiedeman*, 2007]. A PCC having an absolute value close to 1.00 indicates that the two parameters involved likely cannot be estimated uniquely. Generally, absolute values greater than 0.95 are cause for concern, but values as small as 0.85 can affect the uncertainty of parameter estimates. In this model, there were no PCC values greater than 0.85.

3.5.3.1.1.3 The RESIDUAL_ANALYSIS program [*Poeter et al.*, 2005] calculates additional statistics (known as influence statistics) useful in identifying observations that are influential in the regression, which aids in finding observation errors and model construction errors, and highlighting changes in model construction that may lead to more realistic values of model parameters. Two of the statistics calculated are the Cook's D and DFBETAS statistics. The Cook's D statistic identifies observations that, if omitted, would cause the greatest changes in estimated parameter values. The DFBETAS statistics identify observations that are influential in the estimation of each parameter [*Poeter et al.*, 2005]. If nonlinear regression led to unreasonable parameter values, or if regression statistics indicated that a parameter change improved one part of the model but made the fit worse in other areas, these statistics were used to make model changes.

3.5.3.1.2 Nonlinear Regression

Nonlinear regression (UCODE_2005) is used to find parameter values that produce simulations that best fit the observations. The fit between model simulated values and associated observations is quantified using a weighted least-squares objective function [*Hill and Tiedeman*, 2007]. The weighting used in the objective function is based on the observation errors presented in the "Observations Used in Model Calibration" section of this chapter and is a diagonal weight matrix, which assumes that errors in the observations are uncorrelated.

Nonlinear regression adjusts parameter values to minimize the sum of squared weighted residuals. Weighted residuals are dimensionless quantities that reflect model fit in the context of the expected accuracy of the observations [*Hill and Tiedeman*, 2007]. A weighted residual of 2.0, for example, indicates that the unweighted residual is twice the observation error, where the error is defined as standard deviation.

3.5.3.1.3 Evaluation of Parameter Estimates

An advantage to using regression to estimate parameter values is that the regression does not limit the parameter estimates to reasonable values [*Faunt et al.*, 2010]. If a model represents a physical system adequately, and the observations used in the regression provide substantial information about the parameters being estimated, estimated parameter values should be realistic. Unrealistic estimated parameter values can indicate model error [*Hill and Tiedeman*, 2007], and that model changes or further calibration are necessary.

Evaluating estimated parameter values requires that a reasonable range of the parameter values be determined from information other than the model simulation. Few

estimates have been completed in the study area, and estimates of hydraulic and thermal properties are sparse. *Sweetkind et al.* [2011a] present estimates of hydraulic properties (summarized in Table 3-1 in this chapter) that were compiled from aquifer tests in the Death Valley regional groundwater flow system (DVRFS), which are considered representative of hydraulic properties over much of the eastern Great Basin because of similar rock types and HGUs. More detail for the hydraulic properties, given in *Belcher et al.* [2002], allow calculation of the standard deviations of the hydraulic conductivity and is summarized in Table 3-7.

Surficial heat-flow values in the study area, which are generally used as a proxy for basal heat flux, range from 50 to 100 mW/m^2 [*Southern Methodist University*, 2011]. While the surficial heat flow within the study area is likely largely affected by groundwater flow, it was assumed that the reasonable range of basal heat flux within the study area was similar to the range of surficial heat-flow values within the study area.

Parameter estimate uncertainty is measured using linear confidence intervals that are calculated by UCODE [*Poeter et al.*, 2005]. The size of the confidence interval is a measure of the amount of information the observations provide about the parameter; a smaller interval typically means that the observations provide more information to constrain the parameter. A linear, 95-percent confidence interval on a parameter estimate that excludes reasonable values indicates model bias, misinterpreted data on the parameter or observations, or incorrect model construction [*Hill and Tiedeman*, 2007]. An estimated parameter value that falls outside the range of reasonable values, but for which the confidence interval includes reasonable values may or may not indicate similar problems.

Table 3-7. Horizontal hydraulic-conductivity estimates and statistics of hydrogeologic units in the Death Valley regional groundwater flow system and relation to hydrogeologic units used in the Snake Valley area groundwater model. Modified from: *Belcher et al.* [2002] and *Masbruch et al.* [201X], in review.

[**Abbreviations:** AA, alluvial aquifer; ACU, alluvial confining unit; DVRFS, Death Valley regional groundwater flow system; LBFAU, lower basin-fill aquifer unit; LCA, lower carbonate aquifer; LCAU, lower carbonate aquifer unit; LCCU, lower clastic confining unit; NCCU, non-carbonate confining unit; OVU, older volcanic rocks unit; TV, Tertiary volcanic rocks; UBFAU, upper basin-fill aquifer unit; UCA, upper carbonate aquifer; UCAU, upper carbonate aquifer unit; UCCU, upper clastic confining unit; USCU, upper siliciclastic confining unit; VSU, volcaniclastic and seidmentary rocks unit; VU, volcanic unit; YVU, younger volcanic rocks unit. Note: Geometric mean and standard deviation are back-transformed from logarithmic values]

DVRFS hydrogeologic unit or subunit	Snake Valley area hydrogeologic unit	Horizontal hydraulic conductivity (meters per day)					Standard deviation of log values	Number of measurements
		Geometric mean	Arithmetric mean	Minimum	Maximum	95-percent confidence interval		
AA	UBFAU, non-playa	1.5	10.8	0.00006	130	0.005–430	1.26	52
ACU	UBFAU, playa	3.0	10.5	0.003	34	0.02–470	1.12	15
YVU/VSU	LBFAU	0.06	1.5	0.00004	6	0.00005–80	1.58	15
TV	VU	0.12	3.9	0.000002	180	0.0002–78	1.43	172
OVU	VU	0.004	0.07	0.000001	1	0.00002–5	1.38	46
UCA and LCA	UCAU and LCAU	2.5	90.0	0.0001	820	0.0008–7,700	1.78	53
UCCU and LCCU	USCU and NCCU	0.00002	0.2	0.00000003	5	0.0000000001–3	2.67	29

In addition to assessing possible model error, confidence intervals on estimated parameters also were used to assess whether all parameters were warranted [*Faunt et al.*, 2010; *Hill and Tiedeman*, 2007]. For example, if the confidence intervals overlapped for two parameters representing the hydraulic conductivity of rock types of similar hydraulic properties, the rocks were represented by a single hydraulic-conductivity parameter. If the simulation using fewer hydraulic-conductivity parameters yielded a similar model fit to the observations, the available observations are insufficient to distinguish between the two models. Thus, the model with more hydraulic-conductivity parameters represents a level of complexity that is not supported by the available data. If model fit significantly deteriorated, the parameters were not combined.

3.5.3.1.3.1 To encourage understanding of the information that is available from observations, model parameters were not constrained during model construction and calibration, and prior information was not used to keep regressed values close to observed values. Because observations are more accurate than prior information on parameter values, observations should be emphasized in model calibration [*Hill and Tiedeman*, 2007]. For final analysis of sensitivity, parameter correlation, parameter confidence intervals, and prediction uncertainty, prior information was used for parameters with very large calculated confidence intervals to simulate a reasonable degree of uncertainty in these parameters [*Hill and Tiedeman*, 2007]. Nine out of the final 51 parameters required prior information.

3.5.3.2 Model Variations

During calibration, a number of models were evaluated. Evidence of model error or data problems was investigated after each model run, and the model fit to observations

was analyzed. These analyses were used in conjunction with hydrogeologic and thermal data to modify and improve the existing conceptual model and observation data sets. Sensitivity and fit statistics were used to determine if model changes, such as rezoning hydraulic conductivity or recharge parameters, could lead to better model fit and if additional parameters were warranted on the basis of the information provided by the observations. Parameters could be divided, for example, if the CSS of a parameter was significantly greater than 1.0 and large compared to the CSS of other parameters [*Hill and Tiedeman*, 2007].

The initial model used the conceptual recharge from the BCM; conceptual groundwater ETg rates; one value of hydraulic conductivity (HK) for each of the HGU zones defined by *Sweetkind et al.* [2011a] (Figures 3-20 through 3-26); one value of vertical anisotropy (VANI) for the UBFAU and one value of VANI for all other units; one value of spring, river bed, and general-head boundary conductance; no horizontal-flow barriers; and one value each for basal heat flux and dispersivity. This model had 39 parameters. Nonlinear regression converged for this model, but took some parameters to unreasonable values, did not provide discharge to 7 of 20 discharge observations, and reduced the overall groundwater budget to about 79 percent of the estimated budget. This was not considered to be an acceptable representation of the groundwater system. The composite scaled sensitivities for the model indicated that the observations provide more information about the hydraulic conductivity of the UBFAU and LCAU HGUs than about any other hydraulic-conductivity parameter (Figure 3-31).

The first conceptual model described above indicated that more variety was needed in the parameters to achieve reasonable matches to groundwater-level, discharge,

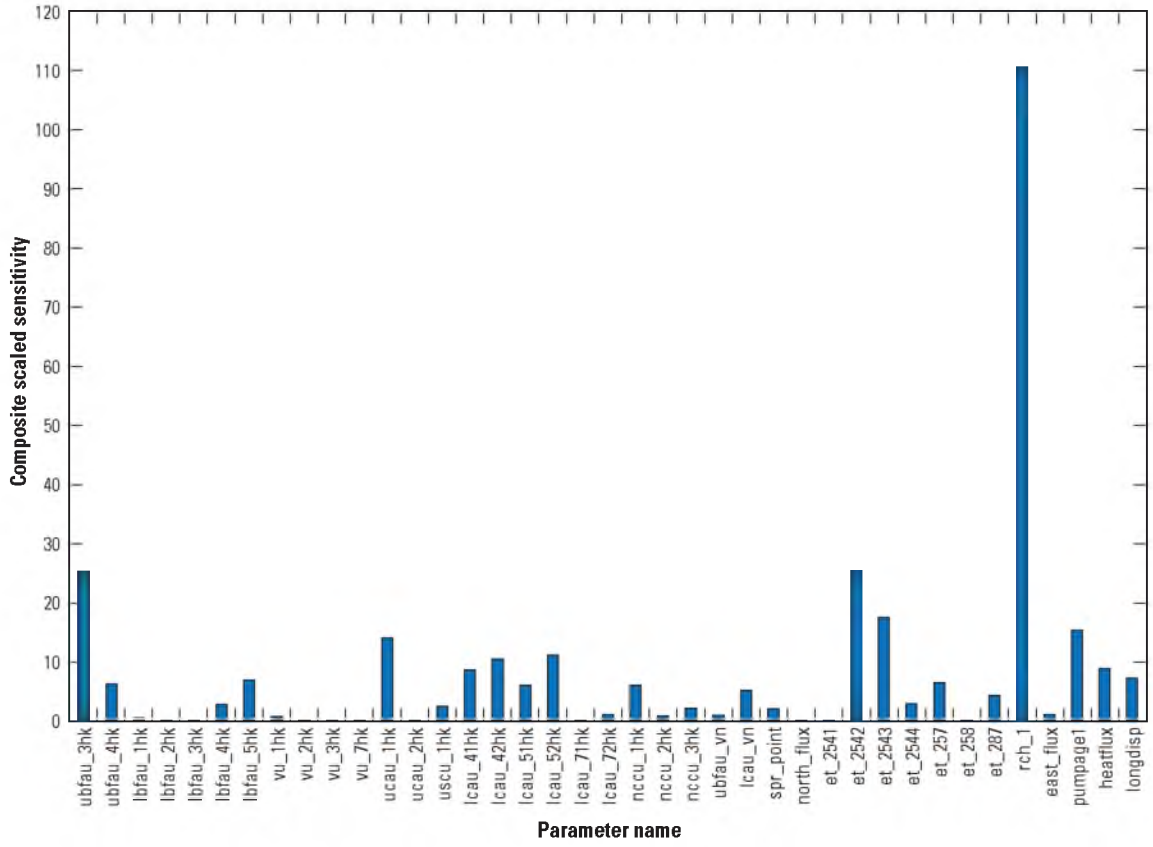

Figure 3-31. Composite scaled sensitivities of parameters used in the initial groundwater model definition of the Snake Valley study area. Modified from: *Masbruch et al.* [201X], in review.

and temperature observations. Additional calibration used the methods discussed in the "Model Calibration Approach" section of this chapter to assign new parameter zones; nonlinear regression was then used to estimate the value of parameters using the new zonation. Multiple versions of the model were created using this method and only changes that improved model fit were retained from one model version to the next, until calibration was achieved; only the final calibrated model construction is discussed in the following sections.

3.5.3.3 Final Calibrated Model

Of the numerous model variations, most differed in how recharge and hydraulic conductivity were represented. The relative likelihood of the different models was evaluated by considering how simulated water levels, discharges, and temperatures compared to the observations, and how the estimated parameters compared to reasonable ranges. The model that yielded the best fit with reasonable parameter values and a reasonable number of parameters was retained. Figure 3-32 shows the composite scaled sensitivities for the final parameter set, and Figure 3-33 shows the calibrated parameter values and their associated 95-percent confidence intervals.

3.5.3.3.1 Recharge

Observations in the Snake Valley area groundwater model are highly sensitive to areal recharge parameters (Figure 3-32; parameters rch_1, rch_2, rch_3, rch_4, and rch_5). As a result, five zones were defined for areal recharge (Figure 3-34). Each recharge parameter refers to one recharge zone. During model calibration, zones were combined and divided on the basis of composite scaled sensitivities and parameter

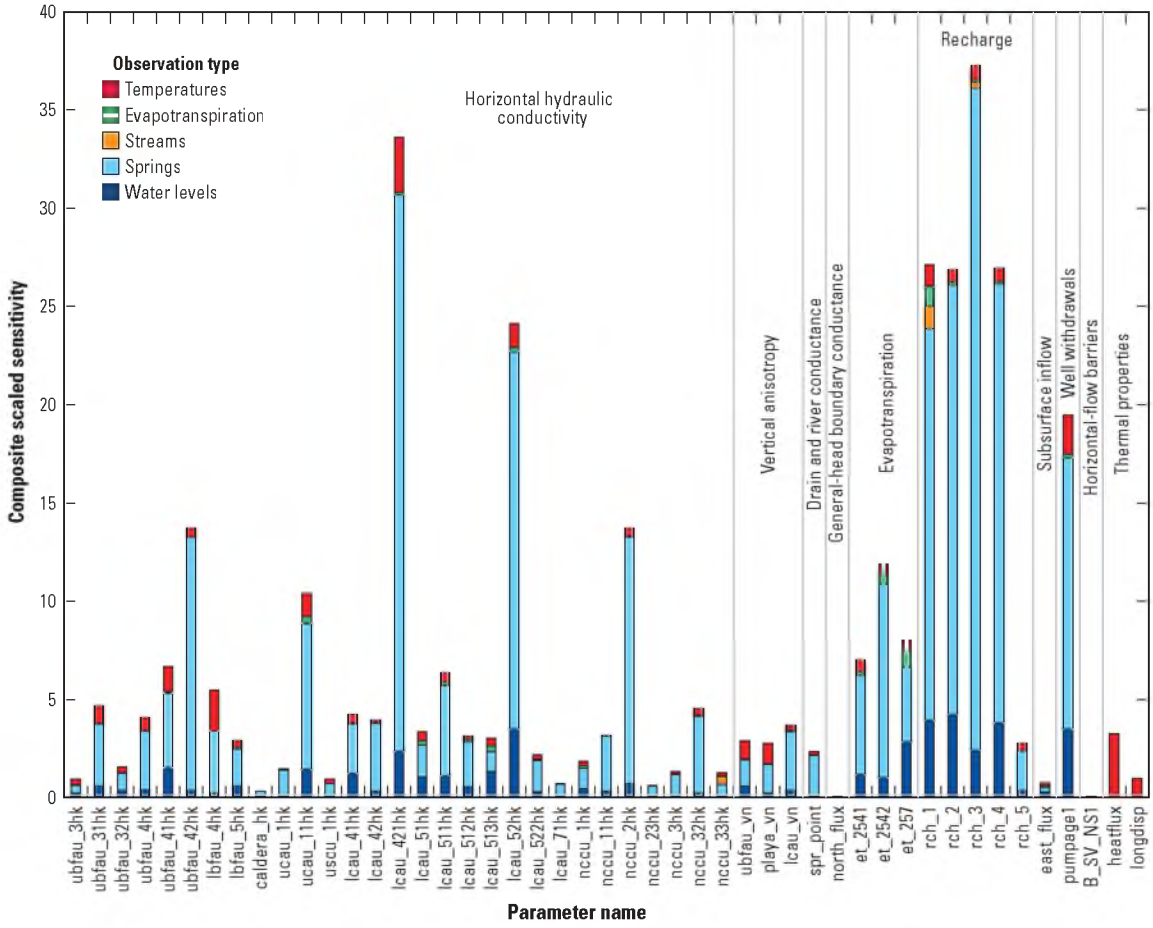

Figure 3-32. Composite scaled sensitivities for parameters used in the final calibrated groundwater model of the Snake Valley study area. Modified from: *Masbruch et al.* [201X], in review.

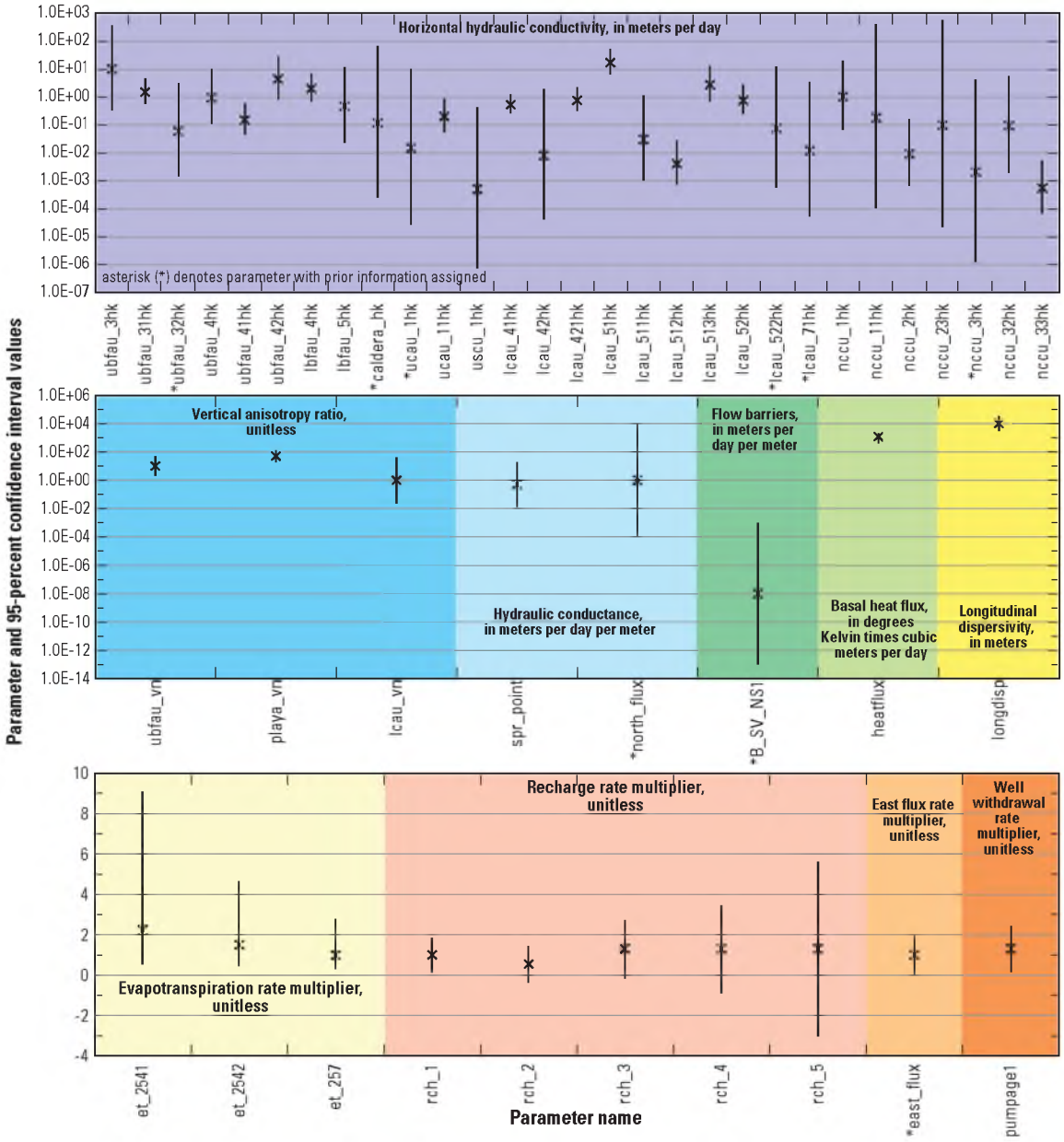

Figure 3-33. Values and linear 95-percent confidence intervals of parameters used in the final calibrated groundwater model of the Snake Valley study area. Modified from: *Masbruch et al.* [201X], in review.

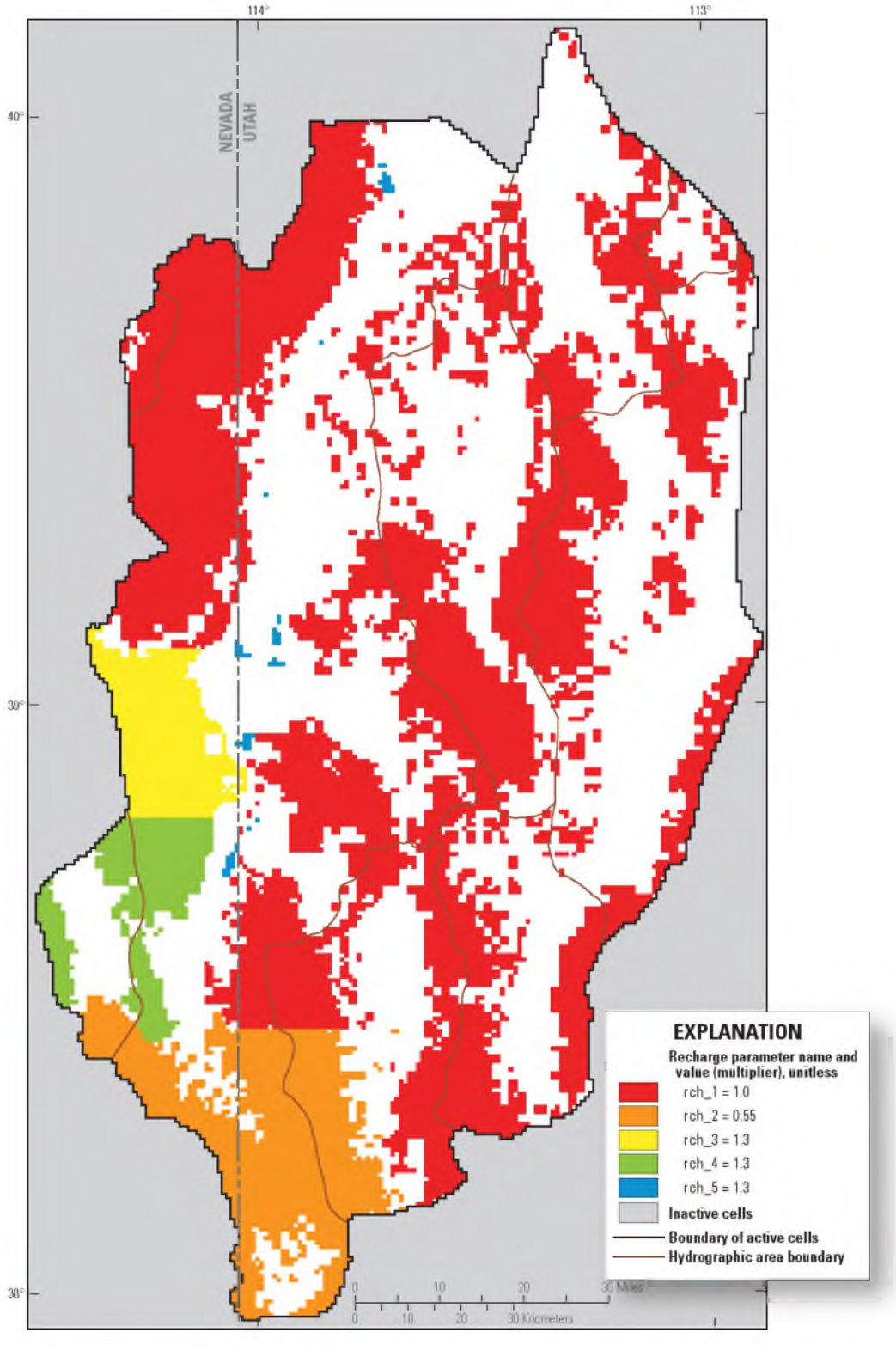

Figure 3-34. Distribution of areal recharge parameters (multipliers) in the Snake Valley area groundwater model. State boundary data from: *U.S. Census Bureau* [2000]. Modified from: *Masbruch et al.* [201X], in review.

confidence intervals. The areal recharge parameter value is a multiplier on the conceptual recharge rate assigned in the model as explained in the "Boundary Conditions" section of this chapter. Generally, the recharge zones were delineated by surficial HGU type; this provides the recharge and variability needed to achieve calibration of this regional model, but should not be considered accurate at the cell-by-cell level. Final areal recharge rates range from 0 to 1.566 mm/d (Figure 3-35).

In the southwestern portion of the study area, recharge over the volcanic units was reduced compared to the BCM with a multiplier of 0.55 to minimize flooding in these mountain blocks and to reduce water-levels in southern Snake and Pine Valleys. Recharge was increased compared to the BCM with a multiplier of 1.3 in the southern Snake Range and in the Fortification Range in Spring Valley, which was indicated by both the temperature and groundwater discharge observations in this area. Recharge from unconsumed irrigation from well withdrawals was increased by a factor of 1.3 because well withdrawals were increased by a factor of 1.3 (see "Discharge" section).

Observations were insensitive to the parameter assigned to the subsurface inflow rates along the eastern boundary of the model (Figures 3-32 and 3-36; parameter east_flux). Because of this insensitivity, a standard deviation of 0.5 was applied to this parameter as prior information.

3.5.3.3.2 Discharge

The conductances of spring (drain), river, and general-head boundary cells, as well as multipliers on the ETg rate and well withdrawal rate were defined as parameters in the groundwater model. Spring, river, and general-head boundary conductances are defined by the conductance factor multiplied by the parameter value. The conductance

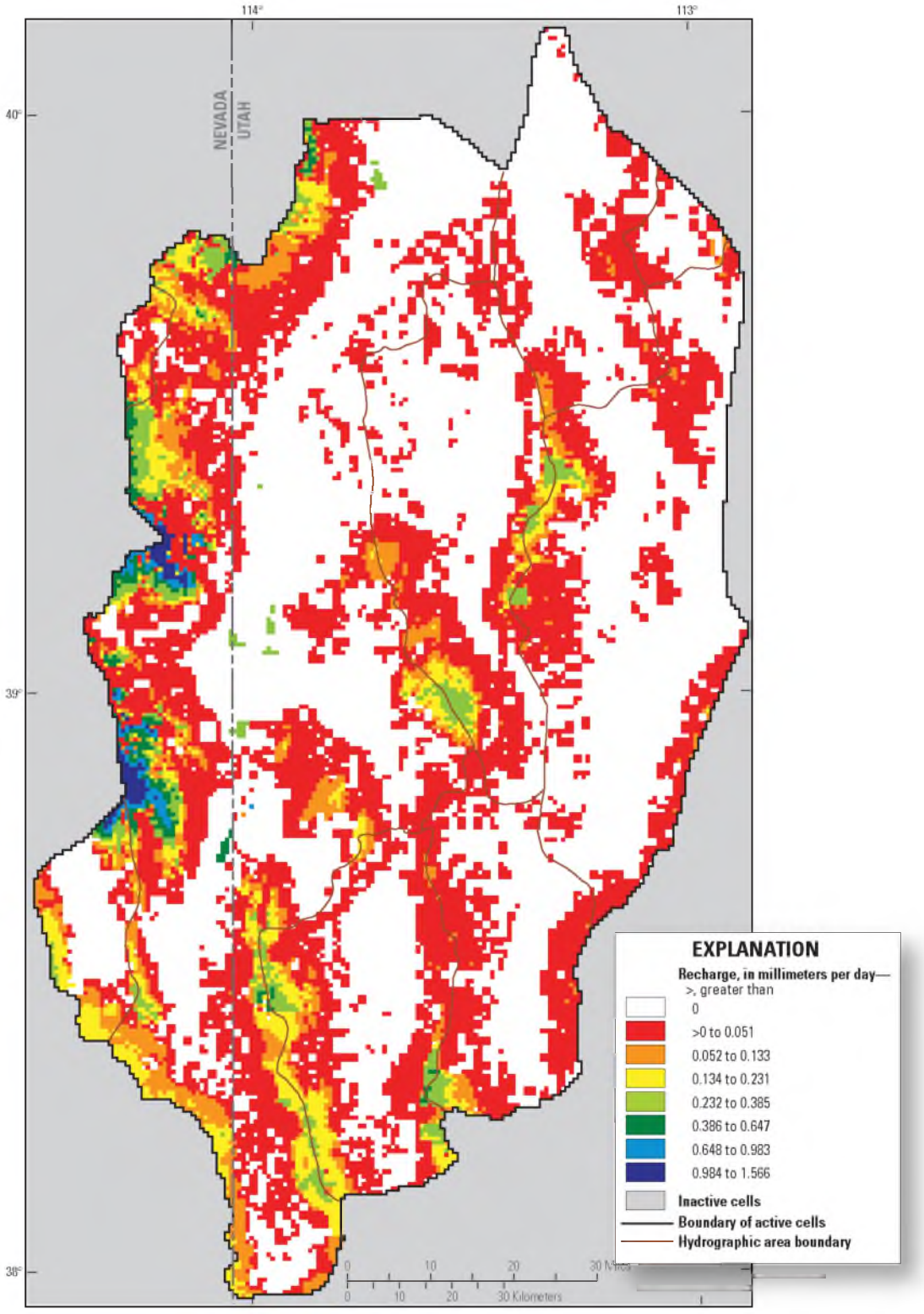

Figure 3-35. Total rate of recharge from precipitation, streams, and irrigation return flow simulated in the Snake Valley area groundwater model. State boundary data from: *U.S. Census Bureau* [2000]. Modified from: *Masbruch et al.* [201X], in review.

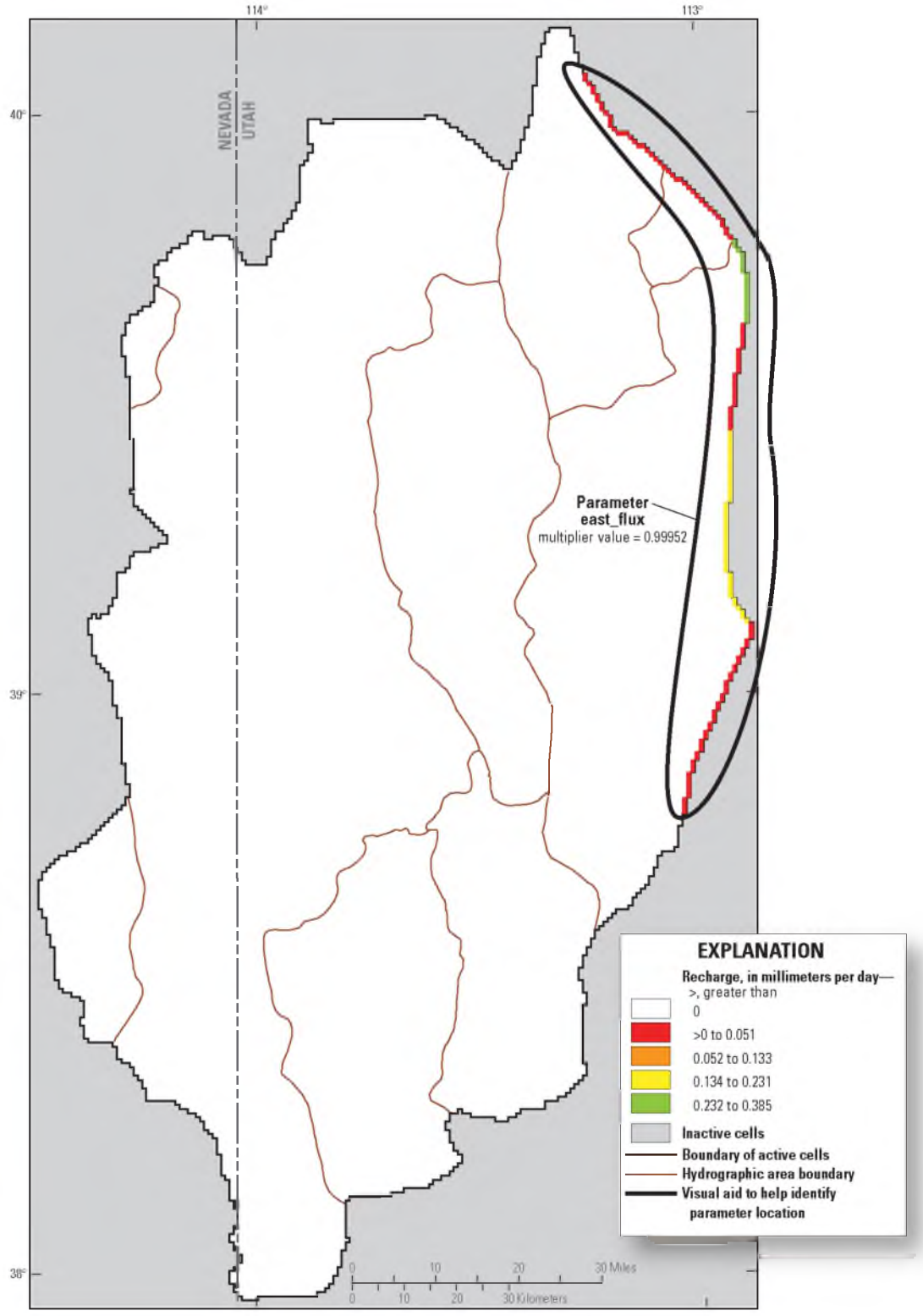

Figure 3-36. Distribution of subsurface inflow recharge parameter (multiplier) and recharge rate simulated in the Snake Valley area groundwater model. State boundary data from: *U.S. Census Bureau* [2000]. Modified from: *Masbruch et al.* [201X], in review.

factor for rivers is the length of river segment in a cell; width was not used because many of the rivers are mountain streams and have similar width. The conductance factor for all point springs is one-tenth of the cell area. The conductance factor for area springs (Fish Springs) is the area of the spring in each cell. Model observations were insensitive to the conductance on the rivers and area springs, but were somewhat sensitive to the conductance on the point springs (Figure 3-32). The conductances for rivers, area springs, and point springs were combined into one parameter (spr_point) in the final calibrated model.

The conductance factor for the general-head boundary cells that simulate flow out of the model boundary to the north was defined as the cross-sectional area of the cell face that is perpendicular to the direction of flow (cell width multiplied by the layer thickness). One parameter (north_flux) was used to define conductance for the general-head boundary. Model observations were insensitive to this parameter (Figure 3-32). Because of this insensitivity, and because conductance is dependent on hydraulic conductivity, a standard deviation of 2.67, the highest standard deviation for hydraulic conductivity (Table 3-7), was applied to the log values of this parameter as prior information.

Model observations were highly sensitive to the multiplier applied to the ETg rate (Figure 3-32). Similar to recharge, the parameter values were defined using zones and early during the modeling process were generally defined at the HA or sub-HA level. During model calibration, zones were combined or divided on the basis of composite scaled sensitivities and parameter confidence intervals. In the final calibrated model three parameters were defined in the model to simulate discharge to ETg (Figure 3-37); this

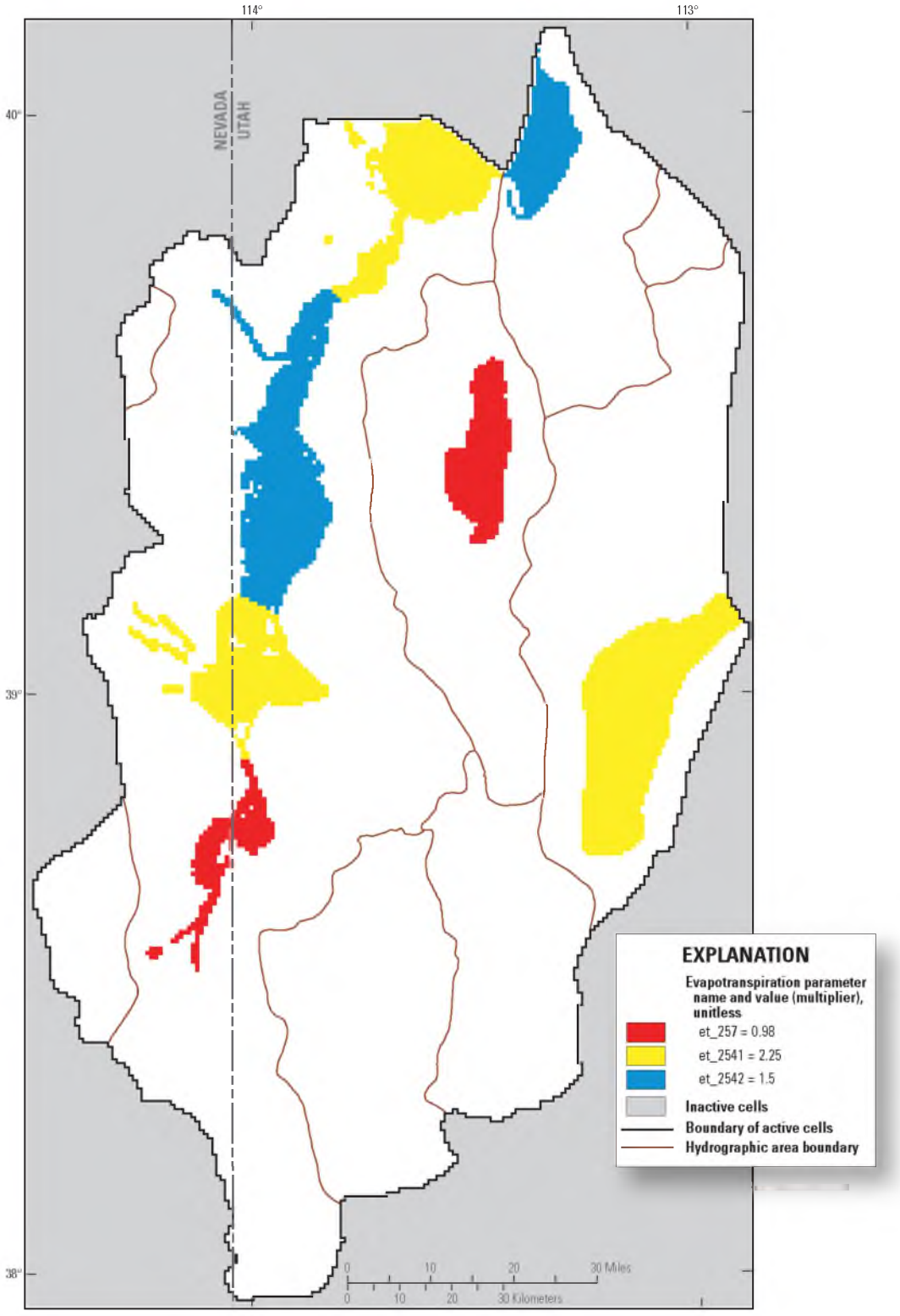

Figure 3-37. Distribution of evapotranspiration parameters (multipliers) in the Snake Valley area groundwater model. State boundary data from: *U.S. Census Bureau* [2000]. Modified from: *Masbruch et al.* [201X], in review.

provides the variability needed to achieve calibration of this regional model, but should not be considered accurate at the cell-by-cell level. Final simulated ETg rates range from 0 to 0.515 mm/d (Figure 3-38).

Model observations were also greatly sensitive to the multiplier applied to the well withdrawal rate (Figure 3-32). One parameter (pumpage) was used to define this multiplier. The value of this parameter, 1.3, was determined by regression within reasonable limits, as the uncertainty on the well withdrawal estimates, which was based on using power records to rate the wells, can be as high as 50 percent [*M. Enright, USGS, oral commun.*, August 2010].

3.5.3.3.3 Horizontal Hydraulic Conductivity

Horizontal hydraulic-conductivity parameters were assigned using the zonation capability of the HUF package [*Anderman and Hill*, 2000]. Model zones are used to define areas with the same simulated properties within individual HGUs. Hydrogeologic evidence was used initially to define model zones (Figures 3-20 through 3-26) of similar horizontal hydraulic conductivity within the HGUs [*Sweetkind et al.*, 2011a]. A parameter defining the horizontal hydraulic conductivity was associated with each model zone. During calibration, however, it became apparent that this zonation does not provide enough variability in hydraulic conductivity to achieve adequate matches to observations. Additional model zones and parameters were added to achieve calibration while minimizing the number of parameters.

These additional model zones were delineated within the original 23 HGU zones described by *Sweetkind et al.* [2011a] (Figures 3-20 through 3-26) using CSS and DFBETAS statistics. These statistics represented the ability and need to define additional

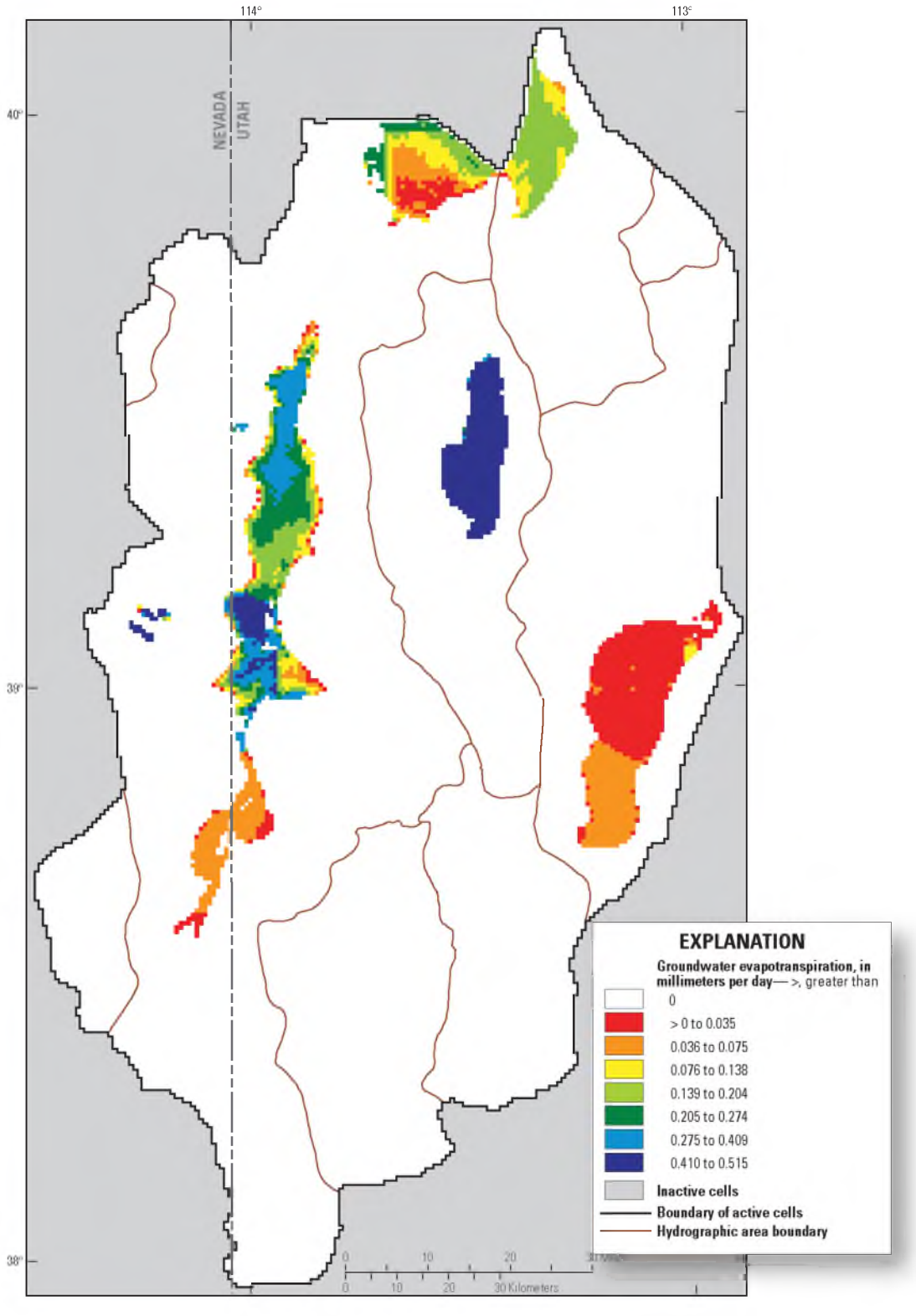

Figure 3-38. Total rate of evapotranspiration simulated in the Snake Valley area groundwater model. State boundary data from: *U.S. Census Bureau* [2000]. Modified from: *Masbruch et al.* [201X], in review.

model zones and parameters to aid the calibration. For instance, a model zone may include a part of NCCU zone 1 (Figure 3-26), but does not include other parts of NCCU zone 1 or any part of NCCU zone 2.

A final set of 29 horizontal hydraulic-conductivity parameters was used to calibrate the model. During calibration, in order to reduce the number of parameters, relatively insensitive hydraulic-conductivity parameters were combined with parameters of similar hydraulic conductivity. As a result, in some cases the hierarchy described above is not maintained, and rocks from different HGUs and different geologic zones within these HGUs (as defined by *Sweetkind et al.* [2011a]) were simulated using the same parameter and the naming convention modified. Calibrated horizontal hydraulic-conductivity parameters are listed in Table 3-8; Figures 3-39 through 3-45 show the distribution of simulated hydraulic conductivity in each HGU. The variability in hydraulic conductivity is adequate to achieve calibration of this regional model but should not be considered accurate at a cell-by-cell level. The zonation and parameter values may not be unique; it is possible that different zones and parameter values could achieve a comparable model fit.

3.5.3.3.3.1 Model observations generally provide good information about the hydraulic conductivity of the NCCU (Figure 3-32) and seven parameters with values ranging from 0.00055 to 1.0 m/d define it in the model (Figure 3-39 and Table 3-8). The estimated values of the parameters are within the expected hydraulic conductivity range reported for the NCCU (Table 3-7), and all except one parameter (nccu_3hk) could be estimated with more certainty than the measured standard deviation of 2.67 on the log values of the parameters (Table 3-7). The measured standard deviation of 2.67 was

Table 3-8. Calibrated horizontal hydraulic-conductivity parameter values and statistics of parameters used in the Snake Valley area groundwater model. Modfied from: *Masbruch et al.* [201X], in review.

[**Model zone:** zone number used in MODFLOW files. **Abbreviations:** LBFAU, lower basin-fill aquifer unit; LCAU, lower carbonate aquifer unit; NCCU, non-carbonate confining unit; UBFAU, upper basin-fill aquifer unit; UCAU, upper carbonate aquifer unit; USCU, upper siliciclastic confining unit; VU, volcanic unit; NA, not applied]

Parameter name	Hydrogeologic unit and zone (from *Sweetkind et al.* [2011a])	Model zone	Horizontal hydaulic conductivity (meters per day)		Standard deviation of log values	Prior information standard deviation of log values[1]
			Calibrated parameter value	95-percent confidence interval		
ubfau_3hk	UBFAU zone 3	ubfau zone 3	10	0.32–320	0.76	NA
ubfau_31hk	UBFAU zone 3	ubfau zone 31	1.5	0.54–4.2	0.23	NA
ubfau_32hk[2]	UBFAU zone 3	ubfau zone 32	0.06	0.013–2.7	0.84	1.12
ubfau_4hk	UBFAU zone 4	ubfau zone 4	0.94	0.10–8.7	0.49	NA
ubfau_41hk	UBFAU zone 4	ubfau zone 41	0.15	0.043–0.54	0.28	NA
ubfau_42hk	UBFAU zone 4	ubfau zone 42	4.4	0.75–26	0.39	NA
lbfau_4hk	LBFAU zone 4	lbfau zone 4	2.0	0.64–6.3	0.25	NA
lbfau_5hk	LBFAU zones 1, 3, and 5	lbfau zone 1, 3, and 5	0.47	0.022–10	0.68	NA
caldera_hk[2]	LBFAU zone 2; VU zones 1, 2, 3, and 7	lbfau zone 2; vu zones 1,2,3, and 7	0.12	0.00024–59	1.36	1.43
ucau_1hk[2]	UCAU zones 1 and 2	ucau zones 1 and 2	0.015	0.000025–8.9	1.40	1.78
ucau_11hk	UCAU zone 1	ucau zone 11	0.20	0.051–0.80	0.30	NA
uscu_1hk	USCU (zone 1)	uscu zone 1	0.00050	0.00000069–0.37	1.45	NA
lcau_41hk	LCAU zone 41;USCU (zone 1)	lcau zone 41; uscu zone 2	0.52	0.25–1.1	0.17	NA
lcau_42hk	LCAU zone 42	lcau zone 42	0.0081	0.000038–1.7	1.18	NA
lcau_421hk	LCAU zones 42 and 51	lcau zones 421 and 514	0.75	0.29–1.9	0.21	NA
lcau_51hk	LCAU zones 51 and 52	lcau zones 51 and 521	17	6.0–47	0.23	NA
lcau_511hk	LCAU zone 51	lcau zone 511	0.031	0.00096–0.98	0.76	NA
lcau_512hk	LCAU zone 51	lcau zone 512	0.0041	0.00068–0.025	0.39	NA
lcau_513hk	LCAU zone 51	lcau zone 513	2.8	0.63–12	0.32	NA
lcau_52hk	LCAU zone 52	lcau zone 52	0.75	0.23–2.4	0.26	NA
lcau_522hk[2]	LCAU zone 52	lcau zone 522	0.075	0.00053–11	1.09	1.78
lcau_71hk[2]	LCAU zones 71 and 72	lcau zones 71 and 72	0.012	0.000050–3.1	1.21	1.78
nccu_1hk	NCCU zone 1	nccu zone 1	1.0	0.064–17	0.61	NA
nccu_11hk	NCCU zone 1	nccu zone 11	0.18	0.000098–350	1.66	NA
nccu_2hk	NCCU zone 2	nccu zone 2	0.0093	0.00060–0.14	0.60	NA
nccu_23hk	NCCU zone 2	nccu zone 23	0.10	0.000020–490	1.87	NA
nccu_3hk[2]	NCCU zone 3	nccu zone 3	0.0021	0.0000012–3.7	1.64	2.67
nccu_32hk	NCCU zone 3	nccu zone 32	0.095	0.0018–5.0	0.87	NA
nccu_33hk	NCCU zone 3	nccu zone 33	0.00055	0.000064–0.0048	0.47	NA

[1]Values from Table 3-7.
[2]Denotes parameter with prior information assigned.

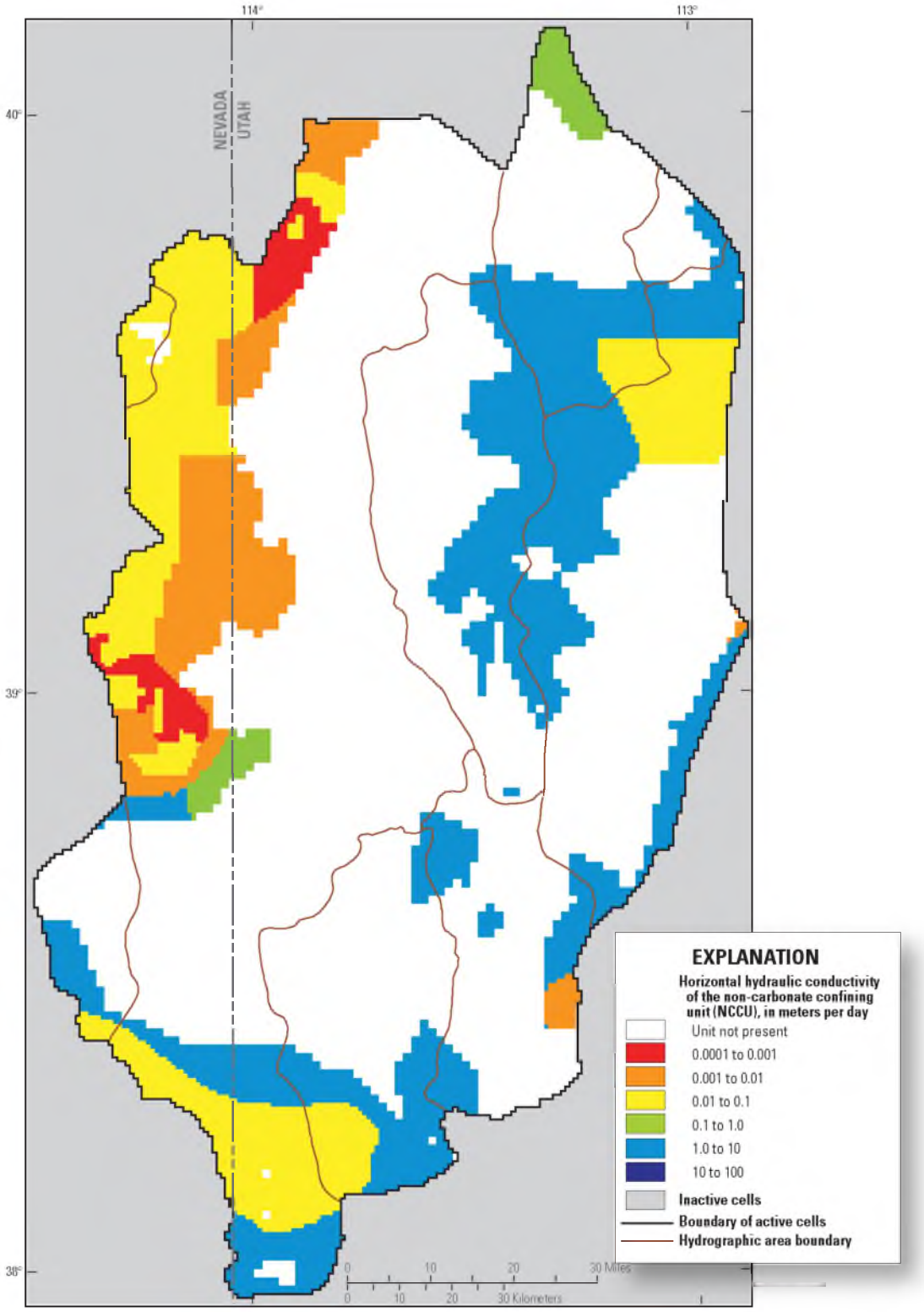

Figure 3-39. Distribution of simulated horizontal hydraulic conductivity of the non-carbonate confining unit (NCCU) in the Snake Valley area groundwater model. State boundary data from: *U.S. Census Bureau* [2000]. Modified from: *Masbruch et al.* [201X], in review.

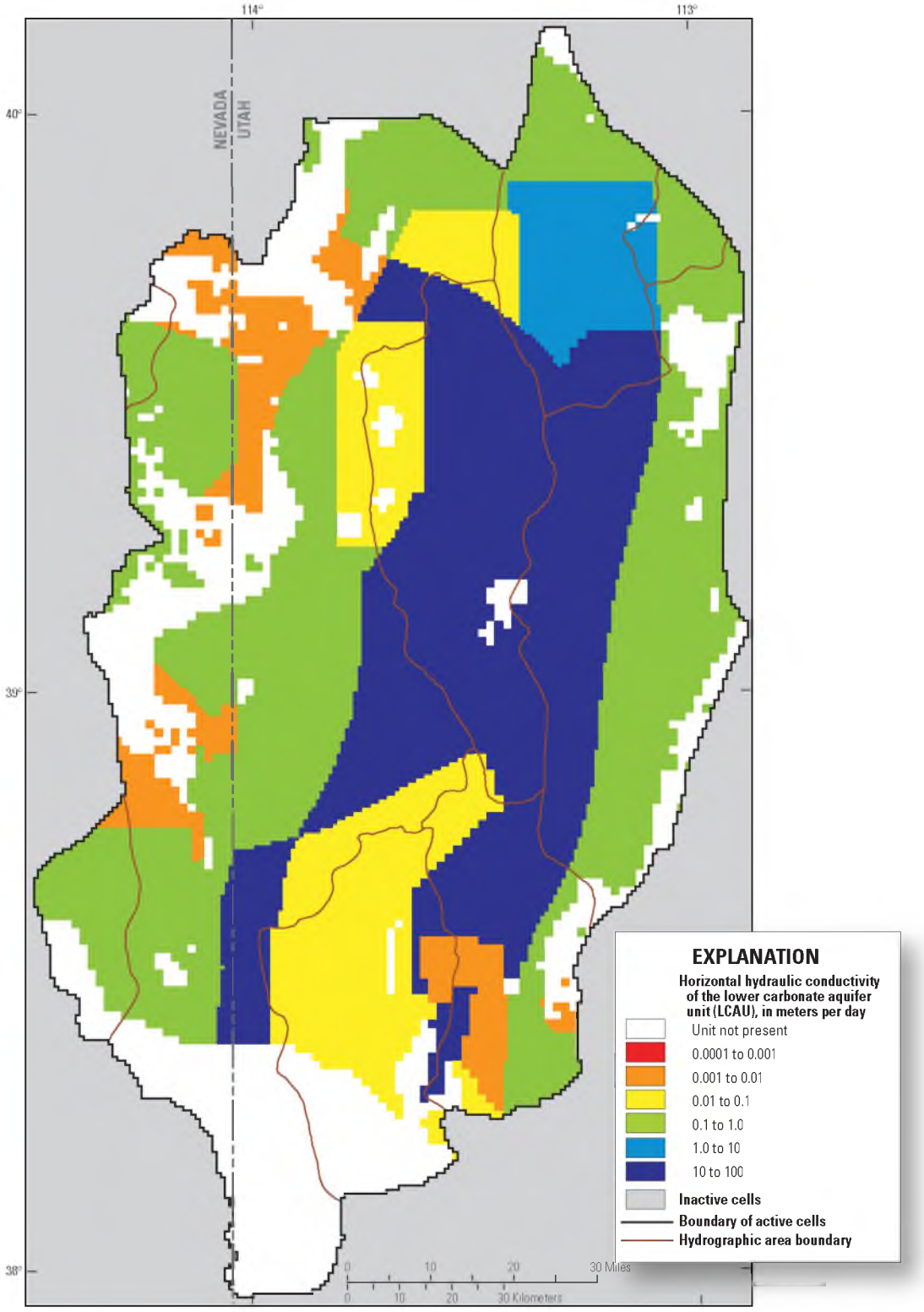

Figure 3-40. Distribution of simulated horizontal hydraulic conductivity of the lower carbonate aquifer unit (LCAU) in the Snake Valley area groundwater model. State boundary data from: *U.S. Census Bureau* [2000]. Modified from: *Masbruch et al.* [201X], in review.

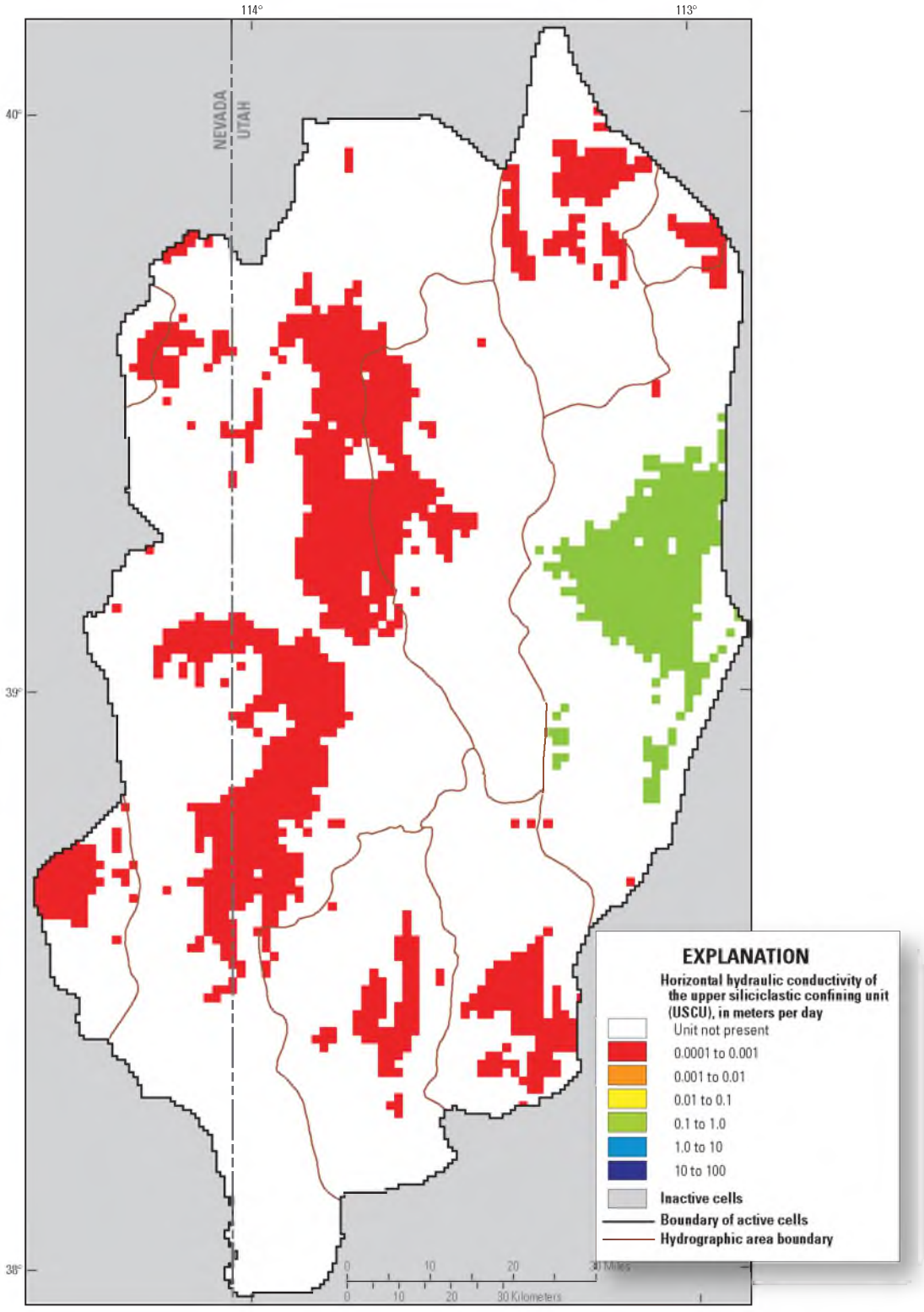

Figure 3-41. Distribution of simulated horizontal hydraulic conductivity of the upper siliciclastic confining unit (USCU) in the Snake Valley area groundwater model. State boundary data from: *U.S. Census Bureau* [2000]. Modified from: *Masbruch et al.* [201X], in review.

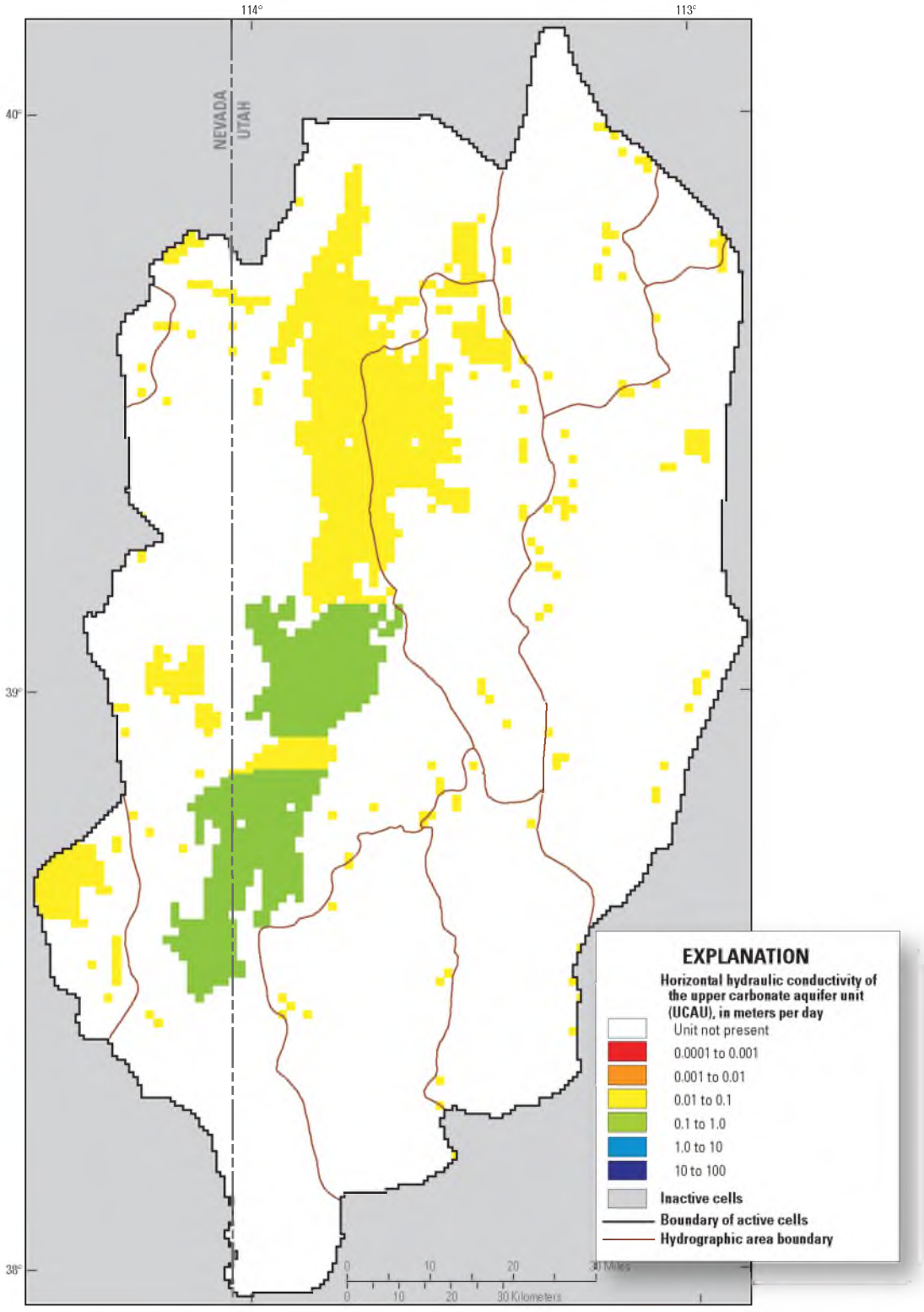

Figure 3-42. Distribution of simulated horizontal hydraulic conductivity of the upper carbonate aquifer unit (UCAU) in the Snake Valley area groundwater model. State boundary data from: *U.S. Census Bureau* [2000]. Modified from: *Masbruch et al.* [201X], in review.

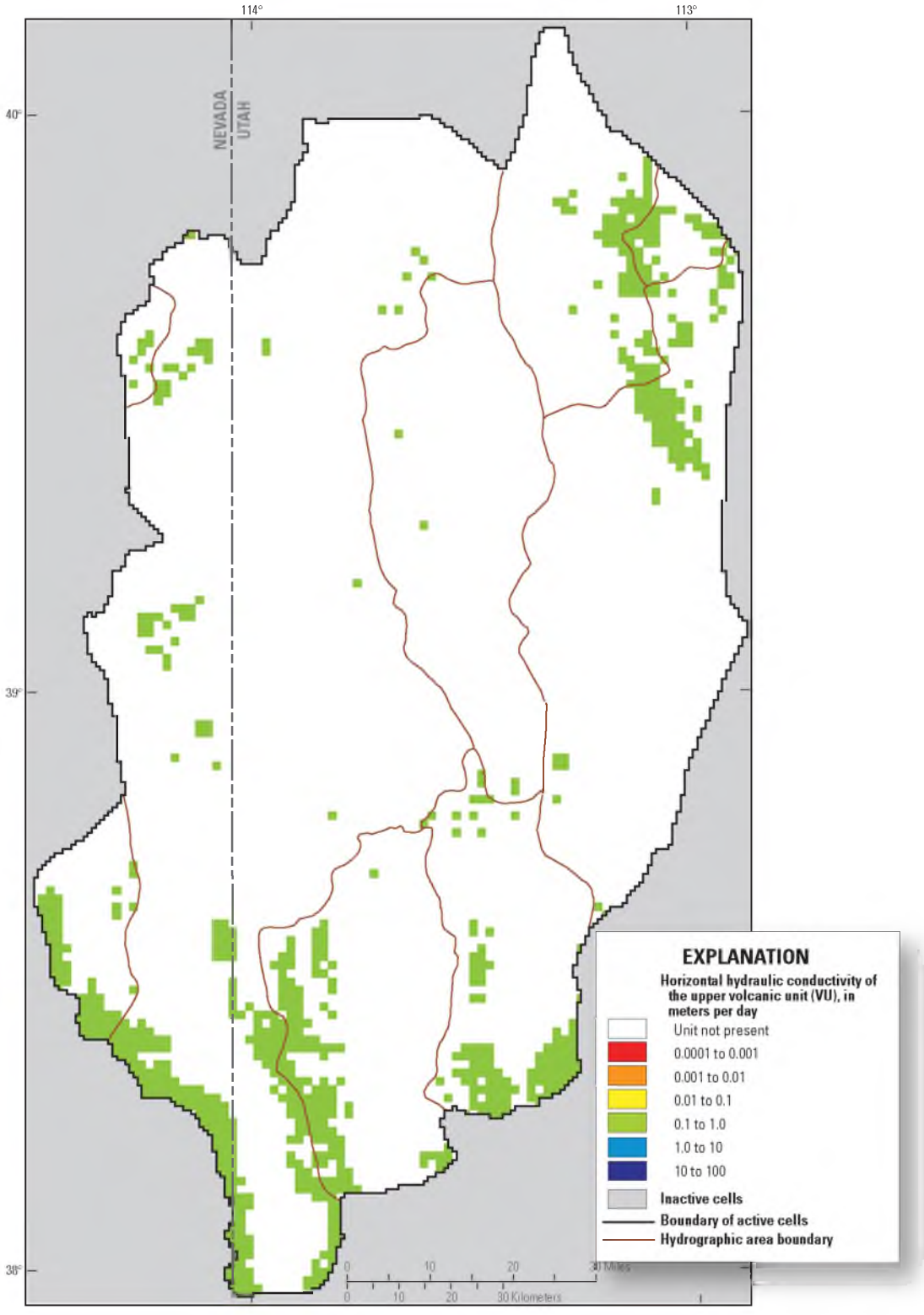

Figure 3-43. Distribution of simulated horizontal hydraulic conductivity of the volcanic unit (VU) in the Snake Valley area groundwater model. State boundary data from: *U.S. Census Bureau* [2000]. Modified from: *Masbruch et al.* [201X], in review.

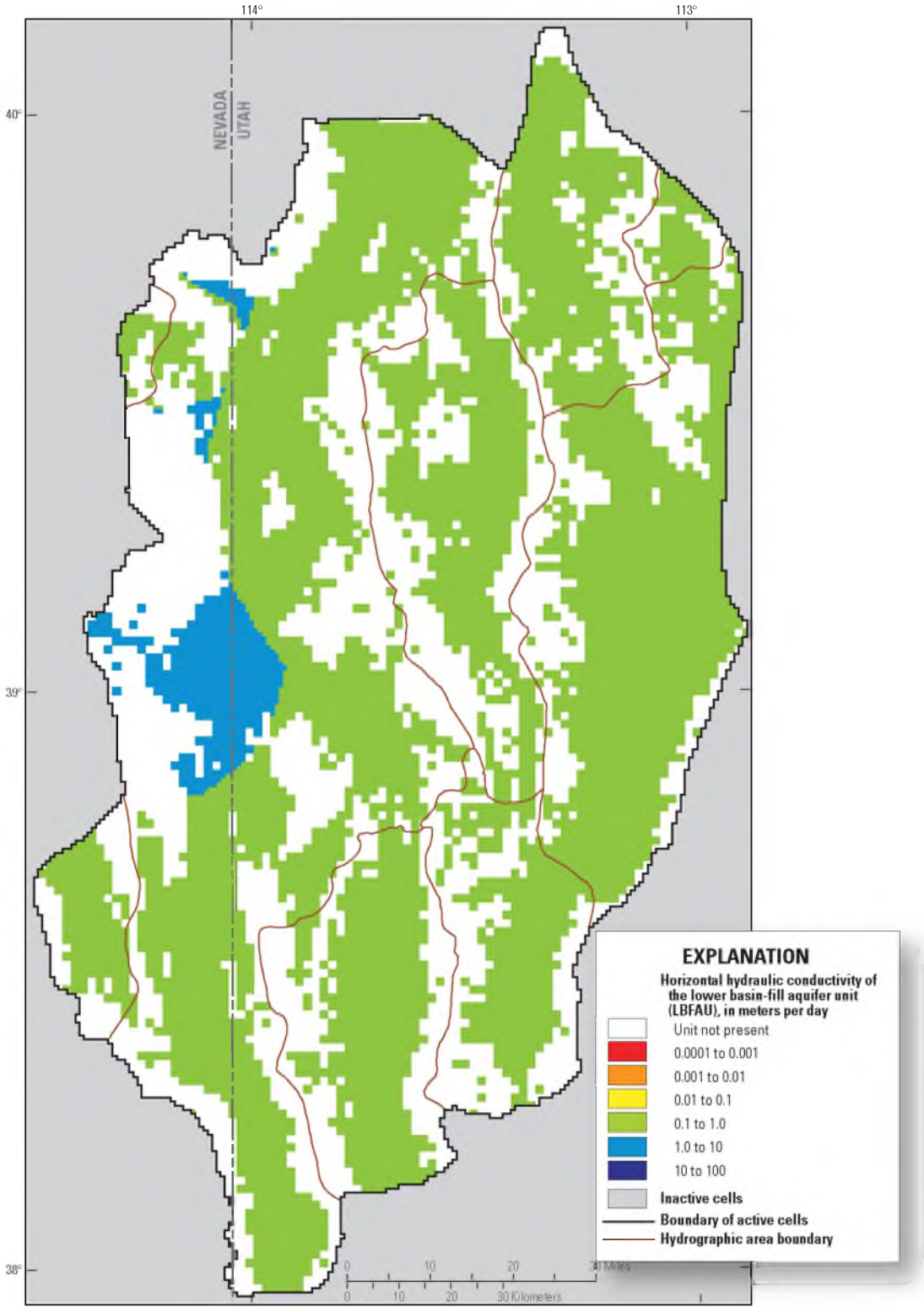

Figure 3-44. Distribution of simulated horizontal hydraulic conductivity of the lower basin-fill aquifer unit (LBFAU) in the Snake Valley area groundwater model. State boundary data from: *U.S. Census Bureau* [2000]. Modified from: *Masbruch et al.* [201X], in review.

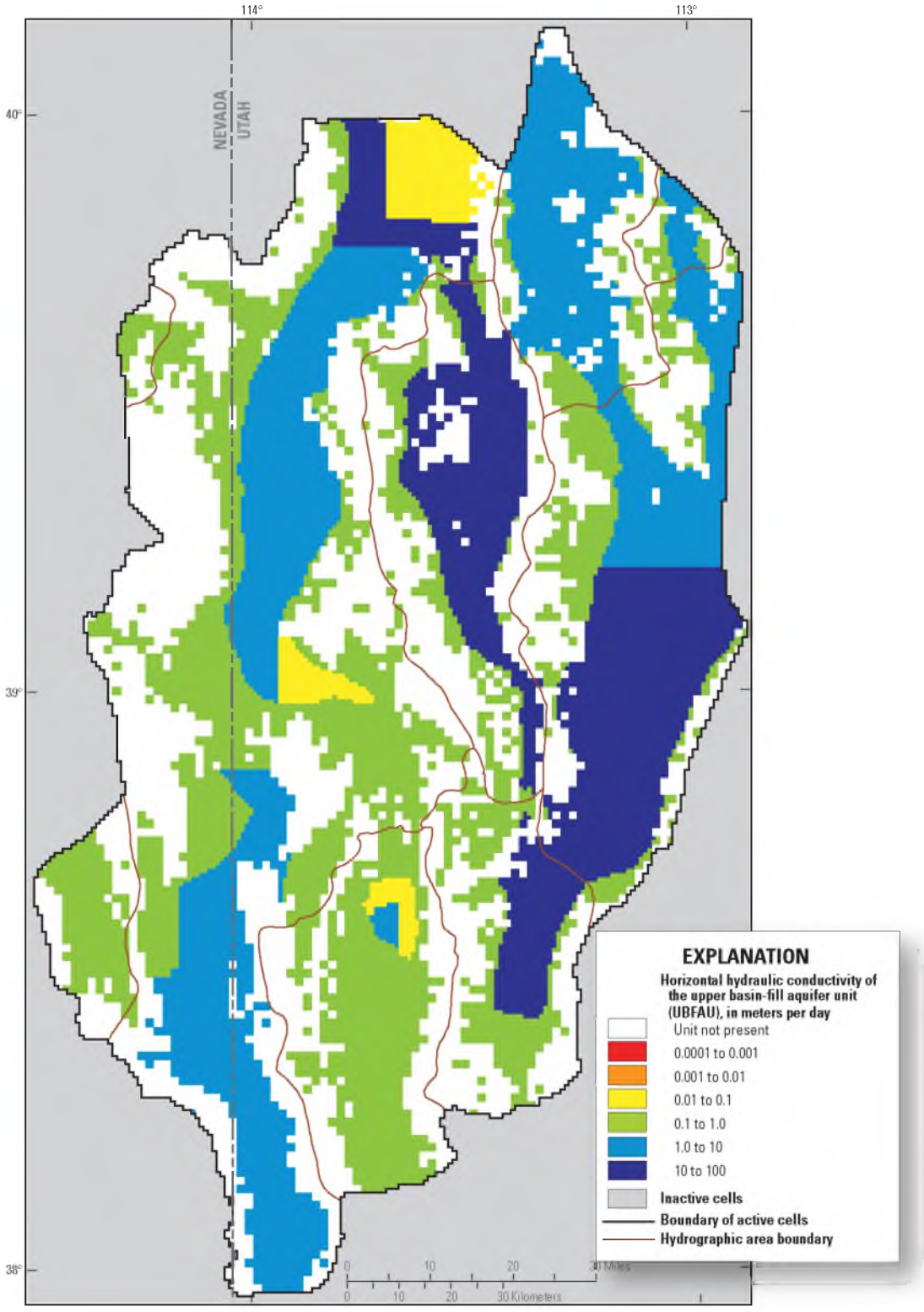

Figure 3-45. Distribution of simulated horizontal hydraulic conductivity of the upper basin-fill aquifer unit (UBFAU) in the Snake Valley area groundwater model. State boundary data from: *U.S. Census Bureau* [2000]. Modified from: *Masbruch et al.* [201X], in review.

applied as prior information to parameter nccu_3hk.

Although hydraulic conductivities of 1 m/d are on the high end of conductivities for the NCCU (Tables 3-7 and 3-8), this higher conductivity was needed to reduce water-level altitudes in Pine, Wah Wah, and Tule Valleys and Sevier Desert, and was needed to move water from these same HAs north towards Fish Springs (Figure 3-39). This higher conductivity is also supported by the fact that this zone (zone 1) of the NCCU is a quartzite that generally has a well-developed fracture network and is classified as having moderate permeability [*Hintze et al.*, 2000; *Ludington et al.*, 1996; *Sweetkind et al.*, 2011a].

3.5.3.3.3.2 Model observations provide good information about the hydraulic conductivity of the LCAU (Figure 3-32) and 10 parameters with values ranging from 0.0041 to 17 m/d define it in the model (Figure 3-40 and Table 3-8). The estimated values of the parameters are within the expected hydraulic conductivity range reported for the LCAU (Table 3-7), and all except two parameters (lcau_52hk and lacu_71hk) could be estimated with more certainty in the model than the measured standard deviation of 1.78 on the log values of the parameters. The measured standard deviation of 1.78 was applied as prior information on the two excepted parameters. Although the parameter with the lowest value (lcau_512hk) occurs in an area where the LCAU should have moderate permeability, it has limited area and was needed to simulate steep gradients and reduce discharge in downgradient areas.

3.5.3.3.3.3 The model observations provide little data about hydraulic conductivity of the USCU (Figure 3-32) and only two parameters ranging in value from 0.00050 to 0.52 m/d define it in the model (Figure 3-41 and Table 3-8). The

estimated values of the parameters are within the expected hydraulic conductivity range reported for the USCU (Table 3-7) and can be estimated in the model with more certainty than the measured standard deviation of 2.67 on the log values of the parameters. The USCU zone with the higher hydraulic conductivity was simulated using an LCAU parameter (lcau_41hk) because during model calibration it was noticed that there was an error in the hydrogeologic framework in this portion of the study area; the USCU units defined in this area of the framework do not exist and should have been defined as LCAU instead [*D.S. Sweetkind, USGS, written commun.*, June 2012].

3.5.3.3.3.4 Model observations generally provide good information about the hydraulic conductivity of the UCAU (Figure 3-32) and two parameters with values of 0.015 and 0.20 m/d define it in the model (Figure 3-42 and Table 3-8). The estimated values of the parameters are within the expected hydraulic conductivity range reported for the UCAU (Table 3-7), and one of the parameters (ucau_11hk) could be estimated with more certainty in the model than the measured standard deviation of 1.78 on the log values of the parameters. The measured standard deviation of 1.78 was applied as prior information on the other parameter (ucau_1hk).

3.5.3.3.3.5 Model observations provide little information about the hydraulic conductivity of the VU (Figure 3-32) and only one parameter (caldera_hk) with a value of 0.19 m/d defines it in the model (Figure 3-43 and Table 3-8). The estimated value of the parameter is within the expected hydraulic conductivity range reported for the VU (Table 3-7); the parameter, however, could not be estimated with more certainty in the model than the measured standard deviation of 1.43 on the log values of the

parameter. The measured standard deviation of 1.43 was applied as prior information on this parameter.

3.5.3.3.3.6 Model observations provide good information about the hydraulic conductivity of the LBFAU (Figure 3-32) and three parameters with values ranging from 0.19 to 2.0 m/d define it in the model (Figure 3-44 and Table 3-8). Volcanic portions of the LBFAU were defined using the same parameter as the VU (caldera_hk). The estimated values of the parameters are within the expected hydraulic conductivity range reported for the LBFAU (Table 3-7) and all parameters could be estimated with more certainty than the measured standard deviation of 1.58 on the log values of the parameters.

3.5.3.3.3.7 Most of the groundwater discharge in the study area and model occurs through the UBFAU as ETg. Model observations generally provide good information about the hydraulic conductivity of the UBFAU (Figure 3-32) and six parameters with values ranging from 0.060 to 10 m/d define it in the model (Figure 3-45 and Table 3-8). The estimated values of the parameters are within the expected hydraulic conductivity range reported for the UBFAU (Table 3-7) and all parameters could be estimated with more certainty than the measured standard deviation of 1.26 on the log values of the parameters.

3.5.3.3.4 Vertical Anisotropy

Two vertical anisotropy parameters were initially defined, one for UBFAU and one for all other HGUs. Initial sensitivity analysis indicated that the observations provide little information about these parameters (Figure 3-31). During calibration, however, vertical anisotropy in the UBFAU and LBFAU was sometimes important to simulate the

observed discharge to evapotranspiration and groundwater temperatures. Two parameters (ubfau_vn and playa_vn) are defined to allow anisotropy in basin-fill units to vary. These units are the most likely to have stratification that would tend to decrease the vertical conductivity relative to the horizontal (anisotropy ratios greater than 1). An additional parameter (lcau_vn) was defined for the consolidated rock HGUs. The estimated values of all vertical-anisotropy parameters range from 1 to 51 (Table 3-9), were determined by regression, are within reasonable limits [*Faunt et al.*, 2010], and have reasonable confidence intervals (Figure 3-33).

3.5.3.3.5 Horizontal-Flow Barriers

Most faults in the study area do not have enough data on either side to determine if they are barriers to groundwater flow. Two HFBs were simulated along selected faults, typically where HGU thickness changes dramatically across the fault and spring discharge observations could not be adequately simulated without the HFB (Figure 3-27). The HFB simulated between Snake Valley and Pine and Tule Valleys corresponds with a steeply, almost vertically, dipping syncline limb of USCU (Figure 3-27) and is evidenced by distinctly different water levels on the east and west sides of this structure. One parameter (B_SV_NS1) representing the hydraulic characteristic of the barrier was defined for all HFBs simulated in the model and was estimated to be four orders of magnitude less than the lowest simulated horizontal hydraulic-conductivity parameter value. The value of this parameter was set to adequately simulate water levels or discharge without causing water levels to be above land surface on the upgradient side of the HFB. Composite-scaled sensitivity to the HFB parameter is low (Figure 3-32), possibly because of its small value [*Hill and Tiedeman*, 2007]. Because of this

Table 3-9. Calibrated horizontal-to-vertical anisotropy parameter values and statistics of parameters used in the Snake Valley area groundwater model. Modified from: *Masbruch et al.* [201X], in review.

[**Model zone:** zone number used in MODFLOW files. **Abbreviations:** LBFAU, lower basin-fill aquifer unit; LCAU, lower carbonate aquifer unit; NCCU, non-carbonate confining unit; UBFAU, upper basin-fill aquifer unit; UCAU, upper carbonate aquifer unit; USCU, upper siliciclastic confining unit; VU, volcanic unit]

Parameter name	Hydrogeologic unit	Model zone	Horizontal-to-vertical anisotropy (unitless)		Standard deviation of log values
			Calibrated parameter value	95-percent confidence interval	
ubfau_vn	UBFAU	ubfau zones 4, 41, and 42	9.9	2.0–49	0.35
	LBFAU	lbfau zones 1, 3, 4, and 5			
playa_vn	UBFAU	ubfau zones 3, 31, and 32	51	19–133	0.21
lcau_vn	LBFAU	lbfau zone 2	1.0	0.017–60	0.90
	VU	all vu zones			
	UCAU	all ucau zones			
	USCU	all uscu zones			
	LCAU	all lcau zones			
	NCCU	all nccu zones			

insensitivity, and because the hydraulic characteristic is dependent on hydraulic conductivity, a standard deviation of 2.67, the greatest standard deviation for hydraulic conductivity (Table 3-7), was applied to the log values of this parameter as prior information.

3.5.3.3.6 Thermal Parameters

Two thermal properties, basal heat flux and longitudinal dispersivity, were defined using parameters (heatflux and longdisp, respectively) that could vary in the model. Model observations generally provide good information about the basal heat flux, and slightly less information about the longitudinal dispersivity (Figure 3-32). The values of these parameters were determined by regression within reasonable limits and with reasonable confidence (Figure 3-33).

3.5.4 Model Evaluation

The calibrated model was evaluated to assess the likely accuracy of simulated results. An advantage of using nonlinear regression to calibrate the model is that a substantial methodology exists for model evaluation that facilitates a better understanding of model strengths and weaknesses [*Faunt et al.*, 2010; *Hill and Tiedeman*, 2007]. A protocol exists to evaluate the likely accuracy of simulated water-level altitudes, groundwater discharge, and groundwater temperatures, estimated and specified parameter values and associated sensitivities and confidence intervals, and other measures of parameter and prediction uncertainty. As part of the model evaluation, comparison of simulated results to the conceptual regional water budget, previously-published regional water-level contours, model fit to observations, and values of parameter estimates and

their associated sensitivities were evaluated. On the basis of this evaluation, as explained in the following sections, this model provides a reasonable representation of this regional groundwater system.

3.5.4.1 Model Fit to Observations

Model fit is evaluated using both unweighted and weighted residuals (the difference between observed and simulated values). Unweighted residuals have the same dimensions as the observations and are clearly understood, but they can be misleading because observations are measured with different accuracy. Two unweighted residuals that are of equal value may not indicate an equally satisfactory model fit. Given the large regional scale of this model, calibration attempts were concentrated to reduce unweighted residuals to 50 m for water levels, 30 percent of flow for discharge observations, and 2 °C for temperature observations. Weighted residuals are used in summary statistics and regression, reflect model fit relative to the expected observation error, but are more difficult to interpret than unweighted residuals.

Summary statistics for model fit are listed in Table 3-10. The square root of the sum of squared weighted residuals (SOSWR) divided by the number of observations (Nobs) is called the standard error of the regression and provides a measure of model fit relative to the weighting that can be compared for different types of observations [*Hill and Tiedeman*, 2007]. A value of 1.0 indicates a match that is, overall, consistent with the observation error evaluation used to determine the weighting. The standard error of the regression can be used to multiply the average standard deviations and coefficients of variation to obtain dimensional values that reflect the fit of any group of observations [*Hill and Tiedeman*, 2007]. The value of $[SOSWR/Nobs]^{1/2}$ of 6.62 for water-level

Table 3-10. Summary statistics for measure of model fit for the Snake Valley area groundwater model. Modified from: *Masbruch et al.* [201X], in review.

[**Abbreviations:** SOSWR, sum of squared weighted residuals; Nobs, number of observations]

Type of observation	Number of observations	Average positive weighted residual	Average negative weighted residual	SOSWR	[SOSWR/ Nobs]$^{1/2}$	Average standard deviation or coefficient of variation (with weighting)
Water levels in wells	123	4.25	-6.30	5,386	6.62	1.75[1]
Discharge	20	3.39	-1.07	178	2.98	0.11[2]
Groundwater temperatures in wells	31	6.79	-3.87	1,984	8.00	0.35[3]

[1]Standard deviation, in meters.
[2]Coefficient of variation.
[3]Standard deviation, in degrees Celsius.

observations from wells multiplied by the average standard deviation of observations from wells of 1.75 m indicate that the model has an overall fit to water levels in wells of 12 m, which is well within the 50 m considered adequate for this regional model. The model statistics for discharge include the weight multiplier that was used in UCODE-2005 to force regressions to match discharge more closely. The value of $[SOSWR/Nobs]^{1/2}$ of 2.98 for discharge observations indicates that the model has an overall fit to discharge observations of a coefficient of variation of 0.33, which is slightly greater than the estimated error in the discharge observations (see the "Groundwater Discharge Observations and Uncertainty" section of this chapter) but is close to the 30 percent considered adequate for this regional model. Similar to discharge, the model statistics for groundwater temperature in wells include the weight multipliers used in UCODE to force regressions to match all types of observations equally, not just the temperatures with small variances. The value of $[SOSWR/Nobs]^{1/2}$ of 8.00 for temperature observations indicates that the model has an overall fit to temperature observations of 2.8 °C, which is only slightly above the 2 °C considered adequate for this regional model.

3.5.4.1.1 Water Levels

The fit of simulated to observed water levels is generally good; 98 percent of the simulated values of water levels in wells are within 30 m of the observation, and 58 percent of them are within 12 m (Table 3-11). Weighted observations plotted against weighted simulated values generally fall on the 1 to 1 line (Figure 3-46A). Positive and negative water-level residuals are distributed randomly around the study area, indicating no systematic model error (Figure 3-47). Graphs of weighted water-level residuals and

Table 3-11. Summary of observed and simulated water-level altitudes for the Snake Valley area groundwater model. Modified from: *Masbruch et al.* [201X], in review.

[Values are rounded and may not exactly match model files. **Abbreviations:** USGS, U.S. Geological Survey]

Observation name	USGS site number	Altitude of well (meters)	Observed water-level altitude (meters)	Variance (square meters)	Simulated water-level altitude (meters)	Residual (oberved minus simulated, in meters)
C281722dda1	382113113435401	1,761	1,646	11.12	1,686	-40
C281711cca1	382259113433701	1,733	1,622	21.26	1,660	-38
C281411abb1	382350113231901	1,585	1,382	43.61	1,411	-29
C271428ddd1	382535113251101	1,552	1,379	15.26	1,401	-22
C271428ddd2	382539113250601	1,551	1,380	13.16	1,400	-20
N086935CDDD1	383023114115301	1,775	1,727	5.23	1,721	6
N076902BABA2	383023114115302	1,781	1,727	6.68	1,721	6
C261425aad1	383131113214301	1,452	1,381	4.47	1,381	0
N087021AADA1	383252114075101	1,741	1,701	6.34	1,716	-15
N086915BCDD1	383325114134901	1,746	1,724	7.07	1,725	-1
C26173cdd1	383357113440601	1,600	1,467	8.98	1,480	-13
C26173cda1	383402113440601	1,601	1,468	9.07	1,479	-11
C26202aad1	383452114023401	1,884	1,703	1.63	1,709	-6
C26202aad2	383452114023402	1,884	1,703	1.64	1,709	-6
N097034DCDC1	383545114070101	1,727	1,693	3.85	1,714	-21
C251618bdd1	383825113410801	1,551	1,459	3.84	1,443	16
N097014DABD1	383826114051201	1,718	1,686	4.22	1,711	-25
N096711DBCD1	383907114253001	1,846	1,761	1.55	1,744	17
N096811BDBD1	383925114190801	1,887	1,739	1.74	1,734	5
C241334ccb1	384042113181601	1,417	1,353	4.08	1,376	-23
C241323ccd1	384215113165701	1,408	1,354	3.90	1,375	-21
N107028CBCB1	384227114082701	1,772	1,703	2.38	1,714	-11
C241215cdc1	384306113112601	1,393	1,368	1.69	1,374	-6
C241913cbd1	384324113554401	1,754	1,723	5.75	1,700	23
C241913cbd2	384324113554402	1,754	1,724	5.85	1,700	24

Table 3-11. Continued

[Values are rounded and may not exactly match model files. **Abbreviations:** USGS, U.S. Geological Survey]

Observation name	USGS site number	Altitude of well (meters)	Observed water-level altitude (meters)	Variance (square meters)	Simulated water-level altitude (meters)	Residual (oberved minus simulated, in meters)
C241916cbb1	384327113591401	1,739	1,662	7.26	1,687	-25
C241916bdb2	384340113585701	1,727	1,661	7.57	1,686	-25
C241916bdb3	384340113585702	1,727	1,661	7.68	1,686	-25
C241916bdb4	384342113585401	1,725	1,661	7.93	1,686	-25
C241916bdb5	384342113585402	1,725	1,661	8.47	1,686	-25
C242014bbc1	384347114025601	1,685	1,660	1.61	1,676	-16
C241313aac1	384351113150501	1,389	1,361	1.51	1,375	-14
C24198baa1	384449113595401	1,677	1,656	7.59	1,678	-22
C24193dbc1	384510113573001	1,702	1,660	3.86	1,685	-25
C24201adc1	384521114014701	1,661	1,660	4.05	1,670	-10
C232025ccd1	384651114025101	1,664	1,655	3.94	1,666	-11
C232025ccd2	384651114025102	1,664	1,655	4.05	1,666	-11
C231924dcc1	384746113554701	1,766	1,658	15.30	1,667	-9
C231920cac1	384755114003301	1,651	1,645	4.03	1,631	14
C231920cac2	384755114003401	1,650	1,645	4.03	1,630	15
C231920cac3	384755114003402	1,650	1,646	1.47	1,639	7
C23126ccd1	385008113145301	1,413	1,350	10.82	1,374	-24
C22141cba1	385542113223601	1,458	1,351	2.72	1,373	-22
C22196bcc1	385607114015601	1,609	1,586	14.24	1,576	10
C22196bac2	385617114013801	1,603	1,584	6.74	1,571	13
C22201aba1	385623114021501	1,610	1,588	5.33	1,577	11
C212036ccc1	385628114025701	1,619	1,590	11.49	1,580	10
C212036ccc2	385628114025702	1,619	1,590	13.01	1,585	5
C212036ccc3	385628114025703	1,619	1,586	14.50	1,583	3
C212036ddd2	385630114020201	1,604	1,584	2.15	1,576	8

Table 3-11. Continued

[Values are rounded and may not exactly match model files. **Abbreviations:** USGS, U.S. Geological Survey]

Observation name	USGS site number	Altitude of well (meters)	Observed water-level altitude (meters)	Variance (square meters)	Simulated water-level altitude (meters)	Residual (oberved minus simulated, in meters)
C212036ddd3	385630114020202	1,604	1,583	2.17	1,579	4
C212036ddd1	385630114020301	1,604	1,585	4.70	1,577	8
C211932dad1	385643113594701	1,623	1,561	2.16	1,582	-21
C211932dad2	385643113594702	1,623	1,562	2.24	1,582	-20
C211932dad3	385649113594601	1,620	1,566	2.73	1,581	-15
C211817add1	385933113530801	1,538	1,520	7.62	1,529	-9
C211812ccd1	385958113493401	1,541	1,507	9.50	1,525	-18
C21178dcc1	390000113463701	1,547	1,479	13.38	1,489	-10
C201932ddd1	390059114000401	1,548	1,532	1.58	1,542	-10
C201932ddd2	390059114000402	1,548	1,537	1.59	1,543	-6
C201932ddd3	390059114000403	1,548	1,537	1.60	1,544	-7
C201832abd1	390141113532901	1,530	1,519	6.60	1,520	-1
C201832aba2	390143113533002	1,530	1,516	4.71	1,528	-12
C201832aba3	390143113533003	1,530	1,516	4.29	1,527	-11
C201921acc1	390312113591701	1,534	1,524	13.34	1,529	-5
C201916aaa1	390425113585201	1,527	1,519	4.57	1,523	-4
C201916aaa2	390426113585201	1,527	1,519	2.02	1,523	-4
C201916aaa3	390426113585202	1,527	1,521	2.04	1,524	-3
C20198bcb1	390503114005901	1,534	1,533	8.87	1,527	6
C20146dda2	390540113272301	1,379	1,352	10.73	1,371	-19
C20191bcc1	390549113562901	1,520	1,521	6.66	1,513	8
C191936cda1	390629113560301	1,537	1,514	5.13	1,511	3
C191936daa2	390637113553102	1,562	1,508	1.89	1,510	-2
C191936daa1	390637113553201	1,562	1,509	59.91	1,510	-1
C191736bcb1	390656113425101	1,784	1,349	41.35	1,371	-22

Table 3-11. Continued

[Values are rounded and may not exactly match model files. **Abbreviations:** USGS, U.S. Geological Survey]

Observation name	USGS site number	Altitude of well (meters)	Observed water-level altitude (meters)	Variance (square meters)	Simulated water-level altitude (meters)	Residual (oberved minus simulated, in meters)
C191128bdb1	390803113054801	1,420	1,354	2.15	1,370	-16
C19107bda1	391050113010101	1,431	1,374	10.96	1,371	3
C181536cdd1	391136113290401	1,382	1,350	10.73	1,369	-19
C181832cbb1	391156113541901	1,524	1,491	1.45	1,489	2
C181832cbb2	391156113541902	1,524	1,492	1.45	1,489	3
C181832cbb3	391156113541903	1,524	1,492	1.45	1,489	3
C181832cbb4	391156113541904	1,524	1,492	1.45	1,489	3
C181831adb1	391205113543401	1,516	1,491	4.01	1,488	3
C181920ddd1	391322114000001	1,522	1,515	13.90	1,489	26
C171534cac1	391704113312001	1,359	1,350	2.03	1,365	-15
C171525cbb1	391801113292201	1,352	1,351	2.05	1,363	-12
C171616cdc1	391926113391801	1,605	1,440	6.74	1,423	17
C171616cdc2	391926113391802	1,605	1,447	6.81	1,423	24
C171517acc2	391951113331601	1,364	1,349	3.09	1,362	-13
C17194add2	392141113585601	1,487	1,473	4.73	1,473	0
C161634bcd2	392229113381701	1,462	1,418	14.89	1,381	37
C161826cba1	392317113504201	1,491	1,478	5.89	1,463	15
C151936bca1	392756113563401	1,470	1,469	4.25	1,467	2
C151532aab3	392840113330401	1,374	1,349	1.63	1,360	-11
C151532aab2	392840113330402	1,374	1,349	1.62	1,360	-11
C151532aab1	392841113330401	1,374	1,349	1.62	1,360	-11
C151819dcc1	392906113550301	1,461	1,460	4.24	1,466	-6
C151630bdd1	392916113343301	1,393	1,349	1.55	1,359	-10
C151422ddd1	392924113235101	1,386	1,348	2.03	1,359	-11
C141832aaa1	393331113533001	1,460	1,459	4.04	1,459	0

Table 3-11. Continued

[Values are rounded and may not exactly match model files. **Abbreviations:** USGS, U.S. Geological Survey]

Observation name	USGS site number	Altitude of well (meters)	Observed water-level altitude (meters)	Variance (square meters)	Simulated water-level altitude (meters)	Residual (oberved minus simulated, in meters)
C141832aaa2	393331113533002	1,460	1,459	4.04	1,459	0
C141832aaa3	393331113533003	1,460	1,460	1.48	1,459	1
C141832aba1	393331113534401	1,461	1,459	4.01	1,460	-1
C141826dbc1	393345113503201	1,513	1,461	14.60	1,453	8
C14139cba1	393701113191101	1,410	1,343	1.58	1,350	-7
C141410acb1	393714113242001	1,438	1,349	3.05	1,355	-6
C14124cbc1	393745113123001	1,467	1,354	1.49	1,347	7
C14132adb2	393803113161601	1,413	1,353	1.62	1,347	6
C14132adb3	393803113161602	1,413	1,353	1.62	1,347	6
C14132adb1	393806113161501	1,412	1,353	1.62	1,347	6
C131833ddc1	393814113522601	1,452	1,449	13.39	1,433	16
C131632abb1	393914113400701	1,580	1,350	1.67	1,356	-6
C131828dab1	393928113522601	1,458	1,450	14.85	1,427	23
C131425dac1	393933113214801	1,360	1,327	3.62	1,347	-20
C131523ccc1	394014113303301	1,494	1,333	10.85	1,356	-23
C131424baa1	394045113222501	1,383	1,327	2.13	1,344	-17
C121312caa1	394727113152901	1,376	1,320	3.79	1,326	-6
C111636cdb1	394905113354101	1,347	1,346	4.99	1,334	12
C111215bba1	395216113111801	1,397	1,320	10.75	1,322	-2
C11124ccd1	395310113123301	1,364	1,318	1.47	1,318	0
C11124cbc1	395331113123901	1,360	1,318	10.74	1,318	0
C11166cbc4	395355112423601	1,320	1,320	5.39	1,326	-6
C20179cad1	390453113454701	1,674	1,490	13.86	1,480	10

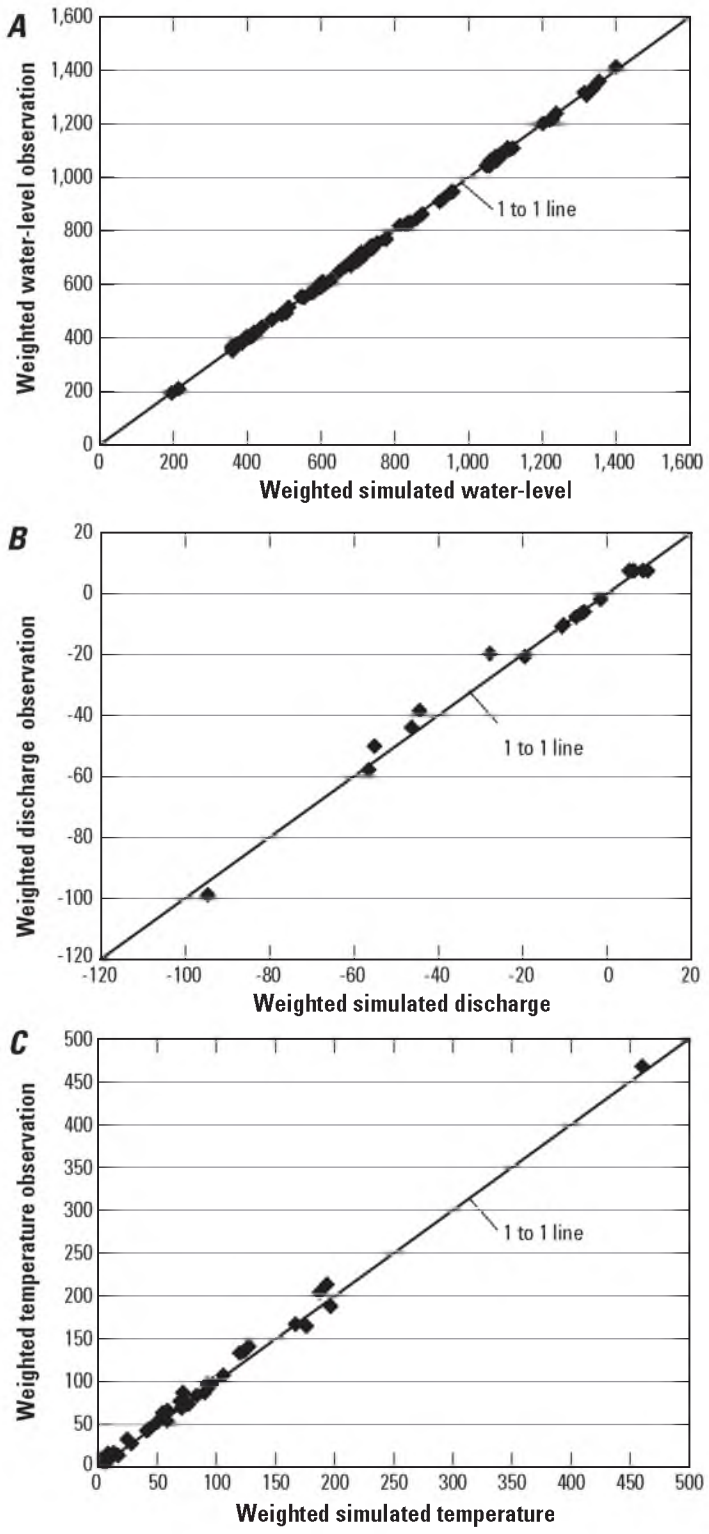

Figure 3-46. Weighted observations compared to weighted simulated values for (*A*) water-levels, (*B*) discharge, and (*C*) temperatures. Modified from: *Masbruch et al.* [201X], in review.

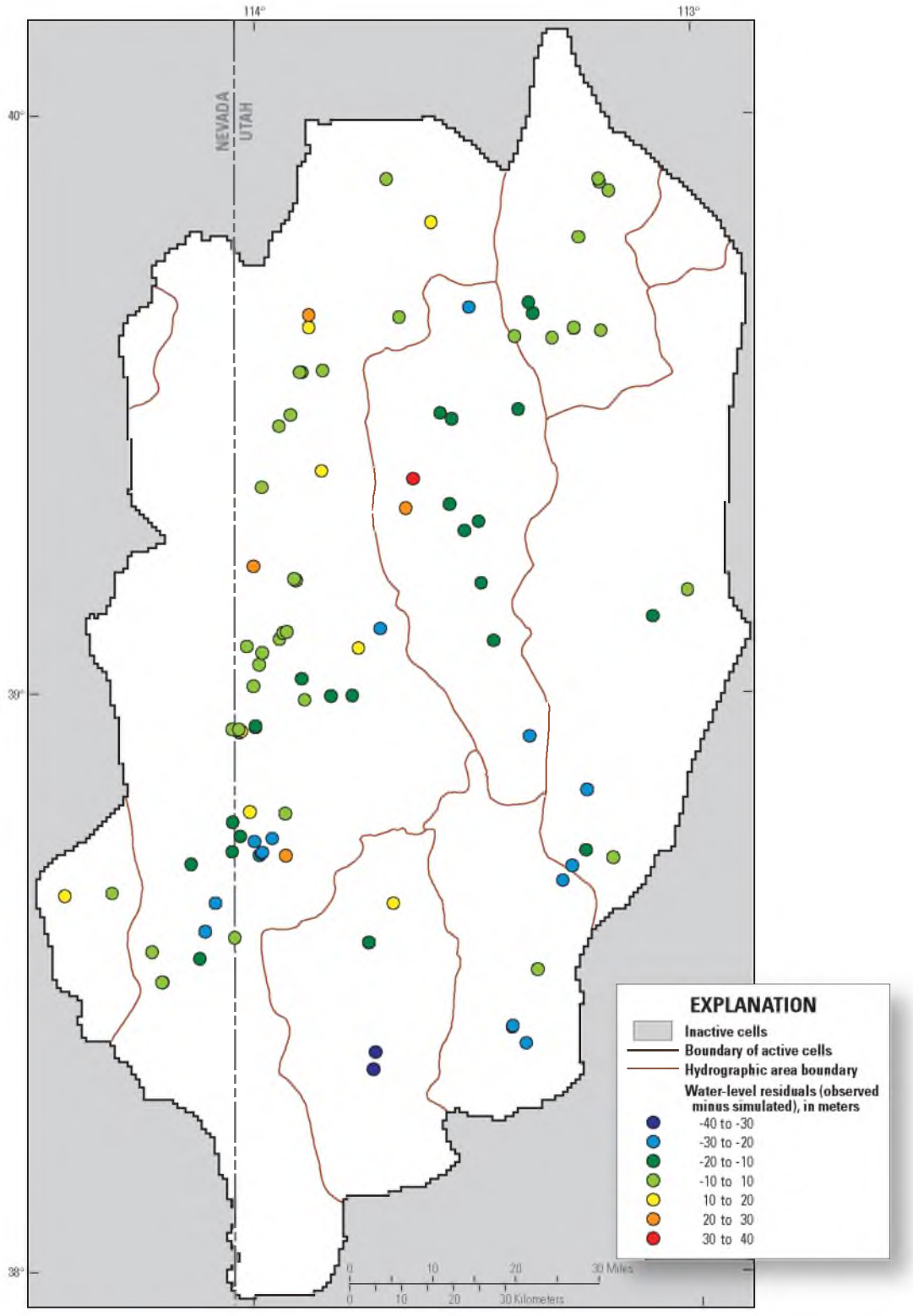

Figure 3-47. Distribution of water-level residuals (observed minus simulated) in the Snake Valley area groundwater model. State boundary data from: *U.S. Census Bureau* [2000]. Modified from: *Masbruch et al.* [201X], in review.

weighted simulated values (Figure 3-48A) also indicate little model bias; most of the weighted residuals vary randomly about a value of zero.

Comparison of the simulated water level altitudes (Figure 3-49) with the potentiometric surface map of *Gardner et al.* [2011] indicates that the groundwater model results adequately depict major features of the water-level altitude distribution and regional patterns of groundwater flow. In general, areas of nearly flat and steep hydraulic gradients are appropriately located.

3.5.4.1.2 Discharge

Calibration was focused on matching groundwater discharge to ETg, springs, and rivers more so than to matching individual water-level observations. Simulating accurate discharge was considered important in simulating the regional budget, in understanding regional sources of water to discharge areas, and in adequately simulating the complex regional aquifer system.

The fit of simulated to observed discharge is generally good; all simulated discharge with the exception of Dearden Springs Group is within 30 percent of the observed discharge (Table 3-12). Dearden Springs Group is within 41 percent of the observed discharge. The discharge at Dearden Springs is difficult to measure; the springs discharge at diffuse areas along Big Springs Creek and cannot be measured directly. The streamflow measured at three flumes upstream and downstream of the springs is used to indirectly measure discharge from the springs. It is possible, therefore, that the observed discharge at Dearden Springs Groups is in error. Weighted discharge observations plotted against weighted simulated values generally fall on the 1 to 1 line (Figure 3-46B). Positive and negative residuals are mostly evenly distributed throughout the study area

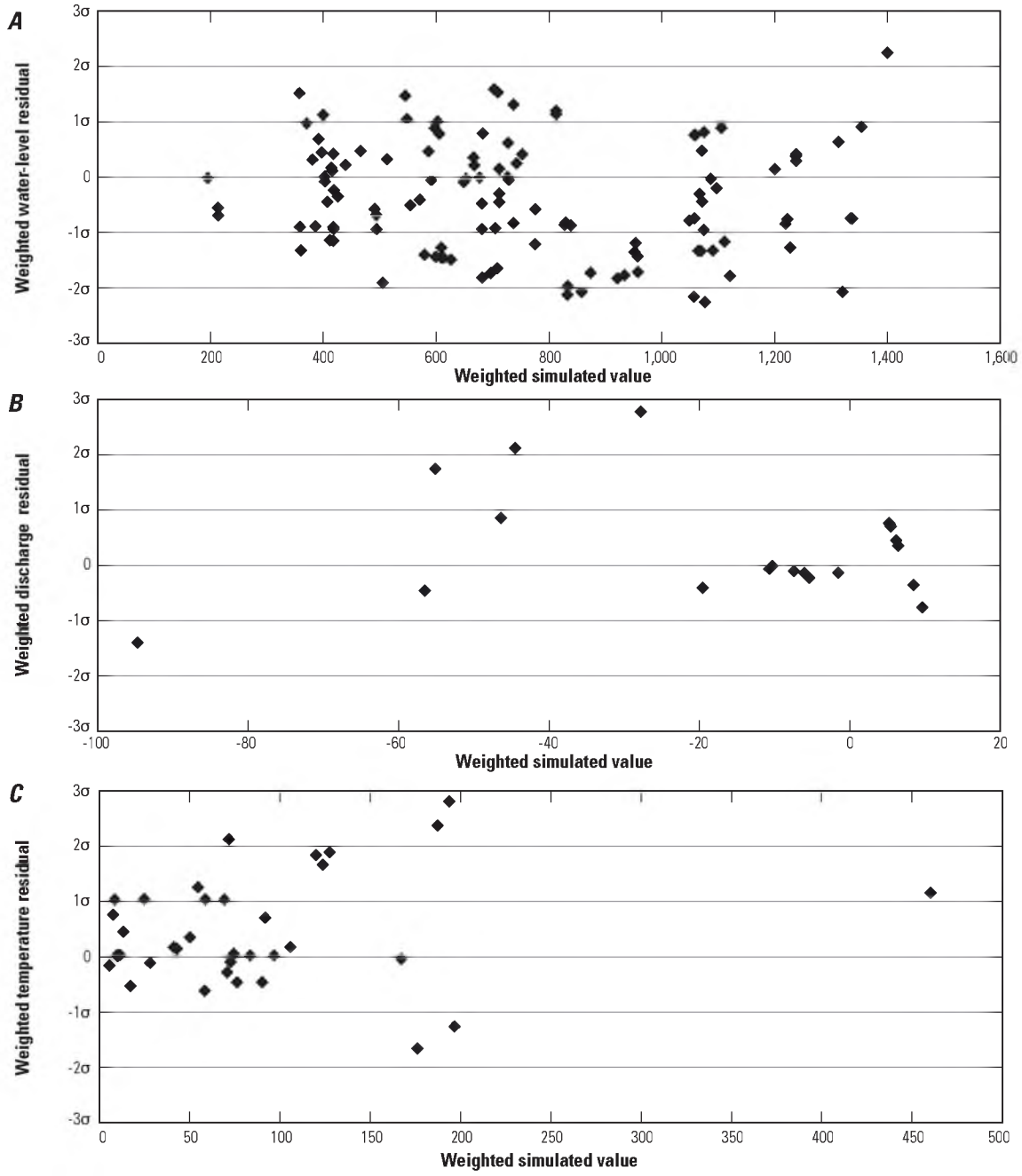

Figure 3-48. Weighted residuals and simulated values for (*A*) water-levels, (*B*) discharge, and (*C*) temperatures. The standard deviations of the weighted residuals are used to define the grid lines. Modified from: *Masbruch et al.* [201X], in review.

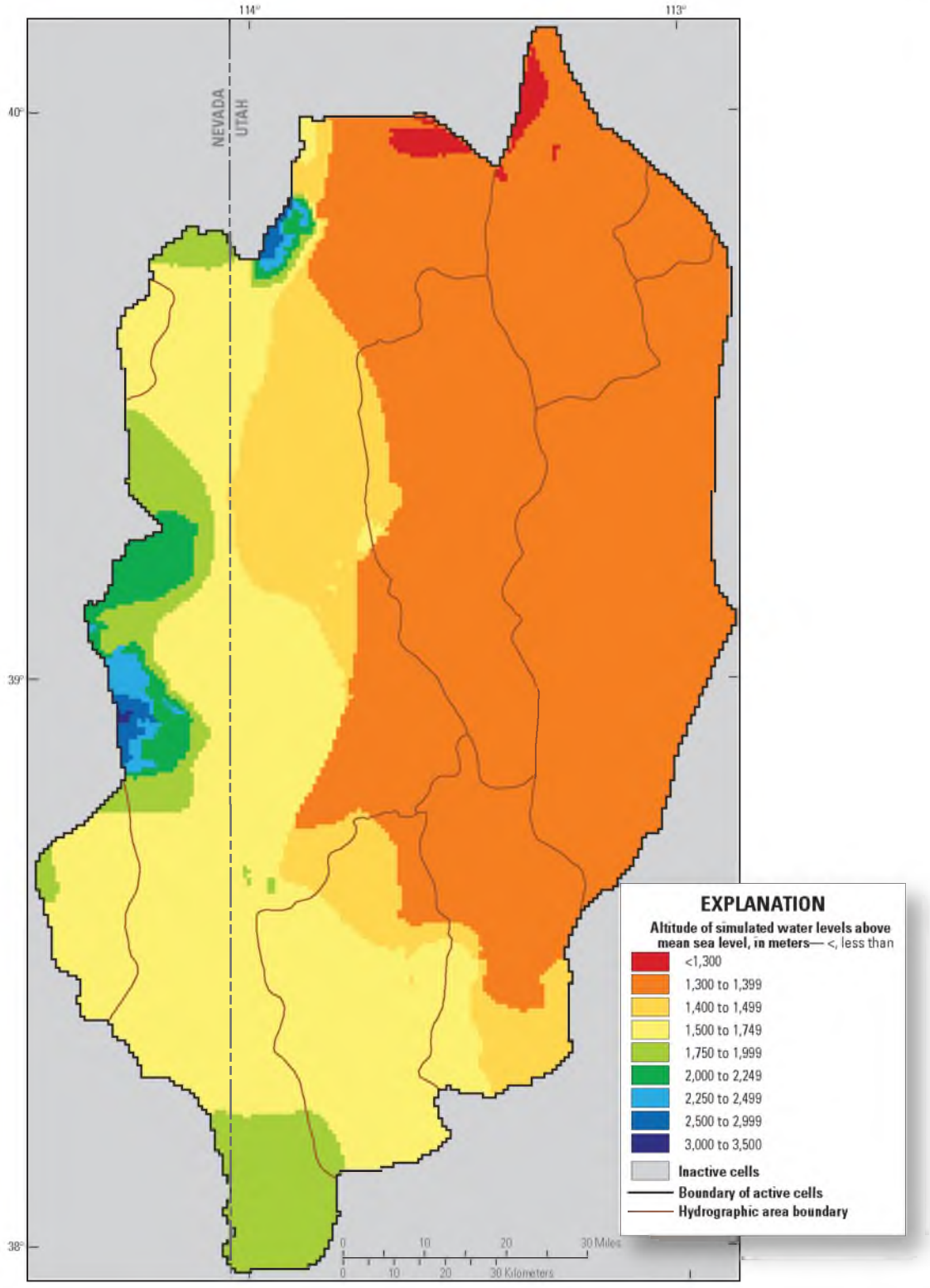

Figure 3-49. Distribution of simulated water-level altitudes in the Snake Valley area groundwater model. State boundary data from: *U.S. Census Bureau* [2000]. Modified from: *Masbruch et al.* [201X], in review.

Table 3-12. Summary of observed and simulated discharge for the Snake Valley area groundwater model. Modified from: *Masbruch et al.* [201X], in review.

[**Abbreviations:** ETg, groundwater evapotranspiration; %, percent]

Groundwater discharge type	Observation name	Observed discharge (cubic meters per day)	Simulated discharge (cubic meters per day)	Simulated discharge as a percent of observed discharge
Snake Valley				
ETg				
North	ET_2541	45,755	32,493	71%
North-central	ET_2542	131,042	95,151	73%
South-central	ET_2543	96,827	83,516	86%
South	ET_2544	7,462	6,156	82%
Springs				
Miller Spring	miller	931	1,025	110%
Gandy Warm Springs	gandy	36,830	34,739	94%
Twin Springs and Foote Reservoir Spring	twin_foote	13,240	12,935	98%
Unnamed Spring	unnamed	4,906	4,820	98%
Rowland Springs	rowland	5,576	5,231	94%
Spring Creek Spring	spring_creek	4,648	4,912	106%
Clay Spring	clay	868	832	96%
Dearden Spring Group	dearden	16,320	22,985	141%
Big Springs	big	24,420	28,342	116%
Mountain streams				
Granite and Trout Creeks	gran_trout	4,761	4,743	100%
Strawberry, Baker, and Snake Creeks	str_bak_snk	7,560	6,005	79%
Wah Wah Valley				
Springs				
Wah Wah Springs	wah_wah	2,725	2,434	89%
Tule Valley				
ETg	ET_257	128,311	146,047	114%
Fish Springs Flat				
ETg	ET_258	27,013	35,019	130%
Springs				
Fish Springs	fish	87,790	84,447	96%
Sevier Desert				
ETg	ET_287	29,039	20,382	70%

(Figure 3-50), but a few trends are evident, most notably discharge to ETg. Simulated discharge to ETg is predominantly more than observed discharge throughout the central portion of the study area, and is less than observed in Snake Valley and Sevier Desert. Graphs of weighted discharge residuals and weighted simulated values (Figure 3-48B) also indicate little model bias; most of the weighted residuals vary randomly about a value of zero.

3.5.4.1.3 Temperatures

The fit of simulated to observed temperatures is generally good; 81 percent of the simulated values of temperatures in wells are within 2 °C of the observation, and 55 percent of them are within 0.75 °C (Table 3-13). The largest temperature residuals generally occur at or near springs. Simulated groundwater temperatures at Gandy Warm Springs (observation gandyT) and Big Springs (observation bigT) are cooler than the observed temperatures by 13 °C and 7.5 °C, respectively. It is possible that there are local effects leading to the warmer observed temperatures at these springs that could not be simulated in this larger regional model. Weighted temperature observations plotted against weighted simulated values generally fall on the 1 to 1 line, indicating good model fit (Figure 3-46C). Positive and negative temperature residuals are distributed randomly around the study area, indicating no systematic model error. Graphs of weighted temperature residuals and weighted simulated values (Figure 3-48C) also indicate little model bias; most of the weighted residuals vary randomly about a value of zero.

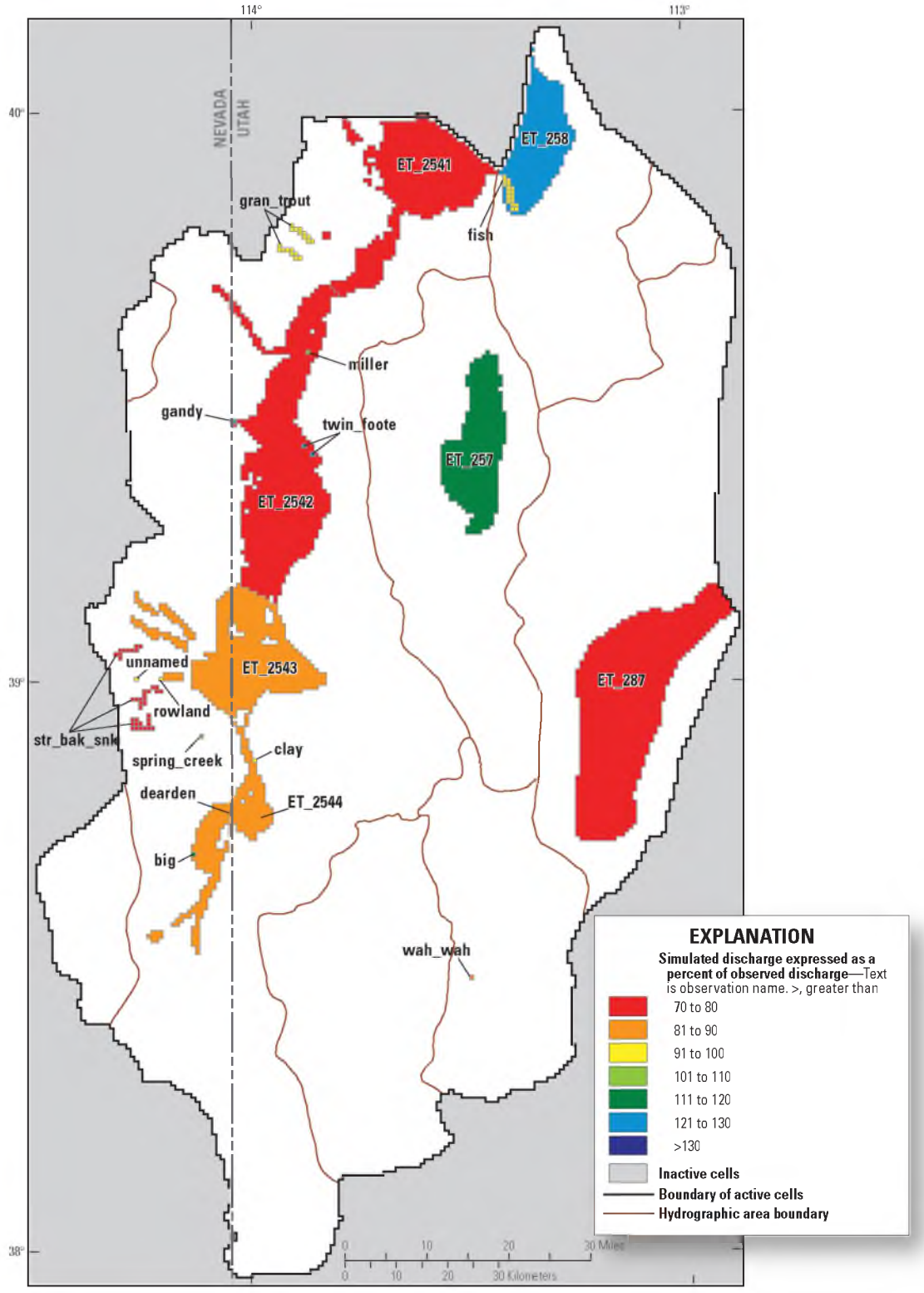

Figure 3-50. Simulated discharge as a percent of observed discharge in the Snake Valley area groundwater model. State boundary data from: *U.S. Census Bureau* [2000]. Modified from: *Masbruch et al.* [201X], in review.

Table 3-13. Summary of observed and simulated groundwater temperatures for the Snake Valley area groundwater model. Modified from: *Masbruch et al.* [201X], in review.

Observation name	Observed temperature (degress Celsius)	Simulated temperature (degress Celsius)	Residual (observed minus simulated, in degrees Celsius)
PW01C2	12.7	13.6	-0.9
PW01C3	13.7	14.8	-1.1
PW01C4	15.6	14.9	0.7
PW01C5	19.1	15.3	3.8
PW02B2	14.8	13.4	1.4
PW02B3	16.7	12.8	3.9
PW03B2	13.2	13.2	0.0
PW03B3	13.3	13.1	0.2
PW04B2	15.7	14.2	1.5
PW05C2	13.8	14.5	-0.6
PW05C3	14.5	15.1	-0.5
PW05C4	15.8	15.5	0.4
PW06D2	18.2	16.4	1.8
PW06D3	18.6	16.0	2.6
PW07B2	13.5	13.5	0.0
PW07B3	14.4	14.9	-0.4
PW07B4	15.4	16.1	-0.7
PW07B5	17.0	17.5	-0.5
PW09B2	16.9	16.9	-0.0
PW09B3	18.0	18.2	-0.2
PW11E2	15.1	14.3	0.8
PW11E3	16.5	14.7	1.8
PW11E4	18.0	14.9	3.1
PW12A2	35.2	31.9	3.3
PW17C2	17.5	17.3	0.2
PW17C3	19.0	18.5	0.5
PW18A2	46.9	42.9	4.1
PW19C2	35.1	32.3	2.9
PW20A2	25.2	25.0	0.1
SG21C1	23.2	29.7	-6.6
SG24C1	16.4	16.1	0.3
clayT	13.6	13.3	0.3
deardenT	13.8	13.7	0.1
gandyT	27.2	14.2	13.0
bigT	17.5	10.0	7.5
unnamedT	5.6	7.1	-1.5

3.5.4.2 Estimated Parameter Values and Sensitivities

Most of the parameters estimated during model calibration are related to recharge, evapotranspiration, horizontal-hydraulic conductivity, vertical anisotropy, well withdrawals, drain and river conductances, and thermal properties. Less sensitive parameters are related to general-head boundary conductances, hydraulic characteristics of HFBs, and subsurface flow across the eastern boundary (Figure 3-32). Of the 51 defined parameters, 40 were estimated using nonlinear regression, and 42 are within reasonable ranges. The other defined parameters were not estimated using regression because CSS values indicate that there is inadequate information to estimate them; most of these are horizontal hydraulic-conductivity parameters. These parameters are often important, however, in defining local flow patterns and gradients, especially in the mountain blocks. Compared to reported hydraulic-conductivity estimates [*Sweetkind et al.*, 2011a], these nonregressed estimated hydraulic conductivity parameter values fall within reasonable ranges (Tables 3-7 and 3-8).

3.5.4.2.1 Reduction of Parameter Uncertainty With the Inclusion of Temperature Observations

Several previous studies [*Bravo et al.*, 2002; *Heilweil et al.*, 2012; *Manning and Solomon*, 2005; *Woodbury and Smith*, 1988] have shown that using temperature observations in numerical models reduces the uncertainty in model parameters more than using only water-level observations and/or groundwater flow (discharge) observations. Most of these studies, however, are at the basin or subbasin scale. This study represents one of the first regional modeling efforts to include calibration to groundwater temperature data.

UCODE_2005 was used to calculate the reduction in parameter uncertainties using groundwater temperature observations over using just water-level and/or groundwater discharge observations. Figure 3-51 shows the 95-percent confidence intervals for model parameters using (1) only water-level observations (blue bars); (2) water-level plus discharge observations (yellow bars); and (3) water-level, discharge, and temperature observations (red bars). Although most parameters are greatly sensitive to the spring discharge observations (Figure 3-32), the inclusion of temperature observations further reduces parameter uncertainty, in some cases quite significantly. For example, the 95-percent confidence interval for parameter lbfau_4hk (representing horizontal-hydraulic conductivity) has a range spanning about 12 orders of magnitude when only water-level observations are used. This range is reduced to about six orders of magnitude with the addition of discharge observations, and is further reduced to about one order of magnitude with the addition of temperature observations.

Because groundwater temperatures are highly affected by the magnitude of groundwater flow, parameters controlling this aspect of the system were more constrained by temperature observations than water-level or groundwater discharge observations (Figure 3-51). These include parameters representing (1) the horizontal-hydraulic conductivity of the basin-fill HGUs (UBFAU and LBFAU) and the carbonate HGUs (UCAU and LCAU); (2) the vertical anisotropy ratio, especially those of the basin fill units (parameters ubfau_vn and playa_vn); (3) spring and river conductance; (4) recharge rate; and (5) well withdrawal rate.

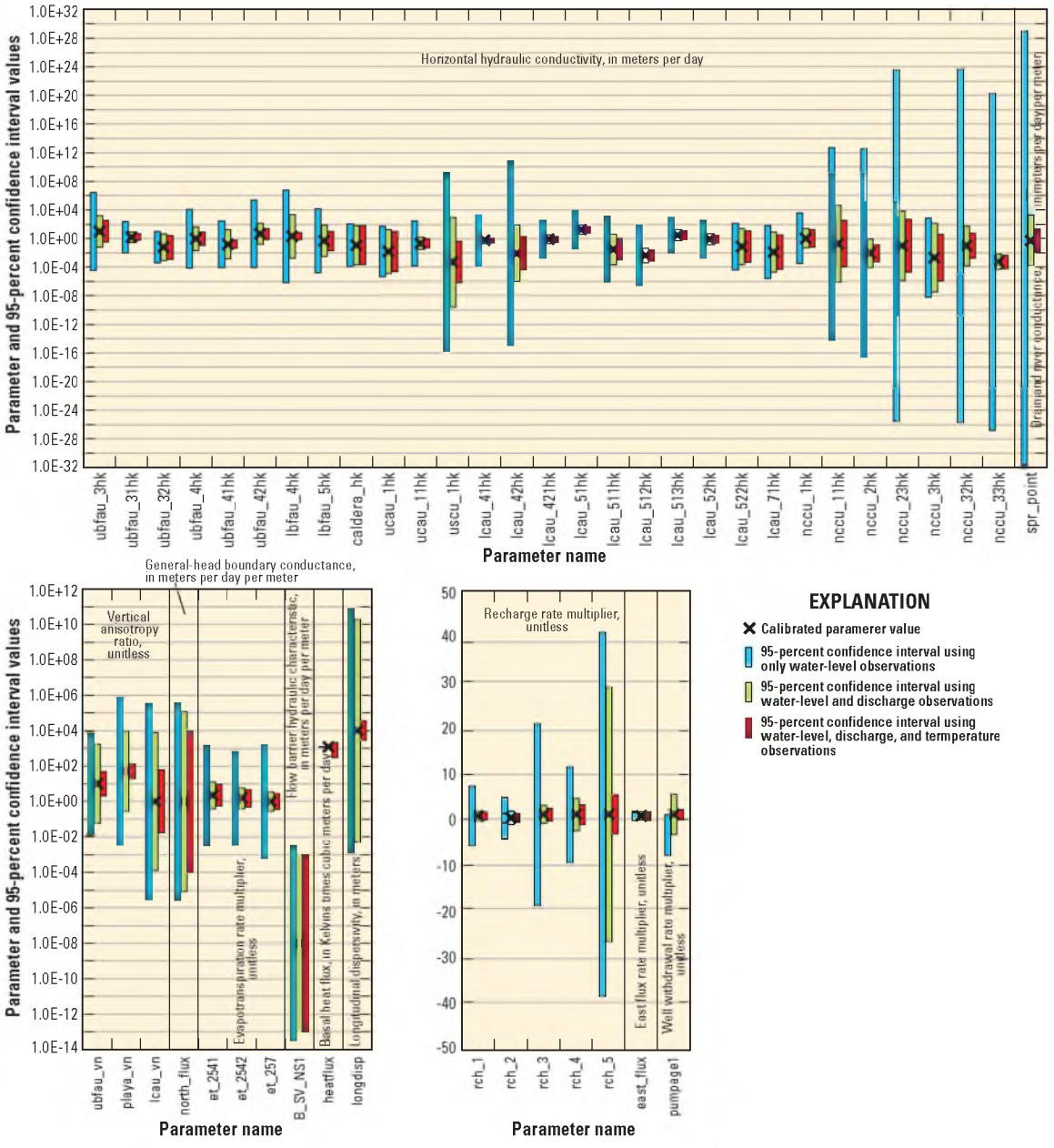

Figure 3-51. Calibrated model parameter values and 95-percent confidence intervals using only water-level observations, water-level plus discharge observations, and water-level plus discharge and temperature observations. Modified from: *Masbruch et al.* [201X], in review.

3.5.4.2 Regional Groundwater Budget

The conceptual and simulated water budgets for the entire study area and also for the eight individual HAs in the study area are listed in Table 3-14. One calibration criteria for the model was to match conceptual recharge and discharge components to within plus or minus 30 percent, because the majority of the discharge measurements had uncertainties of about 30 percent. The model simulated recharge and discharge amounts to within plus or minus 30 percent of the conceptual recharge and discharge amounts with one exception; Pine Valley has simulated areal recharge (in-place+runoff+unconsumed irrigation) that is 68 percent of the conceptual recharge. This is because recharge was reduced in southern Spring, Snake, and Pine Valleys to minimize flooding in the mountain blocks and to reduce simulated water-levels in southern Snake and Pine Valleys. The amount of reduction in recharge is approximately equal to the amount of previously reported groundwater discharge from perched areas to springs, streams, and ETg [*Stephens*, 1976], which would be disconnected from the larger regional flow system. Because the model did not simulate discharge from these perched areas, the reduction in recharge accounts for any groundwater that may have been discharged to these perched areas. Although simulated recharge was reduced in southern Spring and Snake Valleys, simulated areal recharge in Spring and Snake Valleys is more similar to conceptual amounts than in Pine Valley because simulated recharge was increased over conceptual recharge in other portions of these HAs as indicated by both the temperature and groundwater discharge observations. Simulated discharge matches conceptual discharge within the range of plus or minus 30 percent in all HAs. This indicates that the model reasonably represents the movement of water from recharge areas to discharge

Table 3-14. Comparison of simulated, conceptual, and previously reported groundwater budget components for hydrographic areas and the Snake Valley study area. Modified from: *Masbruch et al.* [201X], in review.

[All estimates in acre-feet per year rounded to two significant figures. **Abbrevations:** HA, hydrographic area; —, no data; NE, not estimated]

	Simulated	Conceptual	Previous studies
Spring Valley (HA 184)[1]			
Recharge			
Direct infiltration of precipitation (inplace recharge) + infiltration of runoff (including unconsumed surface-water irrigation) + infiltraiton of mountain stream baseflow + unconsumed irrigation from well withdrawals	15,000	16,000	—
Subsurface inflow	0	NE	—
Discharge			
Groundwater evapotranspiration + springs	0	0	—
Mountain streams	0	0	—
Well withdrawals	0	0	—
Subsurface ouflow	15,000	NE	4,000 to 49,000[2,3,4,5,6,7,8]
Northern Spring Valley to Snake Valley	2,200	NE	16,000[5]
Southern Spring Valley to Snake Valley	13,000	NE	4,000 to 33,000[2,3,4,5,6,7,8]
Snake Valley (HA 254)			
Recharge			
Direct infiltration of precipitation (inplace recharge) + infiltration of runoff (including unconsumed surface-water irrigation) + infiltraiton of mountain stream baseflow + unconsumed irrigation from well withdrawals	160,000	160,000	99,000 to 160,000[2,3,5,9,10]
Subsurface inflow	15,000	NE	4,000 to 49,000[2,3,4,5,6,7,8]
From Northern Spring Valley	2,200	NE	16,000[5]
From Southern Spring Valley	13,000	NE	4,000 to 33,000[2,3,4,5,6,7,8]
Discharge			
Groundwater evapotranspiration + springs	100,000	120,000	64,000 to 130,000[2,3,5,14]
Mountain streams	3,300	3,600	2,800[14]
Well withdrawals	28,000	22,000[11]	11, 000[12,13]
Subsurface ouflow	44,000	NE	25,000 to 43,000[2,3,4,5,7]
To Pine Valley	2,000	NE	—
To Wah Wah Valley	23	NE	—
To Tule Valley	31,000	NE	15,000 to 42,000[2,3,4]
To Fish Springs Flat	790	NE	0[4]
To outside study area	8,400	NE	10,000 to 29,000[2,4,5]

Table 3-14. Continued

[All estimates in acre-feet per year rounded to two significant figures. **Abbrevations:** HA, hydrographic area; —, no data; NE, not estimated]

	Simulated	Conceptual	Previous studies
Pine Valley (HA 255)			
Recharge			
Direct infiltration of precipitation (inplace recharge) + infiltration of runoff (including unconsumed surface-water irrigation) + infiltraiton of mountain stream baseflow + unconsumed irrigation from well withdrawals	18,000	27,000	21,000 to 27,000[3,9,10,15]
Subsurface inflow	2,000	NE	—
From Snake Valley	2,000	NE	—
Discharge			
Groundwater evapotranspiration + springs	0	0	0[3,14,15]
Mountain streams	0	0	0[3,14,15]
Well withdrawals	0	0	5[15]
Subsurface ouflow	20,000	NE	3,000 to 14,000[3,4,15,17]
To Wah Wah Valley	20,000	NE	3,000 to 14,000[4,15,17]
To Tule Valley	0	NE	14,000[3]
Wah Wah Valley (HA 256)			
Recharge			
Direct infiltration of precipitation (inplace recharge) + infiltration of runoff (including unconsumed surface-water irrigation) + infiltraiton of mountain stream baseflow + unconsumed irrigation from well withdrawals	4,700	5,900	6,000 to 7,000[3,9,10,18]
Subsurface inflow	20,000	NE	3,000 to 14,000[4,15,17]
From Snake Valley	23	NE	—
From Pine Valley	20,000	NE	3,000 to 14,000[4,15,17]
Discharge			
Groundwater evapotranspiration + springs	710	740	1,400 to 1,500[3,14,17]
Mountain streams	0	0	0[3,14,17]
Well withdrawals	0	0	110[19]
Subsurface ouflow	24,000	NE	8,500[3,4]
To Tule Valley	11,000	NE	8,500[3,4]
To Sevier Desert	13,000	NE	—

Table 3-14. Continued

[All estimates in acre-feet per year rounded to two significant figures. **Abbrevations:** HA, hydrographic area; —, no data; NE, not estimated]

	Simulated	Conceptual	Previous studies
Tule Valley (HA 257)			
Recharge			
Direct infiltration of precipitation (inplace recharge) + infiltration of runoff (including unconsumed surface-water irrigation) + infiltraiton of mountain stream baseflow + unconsumed irrigation from well withdrawals	14,000	13,000	7,600 to 13,000[3,9,10,18]
Subsurface inflow	44,000	NE	15,000 to 50,000[2,3,4,18,20]
From Snake Valley	31,000	NE	15,000 to 42,000[2,3,4]
From Wah Wah Valley	11,000	NE	8,500 to 32,000[3,4,18]
From Sevier Desert	2,000	NE	9,000[4]
Discharge			
Groundwater evapotranspiration + springs	44,000	39,000	24,000 to 56,000[3,14,18]
Mountain streams	0	0	0[3,14,18]
Well withdrawals	0	0	—
Subsurface ouflow	16,000	NE	27,000 to 31,000[4,21]
To Fish Springs Flat	16,000	NE	27,000[4]
Fish Springs Flat (HA 258)			
Recharge			
Direct infiltration of precipitation (inplace recharge) + infiltration of runoff (including unconsumed surface-water irrigation) + infiltraiton of mountain stream baseflow + unconsumed irrigation from well withdrawals	1,200	1,700	1,600 to 4,000[3,9,10,21]
Subsurface inflow	37,000	NE	27,000 to 31,000[3,4,21]
From Snake Valley	790	NE	0[4]
From Tule Valley	16,000	NE	27,000[4]
From Dugway-Government Creek Valley	5,100	NE	—
From Sevier Desert	15,000	NE	0[4]
From outside of study area	100	NE	—
Discharge			
Groundwater evapotranspiration + springs	35,000	34,000	34,000 to 35,000[3,14,21]
Mountain streams	0	0	0[3,14,21]
Well withdrawals	0	0	—
Subsurface ouflow	2,400	NE	100 to 1,000[3,4]
To outside study area	2,400	NE	1,000[4]

Table 3-14. Continued

[All estimates in acre-feet per year rounded to two significant figures. **Abbrevations:** HA, hydrographic area; —, no data; NE, not estimated]

	Simulated	Conceptual	Previous studies
Dugway-Government Creek Valley (HA 259)[1]			
Recharge			
Direct infiltration of precipitation (inplace recharge) + infiltration of runoff (including unconsumed surface-water irrigation) + infiltraiton of mountain stream baseflow + unconsumed irrigation from well withdrawals	230	300	—
Subsurface inflow	71	NE	—
From outside of study area	71	NE	—
Discharge			
Groundwater evapotranspiration + springs	0	0	—
Mountain streams	0	0	—
Well withdrawals	0	0	—
Subsurface ouflow	5,000	NE	—
To Fish Springs Flat	5,000	NE	—
Sevier Desert (HA 287)[1]			
Recharge			
Direct infiltration of precipitation (inplace recharge) + infiltration of runoff (including unconsumed surface-water irrigation) + infiltraiton of mountain stream baseflow + unconsumed irrigation from well withdrawals	8,900	10,000	—
Subsurface inflow	19,000	NE	—
From Wah Wah Valley	13,000	NE	—
From outside the study area	6,200	NE	—
Discharge			
Groundwater evapotranspiration + springs	6,200	8,600	8,600[22]
Mountain streams	0	0	—
Well withdrawals	0	0	—
Subsurface ouflow	22,000	NE	8,800 to 9,000[4,20]
To Tule Valley	2,000	NE	9,000[4]
To Fish Srings Flat	15,000	NE	0[4]
To Dugway-Government Creek Valley	4,800	NE	—

Table 3-14. Continued

[All estimates in acre-feet per year rounded to two significant figures. **Abbrevations:** HA, hydrographic area; —, no data; NE, not estimated]

	Simulated	Conceptual	Previous studies
Study area total			
Recharge			
Direct infiltration of precipitation (inplace recharge) + infiltration of runoff (including unconsumed surface-water irrigation) + infiltraiton of mountain stream baseflow + unconsumed irrigation from well withdrawals	220,000	240,000	—
Subsurface inflow from outside the study area	6,400	NE	—
Discharge			
Groundwater evapotranspiration + springs	190,000	200,000	—
Mountain streams	3,300	3,600	—
Well withdrawals	28,000	22,000	—
Subsurface ouflow to outside of study area	11,000	NE	—

[1]Partial HA; estimates only for portion of HA within study area.
[2]*Hood and Rush* [1965].
[3]*Gates and Kruer* [1981].
[4]*Harrill et al.* [1988].
[5]*Welch et al.* [2007].
[6]*Rush and Kazmi* [1965].
[7]*Scott et al.* [1971].
[8]*Nichols* [2000].
[9]*Harrill and Prudic* [1998].
[10]*Masbruch* [2011a].
[11]Estimate for the year 2009.
[12]*Masbruch* [2011b].
[13]Estimate for the year 2000.
[14]*Masbruch* [2011c].
[15]*Stephens* [1976].
[16]Estimate for the year 1976.
[17]*Stephens* [1974].
[18]*Stephens* [1977].
[19]Estimate for the year 1974.
[20]*Holmes* [1984].
[21]*Bolke and Sumsion* [1978].
[22]*Wilberg* [1991].

areas and water levels within the discharge areas.

Simulated subsurface flow between HAs and out of the study area, along with uncertainties (Table 3-15), were also calculated for the model using the predictive capabilities of UCODE_2005 [*Poeter et al.*, 2005]. These subsurface flow estimates are HA based, which may include flow between cells along the the topographic divides, and are not just valley to valley flow as has been reported in previous studies. The magnitude of the uncertainties (shown as 95-percent confidence intervals in Table 3-15) of the simulated flow is related to the uncertainty in the model parameters and the sensitivity of the simulated flows to the model parameters [*Hill and Tiedeman*, 2007]. The uncertainties were calculated using simultaneous confidence intervals [*Hill and Tiedeman*, 2007] because no subsurface flow amounts within the study area are known with certainty. Methods used for determining simultaneous confidence intervals tend to produce larger intervals than exact intervals would be for a linear model with normally distributed residuals [*Poeter et al.*, 2005]. Additionally, the confidence intervals get larger as more intervals are calculated because the uncertainty of each individual subsurface flow amount is affected by the uncertainty of all the other subsurface flow amounts. The 95 percent simultaneous confidence intervals have a 95 percent probability of containing their respective true predicted values simultaneously [*Hill and Tiedeman*, 2007]. The negative amounts shown on the lower end of the confidence intervals indicate that subsurface flow between HAs and across the model boundary could go in the opposite direction; no simulated boundary flow has 95-percent confidence in direction. Because the model developed in the current study takes into account the uncertainties of the parameters as well as the observations in calculating the uncertainties of the simulated

Table 3-15. Summary statistics of simulated subsurface flow between hydrographic areas and out of the study area in the Snake Valley groundwater model and comparison to previous estimates. Modified from: *Masbruch et al.* [201X], in review.

[All values in acre-feet per year. **Abbreviations:** NE, no estimate]

Direction of simulated subsurface net flow	Simulated net flow	95-percent confidence interval	Previous estimates of subsurface flow
Northern Spring Valley to Snake Valley	2,248	-471 to 4,967	16,000[1]
Southern Spring Valley to Snake Valley	13,052	-14,283 to 40,388	4,000 to 33,000[1,2,3,4,5,6,7]
Snake Valley to Pine Valley	1,955	-20,298 to 24,208	NE
Snake Valley to Wah Wah Valley	23	-353 to 399	NE
Snake Valley to Tule Valley	31,440	-18,217 to 81,097	15,000 to 42,000[2,3,4]
Snake Valley to Fish Springs Flat	787	-2,442 to 4,015	0[4]
Pine Valley to Wah Wah Valley	20,207	-8,425 to 48,839	3,000 to 14,000[4,8,9]
Wah Wah Valley to Tule Valley	11,302	-5,068 to 27,673	8,500[3,4]
Wah Wah Valley to Sevier Desert	13,017	-292 to 26,326	NE
Tule Valley to Fish Springs Flat	15,553	-20,140 to 51,246	27,000[4]
Dugway-Government Creek Valley to Fish Springs Flat	5,052	-3,647 to 13,752	NE
Sevier Desert to Tule Valley	2,026	-20,692 to 24,743	9,000[4]
Sevier Desert to Fish Springs Flat	15,157	-3,492 to 33,806	0[4]
Sevier Desert to Dugway-Government Creek Valley	4,754	-3,641 to 13,148	NE
Snake Valley to outside model boundary	8,378	-444,001 to 460,758	10,000 to 29,000[1,2,4]
Fish Springs Flat to outside model boundary	2,412	-261,298 to 266,121	1,000[4]

[1]*Welch et al.* [2007].
[2]*Hood and Rush* [1965].
[3]*Gates and Kruer* [1981].
[4]*Harrill et al.* [1988].
[5]*Rush and Kazmi* [1965].
[6]*Scott et al.* [1971].
[7]*Nichols* [2000].
[8]*Stephens* [1974].
[9]*Stephens* [1976].

subsurface flow amounts, these simulated subsurface flow estimates and uncertainties are considered a better quantification of subsurface flow than previously reported estimates.

Simulated subsurface flow estimates between HAs and across the study area boundary, along with their associated uncertainty, are within the range of previously reported estimates, except for subsurface flow from Spring Valley to Snake Valley north of the Snake Range; the simulated subsurface flow and associated uncertainty indicate that flow across this boundary is much less than has recently been estimated [*Welch et al.*, 2007]. Although simulated subsurface flow amounts are more than previously reported from Pine Valley to Wah Wah Valley, Wah Wah Valley to Tule Valley, Sevier Desert to Fish Springs Flat, and Fish Springs Flat to outside the model boundary and are less than previously reported from Tule Valley to Fish Springs Flat, Sevier Desert to Tule Valley, and Snake Valley to outside the model boundary, their 95-percent confidence intervals encompass the range of previous estimates across these boundaries. This indicates that the simulated subsurface flow across these boundaries is actually within the range of the previous estimates.

3.5.5 Implications

The numerical model represents a more robust quantification of groundwater budget components than the previously reported conceptually developed budget estimates (Table 3-14) because the model integrates all components of the groundwater budget. The numerical model represents and simulates the conceptual model of an interconnected groundwater system between consolidated rock and basin fill, and of recharge areas in the mountains connecting flow through the mountains to the basins and to the regional flow system, similar to the conceptual model presented in *Heilweil and Brooks* [2011] for the

eastern Great Basin. The concept of the mountains and basins forming a continuous groundwater system provides a more detailed representation of groundwater budgets and flowpaths compared to previous studies that separated the flow and/or groundwater budget components between the consolidated rock and basin fill [*Harrill and Prudic*, 1998; *Prudic et al.*, 1995; *Welch et al.*, 2007].

The numerical model is also an advancement over previous numerical models, specifically the RASA-GB model [*Halford and Plume*, 2011; *Prudic et al.*, 1995], for several reasons: (1) The model incorporates a more detailed hydrogeologic framework, whereas the RASA-GB model used two layers to represent shallower and deeper flow; (2) the model was calibrated using more observations including several new water-level altitudes from the recently installed UGS monitoring well network and other newer wells in the study area, several new measurements of spring discharge within Snake Valley, including Dearden Springs Group, Clay Spring, Twin Springs, Foote Reservoir, and Miller Spring, discharge to mountain springs and baseflow to mountain streams, and temperature data from the UGS monitoring well network; and (3) the inclusion of calibration to temperature data resulted in a reduction of parameter uncertainty over using just water-level altitude and discharge observations, which is what was used to calibrate the RASA-GB model.

Uncertainty in the estimates of subsurface flow are less than those of previous studies because the model balanced recharge and discharge across the entire simulated area, not just in each HA, and because of the large dataset of observations (water-level altitudes, discharge, and temperatures) used to calibrate the model and the resulting transmissivity distribution. Previous estimates had uncertainty, but it was difficult to

quantify and was seldom specified. Many of the previous estimates of subsurface flow (Table 3-15) were made on the basis of whether estimated recharge exceeded estimated discharge, or the reverse, in a basin or HA. If estimated recharge was greater than estimated discharge within the basin, groundwater was assumed to leave the basin through one or more boundaries. The uncertainties associated with estimated recharge and discharge are additive in determining the uncertainty in the subsurface flow. For example, consider a basin where recharge is 100,000 acre-ft/yr with a 30 percent uncertainty, and discharge is 70,000 acre-ft/yr with a 30 percent uncertainty. It is possible that recharge could be as low as 70,000 acre-ft/yr and discharge could be as high as 91,000 acre-ft/yr, resulting in a deficit of 21,000 acre-ft/yr and, thereby, indicating that the basin receives subsurface inflow. It is also possible that recharge could be as high as 130,000 acre-ft/yr and discharge could be as low as 49,000 acre-ft/yr resulting in an excess of 81,000 acre-ft/yr and, thereby, indicating that the excess water must leave the basin through subsurface outflow. In this example, both the amount and direction of subsurface flow varies by a substantial amount. If a basin could receive or send flow amongst multiple adjacent basins, each subsurface flow amount is even more uncertain. A few of the previous estimates were made on the basis of Darcy's Law using estimates of transmissivity, length of the boundary, and hydraulic gradient across the boundary. These estimates seldom accounted for uncertainty in estimating transmissivity, the length of the permeable boundary, or the hydraulic gradient on the basis of little data.

Because the uncertainties in the subsurface HA flow represent uncertainties in many model parameters at one time, postprocessing model statistic tools could be used to guide data collection that would help reduce uncertainty on model parameters. One

example is OPR-PPR [*Tonkin et al.*, 2007], which can identify potential observations that would most reduce prediction uncertainty. For instance, OPR-PPR could be used to identify possible areas where additional observations would be useful for predicting the reduction of groundwater discharge to springs if increased well withdrawals were occurring.

Although the quantification of groundwater flow across HA boundaries in the model is important in understanding the occurrence and movement of groundwater in and through the study area, it should be noted that the effects of groundwater development on natural discharge are not dependent on the rate and direction of groundwater flow [*Barlow and Leake*, 2012; *Leake*, 2011]. For example, the effects of groundwater withdrawals in southern Spring Valley on natural discharge in southern Snake Valley would be the same whether groundwater was flowing from Spring Valley to Snake Valley or from Snake Valley to Spring Valley (Figure 3-52). As long as aquifer properties remain the same, groundwater withdrawals in southern Spring Valley could capture natural groundwater discharge in Snake Valley, such as at Big Springs or from ETg, regardless of the direction of the interbasin flow. *Barlow and Leake* [2012] show that the locations and timing of depletion and capture of natural groundwater discharge are affected by (1) aquifer properties, specifically the hydraulic diffusivity, which is the hydraulic transmissivity divided by the storage coefficient; and (2) system geometry, specifically the distance between pumping locations and connected groundwater discharge areas. The simulated transmissivity (Figure 3-53) across HA boundaries and the location of natural discharge (Figure 3-6), therefore, provide a better estimate of the effect of groundwater withdrawals on groundwater resources than does the amount and

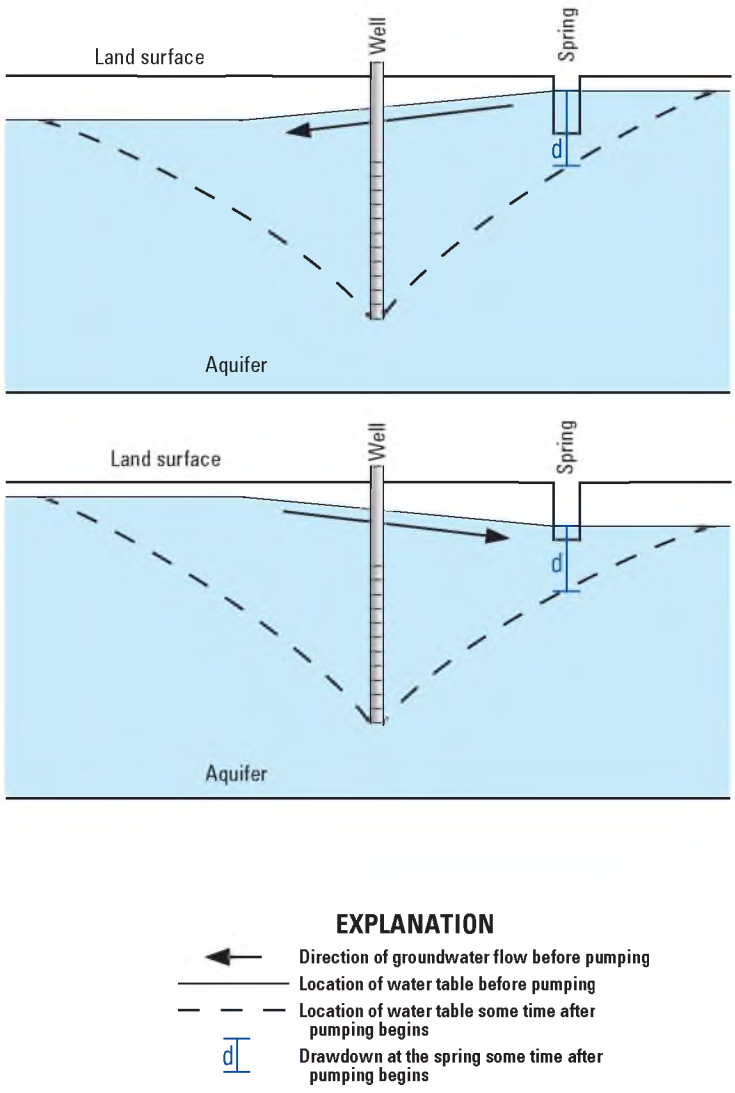

Figure 3-52. Position of a pumped well in relation to a spring with opposing directions of prepumping groundwater flow. As long as aquifer properties are the same in each case, the amount of drawdown (d) at the spring would be the same and, in the case shown, the spring would cease to flow. Modified from: *Barlow and Leake* [2012] and *Masbruch et al.* [201X], in review.

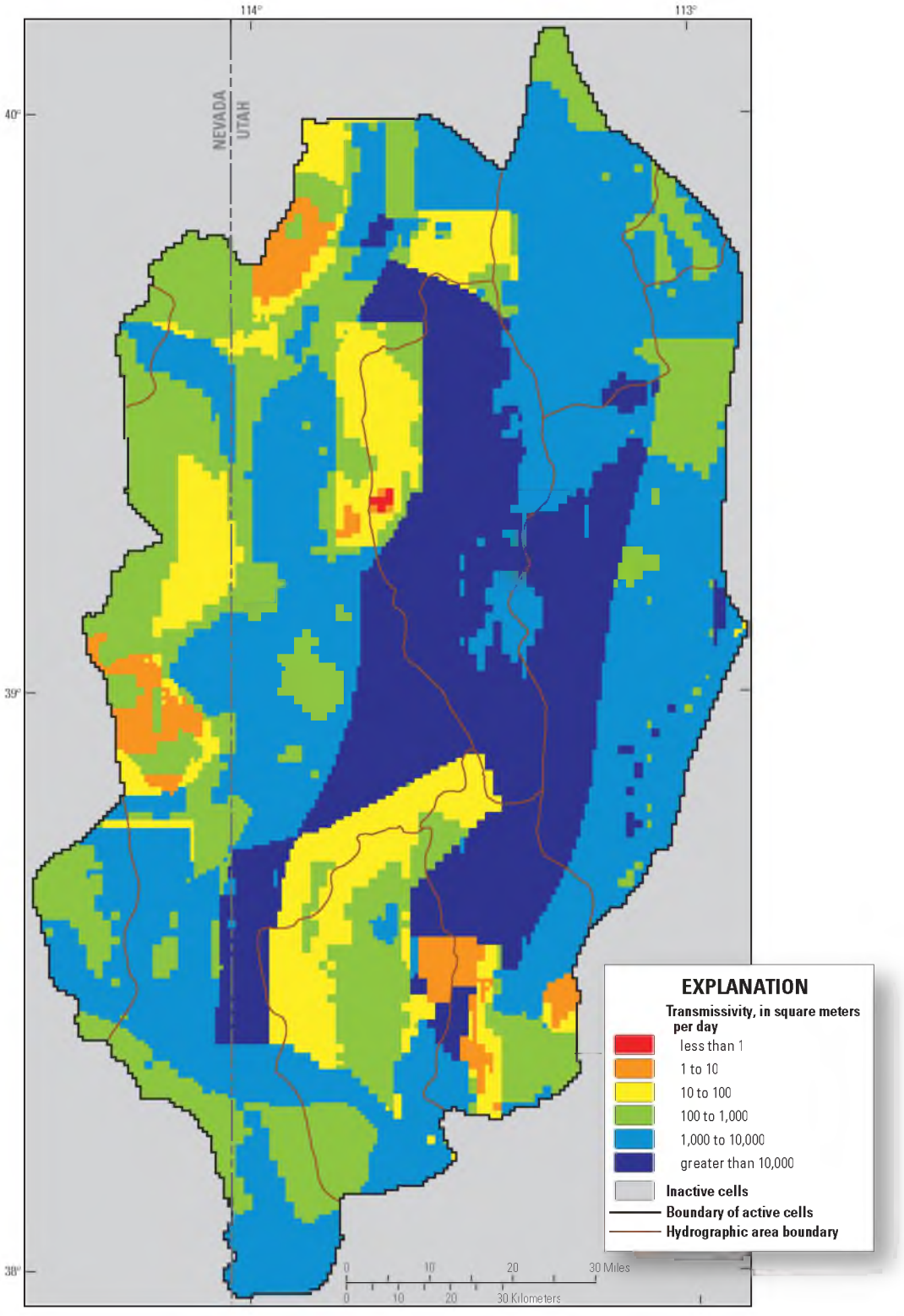

Figure 3-53. Simulated transmissivity in the Snake Valley area groundwater model. State boundary data from: *U.S. Census Bureau* [2000]. Modified from: *Masbruch et al.* [201X], in review.

direction of subsurface flow between HAs.

The distribution of simulated transmissivity (Figure 3-53) includes many areas of high transmissivity within and between HA boundaries. The highest transmissivity occurs in the middle section of the study area, extending from northern Wah Wah Valley through Tule Valley and portions of Sevier Desert and Snake Valley. This corresponds with an area of relatively thick LCAU (Figure 3-25). Other areas of high transmissivity between HAs occurs between southern Spring Valley and southern Snake Valley, southern Snake Valley and southern Pine Valley, northeastern Tule Valley and Fish Springs Flat, northwestern Sevier Desert and Fish Springs Flat, and a small section between northern Spring Valley and Snake Valley. Most of these areas also correspond with thick sections of LCAU. Well withdrawals from these areas of high transmissivity would likely affect natural groundwater discharge through a large portion of the study area. For example, although the model simulates flow from Snake Valley to Pine Valley, the lack of natural discharge in Pine Valley, and the relatively large transmissivity between southern Pine Valley and Snake Valley, indicates that withdrawals in Pine Valley could cause drawdown in Snake Valley that could reduce natural discharge in southern Snake Valley. These reductions in natural discharge could occur at Big Springs, Dearden Spring Group, or from ETg in southern Snake Valley, or from all three discharge areas.

Conversely, there are a few areas where model calibration required zones of low transmissivity (Figure 3-53) in order to simulate discharge at springs. These include the areas between (1) northeastern Tule Valley and northwestern Snake Valley, which was needed to match discharge to Twin Springs, Foote Reservoir, Miller Spring, and Gandy

Warm Springs; (2) northeastern and northern Pine Valley and Snake Valley, which was needed to match discharge at Clay Springs, Big Springs, and Dearden Springs Group; and (3) the area around Wah Wah Springs, which was needed to match discharge at Wah Wah Springs. Other areas of low transmissivity occur in the northern section of the southern Snake Range, the northern Snake Range, and the Deep Creek Range, which correspond with relatively thick sections of lower permeability NCCU (Figure 3-26).

3.5.5.1 Appropriate Uses of the Model

The Snake Valley groundwater model was constructed to simulate regional-scale groundwater flow, thus it can be used to answer questions regarding groundwater flow issues at this scale. The model can provide boundary conditions for local-scale models, but consistency between regional and local-scale models must be ensured. For example, using a regional model to determine boundary heads and then changing hydraulic conductivity extensively in a local model may allow more or less flow through the local model than would occur in the regional model. Programs such as Local Grid Refinement [*Mehl and Hill*, 2006] may be used to derive boundary conditions for local-scale models that stay consistent with regional models.

The model can be used to evaluate alternative conceptualizations of the hydrogeology that are likely to have a regional effect. These might include the effects of decreased recharge caused by drought conditions, different interpretations of the extent or offset of faults, or other conceptual models of depositional environments that would affect the spatial variation of hydraulic properties.

Increased urbanization in the western U.S. necessitates the development of groundwater resources. Because this is a steady-state model, it can be used for examining

the long-term effects of continued or increased groundwater withdrawals on the regional groundwater flow system and natural groundwater discharge, which can aid in effective management of groundwater resources.

3.5.6 Model Limitations

All models are based on a limited amount of data and thus are necessarily simplifications of actual systems. When creating a model of a large region it is necessary to make more simplifications than when creating models of smaller regions. Model limitations are a consequence of uncertainty in three basic aspects of the model, including inadequacies, inaccuracies, or simplifications in (1) observations used in the model, (2) representation of geologic complexity in the hydrogeologic framework, and (3) representation of the groundwater system in the model. It is important to understand how these characteristics limit the use of the model.

3.5.6.1 Observation Limitations

Observations of water levels, groundwater discharge, and temperatures constrain model calibration through parameter estimation [*Faunt et al.*, 2010]. Uncertainty in these observations introduces uncertainty in the results of model simulations. Although water-level, discharge, and temperature observations were analyzed prior to and throughout calibration, there was uncertainty regarding (1) the distribution and quality of the observation data, (2) appropriateness of the hydrogeologic interpretation, and (3) the representation of observations in the numerical model.

3.5.6.1.1 Distribution and Quality of Observations

The clustering of water-level and temperature observations limits the parameter estimation because it results in the overemphasis of observations in data-rich areas [*Hill and Tiedeman*, 2007]. In the eastern (Sevier Desert) and southern (southern Snake Valley, and Pine and Wah Wah Valleys) portions of the study area, and in the mountain blocks, water-level and temperature data are sparse. A method of better distributing weights for these situations may reduce model uncertainty.

Some water-level observations used in the calibration may be affected by pumping. Only 27 wells within the study area had long-term water-level records. At these sites the spring 2009 water-level measurements were found to be similar to long-term average water levels. Additionally, the spring 2009 water-levels measured in wells without long-term records were similar to those with long-term records. The spring 2009 water-level measurements used as observations in the model, therefore, were assumed to represent steady-state conditions. Without long-term water-level records, however, it is difficult to assess if the observations actually do represent steady-state conditions.

Errors in the estimates of flow across the model boundaries also affect the accuracy of the model. Any unknown and/or unsimulated flow diminishes model accuracy. Improving estimates of flow across the boundaries can reduce model uncertainty.

3.5.6.1.2 Interpretation of Observations

It is difficult to assess whether certain water-level observations represent the regional saturated-zone flow system or more local-scale, perched-water conditions. Areas of steep hydraulic gradient, which are important features in the regional groundwater

flow system, also may be an artifact of perched water levels. Further evaluation of water levels in these areas may help reduce model uncertainty.

Evapotranspiration discharge observations were computed on the basis of vegetated areas and previously reported rates of evapotranspiration [*Welch et al.*, 2007]. These reports gave estimates of the amount of groundwater discharge that may have occurred prior to groundwater development; in Snake Valley, however, well-withdrawals have increased and are assumed to have affected the amount of groundwater discharge available for ETg. Although adjustments were made to the observations to try to account for this decreased water availability, these adjustments were based on assumptions that have a great deal of associated uncertainty, namely the amount of recharge that occurs as irrigation return flow. The uncertainty in the discharge observations increases uncertainty in the flow model.

3.5.6.1.3 Representation of Observations

The altitude assigned to drains and ETg affects the ability of the model to simulate groundwater conditions accurately. The extinction-depth altitude used to simulate discharge through ETg likely approximates the extinction depth for all discharge areas, particularly in areas with highly variable root depth of plants and discontinuous areas of capillary fringe. In areas with extensive capillary effects, such as in the fine-grained playas, observed heads may be lower than the drain altitudes or ETg extinction depth and any drain or ETg cell will not discharge if the heads are simulated accurately.

Incised drainages and other focused discharge areas are difficult to simulate accurately at a grid resolution of 804.65 m (0.5 mi) because, in many cases, the hydraulic conductivity of the HGUs at the land surface controls the simulated discharge. Larger

springs were often simulated as being in several layers in the model to minimize this effect and more closely mimic the probable high vertical conductance that occurs at these springs.

The representation of temperatures in the model was difficult given the large grid resolution and layer thicknesses. Local scale effects that may affect groundwater temperatures could not be simulated accurately at this grid resolution. Likewise, small changes in thermal gradients are difficult to capture given the layer thicknesses in the model. To better represent more local dynamics and gradients, smaller grid cells and layer thicknesses or local refinement of the model grid around selected features or in critical areas of the model domain would be required.

3.5.6.2 Hydrogeologic Framework Limitations

The accuracy of the groundwater model depends on the accuracy of the hydrogeologic conceptual model. Limitations exist in the groundwater flow model because of the difficulties inherent in the interpretation and representation of the complex geometry and spatial variability of hydrogeologic materials and structures in the hydrogeologic framework and in the application of that framework to a 804.65 m (0.5 mi) grid cell size. Abrupt changes in rock type and conductivity cannot be located at their exact positions and small but important features may get missed completely at this scale.

The spatial variability of material properties of the HGUs and structures [*Sweetkind et al.*, 2011a] is represented to some degree in the model. Incorporating these features in the groundwater model substantially improved the simulation; however, the model remains a significantly simplified version of reality. Detailed stratigraphy not represented in the hydrogeologic framework probably causes some of the mismatch

between simulated and observed hydraulic gradients and water levels. In the groundwater model, the assumption of homogeneity within a given HGU or hydraulic-conductivity zone removes the potential effects of smaller scale variability.

3.5.6.3 Limitations of Model Representation of the Groundwater System

Three limitations of the groundwater model are inherent in its construction. These inaccuracies are in the representation of the physical framework, representation of the hydrologic conditions, and representation of thermal conditions.

3.5.6.3.1 Representation of Physical Framework

The 804.65 m (0.5 mi) resolution of the model grid is appropriate to represent regional conditions. A smaller grid cell size would improve simulation accuracy, especially in areas of geologic or thermal complexity. The large grid cells generalize important local-scale complexities that can affect regional flowpaths and gradients, or the thermal regime within the system. To represent more local dynamics, smaller grid cells or local refinement of the model grid around selected features or in critical areas of the model domain would be required.

3.5.6.3.2 Representation of Hydrologic Conditions

The hydrologic conditions represented by the model are expressed as boundary conditions and include recharge; discharge from ETg, springs, and streams; and no-flow, specified-flux, and head-dependent flux boundaries at the edges of the model. Of these boundary conditions, the most significant is recharge. The main limitation in the representation of recharge is the uncertainties associated with the BCM [*Flint et al.*,

2011; *Masbruch et al.*, 2011). In addition to the possible errors discussed in *Flint et al.* [2011] and *Masbruch et al.* [2011], the BCM may overestimate recharge in parts of the model domain because it is assumed that all infiltrating water that passes the root zone ultimately reaches the water table. This assumption ignores the possibility that infiltrating water could be intercepted and perched by a lower permeability layer in the unsaturated zone.

Limitations in the definition of lateral boundary flow are the result of an incomplete understanding of natural conditions. Because very little data exist in the areas defined as lateral flow-system boundary segments, all aspects of the assigned boundary conditions are poorly known. Despite these uncertainties, the data used to characterize these boundary flows have been thoroughly analyzed for this model.

3.5.6.3.3 Representation of Thermal Conditions

Thermal conditions represented by the model are expressed as boundary conditions and thermal properties. The main limitation in the representation of boundary conditions is unknown variability in the basal heat flux across the model domain, and having to specify temperatures at the top of the model to account for conductive heat flux. Limitations associated with unknown variability in the basal heat flux are the result of highly limited to no basal heat flux data in the study area. While several studies [*Blackwell*, 1983; *Lachenbruch and Sass*, 1977; 1978; *Sass et al.*, 1971; *Southern Methodist University*, 2011] have identified variability in the surficial heat flow within the Great Basin and Snake Valley study area, it is likely that surficial heat flow in the Snake Valley study area is being highly affected by groundwater flow, which can mask variability in the basal heat flux. By assuming that the basal heat flux is the same across

the model domain, there is associated uncertainty in the heat transport and energy balance throughout the model.

Limitations associated with applying specified temperatures across the top of the model domain are the result of uncertainty in the temperatures at the water table. While there is lots of data and, therefore, good control on water table temperatures in Snake Valley, northern Tule Valley, and western Fish Springs Flat, little data exist in the southern and eastern portions of the study area and in the mountain blocks; consequently water table temperatures in these areas are poorly known. Despite these uncertainties, the data used to characterize temperatures in these areas have been thoroughly analyzed for this model.

Limitations associated with applying a single (bulk) thermal conductivity value for an HGU are the result of limited source data (drill cuttings) to measure these values. Variability in these values within an HGU is highly likely at a local scale; at the resolution of the model grid, however, these variations would be difficult to quantify and represent. There is associated uncertainty, therefore, in the heat transport and energy balance throughout the model due to assuming a single bulk thermal conductivity for each HGU.

3.6 Summary

The Southern Nevada Water Authority (SNWA) has proposed developing unappropriated groundwater resources in Snake Valley and adjacent basins in eastern Nevada in order to supply the growing urban population of Las Vegas, Nevada. A ruling was issued on March 22, 2012, granting SNWA water rights for 61,127 acre-ft/yr of groundwater from Spring Valley, located immediately to the west of Snake Valley.

Furthermore, SNWA holds applications for approximately 50,700 acre-ft/yr of groundwater in Snake Valley.

Because of the magnitude of the SNWA groundwater development project and the interconnected nature of groundwater basins in the region, groundwater users and managers in Utah are concerned about declining groundwater levels and spring flows in western Utah which could result from the proposed groundwater withdrawals. The objective of this study is focused on understanding the links between basin-fill and carbonate aquifer systems, groundwater flow paths, sources of water to springs, and the movement of groundwater between basins in the Snake Valley area. This study lays the foundation for future studies, and will provide a baseline that can be used to assess the effects of future groundwater withdrawals on groundwater resources in the Snake Valley area.

This report describes the groundwater hydrology of the Snake Valley and surrounding area and presents the construction, calibration, and results of a numerical simulation of the groundwater system developed to test the conceptual understanding of the groundwater system. Information from a number of previous and current investigations was compiled to conceptualize and quantify hydrologic and thermal components of the groundwater system, and to provide hydraulic and thermal properties and observation data used in the calibration of the numerical groundwater model. A more complete understanding of the groundwater system and groundwater budget can aid in effective management of groundwater resources.

It was beyond the scope of the current study to develop a transient groundwater model to simulate increased groundwater withdrawals within the study area. The

groundwater model developed in this study, however, can be used as a tool in future studies to assess long-term effects of groundwater withdrawals and to guide the collection of further data that will lead to better predictions of the reduction of groundwater discharge to springs and declining water levels if increased well withdrawals were occurring.

The Snake Valley area regional groundwater flow system was simulated using a three-dimensional model incorporating both groundwater flow and heat transport. The model was constructed with MODFLOW-2000, a version of the U.S. Geological Survey's groundwater flow model, and MT3DMS, a transport model that simulates advection, dispersion, and chemical reactions of solutes or heat in groundwater systems. Observations of groundwater discharge by evapotranspiration, spring flow, mountain stream baseflow, and well withdrawals; groundwater-level altitudes; and groundwater temperatures were used to calibrate the model. UCODE-2005 was used to perform sensitivity analysis, calibration (including parameter estimation through nonlinear regression), and uncertainty evaluation of the groundwater model. Parameter values estimated by regression analyses were reasonable and within the range of expected values.

The model consists of 7 layers, on a finite-difference grid of 310 rows and 175 columns, and uniform, square model cells with a dimension of 804.65 m (0.5 mi) on each side. Model layers are simulated under confined flow conditions, so that the top of each layer and its thickness are defined. Although the top of the actual flow system is unconfined, the model accurately simulates the position of the water table. The model was run as steady-state and, therefore, model parameters were temporally constant.

Recharge into the model is from the simulation of infiltration of direct precipitation (in-place recharge), recharge from runoff, including mountain stream baseflow and unconsumed irrigation from surface-water; and from the simulation of subsurface groundwater inflow across the model boundary. The distribution of simulated recharge varies spatially. Groundwater discharge out of the model is primarily through simulated evapotranspiration, discharge at springs, mountain stream baseflow, and well withdrawals; and, to a lesser extent, by subsurface outflow across the model boundary. Several conceptual models were evaluated during calibration to test the validity of various interpretations about the flow system. The evaluation focused on testing alternative hypotheses concerning (1) the location and type of flow system boundaries (both hydrogeologic and thermal), (2) the definition of recharge areas, and (3) variations in interpretation of the hydrogeologic framework. For each conceptual model, a new set of parameters was estimated, and the resulting simulated water levels, groundwater discharges, and groundwater temperatures were compared to observed values. Only those conceptual model changes contributing to a significant improvement in model fit were retained in the final calibrated model.

This study represents one of the first regional modeling efforts to include calibration to groundwater temperature data. The inclusion of temperature observations reduced parameter uncertainty, in some cases quite significantly, over using just water-level and discharge observations. For instance, of the 39 parameters used to simulate horizontal-hydraulic conductivity, uncertainty on 11 of these parameters was reduced to one order of magnitude or less. Because groundwater temperatures are highly affected by the magnitude of groundwater flow, parameters controlling this aspect of the system were

more constrained by temperature observations than water-level or groundwater discharge observations. These include parameters representing (1) the horizontal-hydraulic conductivity of the higher permeability basin-fill and carbonate HGUs; (2) the vertical anisotropy ratio, especially those of the basin-fill units; (3) spring and river conductance; (4) recharge rates; and (5) well withdrawal rates.

The model provides a good representation of the groundwater system; 98 percent of the simulated values of water-level altitudes in wells are within 30 m of observed water-level altitudes, and 58 percent of them are within 12 m. Nineteen of 20 discharge observations are within 30 percent of observed discharge. Eighty-one percent of the simulated values of temperatures in wells are within 2 °C of the observed values, and 55 percent of them are within 0.75 °C.

The numerical model represents a more robust quantification of groundwater budget components than previous studies because the model integrates all components of the groundwater budget. The model also incorporates several new data including (1) a detailed hydrogeologic framework; (2) and more observations including several new water-level altitudes throughout the study area, several new measurements of spring discharge within Snake Valley which had not previously been monitored, and groundwater temperature data. The numerical model represents and simulates the conceptual model of an interconnected groundwater system between consolidated rock and basin fill, and of recharge areas in the mountains connecting flow through the mountains to the basins and to the regional flow system. The concept of the mountains and basins forming a continuous groundwater system provides a more detailed representation of groundwater budgets and flowpaths compared to previous studies that

separated the flow and/or groundwater budget components between the consolidated rock and basin. Uncertainty in the estimates of subsurface flow are less than those of previous studies because the model balanced recharge and discharge across the entire simulated area, not just in each HA, and because of the large dataset of observations (water-level altitudes, discharge, and temperatures) used to calibrate the model and the resulting transmissivity distribution.

The model simulated recharge and discharge amounts to within plus or minus 30 percent of the conceptual recharge and discharge amounts, which are largely based on previous estimates, with one exception; Pine Valley has simulated areal recharge that is 68 percent of the conceptual recharge. This is because recharge was reduced in southern Spring, Snake, and Pine Valleys to minimize flooding in the mountain blocks and to reduce simulated water-levels in southern Snake and Pine Valleys. The amount of reduction in recharge is approximately equal to the amount of previously reported groundwater discharge from perched areas to springs, streams, and ETg, which would be disconnected from the larger regional flow system. Because the model did not simulate discharge from these perched areas, the reduction in recharge accounts for any groundwater that may have been discharged to these perched areas. Although simulated recharge was reduced in southern Spring and Snake Valleys, simulated areal recharge in Spring and Snake Valleys is more similar to conceptual amounts than in Pine Valley because simulated recharge was increased over conceptual recharge in other portions of these HAs as indicated by both the temperature and groundwater discharge observations. Simulated subsurface flow estimates between HAs along with their associated uncertainty are within the range of previously reported estimates, except for subsurface flow from

Spring Valley to Snake Valley north of the Snake Range; the simulated subsurface flow and associated uncertainty indicate that flow across this boundary is much less than has been previously estimated.

Groundwater recharge from precipitation and unconsumed irrigation in Snake Valley is 160,000 acre-ft/yr, which is within the range of previous estimates. Subsurface inflow from southern Spring Valley to southern Snake Valley is 13,000 acre-ft/yr and is also within the range of previous estimates; subsurface inflow from Spring Valley to Snake Valley north of the Snake Range, however, is only 2,200 acre-ft/yr, which is much less than has been previously estimated. Groundwater discharge from groundwater evapotranspiration and springs is 100,000 acre-ft/yr, and discharge to mountain streams is 3,300 acre-ft/yr; these are within the range of previous estimates. Current well withdrawals are 28,000 acre-ft/yr. Subsurface outflow from Snake Valley occurs to Pine Valley (2,000 acre-ft/yr), Wah Wah Valley (23 acre-ft/yr), Tule Valley (31,000 acre-ft/yr), Fish Springs Flat (790 acre-ft/yr), and outside of the study area towards Great Salt Lake Desert (8,400 acre-ft/yr), totaling 44,000 acre-ft/yr and is within the range of previous estimates.

Although the quantification of groundwater flow across HA boundaries in the model is important in understanding the occurrence and movement of groundwater in and through the study area, it should be noted that the effects of groundwater development on natural discharge are not dependent on the rate and direction of groundwater flow; the simulated transmissivity and the locations of natural discharge provide a better indication of the effect of groundwater withdrawals on groundwater resources than does the amount and direction of subsurface flow between HAs. The distribution of simulated

transmissivity throughout the study area includes many areas of high transmissivity within and between HAs. Increased well withdrawals within these high transmissivity areas will likely affect a large portion of the study area, resulting in decreasing groundwater levels, as well as leading to a decrease in natural discharge to springs and evapotranspiration.

Because this is a regional, steady-state model, it can be used for the evaluation of regional-scale processes including (1) determining boundary conditions for the development of local-scale models; (2) evaluating alternative conceptual models; (3) transport of contaminants and heat; and (4) the analysis of long-term consequences of changed system stresses, such as those that would be imposed on the system by drought or increased groundwater withdrawals.

3.7 References

Anderman, E.R., and M.C. Hill (2000), MODFLOW-2000, the U.S. Geological Survey modular ground-water flow model—Documentation of the Hydrogeologic-Unit Flow (HUF) package, *US Geol. Surv. Open-File Rep. 00–342*, 89 pp.

Anderson, M.P., and W.W. Woessner (2002), *Applied Groundwater Modeling: Simulation of Flow and Advective Transport*, Elsvier, San Diego.

Barlow, P.M., and S.A. Leake (2012), Streamflow depletion by wells—Understanding and managing the effects of groundwater pumping on streamflow, *US Geol. Surv. Circ. 1376*, 84 pp.

Belcher, W.R., P.E. Elliott, and A.L. Geldon (2001), Hydraulic-property estimates for use with a transient ground-water flow model of the Death Valley regional ground-water flow system, Nevada and California, *US Geol. Surv. Water-Resour. Invest. Rep. 01–4210*, 28 pp.

Belcher, W.R., D.S. Sweetkind, and P.E. Elliott (2002), Probability distributions of hydraulic conductivity for the hydrogeologic units of the Death Valley regional ground-water flow system, Nevada and California, *US Geol. Surv. Water-Resour. Invest. Rep. 02–4212*, 24 pp.

Blackett, R.E. (2011), Temperature profiles of water monitoring wells in Snake Valley, Tule Valley, and Fish Springs Flat, Millard and Juab Counties, Utah, *Utah Geol. Surv. Open-File Rep. 578*, 13 pp.

Blackwell, D.D. (1983), Heat flow in the northern Basin and Range province, *Geothermal Resour. Council Spec. Rep. No. 13*, 81–92.

Bolke, E.L., and C.T. Sumsion (1978), Hydrologic reconnaissance of the Fish Springs Flat area, Tooele, Juab, and Millard Counties, Utah, *Utah Dept. of Nat. Resour. Tech. Pub. No. 64*, 30 pp.

Bravo, H.R., Feng Jiang, and R.J. Hunt (2002), Using groundwater temperature data to constrain parameter estimation in a groundwater flow model of a wetland system, *Water Resour. Res.*, *38*, doi: 10.1029/2000WR000172.

Bredehoeft, J.D., and I.S. Papadopulos (1965), Rates of vertical groundwater movement estimated from the earth's thermal profile, *Water Resour. Res.*, *1*, 325–328.

Burden, C.B. et al. (2010), Groundwater conditions in Utah, spring of 2010, *Utah Dept. of Nat. Resour. Coop. Invest. Rep. No. 51*, 135 pp.

Burden, C.B. et al. (2011), Groundwater conditions in Utah, spring of 2011, *Utah Dept. of Nat. Resour. Coop. Invest. Rep. No. 52*, 118 pp.

Buto, S.G. (2011), Description of spatial datasets accompanying the conceptual model of the Great Basin carbonate and alluvial aquifer system, Appendix 6 in Conceptual model of the Great Basin carbonate and alluvial aquifer system, edited by V.M. Heilweil and L.E. Brooks, *US Geol. Surv. Scien. Invest. Rep. 2010–5193*, 177–179.

Cartwright, K. (1970), Groundwater discharge in the Illinois Basin as suggested by temperature anomalies, *Water Resour. Res.*, *6*, 912–918.

Cederberg, J.R., D.S. Sweetkind, S.G. Buto, and M.D. Masbruch (2011), Three-dimensional hydrogeologic framework, Appendix 1 in Conceptual model of the Great Basin carbonate and alluvial aquifer system, edited by V.M. Heilweil and L.E. Brooks, *US Geol. Surv. Scien. Invest. Rep. 2010–5193*, 127–141.

Daly, C., M. Halbleib, J.I. Smith, W.P. Gibson, M.K. Doggett, G.H. Taylor, J. Curtis, and P.A. Pasteris (2008), Physiographically-sensitive mapping of temperature and precipitation across the conterminous United States, *Int. J. of Climatology*, *28*, 1977–2087.

Daly, C., R.P. Neilson, and D.L. Phillips (1994), A statistical-topographic model for mapping climatological precipitation over mountain terrain, *J. App. Met.*, *33*, 140–158.

Domenico, P. A., and F. W. Schwartz (1998), *Physical and Chemical Hydrology*, John Wiley and Sons, New York.

Elliott, P.E., D.A. Beck, and D.E. Prudic (2006), Characterization of surface-water resources in the Great Basin National Park area and their susceptibility to ground-water withdrawals in adjacent valleys, White Pine County, Nevada, *US Geol. Surv. Scien. Invest. Rep. 2006–5099*, 156 pp.

Faunt, C.G., J.B. Blainey, M.C. Hill, F.A. D'Agnese, and G.M. O'Brien (2010), Transient numerical model, Chap. F in Death Valley regional ground-water flow system, Nevada and California—Hydrogeologic framework and transient ground-water flow model, edited by W.R. Belcher, *US Geol. Surv. Prof. Pap. 1711*, 257–344.

Faunt, C.G., A.M. Provost, M.C. Hill, and W.R. Belcher (2011), Comment on "An unconfined groundwater model of the Death Valley Regional Flow System and a comparison to its confinced predecessor" by R.W.H. Carroll, G.M. Pohll and R.L. Hershey [J. Hydrol., 373, 316–328], *J. Hydrol.*, *397*, 306–309.

Fenneman, N.M. (1931), *Physiography of Western United States*, McGraw-Hill Book Company, Inc., New York.

Flint, A.L., and L.E. Flint (2007a), Application of the basin characterization model to estimate in-place recharge and runoff potential in the Basin and Range carbonate-rock aquifer system, White Pine County, Nevada, and adjacent areas in Nevada and Utah, *US Geol. Surv. Scien. Invest. Rep. 2007–5099*, 20 pp.

Flint, A.L., L.E. Flint, and M.D. Masbruch (2011), Input, calibration, uncertainty, and limitations of the Basin Characterization Model, Appendix 3 in Conceptual model of the Great Basin carbonate and alluvial aquifer system, edited by V.M. Heilweil and L.E. Brooks, *US Geol. Surv. Scien. Invest. Rep. 2010–5193*, 149–163.

Flint, L.E., and A.L. Flint (2007b), Regional analysis of ground-water recharge, in Ground-water recharge in the arid and semiarid southwestern United States, edited by D.A. Stonestrom, J. Constantz, T.P.A. Ferré, and S.A. Leake, *US Geol. Surv. Prof. Pap. 1703*, 29–59.

Gardner, P.M., M.D. Masbruch, R.W. Plume, and S.G. Buto (2011), Regional potentiometric-surface map of the Great Basin carbonate and alluvial aquifer system in Snake Valley and surrounding areas, Juab, Millard, and Beaver Counties, Utah, and White Pine and Lincoln Counties, Nevada, *US Geol. Surv. Scien. Invest. Map 3193*, 2 sheets.

Gates, J.S. (1987), Ground water in the Great Basin part of the Basin and Range Province, western Utah: Cenozoic geology of western Utah—Site for precious metal and hydrocarbon accumulations, *Utah Geol. Assoc.*, *Pub. 16*, 75–89.

Gates, J.S., and S.A. Kruer (1981), Hydrologic reconnaissance of the southern Great Salt Lake Desert and summary of the hydrology of west-central Utah, *Utah Dept. of. Nat. Resour. Tech. Pub. No. 71*, 55 pp.

Gelhar, L.W., C. Welty, and K.W. Rehfeldt (1992), A critical review of data on field-scale dispersion in aquifers, *Water Resour. Res.*, *28*, 1955–1974.

Halford, K.J., and R.W. Plume (2011), Potential effects of groundwater pumping on water levels, phreatophytes, and spring discharges in Spring and Snake Valleys, White Pine County, Nevada, and adjacent areas in Nevada and Utah, *US Geol. Surv. Scien. Invest. Rep. 2011–5032*, 52 pp.

Harbaugh, A.W., E.R. Banta, M.C. Hill, and M.G. McDonald (2000), MODFLOW-2000, the U.S. Geological Survey modular ground-water model—User guide to modularization concepts and the Ground-Water Flow Process, *US Geol. Surv. Open-File Rep. 00–92*, 121 pp.

Harrill, J.R., and M.S. Bedinger (2004), Estimated model boundary flows, Appendix 2 in Death Valley regional ground-water flow system, Nevada and California—Hydrologic framework and transient ground-water flow model, edited by W.R. Belcher, *US Geol. Surv. Scien. Invest. Rep. 2004–5205*, 376–408.

Harrill, J.R., J.S. Gates, and J.M. Thomas (1988), Major ground-water flow systems in the Great Basin region of Nevada, Utah, and adjacent states, *US Geol. Surv. Hydrogeo. Invest. Atlas HA–694–C*, 2 sheets.

Harrill, J.R., and D.E. Prudic (1998), Aquifer systems in the Great Basin region of Nevada, Utah, and adjacent states—Summary report, *US Geol. Surv. Prof. Pap. 1409–A*, 66 pp.

Heilweil, V.M., and L.E. Brooks, eds. (2011), Conceptual model of the Great Basin carbonate and alluvial aquifer system, *US Geol. Surv. Scien. Invest. Rep. 2010–5193*, 191 pp.

Heilweil, V.M., R.W. Healy, and R.N. Harris (2012), Noble gases and coupled heat/fluid modeling for evaluating hydrogeologic conditions of volcanic island aquifers, *J. Hydrol.*, *464–465*, 309–327.

Heilweil, V.M., D.S. Sweetkind, and D.D. Susong (2011), Introduction, Chap. A in Conceptual model of the Great Basin carbonate and alluvial aquifer system, edited by V.M. Heilweil and L.E. Brooks, *US Geol. Surv. Scien. Invest. Rep. 2010–5193*, 3–14.

Hevesi, J.A., A.L. Flint, and L.E. Flint (2003), Simulation of net infiltration and potential recharge using a distributed-parameter watershed model of the Death Valley region, Nevada and California, *US Geol. Surv. Water-Resour. Invest. Rep. 03–4090*, 161 pp.

Hill, M.C. (1998), Methods and guidelines for effective model calibration, *US Geol. Surv. Water-Resour. Invest. Rep. 03–4090*, 90 pp.

Hill, M.C., E.R. Banta, A.W. Harbaugh, and E.R. Anderman (2000), MODFLOW-2000, the U.S. Geological Survey modular ground-water model—User guide to the observation, sensitivity, and parameter-estimation processes and three post-processing programs, *US Geol. Surv. Open-File Rep. 00-184*, 209 pp.

Hill, M.C., and C.R. Tiedeman (2007), *Effective Groundwater Model Calibration with Analysis of Data, Sensitivities, Predictions, and Uncertainty*, John Wiley and Sons, Inc., Hoboken, New Jersey.

Hintze, L.F., G.C. Willis, D.Y.M. Laes, D.A. Sprinkel, and K.D. Brown (2000), Digital geologic map of Utah, *Utah Geol. Surv. Map 179 DM*, CD-ROM.

Holmes, W.F. (1984), Ground-water hydrology and the projected effects of ground-water withdrawals in the Sevier Desert, Utah, *State of Utah Dept. of Nat. Resour. Tech. Pub. 79*, 54 pp.

Hood, J.W., and F.E. Rush (1965), Water-resources appraisal of the Snake Valley area, Utah and Nevada, *Nevada Dept. of Conser. and Nat. Resour. Water Resour. Recon. Rep. 34*, 43 pp.

Kirby, S., and H. Hurlow (2005), Hydrogeologic setting of the Snake Valley hydrologic basin, Millard County, Utah, and White Pine and Lincoln Counties, Nevada—Implications for possible effects of proposed water wells, *Utah Geol. Surv. Rep. of Invest. 254*, 22 pp.

Lachenbruch, A.J., and J.H. Sass (1977), Heat flow in the United States and the thermal regime of the crust, in The Earth's Crust, Its Nature and Physical Properties, edited by J.G. Heacock, *Geophysical Monograph 20*, AGU, Washington, D.C., 626–675.

Lachenbruch, A.J., and J.H. Sass (1978), Models of extending lithosphere and heat flow in the Basin and Range province, in Cenozoic Tectonics and Regional Geophysics of the Western Cordillera, edited by R.B. Smith and G.P. Eaton, *Memoir 152*, 209–250.

Langevin, C.D., D.T. Thorne, A.M. Dausman, M.C. Sukop, and Weixing Guo (2008), SEAWAT Version 4: A computer program for simulation of multi-species solute and heat transport, *US Geol. Surv. Tech. and Meth. Book 6, Chapter A22*, 39 pp.

Leake, S.A. (2011), Capture—rates and directions of groundwater flow don't matter!, *Ground Water*, *49*, 456–458.

Leavesley, G.H., R.W. Lichty, B.M. Troutman, and L.G. Saindon (1983), Precipitation-runoff modeling system: User's manual, *US Geol. Surv. Water-Resour. Invest. Rep. 83–4238*, 207 pp.

Ludington, Steve, D.P. Cox, K.R. Leonard, and B.C. Moring (1996), Cenozoic volcanic geology of Nevada, Chap. 5 in An analysis of Nevada's metal-bearing mineral resources, edtied by D.A. Singer, *Nevada Bur. of Mines and Geol. Open-File Rep. 96–2*, 10 pp.

Manning, A.H., and D.K. Solomon (2005), An integrated environmental tracer approach to characterizing groundwater circulation in a mountain block, *Water Resour. Res.*, *41*, W12412, doi: 10.1029/2005WR004178.

Masbruch, M.D. (2011a), Current study groundwater recharge estimates for predevelopment conditions and ranges of previously reported estimates of groundwater recharge for each hydrographic area within the Great Basin carbonate and alluvial aquifer system study area, Appendix 4 in Conceptual model of the Great Basin carbonate and alluvial aquifer system, edited by V.M. Heilweil and L.E. Brooks, *US Geol. Surv. Scien. Invest. Rep. 2010–5193*, 165–170.

Masbruch, M.D. (2011b), Comparison of predevelopment and recent (2000) groundwater budget estimates for each hydrographic area within the Great Basin carbonate and alluvial aquifer system study area, Appendix 7 in Conceptual model of the Great Basin carbonate and alluvial aquifer system, edited by V.M. Heilweil and L.E. Brooks, *US Geol. Surv. Scien. Invest. Rep. 2010–5193*, 181–186.

Masbruch, M.D. (2011c), Current study groundwater discharge estimates for predevelopment conditions and ranges of previously reported estimates of groundwater discharge for each hydrographic area within the Great Basin carbonate and alluvial aquifer system study area, Appendix 5 in Conceptual model of the Great Basin carbonate and alluvial aquifer system, edited by V.M. Heilweil and L.E. Brooks, *US Geol. Surv. Scien. Invest. Rep. 2010–5193*, 171–176.

Masbruch, M.D., P.M. Gardner, and L.E. Brooks, (201X, in review), Hydrology and numerical simulation of groundwater movement and heat transport in Snake Valley and surrounding areas, Juab, Millard, and Beaver Counties, Utah, and White Pine and Lincoln Counties, Nevada, *US Geol. Surv. Scien. Invest. Rep. 201X-XXXX*, XX pp.

Masbruch, M.D., V.M. Heilweil, S.G. Buto, L.E. Brooks, D.D. Susong, A.L. Flint, L.E. Flint, and P.M. Gardner (2011), Estimated groundwater budgets, Chap. D in Conceptual model of the Great Basin carbonate and alluvial aquifer system, edited by V.M. Heilweil and L.E. Brooks, *US Geol. Surv. Scien. Invest. Rep. 2010–5193*, 73–125.

Mathey, S.B., ed. (1998), National Water Information System (NWIS), *US Geol. Surv. Fact Sheet 027–98*, 2 pp.

Maxey, G.B., and T.E. Eakin (1949), Ground water in White River Valley, White Pine, Nye, and Lincoln Counties, Nevada, *Nevada Office of the State Engineer Water Resour. Bull. No. 8*, 59 pp.

McDonald, M.G., and A.W. Harbaugh (1988), A modular three-dimensional finite-difference ground-water flow model, *US Geol. Surv. Tech. of Water-Resour. Invest.*, *Book 6*, *Chap. A1*, variously paginated.

Mehl, S.W., and M.C. Hill (2006), MODFLOW-2005, the U.S. Geological Survey modular ground-water model—Documentation of shared node local grid refinement (LGR) and the boundary flow and head (BFH) package, *US Geol. Surv. Tech. and Meth. 6–A12*, 68 pp.

Moreo, M.T., R.J. Laczniak, and D.I. Stannard (2007), Evapotranspiration rate measurements of vegetation typical of ground-water discharge areas in the Basin and Range carbonate-rock aquifer system, Nevada and Utah, September 2005–August 2006, *US Geol. Surv. Scien. Invest. Rep. 2007–5078*, 36 pp.

Nichols, W.D. (2000), Regional ground-water evapotranspiration and ground-water budgets, Great Basin, Nevada, Chapter C. Regional ground-water budgets and ground-water flow, eastern Nevada, *US Geol. Surv. Prof Pap. 1628*, 82 pp.

Pavelko, M.T. (2007), Spring database for the Basin and Range carbonate-rock aquifer system, White Pine County, Nevada, and adjacent areas in Nevada and Utah, *US Geol. Surv. Data Ser. 272*, 10 pp.

Plume, R.W., and S.M. Carlton (1988), Hydrogeology of the Great Basin region of Nevada, Utah, and adjacent states, *US Geol. Surv. Hydrol. Invest. Atlas HA–694–A*, 1 sheet.

Poeter, E.P., M.C. Hill, E.R. Banta, Steffen Mehl, and Steen Christensen (2005), UCODE_2005 and six other computer codes for universal sensitivity analysis, calibration, and uncertainty evaluation, *US Geol. Surv. Tech. and Meth. 6-A11*, 283 pp.

Prudic, D.E., J.R. Harrill, and T.J. Burbey (1995), Conceptual evaluation of regional ground-water flow in the Carbonate Rock Province of the Great Basin Nevada, Utah, and adjacent states, *US Geol. Surv. Prof Pap. 1409–D*, 102 pp.

Rush, F.E., andS.A.T. Kazmi (1965), Water resources appraisal of Spring Valley, White Pine and Lincoln Counties, Nevada: *State of Nevada Dept. of Conser. and Nat. Resour. Water Resour. Recon. Rep. 33*, 36 pp.

San Juan, C.A., W.R. Belcher, R.J. Laczniak, and H.M. Putnam (2010), Hydrologic components for model development, Chap. C in Death Valley regional ground-water flow system, Nevada and California—Hydrogeologic framework and transient ground-water flow model, edited by W.R. Belcher, *US Geol. Surv. Prof Pap. 1711*, 99–132.

Sass, J.H., A.H. Lachenbruch, R.J. Munroe, G.W. Greene, and T.H. Moses (1971), Heat flow in the western United States, *J. Geophys. Res.*, *76*, 6376–6412.

Scott, B.R., T.J. Smales, F.E. Rush, and A.S. Van Denburgh (1971), Water for Nevada, *Nevada Dept. of Conser. and Nat. Resour. Water Planning Rep. No. 3*, 87 pp.

Smith, J.L., R.J. Laczniak, M.T. Moreo, and T.L. Welborn (2007), Mapping evapotranspiration units in the Basin and Range carbonate-rock aquifer system, White Pine County, Nevada, and adjacent areas in Nevada and Utah, *US Geol. Surv. Scien. Invest. Rep. 2007–5087*, 20 pp.

Smith, Leslie, and D.S. Chapman (1983), On the thermal effects of groundwater flow systems: 1. Regional scale systems, *J. Geophys. Res.*, *88*, 593–608.

Southern Methodist University Geothermal Laboratory (2011), *The geothermal map of North America, 2011 update*, available online at *http://www.google.org/egs/*, accessed on 21 May 2012.

Southern Nevada Water Authority (SNWA) (2011), Southern Nevada Water Authority Clark, Lincoln, and White Pine Counties groundwater development project conceptual plan of development, available via Southern Nevada Water Authority website at, *http://www.snwa.com/assets/pdf/wr_gdp_concept_plan_2011.pdf*, accessed on 31 July 2012, 152 pp.

Stephens, J.C. (1974), Hydrologic reconnaissance of the Wah Wah Valley drainage basin, Millard and Beaver Counties, Utah, *Utah Dept. of Nat. Resour. Tech. Pub. No. 47*, 53 pp.

Stephens, J.C. (1976), Hydrologic reconnaissance of the Pine Valley drainage basin, Millard, Beaver, and Iron Counties, Utah, *Utah Dept. of Nat. Resour. Tech. Pub. No. 51*, 38 pp.

Stephens, J.C. (1977), Hydrologic reconnaissance of the Tule Valley drainage basin, Juab and Millard Counties, Utah, *Utah Dept. of Nat. Resour. Tech. Pub. No. 56*, 37 pp.

Stephens, J.C., and C.T. Sumsion (1978), Hydrologic reconnaissance of the Dugway Valley-Government Creek area, west-central Utah, *Utah Dept. of Nat. Resour. Tech. Pub. No. 59, 1978*, 42 pp.

Stonestrom, D.A., D.E. Prudic, R.J. Laczniak, K.C. Akstin, R.A. Boyd, and K.K. Henkelman (2003), Estimates of deep percolation beneath native vegetation, irrigated fields, and the Amargosa-River channel, Amargosa Desert, Nye County, Nevada, *US Geol. Surv. Open-File Rep. 03–104*, 88 pp.

Susong, D.D. (1995), Water budget and simulation of one-dimensional unsaturated flow for a flood- and sprinkler-irrigated field near Milford, Utah, *US Geol. Surv. Water-Resour. Invest. Rep. 95–4072*, 32 pp.

Sweetkind, D.S., J.R. Cederberg, M.D. Masbruch, and S.G. Buto (2011a), Hydrogeologic framework, Chap. B in Conceptual model of the Great Basin carbonate and alluvial aquifer system, edited by V.M. Heilweil and L.E. Brooks, *US Geol. Surv. Scien. Invest. Rep. 2010–5193*, 15–50.

Sweetkind, D.S., M.D. Masbruch, V.M. Heilweil, and S.G. Buto (2011b), Groundwater flow, Chap. C in Conceptual model of the Great Basin carbonate and alluvial aquifer system, edited by V.M. Heilweil and L.E. Brooks, *US Geol. Surv. Scien. Invest. Rep. 2010–5193*, 51–72.

Thomas, J.M., J.L. Mason, and J.D. Crabtree (1986), Ground-water levels in the Great Basin region of Nevada, Utah, and adjacent states, *US Geol. Surv. Hydrol. Invest. Atlas HA–694–B*, 2 sheets.

Thomas, J.M., A.H. Welch, and M.D. Dettinger (1996), Geochemistry and isotope hydrology of representative aquifers in the Great Basin region of Nevada, Utah, and adjacent states, *US Geol. Surv. Prof Pap. 1409–C*, 100 pp.

Tonkin, M.J., C.R. Tiedeman, D.M. Ely, and M.C. Hill (2007), OPR-PPR, a computer program for assessing data importance to model predictions using linear statistics, *US Geol. Surv. Tech. and Meth. Rep. TM-6E2*, 115 pp.

U.S. Census Bureau (2000), Pre-2010 cartographic boundary file naming conventions and download access, accessed April 21, 2005 at *http://www.census.gov/geo/maps-data/data/prev_cartbndry_names.html*.

U.S. Geological Survey EROS Data Center (1999), 1 arc-second (30-meter) National Elevation Dataset, *US Geol. Surv. dataset*, accessed September 15, 2008 at *http://ned.usgs.gov/*.

Utah Geological Survey, 2009, Snake Valley ground-water monitoring-well project: Snake Valley and adjacent areas, available via Utah Geological Survey website at *http://geology.utah.gov/esp/snake_valley_project/index.htm*, accessed on August 6, 2012.

Welborn, T.L., and M.T. Moreo (2007), Irrigated acreage within the Basin and Range carbonate-rock aquifer system, White Pine County, Nevada, and adjacent areas in Nevada and Utah, *US Geol. Surv.Data Ser. 273*, 18 pp.

Welch, A.H., D.J. Bright, and L.A. Knochenmus, eds. (2007), Water resources of the Basin and Range carbonate-rock aquifer system, White Pine County, Nevada, and adjacent areas in Nevada and Utah, *US Geol. Surv. Scien. Invest. Rep. 2007–5261*, 96 pp.

Wilberg, D.E. (1991), Hydrologic reconnaissance of the Sevier Lake area, west-central Utah, *Utah Dept. of Nat. Resour. Tech. Pub. No. 96*, 51 pp.

Wilkowske, C. D., D.V. Allen, and J.V. Phillips (2003), Drought conditions in Utah during 1999-2002: a historical perspective, *US Geol. Surv. Fact Sheet 037-03*, 6 pp.

Woodbury, A.D., and Leslie Smith (1988), Simultaneous inversion of hydrogeologic and thermal data 2. Incorporation of thermal data, *Water Resour. Res.*, *24*, 356–372.

Zheng, Chunmiao (2010), MT3DMS v5.3: Supplemental user's guide, *US Army Engineer Res. and Dev. Cen. Tech. Rep.*, 51 pp.

Zheng, Chunmiao, and G.D. Bennett (2002), Dispersive transport and mass transfer, Chap. 3 in *Applied Contaminant Transport Modeling (2)*, John Wiley and Sons, Inc., New York, 34–77.

Zheng, Chunmiao, and P.P. Wang 1999, MT3DMS: A modular three-dimensional multispecies transport model for simulation of advection, dispersion, and chemical reactions of contaminants in groundwater systems; documentation and user's guide, *US Army Engineer Res. and Dev. Cen. Contract Rep. SERDP–99–1*, 169 pp.

Zhu, Jianting, M.H. Young, and M.E. Cablk (2007), Uncertainty analysis of estimates of ground-water discharge by evapotranspiration for the BARCAS study area, *Desert Res. Inst., Div. of Hydrol. Sciences Pub. No. 41234*, 28 pp.

APPENDIX A

EQUATIONS AND CALCULATIONS OF THERMAL PROPERTIES USED FOR MODEL INPUT

A.1 Introduction

Input of thermal properties into the transport model code MT3DMS [*Zheng and Wang*, 1999] is done through arrays that represent each model layer. Because a model cell may contain multiple hydrogeologic units (HGUs) with differing properties of porosity and thermal conductivity, a system of thickness-weighted-mean equations was developed to calculate arrays on a layer by layer basis. This appendix presents these equations.

A.2 Porosity

Porosity is entered into the Basic Transport Package of MT3DMS in arrays that represent each model layer [*Zheng and Wang*, 1999]. It was assumed that UBFAU, LBFAU, and VU have a porosity of 0.3 (middle of range of porosities for sediments and basalts reported in *Domenico and Schwartz* [1998]); UCAU and LCAU have a porosity of 0.1 on the basis of the reported range for carbonates in the Great Basin [*Harrill and Prudic*, 1998]; and that USCU and NCCU have a porosity of 0.01 on the basis of a model using similar rock types [*Manning and Solomon*, 2005]. Because a model cell may contain multiple HGUs, the porosity was calculated using a thickness weighted mean for

each HGU within the cell using the following equation:

$$por_n = \left[0.3\left(\frac{thk_{UBFAU_n} + thk_{LBFAU_n} + thk_{VU_n}}{dz_n}\right)\right] + \left[0.1\left(\frac{thk_{UCAU_n} + thk_{LCAU_n}}{dz_n}\right)\right] + \left[0.01\left(\frac{thk_{USCU_n} + thk_{NCCU_n}}{dz_n}\right)\right] \quad \text{(A-1)}$$

where

por_n is the total porosity for layer n of the model cell,

n is the layer number,

thk_{UBFAU_n} is the thickness of UBFAU in layer n,

thk_{LBFAU_n} is the thickness of LBFAU in layer n,

thk_{VU_n} is the thickness of VU in layer n,

dz_n is the thickness of layer n,

thk_{UCAU_n} is the thickness of UCAU in layer n,

thk_{LCAU_n} is the thickness of LCAU in layer n,

thk_{USCU_n} is the thickness of USCU in layer n, and

thk_{NCCU_n} is the thickness of NCCU in layer n.

A.3 Thermal Conductivity and Thermal Diffusivity

Bulk thermal conductivity incorporates both the thermal conductivity of the aquifer solids, as well as the thermal conductivity of the fluid (groundwater) and is needed to calculate the thermal diffusivity, which accounts for the heat transport process of conduction. The thermal conductivity of the aquifer solids was measured at the University of Utah thermal laboratory (contact: David Chapman) from several cuttings

from wells drilled in the study area. Summary statistics for these measurements are given in Table A-1. The measured samples did not include cuttings for VU, USCU, or cuttings from NCCU zones 2 and 3, which are significantly different in lithology from the quartzites of NCCU zone 1 [*Sweetkind et al.*, 2011]. It was assumed that VU had the same aquifer solids thermal conductivity as UBFAU and LBFAU [*Clauser and Huenges*, 1995]. Thermal conductivity for USCU was assumed to be 1.35 watts per meter per degree Kelvin ($Wm^{-1}K^{-1}$), which was the average of the range reported for shales in *Gilliam and Morgan* [1987]; and thermal conductivity for NCCU zones 2 and 3 was assumed to be 3.00 $Wm^{-1}K^{-1}$, which was the average of the range reported for "poor in quartzite" metamorphic rocks in *Clauser and Huenges* [1995].

Similar to porosity, a cell may contain multiple HGUs that can have different aquifer solids thermal conductivities. The solid thermal conductivity for each cell per layer was calculated as a thickness weighted mean by the following equation:

$$k_{Tsolid_n} = \left[k_{Tsed}\left(\frac{thk_{UBFAU_n} + thk_{LBFAU_n} + thk_{VU_n}}{dz_n}\right)\right] + \left[k_{Tcarb}\left(\frac{thk_{UCAU_n} + thk_{LCAU_n}}{dz_n}\right)\right] + \left[k_{Tshale}\left(\frac{thk_{USCU_1}}{dz_n}\right)\right] + \left[k_{Tmeta}\left(\frac{thk_{NCCU_n}}{dz_n}\right)\right] \quad \text{(A-2)}$$

where

k_{Tsolid_n} is the total aquifer solids thermal conductivity for layer n of the model cell, in $Wm^{-1}K^{-1}$,

n is the layer number,

K_{Tsed} is the aquifer solids thermal conductivity for UBFAU, LBFAU, and VU (basin-fill sediments and volcanics), specified as a constant value of 3.88 W $m^{-1}K^{-1}$,

thk_{UBFAU_n} is the thickness of UBFAU in layer n, in meters,

Table A-1. Summary statistics for measured solid thermal conductivity samples from the Snake Valley study area. Modified from: *Masbruch et al.* [201X], in review.

[Thermal conductivity values are in units of watts per meter per Kelvin. **Abbreviations:** LBFAU, lower basin-fill aquifer unit; LCAU, lower carbonate aquifer unit; N, number of samples measured; NCCU, non-carbonate confining unit; UBFAU, upper basin-fill aquiferunit; UCAU, upper carbonate aquifer unit]

Lithology	Hydrologic unit abbreviation	N	Thermal conductivity	
			Mean	Standard deviation
Basin-fill sediments	UBFAU, LBFAU	45	3.88	0.67
Carbonate rocks	UCAU, LCAU	16	4.36	0.60
Quartzite	NCCU (zone 1)	8	5.09	0.74

thk_{LBFAU_n} is the thickness of LBFAU in layer n, in meters,

thk_{VU_n} is the thickness of VU in layer n, in meters,

dz_n is the thickness of layer n, in meters,

k_{Tcarb} is the aquifer solids thermal conductivity for both the UCAU and LCAU (carbonate rocks), specified as a constant value of 4.36 $Wm^{-1}K^{-1}$,

thk_{UCAU_n} is the thickness of UCAU in layer n, in meters,

thk_{LCAU_n} is the thickness of LCAU in layer n, in meters,

k_{Tshale} is the aquifer solids thermal conductivity for the USCU (shale), specified as a constant value of 1.35 $Wm^{-1}K^{-1}$,

thk_{USCU_n} is the thickness of USCU in layer n, in meters,

k_{Tmeta} is the aquifer solids thermal conductivity for NCCU (metamorphic rocks) specified as a constant value of 5.09 $Wm^{-1}K^{-1}$ for NCCU zone 1, and 3.00 $Wm^{-1}K^{-1}$ for NCCU zones 2 and 3, and

thk_{NCCU_n} is the thickness of NCCU in layer n, in meters.

The bulk thermal conductivity for each layer is then calculated using the following equation:

$$k_{Tbulk_n} = k_{Tfluid}^{(por_n)} k_{Tsolid_n}^{(1-por_n)} \qquad \text{(A-3)}$$

where

k_{Tbulk_n} is the bulk thermal conductivity of the aquifer for layer n of the model, in $Wm^{-1}K^{-1}$,

n is the layer number,

k_{Tfluid} is the thermal conductivity of the fluid (groundwater), specified as a constant value of 0.6 $Wm^{-1}K^{-1}$,

por_n is the total porosity for layer n of the model cell, and

k_{Tsolid_n} is the total aquifer solids thermal conductivity for layer n of the model cell, in $Wm^{-1}K^{-1}$.

Because the thermal diffusivity is entered into MT3DMS in arrays that represent each model layer [*Zheng and Wang*, 1999], and is dependent on both the bulk thermal conductivity and porosity, it is calculated as [*Langevin et al.*, 2008]:

$$Dmcoef_n = \frac{k_{Tbulk_n}}{por_n \rho_f c_{Pfluid}} \qquad \text{(A-4)}$$

where

$Dmcoef_n$ is the thermal diffusivity for layer n of the model cell, in m^2/s,

n is the layer number,

k_{Tbulk_n} is the bulk thermal conductivity of the aquifer for layer n of the model, in $Wm^{-1}K^{-1}$,

por_n is the total porosity for layer n of the model cell,

ρ_f is the density of the fluid (groundwater), specified as a constant value of 1,000 kg/m^3 (although the density of water is temperature dependent, it would only vary up to 4 percent over the expected range of temperatures), and

c_{Pfluid} is the heat capacity of the fluid (groundwater), specified as a constant value of 4,186 J/kgK.

A.4 Bulk Density and Thermal Distribution Factor

Because the bulk density is entered into the Chemical Reaction Package of MT3DMS in arrays that represent each model layer [*Zheng and Wang*, 1999] and is dependent on porosity, the bulk density for each cell per layer was calculated using the following equation:

$$\rho_{bn} = \rho_s(1 - por_n) \tag{A-5}$$

where

ρ_{bn} is the bulk density for layer n of the model cell, in kg/m^3,

n is the layer number,

ρ_s is the density of the aquifer solids, specified as a constant value of 2,700 kg/m^3 in this simulation (average of densities of representative rock types reported in *Langevin et al.* [2008]), and

por_n is the total porosity for layer n of the model cell.

The thermal distribution factor, which is also input to the Chemical Reaction Package in MT3DMS [*Zheng and Wang*, 1999] was calculated using the following equation [*Langevin et al.*, 2008]:

$$K_{d\_temp} = \frac{c_{Psolid}}{\rho_f c_{Pfluid}} \tag{A-6}$$

where

K_{d_temp} is the thermal distribution factor of the model cell, in m^3/kg,

c_{Psolid} is the specific heat capacity of the aquifer solids, and is specified as a constant value of 840 J/kgK (Langevin and others, 2008),

ρ_f is fluid (groundwater) density, and is specified as a constant value of 1,000 kg/m^3, and

c_{Pfluid} is the specific heat capacity of the fluid (groundwater), and is specified as a constant value of 4,186 J/kgK.

Consequently, the thermal distribution factor is equal to 0.0002 m^3/kg for all cells in the model.

A.5 References

Clauser, Christoph, and Ernst Huenges (1995), Thermal conductivity of rocks and minerals, section (3-9) in *Rock Physics and Phase Relations: A Handbook of Physical Constants*, edited by T.J. Ahrens, AGU, Washington, D.C., 105–126.

Gilliam, T.M., and I.L. Morgan (1987), Shale: Measurement of thermal properties, *Oak Ridge Nat. Lab. TM-10499*, 139 pp., (accessed at *http://www.ornl.gov/info/reports/1987/3445602782148.pdf* on June 29, 2012).

Harrill, J.R., and D.E. Prudic (1998), Aquifer systems in the Great Basin region of Nevada, Utah, and adjacent states—Summary report, *US Geol. Surv. Prof Pap. 1409–A*, 66 pp.

Langevin, C.D., D.T. Thorne, A.M. Dausman, M.C. Sukop, and Weixing Guo (2008), SEAWAT Version 4: A computer program for simulation of multi-species solute and heat transport, *US Geol. Surv. Tech. and Meth. Book 6, Chapter A22*, 39 pp.

Manning, A.H., and D.K. Solomon (2005), An integrated environmental tracer approach to characterizing groundwater circulation in a mountain block, *Water Resour. Res., 41*, W12412, doi: 10.1029/2005WR004178.

Masbruch, M.D., P.M. Gardner, and L.E. Brooks, (201X, in review), Hydrology and numerical simulation of groundwater movement and heat transport in Snake Valley and surrounding areas, Juab, Millard, and Beaver Counties, Utah, and White Pine and Lincoln Counties, Nevada, *US Geol. Surv. Scien. Invest. Rep. 201X-XXXX*, XX pp.

Sweetkind, D.S., J.R. Cederberg, M.D. Masbruch, and S.G. Buto (2011), Hydrogeologic framework, Chap. B in Conceptual model of the Great Basin carbonate and alluvial aquifer system, edited by V.M. Heilweil and L.E. Brooks, *US Geol. Surv. Scien. Invest. Rep. 2010–5193*, 15–50.

Zheng, Chunmiao, and P.P. Wang 1999, MT3DMS: A modular three-dimensional multispecies transport model for simulation of advection, dispersion, and chemical reactions of contaminants in groundwater systems; documentation and user's guide, *US Army Engineer Res. and Dev. Cen. Contract Rep. SERDP–99–1*, 169 pp.

APPENDIX B

WATER-LEVEL OBSERVATION UNCERTAINTY CALCULATIONS

B.1 Introduction

The uncertainty determined for each water-level observation includes uncertainties related to errors in the well altitude and location, water-level measurement error, nonsimulated transient error, and model discretization. The error for each of these components presented in this appendix was calculated following the procedure outlined by *San Juan et al.* [2010] and *Faunt et al.* [2010].

B.2 Well-Altitude Error

The well-altitude error was computed from the altitude-accuracy code given for each well in the USGS National Water Information Systems (NWIS) database. The altitude-accuracy code is generally expressed as a plus/minus range related to the method by which the land-surface altitude is determined. In the study area, this ranges between ± 0.003 m for high-precision methods, such as differential global positioning system (GPS) surveys, and ± 15 m for estimates determined from topographic maps having large (30 m or 100 ft) contour intervals. The range defined by the altitude-accuracy code is assumed to represent, with 95-percent confidence, the true well-altitude uncertainty. Assuming that the water-level observation represents the mean value and that the error is normally

distributed, the uncertainty of the water-level observation with respect to well-altitude error can be expressed as a standard deviation by the following equation:

$$sd_1 = \frac{AAC}{2} \tag{B-1}$$

where

sd_1 is the standard deviation of the well-altitude error, and

AAC is the value of the NWIS altitude-accuracy code in meters.

Accordingly, the standard deviation for well-altitude water-level error ranges between 0.0015 m and 7.5 m in the study area.

B.3 Well-Location Error

The well-location error was computed as the product of the hydraulic gradient at the well and the locational uncertainty distance determined from the latitude/longitude coordinate accuracy code values given in NWIS. The latitude/longitude coordinate accuracy code is generally expressed as a plus/minus range related to the method by which the latitude/longitude is determined. In the study area this ranges between ±0.01 seconds to ±60 seconds.

The uncertainty distance based on the latitude/longitude accuracy code was calculated using the following formula (which assumes that the Earth is a perfect sphere):

$$DA = (LLAC)(30.9)\cos\left(\frac{\pi Lat}{180}\right) \tag{B-2}$$

where

DA is the distance accuracy, in meters,

$LLAC$ is the value of the NWIS latitude-longitude accuracy code, in seconds,

30.9 is the distance, in meters, of one second at the equator, and

$\cos\left(\frac{\pi Lat}{180}\right)$ is the cosine of the latitude (in decimal degrees) of the well.

Accordingly, the distance accuracy within the study area ranges between ±0.24 m and ±1,422 m.

The hydraulic gradient at the well was estimated from a regional potentiometric-surface map developed by *Gardner and et al.* [2011] for the study area. The gradient ranges between 0.01 percent and 1.2 percent within the study area.

To determine the well-location error, the range defined by the value of the coordinate accuracy is assumed to represent, with 95-percent confidence, the true error in the water-level observation as related to well-location uncertainty. Assuming that the water-level observation represents the mean value and the error is normally distributed, the uncertainty of the water-level observation, with respect to the well-location error, can be expressed as a standard deviation calculated by the following equation:

$$sd_2 = \left(\frac{DA}{2}\right) HG \tag{B-3}$$

where

sd_2 is the standard deviation of the well-location error, in meters,

DA is the distance accuracy, in meters, and

HG is the hydraulic gradient, in percent slope divided by 100.

Accordingly, the standard deviation for well-location water-level error ranges between 0.00028 m and 0.61 m for the study area.

B.4 Measurement Error

Measurement errors result from inaccuracies in the measurement of depth to water and depend primarily on the device used to make the measurement. For the study area, a general value of ±0.003 m (0.01 ft) was assumed to represent the measurement accuracy [*Cunningham and Schalk*, 2011].

To determine the measurement error, the range defined by the measurement accuracy is assumed to represent, with 95-percent confidence, the true error in the water-level observation as related to measurement uncertainty. Assuming that the water-level observation represents the mean value and the the error is normally distributed, the uncertainty of the water-level observation, with respect to the measurement error, can be expressed as a standard deviation calculated by the following equation:

$$sd_3 = \frac{MA}{2} \tag{B-4}$$

where

sd_3 is the standard deviation of the measurement error, in meters, and

MA is the measurement accuracy, in meters.

Accordingly, the standard deviation for the measurement water-level error is 0.0015 m for the study area.

B.5 Nonsimulated Transient Error

Nonsimulated transient errors result from uncertainty in the magnitude of water-level response caused by stresses not simulated in the groundwater model, which are typically seasonal and long-term climate changes. Seasonal fluctuations in wells in Spring and Snake Valleys with known open intervals of less than 30.5 m (100 ft) depth

below land surface can be as high as 2.9 m, with an average of around 1 m; seasonal fluctuations in wells with known open intervals of less than 30.5 m (100 ft) depth below land surface outside these valleys only averages approximately 0.2 m. For wells with known open intervals greater than 30.5 m (100 ft) depth below land surface, average seasonal fluctuations in wells in Spring and Snake Valleys and wells outside of these valleys were 0.15 m and 0.25 m, respectively.

On the basis of the above seasonal water-level fluctuation analysis, seasonal fluctuations were assigned in the following manner:

1. For wells with known open interval depths of less than 30.5 m (~100 ft) below land surface in Spring and Snake Valleys, seasonal fluctuations of 1 m were assigned.
2. For wells with known open interval depths of less than 30.5 m (~100 ft) below land surface outside of Spring and Snake Valley, seasonal fluctuations of 0.2 m were assigned.
3. For wells with known open interval depths of greater than 30.5 m below land surface, an average value for seasonal fluctuations of 0.2 m was assigned for all HAs within the study area.
4. For wells with no open interval data, it was assumed that wells with a total depth of less than 45 m (~150 ft) below land surface could possibly have open interval depths of less than 30.5 m below land surface. Wells with a total depth of more than 45 m were assumed to have open interval depths of greater than 30.5 m below land surface. Seasonal fluctuations for wells with total depths of

less than 45 m and more than 45 m were assigned as above depending on their location.

On the basis of analysis of available water-level data from wells outside of pumping areas, long-term (> 30 years) climate response is relatively small, on average less than 1.2 m, within the study area. The potential error associated with long-term climatic response at each well was not calculated independently as very few wells have long-term water level data. Instead, it was accounted for by adding 1 m to the seasonal fluctuation assigned to each well.

The range defined by this sum is assumed to represent, with 95-percent confidence, the true error in the water-level observation as related to nonsimulated transient uncertainty. Assuming that the water-level observation represents the mean value and the error is normally distributed, the uncertainty of the water-level observation, with respect to the nonsimulated transient error, can be expressed as a standard deviation calculated by the following equation:

$$sd_4 = \frac{(SF + LTF)}{4} \qquad \text{(B-5)}$$

where

sd_4 is the standard deviation of the nonsimulated transient error, in meters,

SF is the seasonal fluctuation, in meters, and

LTF is the long-term fluctuation, and is equal to 1 m.

Accordingly, the standard deviation for nonsimulated transient water-level error for wells outside of Spring and Snake Valleys is 0.3 m; the standard deviation for wells inside Spring and Snake Valleys is 0.5 m for wells having an open interval within 30.5 m (100 ft) of land surface, and 0.3 m for deeper wells.

B.6 Model-Discretization Error

Model-discretization error results from inaccuracies in the geometric representation of HGUs and major structural features in the model [*Hill and Tiedeman*, 2007]. The magnitude of these errors is assumed to be a function of:

1. Nodal width; larger widths result in a less accurate representation of the geometry of HGUs and major structural features relative to well location.
2. Hydraulic gradient; inaccurate geometric representations tend to shift the location of local hydraulic gradients.
3. Well-opening depth; there is a decrease in knowledge of HGUs and structures with depth)

Model-discretization error is the product of the nodal width, hydraulic gradient, and a scalar representing the error associated with well-opening depth. The nodal width used in the model is 804.65 m (0.5 mi). The hydraulic gradient at the well was estimated from a regional potentiometric-surface map developed for the study area [*Gardner et al.*, 2011], and ranges between 0.01 percent and 1.2 percent. The potential error attributed to a decrease in geologic certainty with depth is calculated using a scalar that is a function of the well-opening depth. The scalar is calculated as 2 plus the quotient of the depth of the top of the open interval and the approximate thickness of the aquifer material in the model (assumed to be 1,450 m based on the average thickness of basin-fill, volcanic, and Paleozoic carbonates in the model).

The range defined by this product is assumed to represent, with 95-percent confidence, the true error in the water-level observation as related to model-discretization error. Assuming that the water-level observation represents the mean value and the error

is normally distributed, the uncertainty of the water-level observation, with respect to model-discretization error, can be expressed as a standard deviation calculated by the following equation:

$$sd_5 = \frac{(NW)(HG)\left[\frac{TOPUPOPEN}{MT} + 2\right]}{4} \quad \text{(B-6)}$$

where

sd_5 is the standard deviation of the model-discretization error, in meters,

NW is the nodal width, and is equal to 804.65 m,

HG is the hydraulic gradient, in percent slope divided by 100

$TOPUPOPEN$ is the top of the upper well opening, in meters below land surface,

and MT is the approximate thickness of aquifer material in the model, specified as 1,450 m for this study.

Accordingly, the standard deviation for the model-discretization water-level error ranges between 0.045 m and 5.5 m for the study area.

B.7 Total Water-Level Observation Error

The total uncertainty associated with each water-level observation is the composite of all errors contributed by the different components. This uncertainty can be expressed as a standard deviation calculated as:

$$sd_h = \sqrt{\left(sd_1^2 + sd_2^2 + sd_3^2 + sd_4^2 + sd_5^2\right)} \quad \text{(B-7)}$$

where

sd_h is the total standard deviation for each water-level observation, in meters,

sd_1 is the standard deviation of the well-altitude error, in meters,

sd_2 is the standard deviation of the well-location error, in meters,

sd_3 is the standard deviation of the measurement error, in meters,

sd_4 is the standard deviation of the nonsimulated transient error, in meters, and

sd_5 is the standard deviation of the model-discretization error.

Accordingly, the total standard deviations of water-level observations range from 1.2 m to 7.7 m, and average 2.3 m.

B.8 References

Cunningham, W.L., and C.W. Schalk, comps. (2011), Groundwater technical procedures of the U.S. Geological Survey, *US Geol. Surv. Tech. and Meth. 1–A1*, 151 pp.

Faunt, C.G., J.B. Blainey, M.C. Hill, F.A. D'Agnese, and G.M. O'Brien (2010), Transient numerical model, Chap. F in Death Valley regional ground-water flow system, Nevada and California—Hydrogeologic framework and transient ground-water flow model, edited by W.R. Belcher, *US Geol. Surv. Prof. Pap. 1711*, 257–344.

Gardner, P.M., M.D. Masbruch, R.W. Plume, and S.G. Buto (2011), Regional potentiometric-surface map of the Great Basin carbonate and alluvial aquifer system in Snake Valley and surrounding areas, Juab, Millard, and Beaver Counties, Utah, and White Pine and Lincoln Counties, Nevada, *US Geol. Surv. Scien. Invest. Map 3193*, 2 sheets.

Hill, M.C., and C.R. Tiedeman (2007), *Effective Groundwater Model Calibration with Analysis of Data, Sensitivities, Predictions, and Uncertainty*, John Wiley and Sons, Inc., Hoboken, New Jersey.

San Juan, C.A., W.R. Belcher, R.J. Laczniak, and H.M. Putnam (2010), Hydrologic components for model development, Chap. C in Death Valley regional ground-water flow system, Nevada and California—Hydrogeologic framework and transient ground-water flow model, edited by W.R. Belcher, *US Geol. Surv. Prof. Pap. 1711*, 99–132.

APPENDIX C

GROUNDWATER TEMPERATURE OBSERVATION UNCERTAINTY CALCULATIONS

C.1 Introduction

The uncertainty determined for each temperature observation includes uncertainties related to errors in the temperature measurement error and model vertical discretization error, and are discussed below.

C.2 Measurement Error

Measurement errors result from inaccuracies in the measurement of temperature and depend primarily on the device used to make the measurement. For the temperature observations measured in the UGS wells, the temperature equipment used had a measurement precision of 0.01 °C [*Blackett*, 2011]. For spring temperature data taken from NWIS, it was assumed that these measurements had a precision of 0.5 °C.

To determine the measurement error, the range defined by the measurement accuracy is assumed to represent, with 95-percent confidence, the true error in the temperature observation as related to measurement uncertainty. Assuming that the temperature observation represents the mean value and that the error is normally distributed, the uncertainty of the temperature observation, with respect to the measurement error, can be expressed as a standard deviation calculated by the following

equation:

$$sd_1 = \frac{MA}{2} \quad \text{(C-1)}$$

where

sd_1 is the standard deviation of the measurement error, in °C, and

MA is the measurement accuracy, and is equal to either 0.01 °C or 0.5 °C.

Accordingly, the standard deviation for the measurement error is 0.005 °C for temperatures measured in wells in the study area, and 0.25 °C for temperatures measured from springs in the study area.

C.3 Model Vertical Discretization Error

Model vertical discretization error results from model layer thickness discretization. The magnitude of this error is assumed to be a function of model layer thickness and the thermal gradient (temperature vs. depth) within each layer.

For UGS wells (except for those adjacent to springs) penetrating the entire model layer, the model discretization error was calculated as the standard deviation of all temperature measurements taken within that layer.

For UGS wells that do not penetrate the entire layer, including those adjacent to springs, the gradient across the entire layer could not be accounted for, and the following assumptions were made:

1. For wells that reach the middle of the layer and are not adjacent to a spring, the thermal gradient for the upper portion of the layer was assumed to extend to the bottom of the layer.
2. For wells that do not reach the middle of the layers and are not adjacent to

a spring, the thermal gradient was assumed to be the same as the thermal gradient for the layer above.

3. For wells that are adjacent to springs, since the thermal gradient changes dramatically across the depth of the well, the gradient was calculated using the highest and lowest temperature measurements within the well.

The model vertical discretization error for these wells is calculated as the product of the layer thickness and the thermal gradient across the layer. The range defined by this product is assumed to represent, with 95-percent confidence, the true error in the temperature observation as related to model vertical discretization error. Assuming that the temperature observation represents the mean value and the error is normally distributed, the uncertainty of the temperature observation, with respect to model vertical discretization error, can be expressed as a standard deviation calculated by the following equation:

$$sd_2 = \frac{(dz)(gradT)}{4} \qquad \text{(C-2)}$$

where

sd_2 is the standard deviation of the model vertical discretization error, in ºC,

dz is the layer thickness, in meters, and

$gradT$ is the thermal gradient across the layer, in ºC per meter.

For spring temperature data from NWIS, the model vertical discretization error was calculated as follows:

1. For Clay, Dearden, Unnamed, and Big Springs, the error was calculated as the mean of the error calculated for UGS wells SG24C and SG25C

[*Blackett*, 2011], which were assumed to be most likely representative of thermal gradients at cold springs within the study area.

2. For Gandy Warm Springs, the error was assumed to be the same as the error calculated for UGS well SG21C [*Blackett*, 2011] as this site was assumed to be most representative of the thermal gradient at warm springs within the study area.

Accordingly, the standard deviation for the model vertical discretization error ranges between ± 0.0039 and 1.8 °C within the study area.

C.4 Total Temperature Observation Error

The total uncertainty associated with each temperature observation is the composite of all errors contributed by the different components. This uncertainty can be expressed as a standard deviation calculated as:

$$sd_T = \sqrt{\left(sd_1^2 + sd_2^2\right)} \tag{C-3}$$

where

sd_T is the total standard deviation for each temperature observation, in °C,

sd_1 is the standard deviation of the measurement error, in °C, and

sd_2 is the standard deviation of the model vertical discretization error, in °C.

Accordingly, the total standard deviations of temperature observations range from 0.0064 °C to 1.8 °C.

C.5 References

Blackett, R.E. (2011), Temperature profiles of water monitoring wells in Snake Valley, Tule Valley, and Fish Springs Flat, Millard and Juab Counties, Utah, *Utah Geol. Surv. Open-File Rep. 578*, 13 pp.